PHD

The Protection of Transmission Networks Containing AC and DC Circuits

Wang, Hualei

Award date:
2015

Awarding institution:
University of Bath

The Protection of Transmission Networks Containing AC and DC Circuits

Hualei Wang

A thesis submitted for the degree of Doctor of Philosophy

University of Bath

Department of Electronic and Electrical Engineering

November 2014

COPYRIGHT

Contents

Abstract

In 14th August 2003, the Northeast USA suffered its worst power outage event in history. The power disturbance spreading through the system caused mal-trips of the distance relay remote back-up protections, which indeed contributed to the power outage cascading a wide area.

The power outage in the Northeast USA was constrained by the presence of HVDC interconnections between the HVAC networks in Ontario and New York. The system collapse did not progress beyond the HVDC interconnection interface with Quebec. The HVDC link can regulate the voltage and current therefore impacts on the performance of the protection and system stability.

The distance relay mal-operations were one of the main cause of the Northeast USA blackout as well as the other recent major large area blackouts which were pointed out by the previous papers.

This thesis is focus on investigate how HVDC interconnections contribute to maintaining the power system stability. The research work investigated the performance of a distance relay to faults and disturbance on networks containing HVDC interconnection.

The research work was carried out by modelling and testing a classic signal processing distance relay in a simple AC network which was based on Kunder's two areas system using MATLAB/SIMULINK at first. Then the modeled distance relay's performance was investigated by combining the distance relay and a simple HVDC link based on the Kunder's two areas system. The research work firstly combined the signal processing distance relay and the HVDC link together to investigate the distance relay's performance when the protected feeder containing DC link. The distance relay's performance was investigated when the protected feeders containing HVDC link under fault conditions and power swing conditions. For comparison, a similar power system without HVDC link was also simulated.

Acknowledgements

Firstly, I would like to express my gratitude to my supervisor Dr. Mile Redfern for his support and guidance throughout my PhD research.

Secondly, I would like to take the opportunity to express my thanks to my beloved families for their support and encouragement in my life. Special thanks to my girlfriend PengfeiGao for her patience and encouragement in the last year of my PhD life.

I would like to thank to Dr. Francis Robinson, Dr. Xin Sun, Dr.ChenghongGu, Dr.Shufeng Dong, Dr.Jiahui Zhu, and Dr.ZhangehuaZheng for discussing with me and sharing knowledge with me.

I would like to thank to my office colleagues, Dr. Chao Gao, Dr.ChenChen Yuan, Dr.Zhiming Wang, Mr. Jiangtao Li, Mr. Ran Li and Mr. Fan Yi, those who gave me much inspiration during my research work.

And, I would express my thanks to all my kind friends including Dr.Mingju Ma, Dr. Bo Li, Dr.Yan Zhang, Dr.Shuang Yu, Dr. Xiao Sun, Mr. Ge Song, Mr. Jun Li for their help in my PhD life. Special thanks to Prof.Furong Li for her help in my PhD life.

List of Figures

List of Tables

List of Abbreviations

Alternating Current	AC
A regional transmission organization in the United States	PJM
Capacitor Commutated Converter	CCC
Carbon Dioxide	CO_2
Constant Current	CC
Constant Extinction Angle	CEA
Constant Ignition Angle	CIA
Current Sources Converter	CSC
Current Transformer	CT
Digital Signal Processing	DSP
Direct Current	DC
Discrete Fourier Transformer	DFT
Effective Short-Circuit Ratio	ESCR
Electricity Distribution Company in Germany	E.onNetz
Electromagnetic Transients including DC	EMTDC
Flexible AC Transmission Systems	FACTS
Gate Turn Off Thyristors	GTOs
Greece-Italy	GRITA
High-Voltage Alternating Current	HVAC
High-Voltage Direct Current	HVDC
International Council on Large Electric Systems	CIGRE
Institute of Electrical and Electronic Engineers	IEEE
Insulate Gate Bipolar Transistors	IGBTs
Matrix Laboratory	MATLAB
Power System Block	PSB
Power System Computer Aided Design	PSCAD
Rheinisch-WestfälischeElektrizitätswerke	RWE

Root-Mean-Square	RMS
Sardinia-Corsica	SACOI
Short-Circuit Ratio	SCR
Transmission System Operator	TSO
Union for the Co-ordination of Transmission of Electricity	UCTE
Voltage Dependent Current Order Limit	VDCOL
Voltage Source Converter	VSC
Voltage Transformer	VT

Chapter 1

Introduction

1.1 Research Back Ground

Modern power systems are driven by the growth of power demand to large interconnected and high voltage level complex networks [1]. The neighbouring power systems are interconnected together by HVAC interconnections in order to transport energy from areas with extra capacity to those with shortage and satisfy the continuing increase in demand [2]. The regional systems are interconnected together by national grids. These large highly integrated grids give opportunities to use larger and more economical power plants, utilize renewable energy resources and reduce the reserve capacity in the systems [1]. Furthermore, the interconnected power systems give savings in costs. It has been estimated that interconnections in North America saved about $20 billion in the 1990s [2].

However, these HVAC interconnections are not as simple as a few connecting wires. Highly interconnected systems are complicated. These HVAC interconnections bring risks of large propagated disturbances [2]. The highly integrated power grids may lead to stability problems and raise the risks of uncontrollable cascading effects. Loehr [3] has been advocating the breaking up of the two gigantic interconnections or grids that straddle North America into a number of smaller ones since 1999. In his suggestion, these mini-grids can be interconnected by HVDC instead of current AC ties. As Loehr explained, "With ac ties, what happens in one place on the grid affects everywhere else. A major disturbance in Ontario is felt as far away as Oklahoma, Florida and Maine. This doesn't happen with DC links – since they insulate one small grid from the others, but still permits power exchange [3]."

An outage could occur in these highly interconnected grids which at first would seem of little importance but then spread through a wide area and cause large blackout [3]. Such situations have been reported in North America blackout. On 14th August 2003, Northeast U.S.A suffered a severe power outage event which affected a wide area and many millions of people [4-10]. According to [10], the 2003 Blackout was the worst outage event in the history of U.S. The blackout led to about 61.8GW power lost, which equates to approximately 11% of the total load served in the Eastern Interconnection of the North American system. It affected about 50 million people in Ontario and the eight states in U.S. Northeast. During the event, over 400

transmission lines and 531 generating units at 261 power plants tripped. The outage was caused by the failure of two 345kV transmission lines due to tree contact and the outage of a 597MW power plant [10]. The event started slowly but spread quickly. The outage then caused widespread voltage collapse in both Canada and the Northeast of the United States. Fig.1-1 shows the affected areas during the blackout. Detailed information of the 2003 blackout will be reviewed in next chapter.

Figure 1-1 Affected areas during the 2003 blackout [4]

The voltage collapse broke the balance of the power networks and resulted in a large power swing. The changing swing voltages and currents caused the apparent impedance detected by distance relays to enter the protection zones and therefore caused relays to trip. Many key lines were tripped by distance relays due to the power swing. These accelerated the blackout which spread to a wide area [11].

However, during the 2003 blackout, the Quebec network was not affected by the disturbance [1, 7, 12]. The Quebec was interconnected to the U.S. system via HVDC interconnection. The HVDC link blocked the power swing and acted as a 'firewall' against the cascade [1, 3]. Quebec survived the blackout [1, 7, 12].

Such evidence that the HVDC interconnection prevented the voltage outage could also be found in recent blackouts listed below.

- 2003 Sweden and Denmark Blackout
- 2003 Italy Blackout

- 2006 European Blackout
- 2010 Namibian and Zambian Eventual Blackout

These recent blackouts are reviewed in next chapter.

1.2 Research Motivation

The growing need for high voltage electrical networks has raised concerns over the potential impacts of wide area blackouts. A catalogue of these events in the USA has highlighted the need for research into introducing new and novel solution to minimize such events.

Studies of several wide area blackouts have suggested that inappropriate operation of the transmission line protection has a major impact on the propagation of such system collapse, principally the operation of distance protection. More recent blackouts have also suggested that including HVDC interconnections in predominately HVAC networks can constrain the collapse.

These findings have prompted this research into the behaviour of classical distance relay system to events on networks containing both HVAC and HVDC lines.

The work was prompted by question being raised in China over the expansion of their high voltage networks to transport power over long distances. It is however appropriate to many other areas of the world including the USA, Europe, the Middle-East, Africa, etc.

HVDC transmission technology has been introduced first half of last century. It offers new solutions for bulk power long distance delivery and power system interconnections. HVDC transmission was developed from transmitting a few hundreds MW up to 3-4 GW over long distance by just one bipolar line [13, 14]. HVDC transmission has become a mature and reliable technology. HVDC transmission systems are used worldwide, with about 50 GW capacity installed as shown in fig.1-2[13].

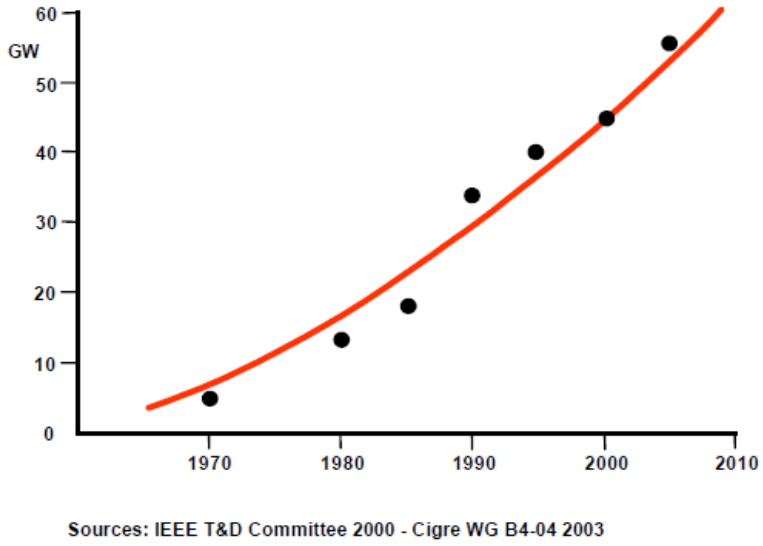

Figure 1-2 Worldwide installed capacities of HVDC systems[13]

HVDC systems provide an alternative method of power system interconnection. HVAC interconnections are technically feasible and economically justified, but HVDC interconnections offer technical benefits and offer more economical solutions when compared to HVAC interconnections [13]. Hybrid interconnections, consisting of HVAC and HVDC links, are the further solutions. The HVDC links support the HVAC interconnections and improve the transmission reliability [2, 13]. The alternatives of the power system interconnections are shown in fig.1-3 [13].

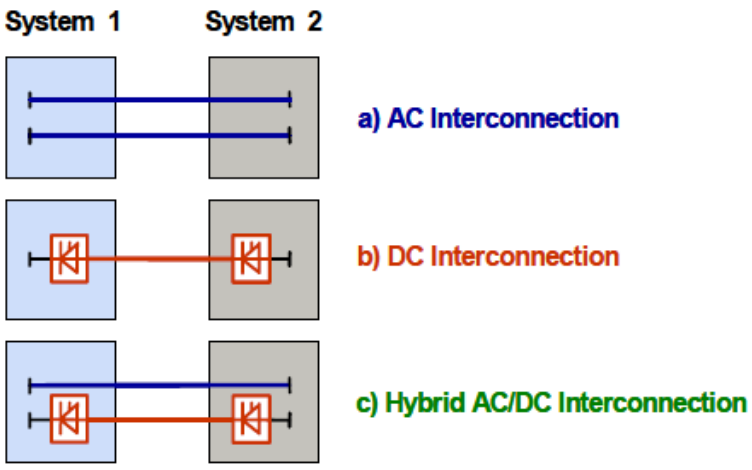

Figure 1-3 Alternatives of the power system interconnections[13]

A decade since 2003 Northeast Blackout, through the electric power industry has undergone great improvements to increase the power grid security and reduction in the risk of failure, HVAC systems still remain vulnerable to large blackouts [15].

After the 2003 Northeast Blackout the North American Electric Reliability Council in its technical report suggested using HVDC transmission systems to improve a power networks' reliability [5]. The use of HVDC interconnections together with HVAC feeders can prevent the propagation of disturbance passing through the network. Such cascades like several of the recent major blackouts could have been avoided if power was delivered via HVDC transmission technology [16]. Fast control of active and reactive power gives HVDC systems advantages that can improve power system dynamic performance under voltage disturbance. Together with power control, the use of HVDC interconnections can increase power grid stability and flexibility [3, 16-19].

As part of the South China power interconnected system, a HVDC interconnection was integrated into the network and operated in parallel with an AC interconnection as shown in fig.1-4 [13]. As shown, with only AC interconnection, the AC systems suffered severe power oscillations after AC system faults. The large power systems became unstable due to fault contingencies and lead to severe outages [13]. With a HVDC interconnection in constant power mode, after fault occurred, the oscillations were damped effectively and potential severe power oscillations were prevented [13].

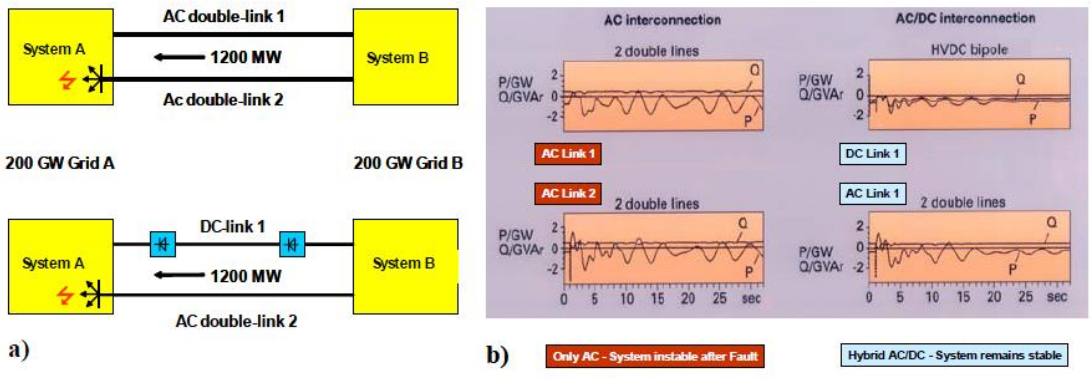

Figure 1-4 Comparison of System stability with AC interconnections and Hybrid AC/DC interconnections (a) System configurations (b) Dynamic results

HVDC transmission systems are playing a more and more important role in modern power systems and more are being constructed all over the world. There are deep interactions between AC and DC transmission systems [20]. Therefore the investigation of cascading failure and blackout should not only consider the HVAC interconnections but also the HVDC links in integrated HVAC/HVDC networks.

Recent major blackouts have demonstrated that the mal-trips of the protective relays contributed to the spreading of the cascading failure and blackouts. Distance relays are the most widely used protection in modern power systems to protect transmission lines [21]. The distance relay compares the apparent impedance with the tripping impedance characteristic to determine fault. If the apparent impedance is within the trip characteristic, the distance relay trips. During power system dynamic conditions, the changing voltages and currents may cause the apparent impedances as seen by distance relays enter the protection zones and therefore cause unwanted tripping.

During 2003 Northeast America blackout, one of the key 345kV lines, Sammis-Star, was tripped by the unwanted distance relay operation leading to widespread cascading in Ohio and beyond [4]. The apparent impedance seen by distance protection during the event is shown in fig.1-5 [7]. The apparent impedance moved from normal steady operation point into the protection zone due to cascading outage and caused the unwanted trip of distance relay.

Figure 1-5 Sammis-Star 345 kV line trip [7]

During normal operation the apparent impedance is outside of the trip characteristic whereas during a fault condition it enters the characteristic [22]. Zone 3 protection provides remote back-up protection which covers a large area of the protected feeders. The apparent impedance seen by distance relay during fault moves from the load area into the protection zones causing the relay to trip. The apparent impedance seen by a relay during a power swing may move from the load area into the protection zone and cause unwanted relay tripping as shown in fig.1-6 [23, 24].

During the cascading failure leading to blackout, the unwanted distance relay operations accelerated the cascading outages. Therefore, it is necessary to consider the distance relay operations during cascading outages. Furthermore, with the increasing use of HVDC systems all over the world, the distance relay's behaviour when the protected feeders containing both HVAC and HVDC interconnections needs to be investigated.

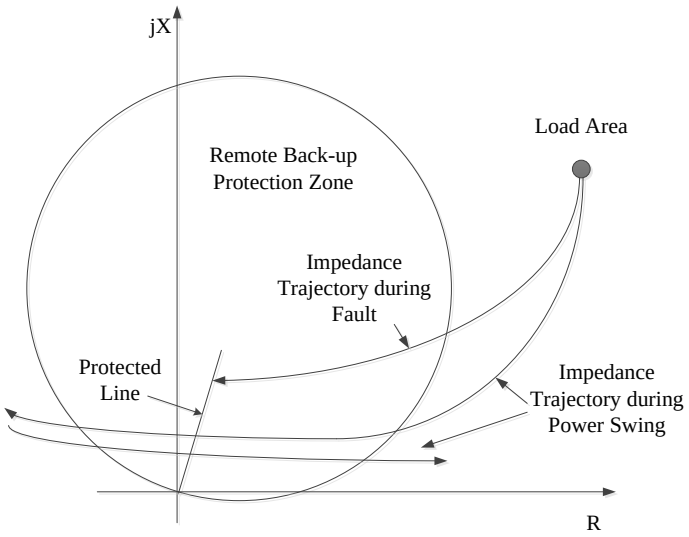

Figure 1-6 Impedance seen by distance relay during fault and power swing[23, 24]

1.3 Research Objectives

This project is to investigate the impact of power system performance on protection relays and the consequences of introducing HVDC interconnections into HVAC networks. The research objectives are summarized as follows:

- To study the HVDC operation during the fault conditions and power swing conditions and investigate the mechanisms by which a HVDC link acts as a 'firewall' against the voltage outages and prevents the cascading outage developing throughout the HVAC networks.
- To study the response of distance relay protection during the faults and voltage collapses in HVAC/HVDC and HVAC networks. Recent blackouts showed that the distance relay remote back-up protection mal-operation during power outages contributed cascading effect throughout a network.
- To investigate the impact of HVDC interconnections in HVAC/HVDC networks on distance relay performance during fault conditions.
- To investigate how the presence of a HVDC interconnection impacts on distance relay performance during a power swing.

1.4 Outline of the thesis

Chapter 2 reviews recent wide area blackouts. The distance relays operations during the blackouts are of particular interest as is the impact of HVDC interconnections in HVAC/HVDC networks.

Chapter 3 provides a literature review of the HVDC technologies. It reviews the development of HVDC technologies, the basic control of HVDC, the advantages and disadvantages of the HVDC interconnections.

Chapter 4 gives an overview of the operation of distance relays. The chapter reviews distance relay basic principles, the different types of fault impedance calculations and the distance relay's Mho characteristic. This chapter also reviews the block-average comparator and signals processing technologies. Furthermore, this chapter reviews the behaviour of a distance relay during a power swing.

Chapter 5 presents simulation studies of a HVDC link's response to fault conditions. The simulation work was carried out in MATLAB/SIMULINK.

Chapter 6 presents simulation studies of a distance relay's behaviour, together with that of a signal processing distance relay to test in a simple ac system.

Chapter 7 presents the results of simulation studies into distance relay operation when the protected system includes a HVDC link. The investigations were carried out in a basic HVAC power system, connected to an infinite bus and included both HVAC and HVDC interconnections. A comparison with a HVAC system was also simulated. The investigation was carried out by applying a selection of faults at different locations of the feeders and studying the distance relay's operation.

Chapter 8 presents the results of studies into the HVDC impacts on distance relay performance during power swings. The investigation was carried on a power system that included HVAC and HVDC interconnections to a load with local generation. The behaviour of a system with two main generators and two loads was investigated.

Chapter 9 summarizes the key findings from the research and the major contributions of the work. Potential future work is given in this chapter.

Chapter 2

Overview of Recent Major Blackouts

2.1 2003 Northeast America Blackout

Based on [5, 7, 12], on 14th August, the power system was running stable prior to the start of the blackout. Electricity demand was high due to the continual increasing using of air-conditioners. Such large air-conditioning loads lead to high reactive power demand in the Indiana and Ohio areas and were known to cause control and protection problems [4]. The investigators determined that the power system in Northeaster Ohio was near to voltage collapse due to low voltage and low reactive power margins [5].

At 12:08EDT, several 345, 230 and 138kV transmission lines experienced a series of outages. At 13:31, a major source of reactive power support unit, Eastlake Unit 5, was tripped due to over-excitation problem. Loss of the Eastlake Unit 5 was the first major event during the blackout [1, 4].

At 14:02, the Stuart-Atlanta 345kV line was tripped due to tree contact [7, 9, 12]. The report of the line failure was not communicated until 15:29 when the operators updated the status of the line being out of service. The Stuart-Atlanta 345kV line failure did not contribute to or lead to the blackout but caused co-operation failures between operators.

From 15:05, within one hour, three 345kV transmission lines tripped due to independent tree contacts [4-7, 9]. Fig.2-1 gives locations of the three tripped lines [5].

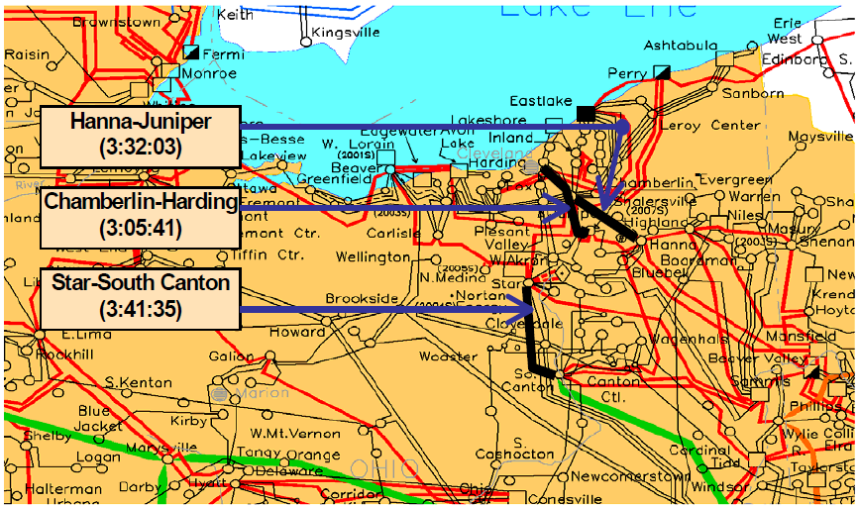

Figure 2-1 Location of three tripped lines [5]

Fig.2-2 gives 345kV line flows [7]. At 15:05, the Chamberlin-Harding 345kV line tripped. The line was loaded at 43.5% of its normal ratings [5, 25]. At 15:32, the Hanna-Juniper 345kV line tripped with 88% of its summer emergency rating [4]. Loss of the Hanna-Juniper line led to a deficit of over 1,200 MVA of power flow to Cleveland, which led to Star-Juniper having to carry the bulk of the power [7]. At 15:41 the Star-Canton 345kV line tripped with 93% of its normal rating [6].

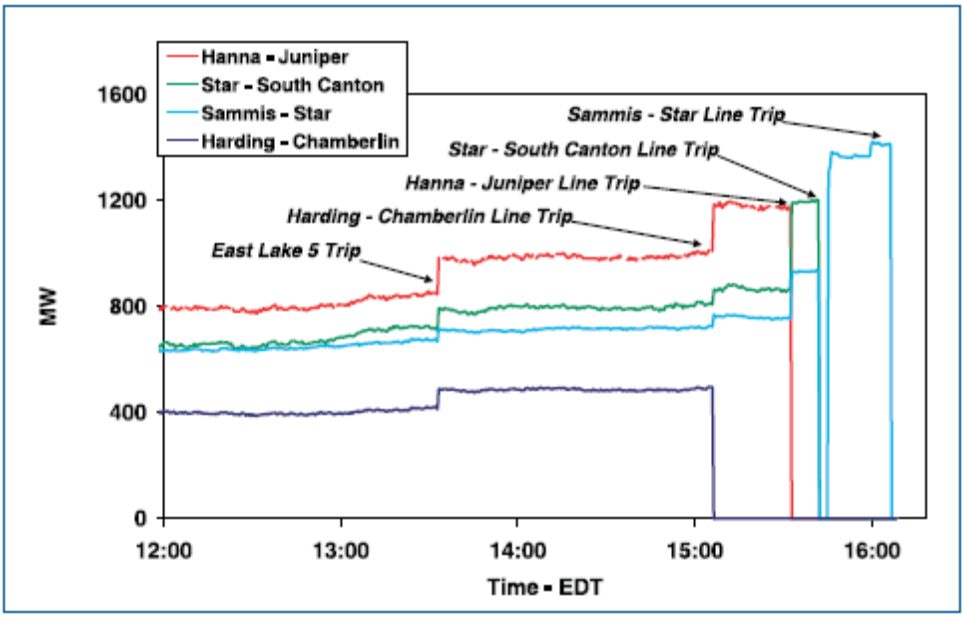

Figure 2-2 345-kV Line Flows [7]

Due to Energy Management System software failure at the control centres, corrective actions were not taken [4, 6]. The loss of these three lines pushed power to several 138kV lines and making these lines overloaded. The voltage began to degrade.

At 16:05, the Sammis-Star 345kV line was tripped by the Zone 3 distance relay as it detected high current and voltage dip consistent with a distance fault [4-7, 9]. Fig.2-3 shows the relay's operation characteristic and the seen impedance causing the Sammis-Star line to be tripped [7]. Fig.2-4 gives a time chart with the trip of the Sammis-Star line [7]. There was no fault or power swing but the system presented a low apparent impedance for the relay to trip the line. The relay could not discriminate a remote fault or high line-load condition. In addition, Sammis-Star carried ten times as much reactive power than its normal load. Loss of that line was a critical event leading to widespread cascading in Ohio [4, 6]. Soon after the Sammis-Star 345kV line tripped, many other 345kV lines which had remained in service were tripped. Losing these lines caused frequency in eastern interconnection increased by 0.02Hz [7, 12]. After the loss of the Sammis-Star line, the power network was temporarily stable.

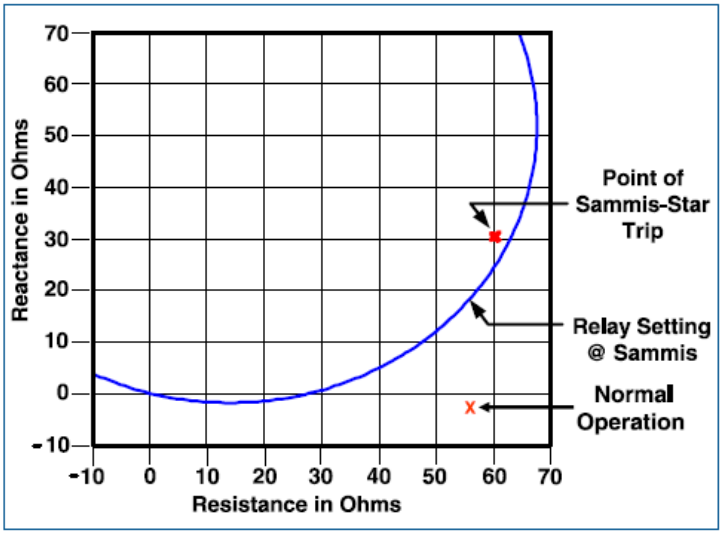

Figure 2-3 Sammis-Star 345-kV Relay Operation [7]

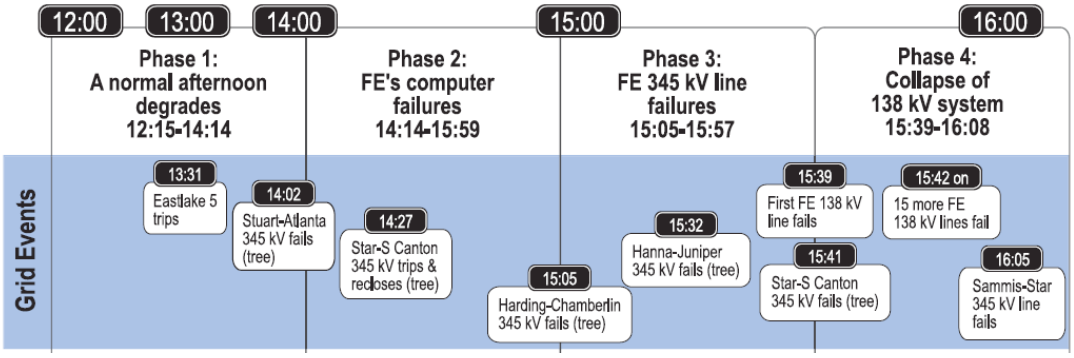

Figure 2-4 Time chart till 16:05 [7]

Soon after the Sammis-Star line tripped, four 48 MW generating units tripped off-line [7]. After the loss of the Sammis-Star at 16:09, the main energy path East Lima-Fostoria Central that connects south and west to Cleveland and Toledo tripped. Loss of this path caused a significant power swing of about 500-700 MW from Pennsylvania and New York through Ontario to Michigan [5, 7]. Fig.2-5shows the power flow along the New York interface [7].

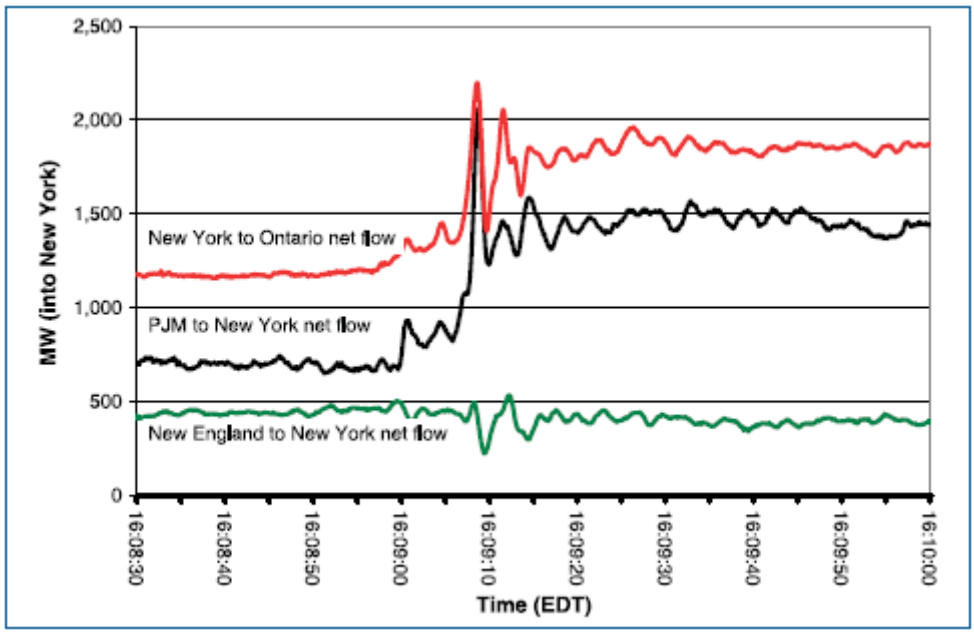

Figure 2-5 Power flow metered at New York interface [7]

The full cascade started at16:10. After 16:10, more 345kV transmission lines and generating units tripped. Between 16:10:36 and 16:10:37 three 345kV transmission lines tripped and several generating units about 20 generators loaded at 2,174 MW tipped off-line [5, 7, 12]. Between 16:10:37 and 38, the Hampton-Pontiac and Thetford-Jewell 345kV lines tripped. Those two lines were the only lines connecting

Detroit to the grid. These trips separated the eastern high voltage transmission system from western Michigan [5]. Fig.2-6 describes some tripped transmission lines due to Zone 3 relay operation around Ohio and Michigan area from 16:05 to 16:10 [7].

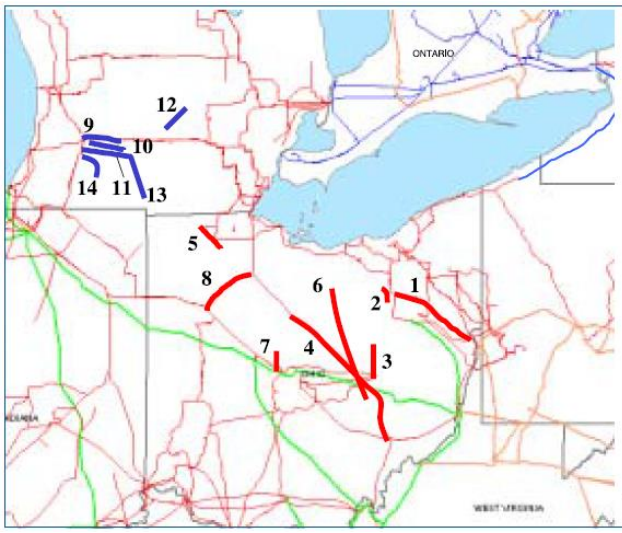

	Zone 3 Tripped Lines	State	Trip Time (EDT)
1	Sammis - Star (345 kV)	Ohio	16:05:57.504
2	Star (138/69 kV) Transformer # 6 Star - Dale (69kV)	Ohio	16:06:01
3	Ohio CTL - Wooster (138 kV)	Ohio	16:08:58
4	Galion - Ohio CTL - Muskingum (345 kV) @ Muskingum	Ohio	16:08:59.158
5	Richland - Wauseon - Midway (138 kV)	Ohio	16:09:00
6	Academia - Howard (138 kV) Philo - Howard (138 kV)	Ohio	16:09:05
7	Tangy - Kirby (138 kV) Tangy - Crissinger (138 kV)	Ohio	16:09:06
8	E. Lima - Fostoria (345 kV)	Ohio	16:09:06.311
9	Argenta - Battle Ck (345 kV)	Michigan	16:10:36.230
10	Argenta - Tompkins (345 kV) Battle Ck - Oneida	Michigan	16:10:36.310
11	Argenta - Verona (138 kV)	Michigan	16:10:37.550
12	Delhi - Island Road (138 kV)	Michigan	16:10:37.870
13	Verona - Batavia (138 kV)	Michigan	16:10:37.900
14	Argenta - Morrow (138 kV)	Michigan	16:10:38.350

Figure 2-6 Tripped transmission lines due to zone 3 relay operation [7]

Around 16:10:38, another three 345kV transmission lines tripped including Perry-Ashtabula line which was tripped by a zone 3 relay operation [5, 25]. The trip of this line was the point that the Northeast entered transient instability [7]. Loss of the line caused a large power swing that affected Ontario, Michigan, New York, and New England [7, 26]. The power swing caused a sudden increase in frequency from 60.0Hz to 60.7Hz at Lambton and 60.4Hz at Niagara [5, 7]. Unbalanced demands and generation led to heavy power flows moving north through the remaining tie lines which accelerated the power swing. Heavy power flows moved from Ontario into Michigan, New York into Ontario, New York into New England and PJM into New York [5, 7, 26].

As been described in [7], the power swing started at 16:10:38 because the loads of Cleveland, Toledo and Detroit were separated from Michigan and Ontario [7]. The power flow was forced to shift to meet the demands. The power flows from Ontario into Michigan increased from 1,000MW to around 3,700MW after the start of power swing. However, the flows reversed back from Michigan into Ontario by dropping from 3,700MW to around 2,100MW [7].

Between 16:10:39 and 16:10:42, several 345kV lines tripped resulting in the Toledo and Cleveland area becoming islanded from Detroit. The frequency around Detroit spiked to 61.7Hz then began to decay and the generators were in under-speed conditions [1, 5, 7, 12, 25, 26]. The Cleveland area was completely isolated after the Beaver-Davis Besse 345kV line tripped [7].

Pennsylvania was separated from New York due to Zone 1 relay operation on the 345kV lines, Homer City-Watercure and Homer City-Stolle Road. There was a power swing into New York and PJM between 16:10:39 to 16:10:44 [5, 7, 12, 25, 26]. These two 345-kV tie lines are long and thus have a high line impedance. High line impedance enlarges relay Zone 1 circle and makes it more likely to be tripped by a power swing [5, 7]. During the power swing, distance relays on these lines responded to the overloads and depressed voltage conditions rather than true faults [25].

Soon after Pennsylvania separated from New York, the Eastern Interconnection was divided into two major parts: to the north and east of the separation containing New York City, northern New Jersey, New York state, New England, the Canadian Maritimes provinces, eastern Michigan, the majority of Ontario, and the Quebec system [5, 7, 12, 25]. The rest of the Eastern Interconnection was not seriously affected by the blackout. After the separation of the Eastern Interconnection, the entire northeastern suffered large oscillations.

The 2003 event became a race between the power surges and the protective relays [5]. The transmission lines that were tripped by the relays' operation due to the power surge accelerated blackout. Longer lines that were having larger apparent impedance tripping zones made the relay prone to tripped during a power swing.

The Quebec system however survived during the event. The Quebec system was connected to the Eastern Interconnection via a High-Voltage Direct Current (HVDC) link instead of AC transmission line [5, 7, 12]. The DC link acted as a 'firewall' against cascading events [1]. Moreover, the HVDC links connected to New York and New England helped stabilize these two islands and support the demand in these areas [1].

2.2 Protection Relay Operation During Recent Blackouts

Evidence has shown that the unwanted zone 3 relay operations contributed to the cascading outage that led to other blackouts like the 2003 Blackout.

The U.S.-Canada Power System Outage Task Force Report [7] on the 2003 Blackout pointed out that some key 345-kV transmission lines that were tripped by zone 3 impedance relays had accelerated the spread of the cascade outage. Horowitz and Phadke [27] argued that the unwanted operation of zone 3 has been identified as the most obvious protective relay characteristic since the 2003 North America Blackout. The same option is also given by Apostolov [11]. He added that combining the protection device with a wide area automatic control could offer the solution to prevent, slow down or reduce the impact of a large-scale disturbance. Suwannakarn and Hoonchareon [28] described the false tripping of the zone 3 activation of the distance relay as one of the main reasons for the 2003 Blackout. They also pointed out that load increase and voltage instability was primarily responsible for such a mis-operation. Richards and Tholomier [29] indicates that the relay settings for generators, transmission lines and under-frequency load-shedding in the Northeast America area may not be sufficient to reduce the effects of cascade. Hodaei et al [30] described the 2003 America Blackout as the most well known incident where zone 3 relay unwanted trips occurred giving rise to the collapse. However, distance relay mis-operation contributing to cascading outage was not only seen in the 2003 North America Blackout but also could be found in many other major blackouts [31-34].

2.2.1 1965 Northeast America Blackout[31, 34]

On 9th November 1965, the most severe power system blackout up to that time affected over 80,000 square miles including the cities of New York, Boston and Toronto and about 30 million people. The event was triggered by the operation of impedance relays due to overload. Five 230kV transmission lines connecting the Beck and Canadian Toronto area were tripped by distance relays sequentially due to heavy load conditions at the start of the cascade trips. Tripping of the lines led to left tie lines suffering from a massive power shortage. Increased power from the U.S. to Canada caused the 230kV tie lines to be tripped by overcurrent relays. After four

seconds the system separated into 5 islands. The cause of the event was identified as mis-operation of distance relays responding to heavy load condition rather than a fault.

2.2.2 1996 North Western America Blackout [35-38]

The July 2nd 1996 outage in the Western Electric Coordinating Council (WECC) system was another significant example of zone 3 mis-operation giving rise to system collapse. The outage resulted in an 11,743 MW load and 9,909 MW generation loss. The event was initiated by a 345kV transmission line which connected the Jim Bridger and Kinport fault. Shortly after the line tripped, the parallel 345kV transmission line connecting Jim Bridger and Goshen was tripped by the relay trip. These two lines were the connection between the 2,000 MW Jim Bridger power plant and the Pacific Northwest load centres. About 20 seconds later, a key 230kV line between Western Montana and South Idaho was tripped by the zone 3 relay operation due to overloading and voltage depression. The loss of the line caused a power swing through Eastern Washington and Eastern Oregon and further cascading led to the separation of the power system.

2.2.3 2003 Sweden and Denmark Blackout [1, 4, 39-41]

On September 23, 2003, Sweden and Denmark suffered a serious power failure. Over 4 million people were affected and about 6,550 MW load was disconnected. The event was started by the loss of a 1,200 MW nuclear power plant. Loss of the power plant resulted in a voltage drop of around 5 kV. Following two busbar faults in a nuclear power station, the power grid lost its transmission capacity along the west coast. The system suffered power oscillations. Tap-changer transformers' operation dropped voltage on the 400kV grid to critical levels. During power oscillation, distance protection devices tripped due to low impedance criteria. Operation of distance protection devices contributed to the splitting. Finally the entire system collapsed. During the event, two HVDC links to Germany and Poland rated at 600 MW connected to the 400kV grid were out of service due to annual inspection. Recommendations were made after the event. One of which suggested

that the protection system needed to be developed to detect a voltage collapse situation.

2.2.4 2003 Italy Blackout [42-46]

On September 28, 2003, Italy suffered the largest blackout in history. A cascade tripping of transmission lines separated Italy from the Europe grid. For economic reasons, Italy imported a large amount of power from European countries. The Italian system was connected to the European grid through six 400kV lines and nine 220kV lines as shown in fig.2-7, during the event, these lines were lost [45].

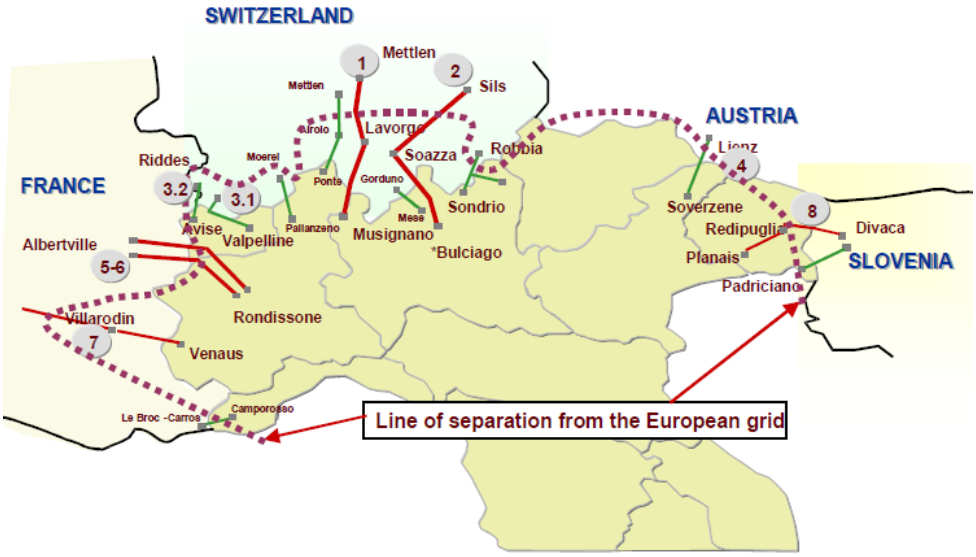

Figure 2-7 Line of separation from Europe [45]

On Sunday September 28, 2003, the Italian load was 27.7 GW and total imported power was 3,500 MW. Several power stations in Italy were off-line due to economic reasons.

The first event occurred in the Swiss grid. A 380-kV transmission line was tripped due to tree contact. Several seconds later the protection device tripped the Airo 10-Mettlen 220kV line because it was overloaded. The tripping of the lines left the 220kV interconnection lines between Switzerland and Italy overloaded and hence they tripped. Loss of these lines led to frequency and voltage decrease. Due to the overload and the lower voltage conditions, local distance relays tripped several transmission lines around Italy and the surrounding countries. This led to the

complete separation of Italy from the European grid. During the event, the HVDC link connecting Italy and Greece was tripped after the collapse of the Italian Grid.

2.2.5 2006 European Blackout [19, 47-51]

On 4th November 2006, the Union for the Co-ordination of Transmission of Electricity (UCTE) suffered the most severe disturbance in its history. About 15 million people in more than 10 countries were affected and a 14.5 GW load was interrupted. The event started from a scheduled disconnection of the double-circuit 380kV Conneforde-Diele line. After switching off the line, the TSO network received several warning messages about high power flows.

At 21:41, the Labdebergen-Wehrendorf line between the E.ON Netz and the RWE TSOs approached near its safe limit of 1795 A. The protection settings on the different sides of the line were different. At 22:00 the lines towards the west was over loaded. At 22:06, the current on Landesbergen-Wehrendorf increased to 1900A and exceeded its safety limit. At 22:10, the protection relay tripped the Landesbergen-Wehrendorf line due to overload rather than a true fault. Another two lines were tripped within five seconds and caused a cascading effect towards the south. The out-of -step conditions led to the tripping of another thirty 400, 380 and 220 kV lines within one second. The UCTE grid was finally separated into three sub-grids with different frequencies, as shown in fig.2-8.

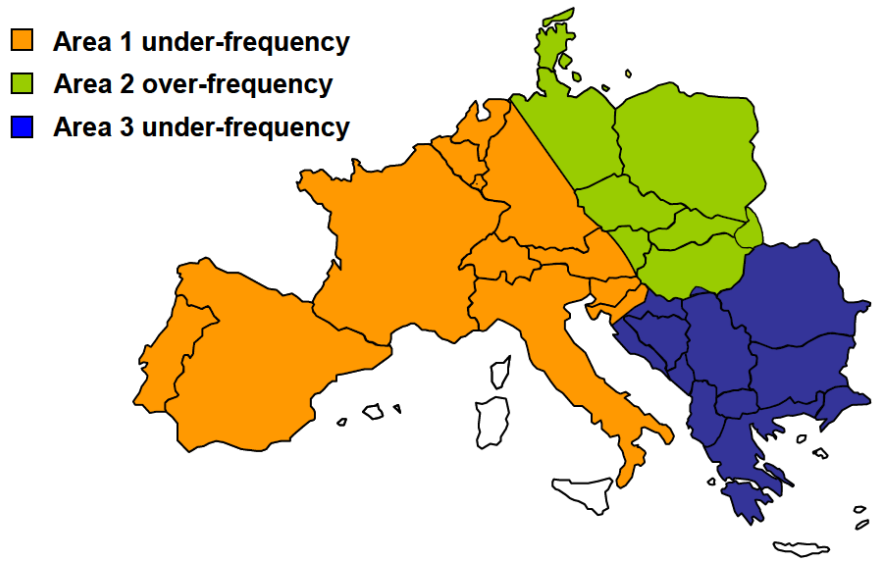

Figure 2-8 Separation of UCTE grid into 3 sub-grids

Area 1 and 3 suffered under-frequency conditions while area2 suffered over-frequency condition. The frequency in area 1 and 3 dropped to 49 Hz and 49.7 Hz respectively. The frequency in area 2 raised to 51.4 Hz.

It should be noted that the area1 and 3 remained asynchronously connected through the HVDC link between Italy and Greece during the whole event. The power exchange on the HVDC link between Italy and Greece was 312 MW towards Greece. Four TSOs of North-East area and Nordel power systems were connected by submarine DC cables transferring total 2,200 MW power from UCTE to Nordel area. These DC cables were not disturbed when the UCTE system split and the available capacities of all these cables were almost fully used. The DC connections to Nordel systems helped to export the surplus of capacity from the UCTE over frequency area without disturbed Nordel system at all.

2.2.62010 Namibian and Zambian eventual blackout

On 3rd June 2010, the HVDC interconnection project was tested for the first time to transmit power from Namibia to Zambia [16, 52]. The project was a 300MW, 345kV monopole HVDC scheme that connects the Namibian and Zambian power systems through a 952 km overhead line [52]. There was a sudden trip of a 220kV line in Nampower's 220kV bus zone because of an overload protection operation. Loss of the line led to an island condition and a large frequency dip in the Namibian power grid [16]. On emergency control at both converter stations, the Namibian grid was restored to stability about 1 second after the outage [16]. On 6th June 2010, a continuing test was carried on. When the power ramped up to about 30 MW on the HVDC link, a line in the Zambian grid was overloaded and tripped [16]. This again resulted in an island condition in the Zambian grid. The Zambezi converter station switched to voltage and frequency stabilization control mode. Within 500ms, the voltage and frequency resumed to pre-outage level [16]. An eventual blackout was avoided.

2.3 Chapter Summary

This chapter reviewed recent major blackouts over the world. These recent blackouts demonstrated that protection devices play an important role during the event. The unwanted trip of protective relays when there was a voltage disturbance quickly contributed to the cascading outage. The setting of distance relays should ensure that the relays will not operate when no fault occurs. Zone 3 protection is applied for backup protection and has wide coverage. When a power swing occurs, a lower voltage level combines with higher load current results in the apparent impedance entered the Zone 3 protection characteristic, leading to tripping and accelerating the cascading outage.

The HVDC systems acted as a 'firewall' against the system collapse can be found in 2003 Northeast America blackout. During 2006 Europe blackout, the DC connections kept in service without disturbing the Nordel system operations. In 2010, the HVDC interconnection between Namibian and Zambian blocked the fault current and prevented the potential blackout.

Chapter 3

Overview of High-Voltage Direct Current (HVDC) Transmission System

The HVDC transmission system, High Voltage Direct Current transmission system has been widely used to transmit long distance bulk power and connect two separate AC systems since it was first introduced in 1950s[53].

3.1 History Background of HVDC

Work on HVDC systems goes back to Thomas Alva Edison who established his research laboratory in 1876 at Menlo Park, New Jersey, USA [54]. It has been widely documented that the first commercial electricity generator designed by Thomas Alva Edison, was Direct Current (DC) electrical power as well as the first electricity transmission system was also the direct current system [53]. However, early DC power was at a low voltage and could not be transmitted over a long distance. Compared to DC transmission technologies, Alternating Current (AC) technologies offered better efficiency which led to the rise of Alternating Current (AC) technologies [54]. Though DC transmission systems lost out in the competition with AC transmission systems, there were still some attempts to improve the DC system. Engineers built a high-voltage transmission system with series connected dc generators and motors but this was unsuccessful commercially [54].

The first attempts of transferring DC voltage to higher or lower levels relied on mechanical methods, which were not practical [55]. HVDC technologies were limited by materials, devices and construction issues. Engineers still carried on. Technical papers were also be found on HVDC technologies including the development of static converter theory for transferring ac to dc and vice versa, economy of dc transmission systems and converter systems [55].

With the fast development of electronic devices, in the 1950s, the world's first commercial HVDC line was installed successfully between Gotland and the Swedish mainland [55-59]. The HVDC transmission system was a 98kM long DC cable connection rating at 20 MW, 200 A and 100kV [54]. After the success of the Gotland and Swedish HVDC project, work had been continued on developing thyristor valves. Some earlier HVDC projects (1960-1970s) were spreading over the world, some of which are listed below [57, 59, 60]:

- 1961 Cross Channel HVDC link between France and England. The system was operated at 100kV and 160 MW.
- 1964 Konti-Scan HVDC link between Denmark and Sweden, which was a 250kV and 250 MW cable link.
- 1964 Voltogard-Donbass HVDC link in Russia. The scheme was a +/-400kV, 750 MW long distance transmission project.
- 1965 Japan HVDC interconnection with 125kV and a capacity of 300 MW. The HVDC link connected two areas with different frequencies: 50Hz and 60Hz.
- 1970 Pacific DC Intertie in United States. The scheme was a 1,362 km long distance overhead line connecting hydro-electric power stations in Oregon and the load centre in Los Angeles that operated at 500kV and 3,100 MW. The project was also the world's first transmission system controlled by a distributed computer system.
- 1971 Manitoba Hydro scheme in northern Canada, which was the first bipole scheme.
- 1972 Eel River scheme in Canada which was the first HVDC project using exclusively thyristors in converter stations.

According to Carlsson [61], since 1990, HVDC technology development can be characterized as follows. The traditional 'classical' HVDC technology still dominates but with improved equipment and sub-systems (eg, valves, ac-filters, dc-filters, etc); the new concept of Capacitor Commutated Converter (CCC), which significantly improves the performance of the traditional converter; using of Voltage Source Converter (VSC) with Insulated Gate Bipolar Transistors (IGBTs) in place of thyristors. According to [53], some of the important milestones in the earlier development of HVDC transmission technology are given below:

- Hewitt's mercury-vapour rectifier, which appeared in 1901.
- Experiments with thyratrons in America and mercury arc valves in Europe before 1940.

- First commercial HVDC transmission, Gotland 1 in Sweden in 1954.
- First solid state semiconductor valves in 1970.
- First microcomputer based control equipment for HVDC in 1979.
- Highest DC transmission voltage (+/- 600kV) in Brazil 1984.
- First active DC filters for outstanding filtering performance in 1994.
- First Capacitor Commutated Converter (CCC) in Argentina-Brazil interconnection 1998
- First Voltage Source Converter for transmission in Gotland 1999.

The rapid increase in voltage and capacity of the modern power system drew attentions to HVDC technology. With the rapid development of power electronics, there are growing numbers of HVDC projects over the world. Fig. 3-1 [55] shows the power that transmitted via HVDC systems in the world from 1950 to 2010.

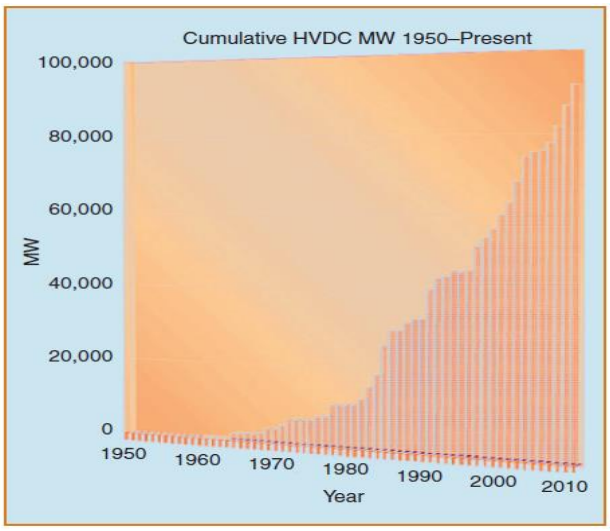

Figure 3-1 Power transmitted via HVDC from 1950 to 2010 [55]

As can be seen in the fig.3-1, there was a significant increase in the power that has been transmitted via HVDC since 1990. Some research results have shown that 800kV is a reliable voltage, for which suitable equipment can be made [59]. The world's first +/- 800kV HVDC project: Yunnan-Guangdong HVDC transmission system was commissioned in 2010 [62]. The project is a 1,418km long distance

HVDC link with a rated capacity of 5000 MW. Fig.3-2 gives the overview of the project.

Figure 3-2The world's first +/-800-kV HVDC system in South of China

The growth in using offshore wind farms and other renewable power stations, including solar power and hydro power, that are located far from load centres gives the opportunity to use HVDC to meet these demands. Fig.3-3 [63] shows the future possible use of HVDC links interconnect large renewable energy resources in Europe. If all renewable energy would be used where they are best available around Europe, wind power from western coasts, solar energy would mainly come from the Mediterranean and hydro power from Scandinavia. Using these renewable energies gives significant benefit in Environments and reduction of CO_2.

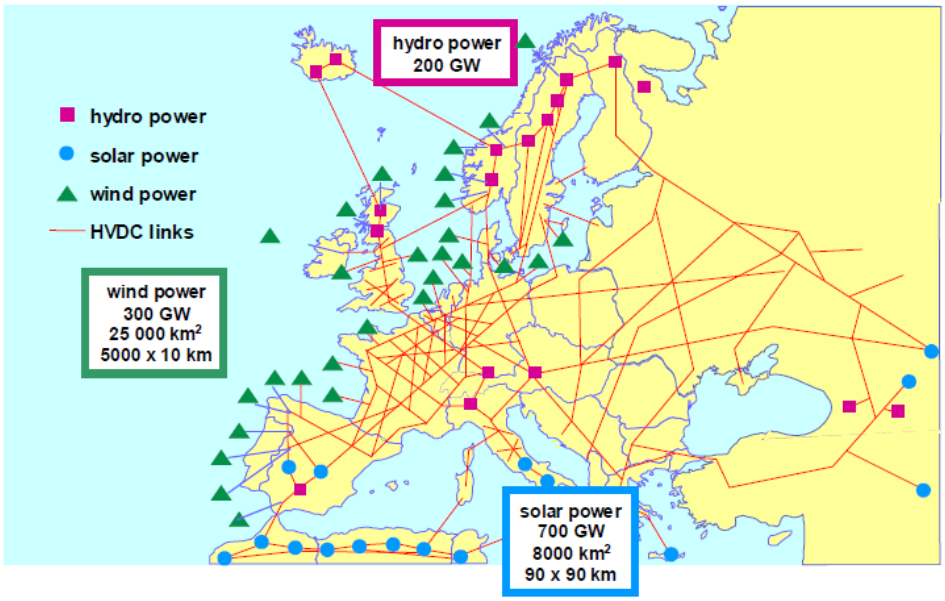

Figure 3-3 Future HVDC integrates renewable energy resource in Europe

3.2 HVDC System

The High Voltage Direct Current transmission system (HVDC) has now been widely used to transmit long distance bulk power and connect separate AC systems.

ABB defines HVDC as follows [64]:

"In a HVDC system, electricity is taken from an AC power network, converted to DC in a converter station and transmitted to the receiving point by a transmission line or cable. It is then converted back to AC in another converter station and injected into the receiving AC network. HVDC enables the power flow to be controlled rapidly and accurately, and improves the performance, efficiency and economy of the connected AC networks."

Siemens presents HVDC technology as follows [65]:

"HVDC (High Voltage Direct Current) transmission systems connect two separate high voltage AC Systems via a DC link. The basic principle of the operation of an HVDC system is based on the conversion of AC to DC and vice-versa by means of converter valves comprising power thyristors, which are at the heart of a converter station."

Fig.3-4 shows the basic HVDC system. The HVDC scheme connects two AC systems. At the sending end, AC power is fed into a converter operating as a rectifier following the power transformer. The output of the rectifier is DC power which will be transmitted through a conducting medium, an overhead line, cable or a short distance busbar, to a second converter which is operated as an inverter [66]. The inverter transfers DC power to AC power and sends it to the AC system through the power transformer at the receiving end.

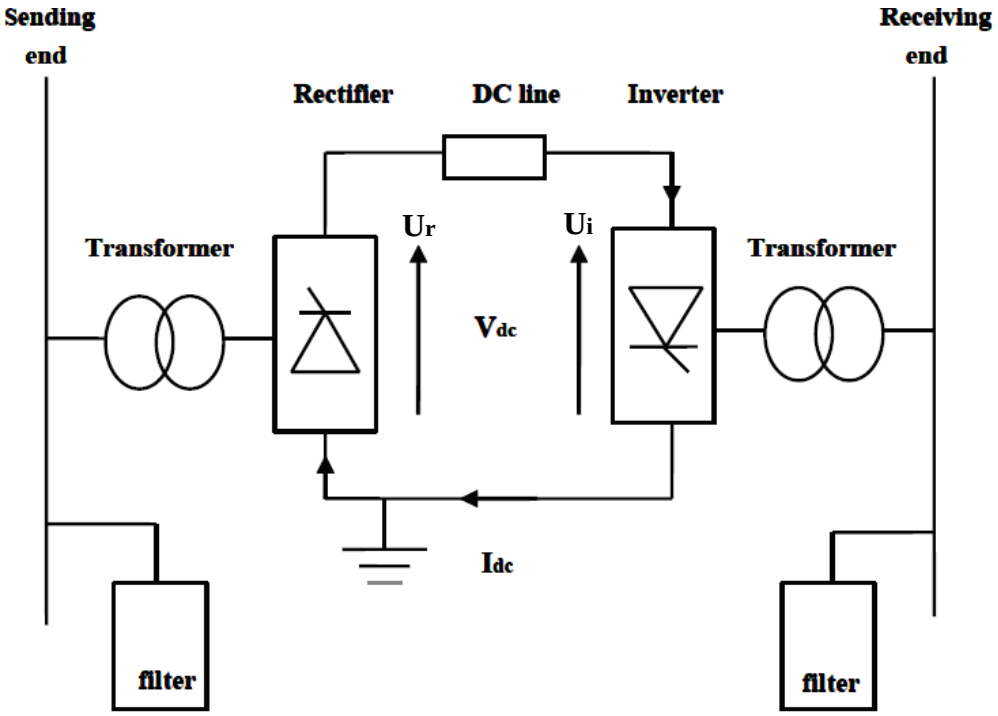

Figure 3-4The basic HVDC system

In fig.3-4, the dc current is defied by I_{dc} which can be calculated as:

$$I_{dc} = \frac{U_r - U_i}{R} \tag{3.1}$$

where:

I_{dc} is the dc current along DC transmission line;

U_r is the voltage at the rectifier;

U_i is the voltage at the inverter;

R is the resistance along the transmission line.

The power transmitted through HVDC system can be calculated as:

$$P = V_d \times I_d \tag{3.2}$$

Where:

V_d is the dc voltage of the DC transmission line;

I_d is the dc current along DC transmission line.

The converter station could be used as either a rectifier or an inverter. When converting AC to DC, the converter is called a rectifier. When converting DC to AC, the converter is called an inverter.

The power transmission direction could be bidirectional. When $U_r > U_i$, the power is transmitted from the rectifier side to the inverter side, while when $U_r < U_i$, the power transmission direction is in the other direction.

3.2.1 Components of an HVDC system

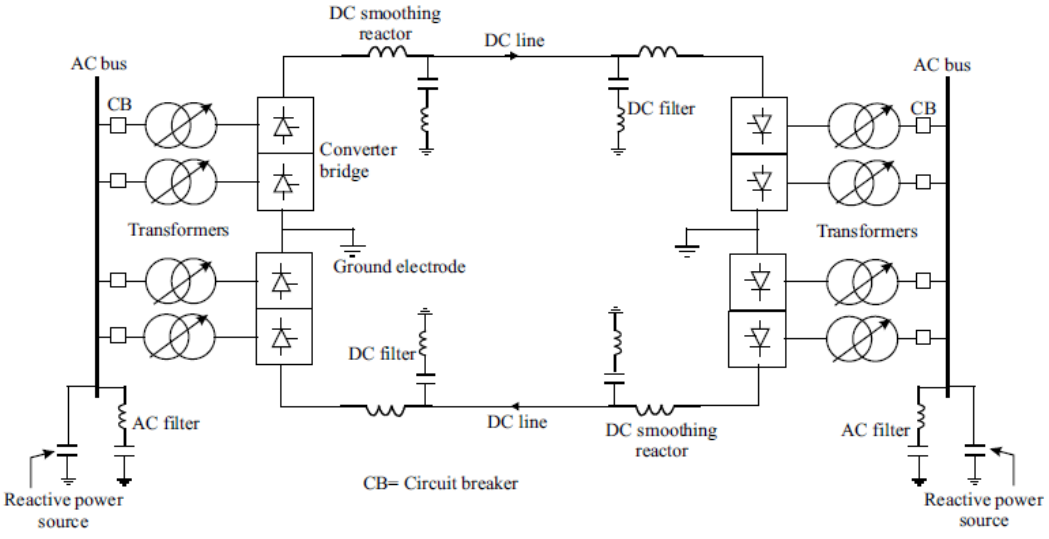

Figure 3-5 Classic bipolar HVDC system [58]

Fig.3-5 presents a classic bipolar HVDC system, which consists of ac filters, smoothing rectors, converters, converter transformers, dc filters and dc lines [67].

3.2.1.1 Converters

The converter is the most important component in a HVDC transmission system. It performs the conversion from ac to dc (rectifier) and from dc to ac (inverter) [67]. The converter is connected to ac system by converter transformer including tap changers.

The classic HVDC converter is current source converter (CSC) [67]. Under normal operation, the dc current is kept constant. Power flow is controlled by dc voltage. The converter consists of thyristor valve bridges and a converter transformer. Thyristor valve bridges consist of high-voltage valves connected in a 6-pulse or 12-pulse arrangement which known as Graetz bridge [68]. Fig.3-6 gives a basic 6-pulse valve bridge.

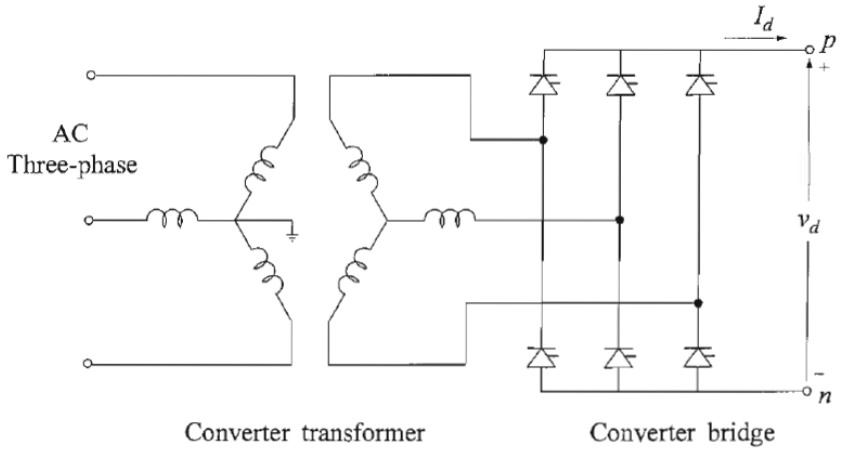

Figure 3-6 Basic 6-pulse valve bridge

3.2.1.2 Converter Transformer

The converter transformer, which always was a tap-changer transformer, connects ac system and converter. It transfers ac voltage on the rectifier terminal to a required level for the conversion process [69]. On the inverter terminal, it connects dc terminal and ac system. The converter transformer windings on ac system side are connected in star and on converter side are connected in delta for the converter. For

12-pulse converters, the 12 devices of the converter bridge are formed by a star and a delta connected transformers effectively providing six phase supply [67].

The converter transformer rating can be calculated as:

$$S = \sqrt{2} \times I_{dN} \times U \quad (3.3)$$

Where:

I_{dN} is nominal DC current;

U is transformer secondary ac voltage (on Rectifier of Inverter side)

3.2.1.3 Smoothing Reactors

Smoothing reactors are large inductors having an inductance up to 1.0 H [68, 70]. These large inductors are connected in series on the dc side of converter.

Siemens [71] lists the main functions of the smoothing reactors as bellow:

- Prevention of intermittent current
- Limitation of the DC fault currents
- Prevention of resonance in the DC circuit
- Reducing harmonic current including limitation of telephone interference

3.2.1.4 AC side filters

The converters generate harmonic voltages and currents on ac side. These harmonics cause overheating of capacitors and generators as well as radio interference[70]. Filters are installed to limit harmonics to an allowed level for connected networks. According to the Siemens Company [71], there are two main duties for ac side filters:

- To absorb harmonic currents generated by HVDC converter and thus to reduce the impact of the harmonic on the connected ac systems
- To supply reactive power for the converter station

During conversion procession, the converter absorbs a large amount of reactive power, normal 50%-60% of the transmitted active power [70]. Under transient

conditions, the consumption of reactive power can be even higher. The ac filters are installed next to converter stations.

3.2.1.5 DC filters

The HVDC converter not only generates harmonics to connected ac networks but also a ripple voltage on dc line. This ripple voltage may cause interference to telephone circuits near the dc line [67]. DC filters are used to reduce the ripple. Usually, there is no need to use dc filters for pure cable transmission or back-to-back scheme, but, filters are needed when overhead lines are used in the HVDC transmission system [67].

3.2.1.6 HVDC lines

The DC transmission lines may be either overhead lines or cables [70]. HVDC cables are normal used for underground or submarine transmission. Compared to ac transmission lines, dc lines have advantages both in number of conductors and space.

3.2.1.7 Circuit breakers

Circuit breakers are used for clearing transformer faults and taking dc line out of service on the ac side [68, 70]. DC line faults can be cleared rapidly by controlling the converter system. ABB announced that they have successfully designed and developed a hybrid DC breaker that can interrupt power flows within 5 milliseconds [72].

3.2.2 Basic Configurations of HVDC System

HVDC transmission system can be configured in many ways. The most common configurations are the back-to-back, bipolar and monopolar schemes [70].

3.2.2.1 Back-to-Back HVDC System

Back-to-back HVDC interconnection is the simplest HVDC configuration [73]. There no transmission lines or cables used in this scheme. These converters are connected directly next to each other. The two converter stations are located at the same site [67].

Back-to-Back scheme could be cheaper than the other schemes because it does not have long transmission lines [73]. The ac systems linked by the back-to-back HVDC system may have different frequencies, for example 50Hz and 60Hz [71]. Voltage levels are quite low normally between 50kV and 150kV. Fig.3-7 gives the overview of back-to-back HVDC scheme.

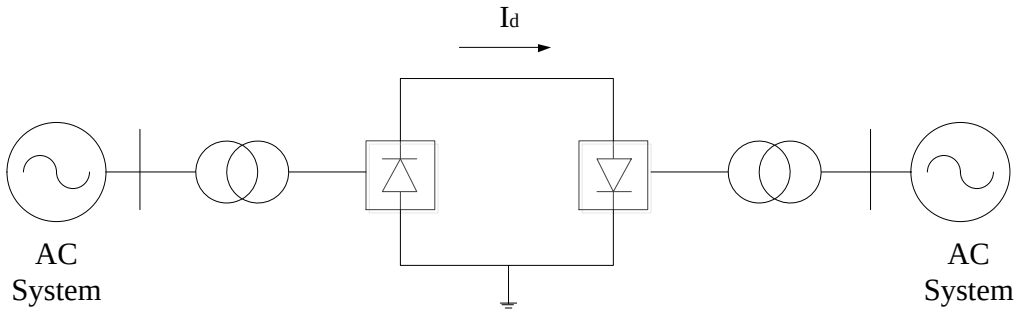

Figure 3-7 Back-to-back HVDC scheme [61]

3.2.2.2 Monopolar HVDC Scheme

The monopolar HVDC scheme consist two converters connected with a single conductor. Usually the ground or sea is used for return path [68, 70, 73]. The typical rating is up to 1500 MW [65]. The monopolar scheme is often used for very long distance particular very long sea cable transmissions. Fig.3-8 presents a classic monopolar HVDC scheme.

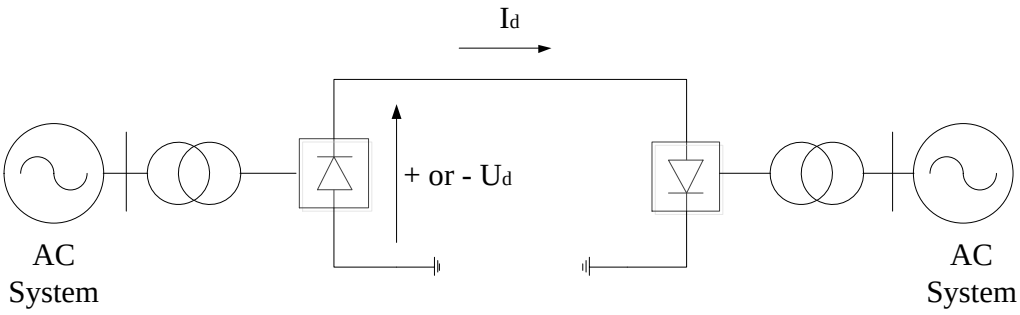

Figure 3-8 Monopolar HVDC scheme [61]

3.2.2.3 Bipolar HVDC Scheme

The bipolar HVDC link is the most widely used [70]. The bipolar scheme has two conductors, often overhead lines, one of which is positive and the other negative [68]. Each pole has two converters of equal rated voltage. The two terminals have equal

dc current under normal operation and have no ground current. Each terminal can be operated independently if both use a ground return, which contributes to reliability [67, 70]. The typical rating is up to 3000 MW [65]. Fig.3-9 shows a bipolar HVDC scheme.

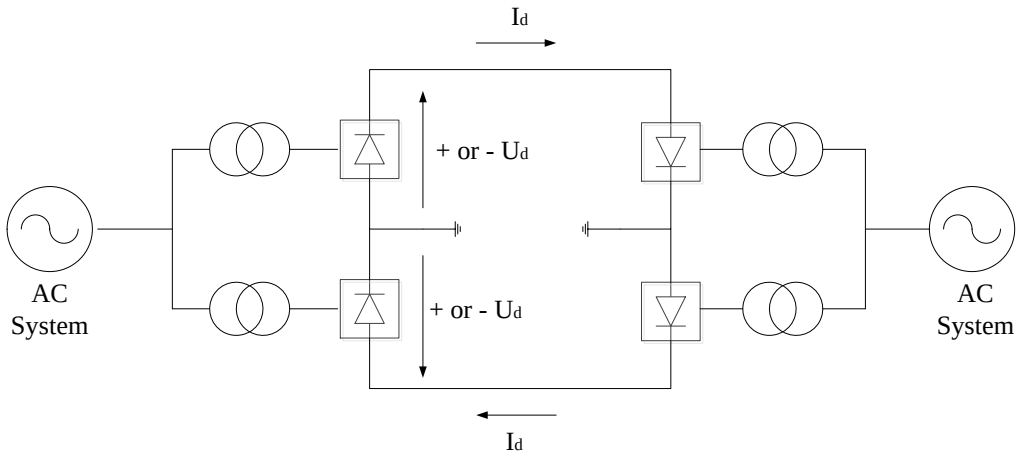

Figure 3-9 Bipolar HVDC scheme [61]

3.2.3 Converter Technologies

Converters are the most important part of the HVDC transmission system. They are the key to convert ac into dc and vice-versa. Bahrman [74] described there are two basic converter technologies used in modern HVDC transmission systems,:

- Line-commutated, current source converters (CSC)
- Self-commutated, voltage source converters (VSC)

3.2.3.1 Line-Commutated Current Source Converter, CSC

These converters, based on mercury valves or thyristor valves, are called line-commutated converters (LCCs) or current-source converters (CSCs) [75]. The basic block used in CSC converter is the three-phase, full wave bridge known as 6-pulse Graetz bridge which presented in fig.3-6[75-78]. Each bridge is formed using six thyristor valves. The Graetz Bridge can transmit power in either direction as it can be controlled in rectifier or inverter mode by changing the firing angle. If the firing angle is lower than 90°, the converter is operated as a rectifier and transmits ac power to dc power. If the firing angle is between 90° and 180°, the converter is operated as

an inverter and transmits dc power to ac power. The active power between two convertors is well controlled and gives some benefits including that voltage phase angle or frequency at the either end of the HVDC scheme does not need to be considered [78]. Fig.3-10 shows a typical CSC HVDC system.

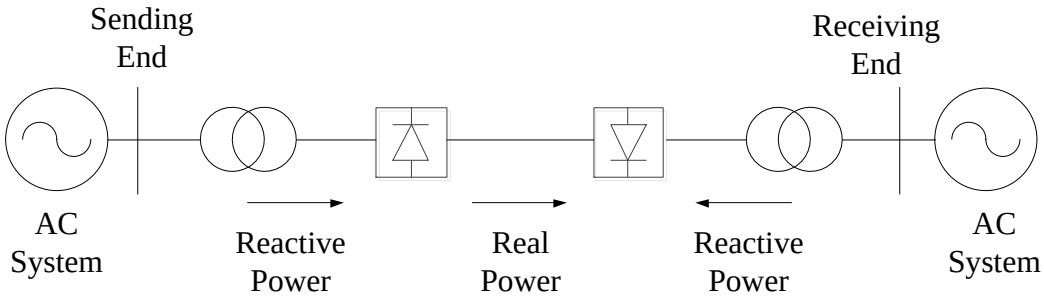

Figure 3-10 CSC HVDC transmission system

The most modern CSC HVDC transmission systems use 12-pulse converters, which use two 6-pulse valves connected in series [77]. Using of 12-pulse converters gives the immediate benefit of reducing harmonics, especially the 5th and 7th on AC side and the 6th on dc side.

The CSC converters need ac voltage to commutate and therefore CSC HVDC links can only operate to transfer power between two active AC systems [79]. The CSCs can only operate with the ac current lagging the voltage and hence they consume a large amount of reactive power during the conversion process, about 50%-60% of the transmitted power [75, 76, 78, 80]. The reactive power is provided by ac filters at the converter stations which results in increasing costs and the system occupies a large amount of space. CSC HVDC systems have common commutation failures, especially caused by inverter side ac system disturbance [75]. A number of serious commutation failures may force HVDC link to trip [75].

3.2.3.2 Self-Commutated Voltage Source Converter, VSC

The Voltage-source converter (VSC) utilizes self-commutating switches, such as gate turn off thyristors (GTOs) or insulated-gate bipolar transistors (IGBTs) [75]. GTOs and IGBTs can be turned on or off freely by gate signals. This is in contrast to the CSC converters, where the thyrstor valves can only be turned off by reversed voltages [75]. Diodes are needed to be connected in anti parallel mode because

IGBTs can only block voltage and conduct current in one direction [81]. The VSC converters are operated at high frequency, about 1 kHz to eliminate low order harmonics [78]. Fig.3-11 gives a diagram of VSC-HVDC transmission system.

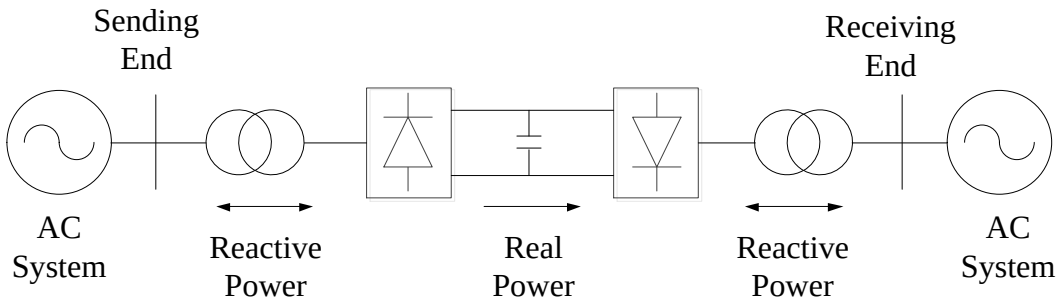

Figure 3-11 VSC-HVDC system

VSC converter technology can control both active and reactive power independently, and independent of dc voltage level [80]. This controllability gives VSC-HVDC transmission system flexibility to be placed anywhere in the connected AC systems. VSC-HVDC schemes give benefits in dynamic support of the ac voltage, improving voltage stability and increasing power transfer capability [76, 80]. Unlike conventional CSC HVDC systems, VSCs do not need reactive power support and can control reactive power to regulate the ac system voltage. The ability to control reactive power is the most significantly difference between a VSC-HVDC system and a CSC-HVDC system [78].

When connected to an ac system, the VSC-HVDC system is equivalent to a voltage source with an amplitude and phase angle determined by control system [81]. Compared with CSC-HVDC systems, VSCs can instantly reverse the active power. The VSC-HVDC systems have the potential to be connected to any kind of ac system with any number of links [75].

The main differences between CSC converter and VSC converter technologies are given in table.3-1 [82].

	CSC Converter	VSC Converter
	Acts as a constant voltage source;	Acts as a constant current source;

On AC Side	Capacitor required for energy storage; Large AC filters required for harmonic elimination; Reactive power supply necessary for power factor correction	Inductor needed for energy storage; Only a small AC filter needed for higher harmonics elimination; No reactive power supply needed
On DC Side	Acts as a constant current source; Inductor needed for energy storage; DC filters required; Provides inherent fault current limiting features;	Act as a constant voltage source; Capacitor needed for energy storage; No need for DC filtering; Problems with DC line faults since the capacitor discharges into the fault;
Switches	Line commutated or force commutated with a series capacitor; Switching at line frequency; Lower switching losses	Self-commutated; Switching at high frequency; Higher switching losses

Table 3-1 Main differences between CSCs and VSCs

3.3 Advantages of HVDC Systems

HVDC Transmission is widely used for bulk power transmission over long distance today. HVDC becomes financially viable from around 1000MW and 600km upward [83]. The HVDC project under constructing in China, which will transmit at 800kV and 1400km long, will set a new record in the world. Compared to 765kV AC line, HVDC Transmission will save about 36% in costs over a 30-year service life [83]. Germany is planning to construct 2100 km of HVDC lines to transmit wind power from its north coast line to the mainland with minimal loss [83].

ABB reviews the reason for using HVDC in two main groups [84], namely:

- HVDC is necessary and desirable from the technical point of view (i.e. controllability).
- HVDC results in a lower total investment (including lower losses) and is environmentally superior.

HVDC transmission systems offer the benefits of providing long-distance bulk power delivery, providing power transfer between asynchronous AC networks, limiting short circuit currents, economic transfers and benefits for the environment. HVDC transmission provides a complement to AC transmission networks.

3.3.1 High Level of Power Transmitted Compared to AC

Compared to AC transmission system, HVDC system can transmit more power per conductor per circuit [57].

For the same insulation, dc voltage V_d is equal to the peak value of the alternating voltage, which can be presented as:

$$V_d = \sqrt{2} \times V_a \tag{3.4}$$

Where:

V_a is the rms value of alternating voltage

For the same conductor size, without consideration of skin effect, the same current can be transmitted with both ac and dc can be presented as:

$$I_d = I_a \tag{3.5}$$

Where:

I_d is dc current while I_a is ac current

Thus the dc power P_d and ac power P_a is presented as:

$$P_d = V_d \times I_d \tag{3.6}$$

$$P_a = V_a \times I_a \times \cos \Phi \tag{3.7}$$

Where:

cosΦ is the power factor

Comparing equation 3.6 and 3.7 can get dc power over ac power as:

$$\frac{P_d}{P_a} = \frac{\sqrt{2}}{\cos \Phi} \tag{3.8}$$

From equation 3.8, it can be determined that the power ratio would be 1.414 @ p.f equals unity or 1.768 @ p.f equals 0.8.

From calculations above, it is shown that capacity of dc transmission is higher than that ac transmission under the similar conditions.

3.3.2 HVDC Interconnections to Enhance AC Networks

A major advantage of HVDC interconnection is that it can contribute in preventing cascading outage pass through the networks and therefore enhance power systems. This was clearly demonstrated in the 2003 North America Blackout, 2006 Europe Blackout and the 2010 Namibian and Zambian eventual blackout [76, 85].

Carlsson [3] reported that HVDC provides a good control of the transmitted power. When using HVDC, the power direction can also be changed rapidly. With the ability to change the operating point instantaneously the HVDC link can feed/reduce active power into the receiving system to control the frequency much faster than a normally controlled generator [86]. Carlsson [3]reported that classical HVDC transmission can vary the power level from minimum load, which normally between 5% and 10%, to max load 100% very quickly. He suggested that the DC interconnection could be designed to automatically adapt its power flow during a system disturbance. The power flow can be limited to protect the network. He also claimed that HVDC can help to reduce voltage oscillations by connecting capacitors to the network or by modulating the station's reactive power using firing angle control.

HVDC transmission link offers good performance when connected to AC system under fault conditions. Such specific actions, like normal power control, emergency power control and voltage control, can all help during disturbances. The most important feature of HVDC is that it cannot become overloaded [87].

Pan et al [17] claimed that by fast power run-up or run-back control functions, HVDC can help maintain power grid stability. With the ability to control both active power and reactive power, HVDC can provide an effective means of damping oscillations and improve voltage stability.

According to Zhang [75], when one of the systems enters oscillation mode between two generator groups, HVDC has the best active power damping effect if the converter station is electrically close to one of the oscillating generator group. The best location for reactive power damping is the electrical middle point between the oscillating generator groups [75]. HVDC system is provided with power modulation features for stabilization of AC system [86]. With this function, the HVDC link can reduce power swings and stabilize the system in a minimal time.

Fig.3-12 gives an example of how a power system can behave with and without HVDC power modulation function [17].

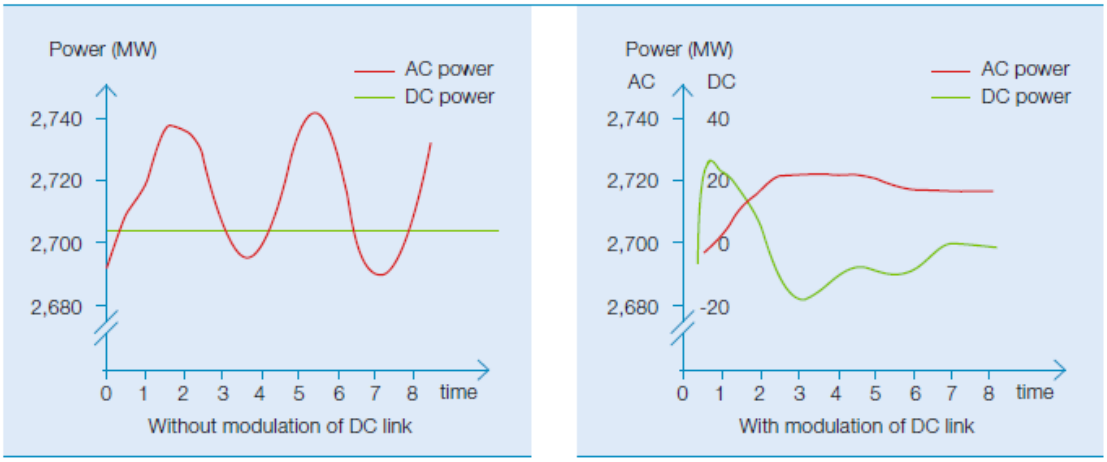

Figure 3-12 Results with and without DC modulation function [77]

Several researchers are investigating how the HVDC can function a damper of oscillations as was proven in 2003 northeast American blackout. Hafner and Manchen in [88] used the Caprivi Link Interconnector HVDC Light project to study the strong voltage and frequency stabilization function of HVDC systems to avoid a blackout. Based on commissioning tests, they showed that the HVDC link had a good performance with islanded AC networks and normal AC faults. They suggested that HVDC systems are able to enhance the stability of extremely weak AC system and to prevent a blackout from cascading. Pan et al [89] examined enhancing power

system stability through controlling HVDC power flow. Ozerdem and Habboob [90] used a MATLAB simulation of the Turkey to TRNC HVDC submarine interconnection and by comparing VSC-based HVDC and CSC-based HVDC performance under the same applied AC fault, they found that VSC-based HVDC had a better performance than CSC-based HVDC.

In 1993 Lee et al [91] suggested to use potential DC system support to enhance AC system in the western U.S.

Corsi et al [92] discussed the Sardinia-Corsica HVDC link (SACOI) in Italy and the Italy-Greece HVDC link (GRITA) by simulation tests and commissioning results, they demonstrated that using HVDC power modulation can achieve high control flexibility and regulation performance, which could contribute to face unexpected contingencies.

Arro and Silavwe [82] discussed what influence a line-to-ground fault occurring on HVDC line will bring to networks involving both AC and DC lines. In order to study the phenomenon, simulation studies were carried using PSCAD/EMTDC. A bipolar HVDC connection between the Swedish and Finnish power systems was simulated. Based on simulation work, there was no unwanted tripping in AC lines due to a line-to-ground fault that occurred on HVDC lines[82].

Paulinder [70] claimed that an HVDC link has an obvious contribution to power system's stability during disturbance through modelling CIGRE Nordic 32 system.

Du in [67] investigated the VSC-based HVDC control system's operations under steady-state and different fault conditions. The HVDC link was used different control strategies and faults were injected at inverter side and converter side separately. He concluded that for unbalanced faults the voltage dips in the dc-supplied ac system were less severe than in a pure ac system.

HVDC and Flexible AC Transmission Systems (FACTS) were strongly advised to provide a secure and stable solution for power delivery [13, 80, 85, 93-97]. As described in [85] 'FACTS, based on power electronics, have been developed to improve the performance of weak AC Systems and for long distance AC transmission. FACTS controllers can, however, also contribute to solve technical

problems in the interconnected power systems. FACTS are applicable in parallel connection, in series connection, or in combination of both to control load flow and to improve dynamic conditions. By these means, FACTS contributes to Blackout prevention too.' They concluded that developing large hybrid transmission systems, consisting of HVDC and FACTS, offers many advantages.

Fig.3-13 gives a brief view of such hybrid AC/DC system. The power exchange among the two nearby systems can be achieved by HVAC interconnections together with the FACTS equipment. The FACTS gives the additional support to HVAC interconnections in improving the dynamic conditions [93]. The Back-to-Back HVDC interconnections can be applied to avoid a spread of large disturbances through to whole system. HVDC transmission systems are utilized to transmit large power in long distance, for example, from the generation to load location [91]. The HVDC systems can also improve the HVAC systems' performances to avoid possible dynamic problems [91-93]. Such hybrid transmission system offers significant advantages in system reliability [85, 93-95]. The performance of AC lines can be improved by FACTS both in transmission capability and reliability. Long-distance bulk power can be transmitted by HVDC. With DC interconnections, high system security could be achieved.

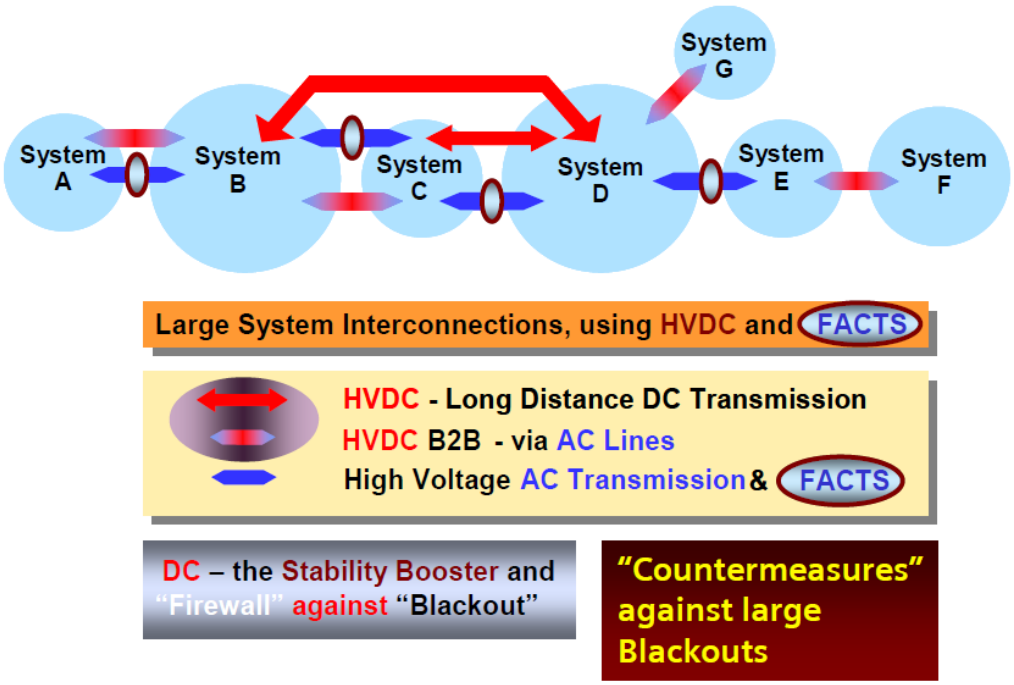

Figure 3-13 Hybrid AC/DC system [85]

3.3.3 Long Distance Bulk Power Delivery

HVDC transmission system provides several advantages for long distance bulk power deliveries. This includes transporting power from remote generation to load centres and connection between major power networks. Remote bulk generation includes hydro power station, solar power stations and large offshore wind farms.

HVDC can transmit more power in fewer lines than an AC transmission system in the same location [74]. In a long AC transmission system, the large cable capacitance causing reactive power flow will limit the maximum transmission distance. Furthermore, reactive power compensation is needed in ac transmission system for long distance power delivery in order to keep the voltage levels within normal operating limits [98]. HVDC systems offer lower line losses and economic benefits make HVDC an alternative choice for long-distance power delivery [74]. Fig.3-14 shows a comparison of DC and AC transmission system losses at same distance [99]. As can be seen from the figure, the longer transmission lines are, higher power losses exist for AC systems.

There are few technical limitations for HVDC cable transmission [100]. This gives HVDC immediate benefits in long distance power transmission especially for an under water cable transmission. DC submarine cables have lower inductances and higher capacitances than AC overhead lines and offer economical benefits. HVDC links are therefore chosen to connect large off-shore wind farms to load centres.

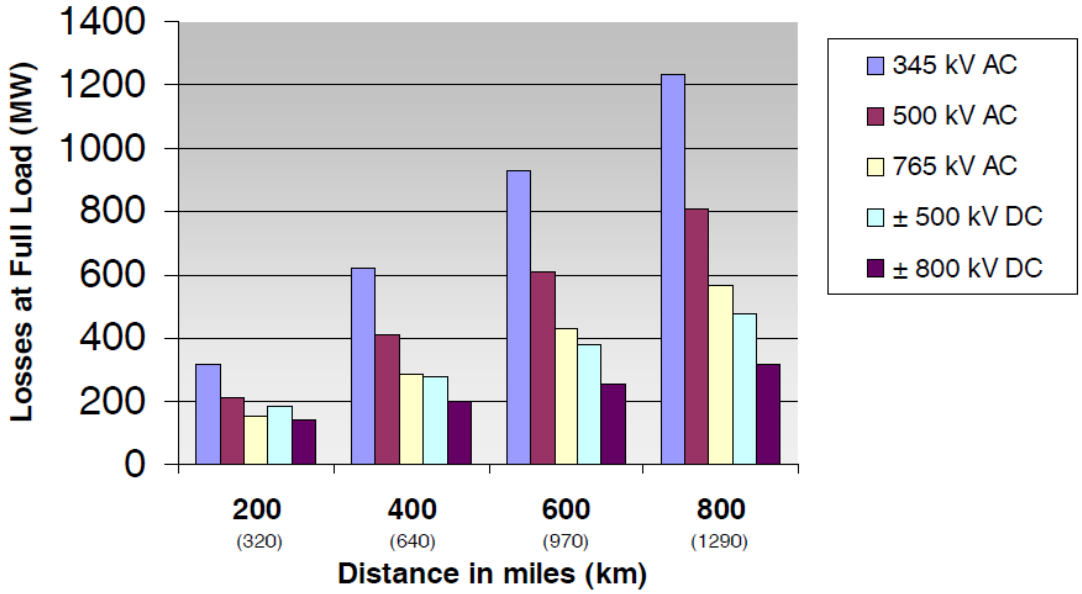

Figure 3-14 Loss comparison for DC and AC transmission systems

3.3.4 Economical Benefits

For the same transmission capacity, HVDC transmission lines cost less than HVAC systems above a certain distance. This is called the 'break-even-distance' [74, 100, 101]. This is a result of the cost of the consider situations. Fig.3-15 shows the investment costs for overhead line transmission with AC and HVDC.

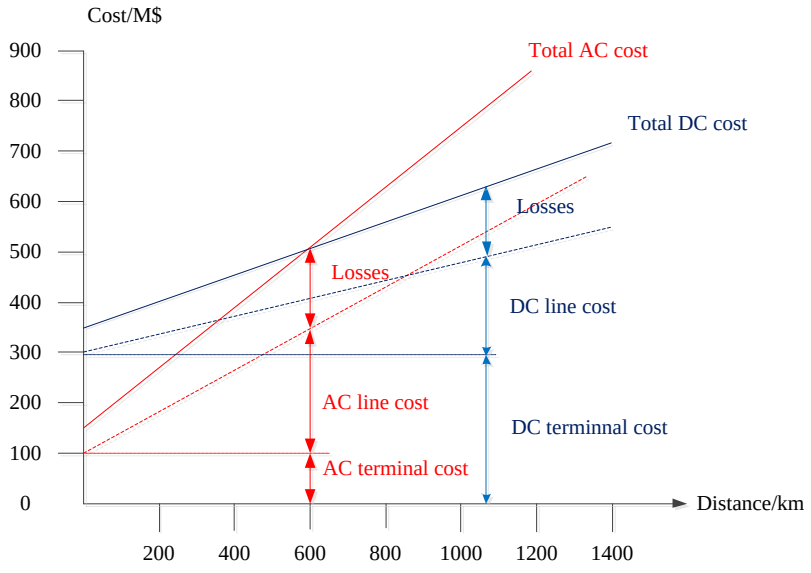

Figure 3-15 HVDC-HVAC cost comparison

As can be seen from the fig.3-15, above a certain distance, normally 600-800 km, the costs of HVDC transmission lines are smaller than AC transmission lines. A bipolar HVDC system has two lines compared to the three lines in an AC circuit. Savings also can be found in tower design which are shown in fig.3-16 and a reduced number of conductors [101]. Both electrical and mechanical considerations dictate a smaller tower which leads to a reduced cost.

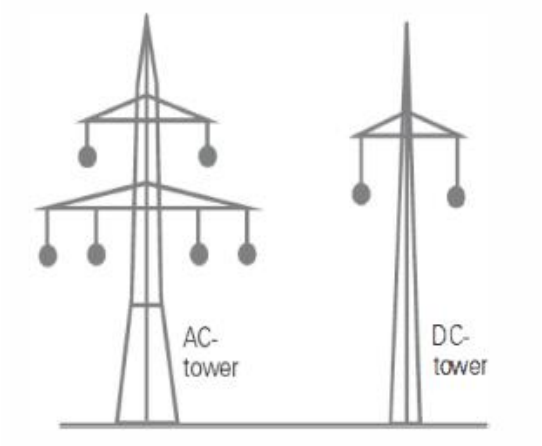

Figure 3-16 Typical transmission tower structures for approximately 1000 MW

In the developing of the Three Gorges Project in China it was shown that it would require five 500 kV HVAC lines compared to two ±500 kV bipolar HVDC lines used [74].

Fig.3-17 gives cost comparisons between AC and DC transmission systems [99]. HVDC has a cost advantage for 400 mile lines and beyond.

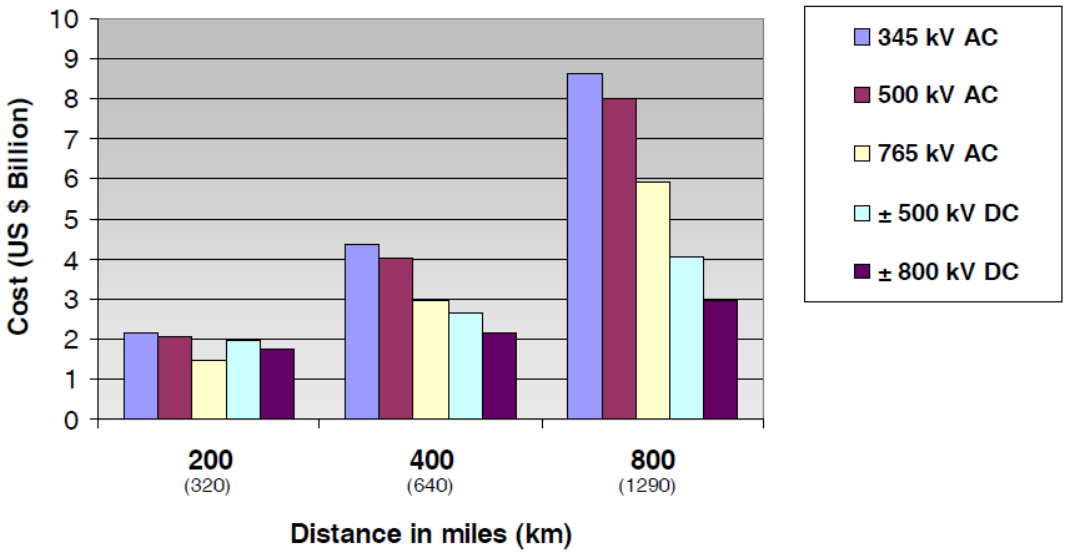

Figure 3-17 Cost comparisons between AC and DC systems [90]

3.3.5 Environmental Benefits

HVDC lines have also been shown to have a lower impact on the surrounding environment than HVAC lines [98]. Many HVDC links have been installed to connect existing power plants to load centres. These links not only improve power system capacity and efficiency but also give benefit to the environment by considering the need to build new power stations. CO_2 generation can therefore be reduced.

Using HVDC to connect hydro generation is another environmental benefit. Behrman [74] highlighted that there is no induction or alternating electro-magnetic fields from HVDC transmission lines. No skin effects, effective cable transmission and lower power losses ensure that there are less environmental impacts.

3.4 Challenges of HVDC Transmission System

HVDC transmission technology is playing an important role in modern power systems. However, there are a number of challenges when combining HVDC and HVAC networks.

3.4.1 Costs

The cost for an HVDC transmission system is high. The HVDC system needs filters, converters, power electronics and other equipment at both terminals to the line. It is hard to estimate the HVDC costs as it depends on many factors such as power capacity, type of transmission medium and environmental conditions [69]. A typical converter station cost structure can be found in fig.3-18. The highest cost is spent on converter stations.

To build a converter station is much more expensive than an ordinary ac substation of similar rating because the greater sophistication of an HVDC needs more components [78].

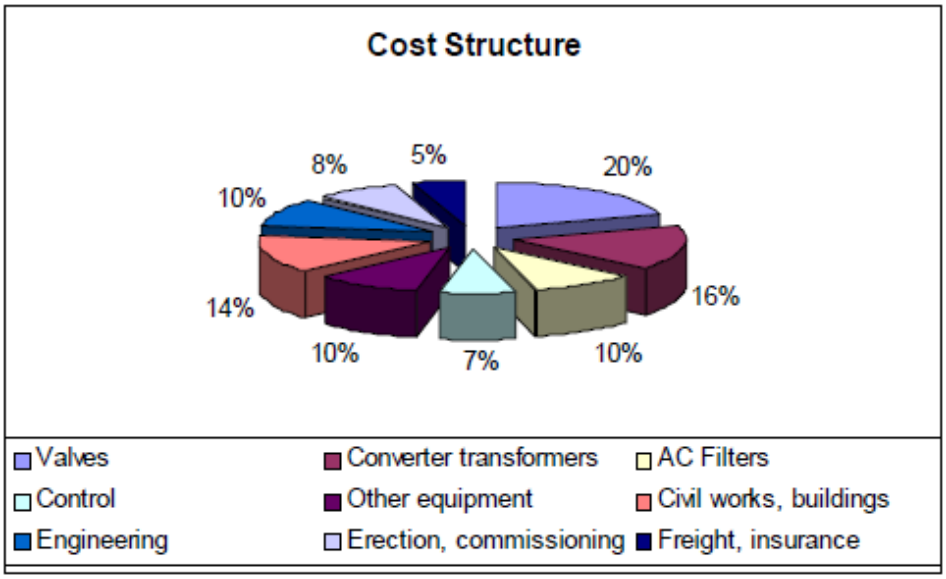

Figure 3-18 Cost structure [60]

3.4.2 Harmonics

All power converters produce harmonics during the converter process. These harmonics affect both the dc and ac sides. If not filtered, these harmonics will create many concerns including neutral circuit overloading in three phase circuit, motor and transformer overheating, metering inaccuracies and control system malfunctions [86]. Usually filters and smoothing reactors are used to reduce these harmonics but these result in additional costs.

Some studies show that even after filtering, some harmonics still enter into the system, typically 3rd and 5th order harmonics [86].

With an increasing number of converters connected to ac networks, the difficulty of reducing harmonics increases the construction costs [78].

3.4.3 Integration of HVDC scheme in AC network

Connecting an HVDC system to an HVAC system is challenging and needs highly trained engineers. An HVDC system, especially an CSC HVDC system, needs large ac harmonic filters to be installed at both ends of the terminals, which makes the system more complex. These large ac filters can cause over-voltages during fault recovery [78].

An HVDC scheme is complicated to maintain. The converter stations consist of a series of connected thyristors, transformers, filters and monitors. It is hard to find internal faults quickly. What is more, the reactive power support devices, such as filters and shunt capacitors connected in ac system, complicate the power networks.

3.5 Chapter Summary

This chapter reviews the HVDC general information including HVDC components, basic HVDC configurations and converter technologies. Furthermore, the advantages and disadvantages were also reviewed.

Since the world's first commercial HVDC line was installed successfully between Gotland and the Swedish mainland in 1950's, the HVDC transmission system draw engineers attentions in large power long distance transmission and systems interconnection. The HVDC transmission system offers benefits in long distance power delivery, system interconnection, economics and environments. However, the HVDC system has its disadvantages in constructing cost, harmonics and integration of HVDC scheme in AC networks.

The HVDC interconnection acts as a 'firewall' against the voltage disturbance and presents the cascading outage pass through therefore avoid the potential wide area

blackout. This was clearly demonstrated in 2003 North America block and other recent major blackouts. The HVDC links combine with HVAC interconnections can offer significant improvements in power system reliability and stability. Such hybrid AC/DC system satisfies the modern power systems in secure power delivery. The HVDC interconnection that constrains the fault current and voltage will be investigated in the following chapters.

Chapter 4

Overview of Distance Relay

Modern power systems involve power plants, transmission networks, distribution networks, loads and customers. The purpose of an electric power system is to provide energy from power plants to customers in a reliable, secure, constant and economic manner. The power system is growing in voltage levels, transmission capacity and complexity; therefore, faults increasingly occur in power systems. One of the most important equipment that keeps power systems working in order is the protection system. When faults occur, the protection systems are needed to remove the faults as speedily as possible. If faults remain connected without being cleared speedily, the power system may suffer three main effects which are named below [102]:

1. a risk of damage to the affected power plant;
2. a risk of damage to a healthy plant;
3. a risk of the power system falling out of step with consequent splitting.

The power system protections are sets of equipment that detect faults in the protected power systems, disconnect the faulted plant and re-establishes the service [21]. The main functions of protection systems are [103]:

1. automatically, speedily remove faults from the faulted power system and ensure the remaining parts operation correctly;
2. monitor the abnormal operation in the power system;
3. ensure the power system operates in a stable manner.

The operation of protection schemes occasionally causes wide area blackouts. Inappropriate tripping of the protection schemes contributed and accelerated the disturbance. This chapter will mainly investigated the operation principles of protection relays.

4.1 Protective Relays

The protective relays are the most important equipment in the protection systems. The Institute of Electrical and Electronic Engineers (IEEE) defines a relay as “an electric device that is designed to respond to input conditions in a prescribed manner and, after specified conditions are met, to cause contact operation or similar abrupt

change in associated electric control circuits." [104] IEEE defines protective relay as "a relay whose function is to detect defective lines or apparatus or other power conditions of an abnormal or dangerous nature and to initiate appropriate control circuit action." [104]

4.2Basic Objectives of Protective Relays

The main purpose of protective relays is to detect and clear a fault as reliably and quickly as possible. Protective relays minimize damage to the power network and maintain the quality of delivering electrical energy supplies. The performance of the protective relay must satisfy the following requirements: reliability, selectivity, speed and sensitivity [103, 105-108].

4.2.1 Reliability

Reliability has two aspects which are dependability and security [103, 108]. Dependability means the protective relay operates correctly when required, that is, no mal-operation when not necessary. Security indicates that the protective relay can avoid unnecessary operations when faults or problems are outside protecting zones. There may be tolerable transients when the power system is under normal operation. The protective relays should not operate on these tolerable transients but trip when there are intolerable transients and permanent faults [108].

4.2.2 Selectivity

Protective relays are designed to operate when faults occur inside a protection zone. However, protective relays may respond to conditions outside a protection zone. When protective relays need to operate, they should disconnect the faulted line correctly and ensure that the remainder of the power system continues its operation. If the protection relay cannot isolate a fault correctly, this may affect power system stability and result in widespread blackouts [105].

4.2.3 Speed

Faults should be isolated or cleared as quickly as possible by protective relays. Rapid operation can minimise damage to a power system. If faults are not cleared rapidly, this may result in serious consequences; for example, a whole power system may lose synchronization or a wide area blackout may occur. Normally, operating time for protective relays are measured in milliseconds [103]. A high-speed relay operates in 50ms or even less [108]. In a distribution system, protective relays are not required to operate within 50ms. The operating time will be slower, typically between 0.2-1.5s [108].

4.2.4 Sensitivity

Sensitivity is the ability that protective relays' response capability to faults inside the protection zone. The protective relays can detect system conditions and initiate successful protective action when there is a fault.

4.3 Distance Relay

Distance relay is the most widely protection relay used to protect transmission lines because of its reliability, selectivity, simplicity, suitability and economy [21]. The distance relay uses the impedance between the relay point and the fault location to determine operation. If the fault impedance is within the protection characteristic, the relay will trip. If the fault impedance is outside the protection characteristic, it will not trip.

4.3.1 Principle of Distance Relay

A distance relay uses the apparent impedance derived from the measured voltage and current at the relay point. The distance from relay point to the fault point is proportional to the apparent impedance seen by the distance relay[109]. During normal operation the apparent impedance is large whereas during fault condition the apparent impedance is small [22]. Fig.4-1 shows a typical distance relay protecting a transmission line AB. The generator G is supplying power to load L via AB. The

distance relay is set to protect line AB at point A. The distance relay has a pre-set protecting distance L_{set}. When the fault is inside a pre-set zone, the relay will trip. As can be seen from fig.4-1, if a fault occurs at f1, the distance from A to f1 L_{f1} is smaller than L_{set}, relay trips. When a fault occurs at f2, due to L_{f2} being larger than L_{set}, the relay does not trip.

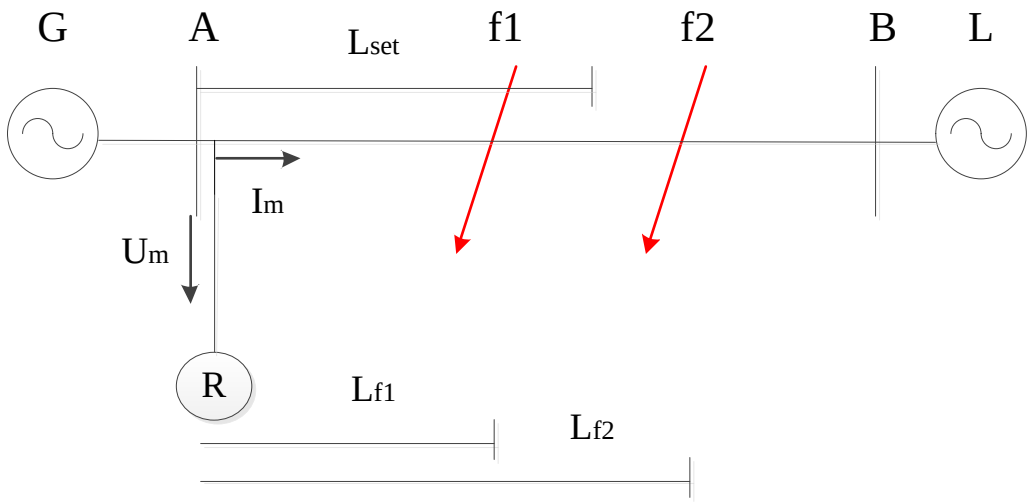

Figure 4-1 Typical distance relay protecting line

The Voltage Transformer (VT) and Current Transformer (CT) are used to transfer primary voltage and current from transmission line to relay for calculating the apparent impedance. The apparent impedance is then calculated as [103]:

$$Z_m = \left(\frac{U_m}{VT_{ratio}}\right) / \left(\frac{I_m}{CT_{ratio}}\right) \tag{4.1}$$

$$Z_m = \left(\frac{U_m}{I_m}\right) \times \left(\frac{CT_{ratio}}{VT_{ratio}}\right) \tag{4.2}$$

Where:

Z_m is the apparent impedance;

U_m is the measured voltage;

I_m is the measured current;

VT_{ratio} is the voltage ratio between VT primary and secondary;

CT_{ratio} is the current ratio between CT primary and secondary.

The apparent impedance is a vector, and it can be represented as [103, 106]:

$$Z_m = |Z_m| \angle \varphi_m = R_m + jX_m \quad (4.3)$$

Where:

$|Z_m|$ is the apparent impedance magnitude value;

φ_m is the apparent impedance phase angle;

R_m is the measured resistance;

X_m is the measured reactance.

$|Z_m|$ and φ_m can be represented as [106]:

$$|Z_m| = \sqrt{{R_m}^2 + {X_m}^2} \quad (4.4)$$

$$\varphi_m = tan^{-1} \frac{X_m}{R_m} \quad (4.5)$$

The apparent impedance Z_m can be presented in rectangular coordinate system as shown in fig.4-2.

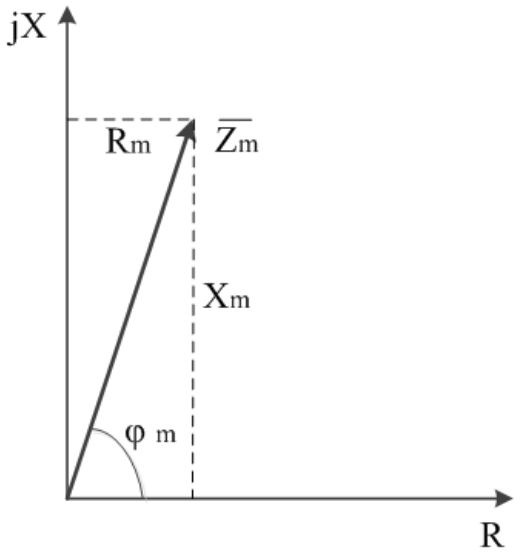

Figure 4-2 RX-diagram for apparent impedance

Similarly, the line impedances and load impedance of fig.4-1 can also be presented in RX-diagram, as shown in fig.4-3. When the power system is under steady

operation, the voltage and current at the relay is rated voltage and current. The apparent impedance seen by distance relay is the load impedance Z_{load} as shown in fig.4-3. The load impedance phase angle is generally small due to high power factor. Usually, the power factor is greater than 0.9 and the impedance phase angle is less than 25.8° [103]. When a fault occurs on the protected transmission line AB, the distance relay measured voltage decreases and current increases. The apparent impedance seen by distance relay becomes the line impedance from the distance relay to the fault location. The relationship of fault impedance and fault location can be presented as [103]:

$$Z_m = Z_f = z_1 \times L_f = (r_1 + jx_1) \times L_k \quad (4.6)$$

Where:

Z_m is the apparent impedance;

Z_f is the fault impedance;

z_1 is the line impedance in unit length;

r_1 is the line resistance in unit length;

x_1 is the line reactance in unit length;

L_k is the line length from distance relay to fault location.

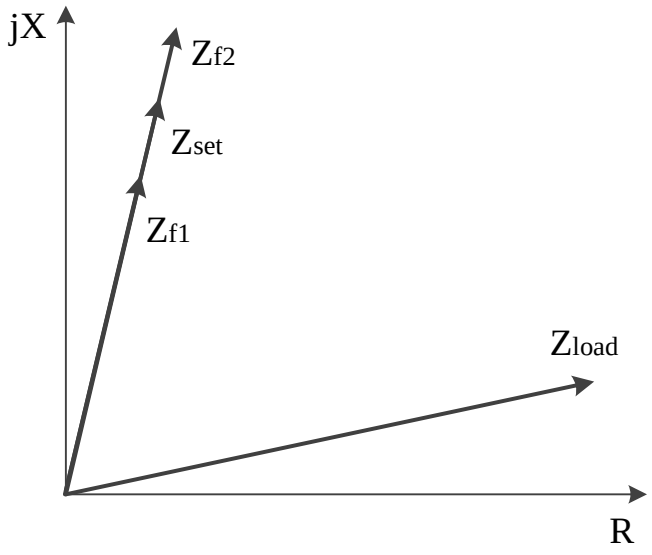

Figure 4-3 Load impedance and line Impedance seen by distance relay

Fig.4-3 also shows the line impedance seen by distance relay when fault occurs. Z_{f1} is the fault impedance seen by distance relay when fault occurs at F1 while Z_{f2} is the fault impedance when fault occurs at F2. Z_{set} presents the pre-setting impedance at distance relay. By comparing $Z_{f1,}$ Z_{f2} and Z_{set} the distance relay determines where the fault location is. If $Z_f<Z_{set}$, the relay trips. When $Z_f>Z_{set}$, as for fault F2, the relay does not trip. The fault impedance phase angle is equivalent to transmission line phase angle. For the transmission line at 220kV and above, the phase angle is usually greater than 75° [103].

The pre-set impedance Z_{set} depends on the protected line length L_{set}, and is normal equal to 80% of the protected line [22, 103, 109]. Z_{set} can be presented as:

$$Z_{set} = z_1 \times L_{set} \tag{4.7}$$

Where:

L_{set} is the setting protected distance.

The distance relay comparing Z_m and Z_{set} means comparing L_k and $L_{set.}$ If $Z_m<Z_{set}$, means $L_k<L_{set}$, relay trips. If $Z_m>Z_{set}$, means $L_k>L_{set}$, the relay does not trip. The 80% setting ensures that a fault beyond the end of the line will not cause tripping.

4.3.2 Protection Zones

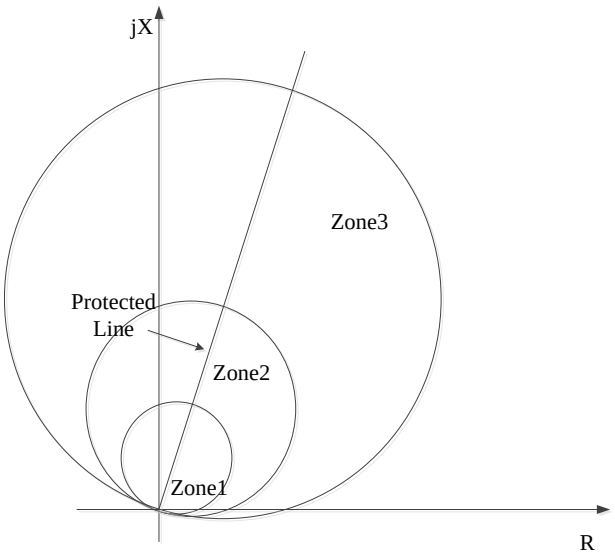

Figure 4-4 Three protection zones

A typical configuration for a distance relay has three protection zones: zone 1, zone 2 and zone 3, as shown in fig.4-4. Zone 1 is usually set up to 80% of the protected line impedance. Zone 2 should be at least 120% of the protected line impedance or the protected feeder plus 50% of the shortest following line impedance. Zone 3 is set up to the protected feeder plus the longest following feeder plus 25% of the shortest subsequent feeder or 120% of the protected feeder plus the longest following feeder [21, 22, 106, 110].

The Zone 1 setting of 80% of the protected line, leaves the remaining 20% of the line impedance as a safety margin. The safety margin prevents the errors introduced by current and voltage transformers and processes in calculating fault impedances [21]. Zone 1 is required to operate instantaneously, without time delay, when a fault occurs.

The Zone 2 setting is 120% of the protected line. It covers not only the protected line but also 20% of next line, which ensures the fault clearing for any fault on the line. To ensure the selectivity of distance relay and avoid unnecessary operation, Zone 2 is given a time delay, normally between 0.2s-0.5s [111]. As shown in fig.4-5, if a fault occurs on BC line at 10%, the fault is covered both by R1 Zone 2 and R2 Zone 1. Time delay Δt_1 of Zone 2 avoids unnecessary operation of R1 Zone 2.

Zone 3 is set as remote back-up protection for faults on adjacent lines. It covers at least 1.2 times the longest adjacent line [22, 106]. There is a typical 1.0s-2.5s time delay for Zone 3 [111]. When a fault occurs on BC line at 90%, it covers by R1 Zone 3 protection and R2 Zone 2 protection. If R2 fails to trip the fault the R1 will operate as remote back-up protection.

Fig.4-5 demonstrates how a transmission line network is protected and shows the reach of each zones and time delay for each zone. Zone 1 and Zone 2 are mainly used to clear local faults. Zone 3 is mainly used for remote back-up protection.

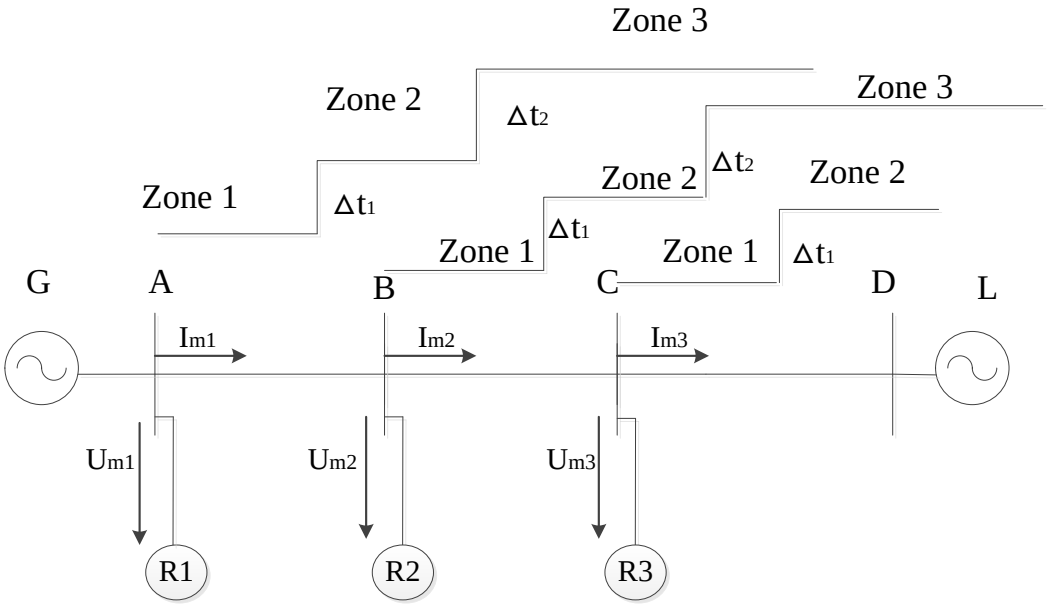

Figure 4-5 The reach of each zones and time delays of each zones

The faults occurring on a three phase transmission line are characterised as: single phase to ground fault (A-G, B-G, C-G), phase to phase fault (A-B, B-C, C-A), phase to phase to ground fault (A-B-G, B-C-G, C-A-G) and three phases fault (A-B-C, A-B-C-G). In order to discriminate between the different fault types, a full scheme distance relay combining zones and time delay settings is shown in fig.4-6.

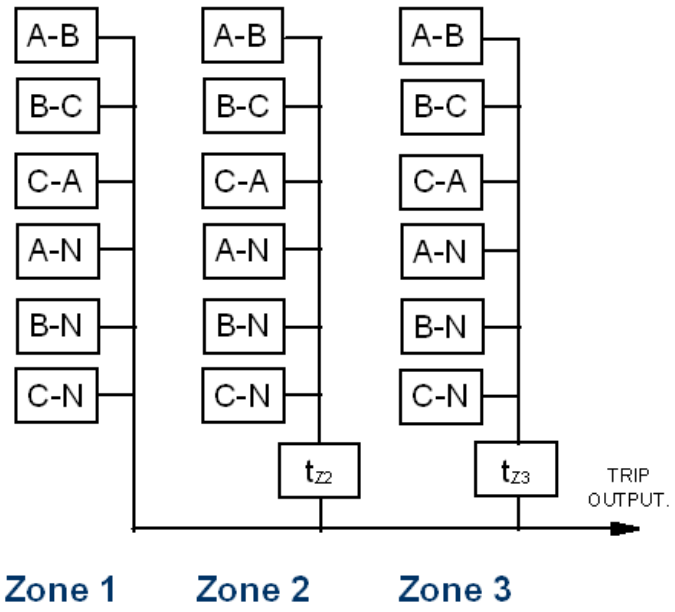

Figure 4-6 Full scheme distance relay

4.4 Fault Impedance Calculation

As shown in fig.4-7, the distance relay at busbar M is used to protect transmission line MN. When a fault occurs at location k, it uses the voltages and currents to determine what action is required.

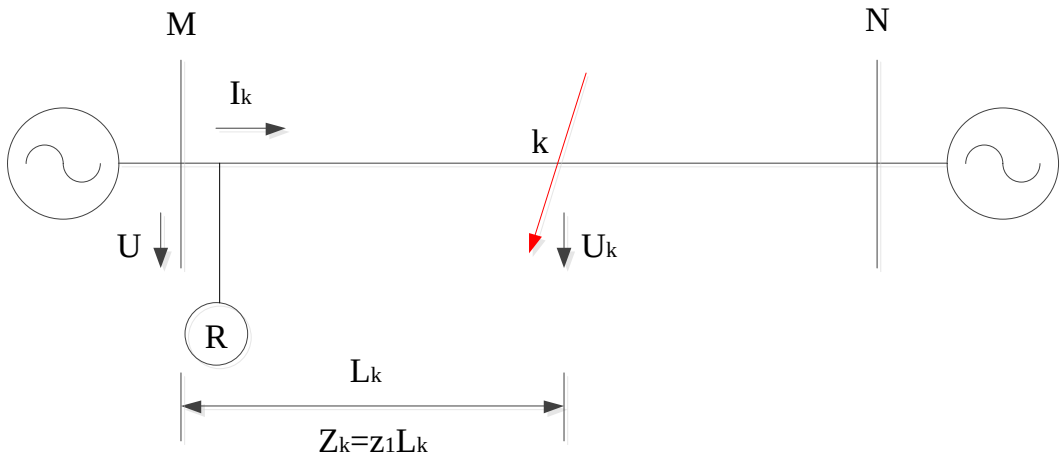

Figure 4-7 Transmission line protected by distance relay

The distance relay calculates the apparent impedance as below:

$$U_m = I_m Z_m = I_m Z_f = I_m z_1 L_f \qquad (4.8)$$

Where:

U_m, I_m and Z_m are the measured voltage, current and impedance at the relay separately;

Z_f is the fault impedance;

z_1 is the positive sequence impedance of the protected line;

L_f is the distance from relay location to fault location.

The distance relay has different parts to protect each type of faults. For single phase to ground fault, it is protected by phase-to-ground relay: A-G, B-G and C-G. For phase to phase fault, it is covered by phase-to-phase relay: A-B, B-C and C-A.

The power system has three phases: A, B and C. Using symmetrical components where [21, 22, 106, 112]:

$$I_a = I_1 + I_2 + I_0$$
$$I_b = a^2 I_1 + a I_2 + I_0$$
$$I_c = a I_1 + a^2 I_2 + I_0 \quad (4.9)$$

and:

$$V_a = V_1 + V_2 + V_0$$
$$V_b = a^2 V_1 + a V_2 + V_0$$
$$V_c = a V_1 + a^2 V_2 + V_0 \quad (4.10)$$

Where:

I_a, I_b and I_c are the phase current at relay location;

V_a, V_b and V_c are the phase voltage at relay location;

I_1 is the positive-sequence current at relay location;

I_2 is the negative-sequence current at relay location;

I_0 is the zero-sequence current at relay location;

V_1 is the positive-sequence voltage at relay location;

V_2 is the negative-sequence voltage at relay location;

V_0 is the zero-sequence voltage at relay location.

In fig.4-7, the phase a voltage at relay location can be calculated as [21]:

$$U_a = I_{a1} z_1 L_k + I_{a2} z_2 L_k + I_{a0} z_0 L_k + U_{ka} \quad (4.11)$$

Where:

U_a is the phase A voltage at relay location;

U_{ka} is the voltage at fault location;

I_{a1}, I_{a2}, I_{a0} are the phase a positive-sequence current, negative-sequence current and zero-sequence current at relay location separately;

z_1, z_2, z_0 are the protected line positive-sequence impedance, negative-sequence impedance and zero-sequence impedance per unit length separately;

L_k is the line distance from relay location to fault location.

Because $z_1=z_2$[103], therefore equation 4.11 equals:

$$\begin{aligned} U_a &= [(I_{a1}+I_{a2})z_1L_k + I_{a0}z_0L_k] + U_{ka} \\ &= [(I_{a1}+I_{a2}+I_{a0})z_1L_k + I_{a0}(z_0-z_1)L_k] + U_{ka} \\ &= \left[(I_{a1}+I_{a2}+I_{a0}) + 3I_{a0}\left(\frac{z_0-z_1}{3z_1}\right)\right] z_1L_k + U_{ka} \end{aligned} \quad (4.12)$$

Because $I_a=I_{a1}+I_{a2}+I_{a0}$ and letting $k=\frac{z_0-z_1}{3z_1}$, then equation 4.12 becomes[103]:

$$U_a = (I_a + 3kI_0)z_1L_k + U_{ka} \quad (4.13)$$

Similarly, phase b and c voltage can be presented as [103]:

$$U_b = (I_b + 3kI_0)z_1L_k + U_{kb} \quad (4.14)$$

$$U_c = (I_c + 3kI_0)z_1L_k + U_{kc} \quad (4.15)$$

Where:

U_b,U_c are the phase b and phase c voltage at relay location;

U_{kb}, U_{kc} are the phase b and phase c voltage at fault location;

I_b, $I_c$are the phase b and phase c current at relay location.

4.4.1 Impedance seen during single-phase-to-ground fault

Assuming a-to-ground fault occurred in fig.4-7 at k, $U_{ka}=0$, then equation 4.13 becomes[103]:

$$U_a = (I_a + 3kI_0)z_1L_k \quad (4.16)$$

Letting $z_a=z_1L_k$, equation 4.16 could be:

$$U_a = (I_a + 3kI_0)z_a \tag{4.17}$$

Therefore [21, 22, 103, 106, 112]:

$$z_a = \frac{U_a}{I_a + 3kI_0} \tag{4.18}$$

z_a is the fault impedance seen by distance relay when there was a a-to-ground fault at k.

Similarly, the fault impedance seen by distance relay when b-to-ground and c-to-ground fault is [21, 22, 103, 106, 112]:

$$z_b = \frac{U_b}{I_b + 3kI_0} \tag{4.19}$$

$$z_c = \frac{U_c}{I_c + 3kI_0} \tag{4.20}$$

z_b and z_c are the fault impedance seen by distance relay.

The fault phase voltage and current may lead to the corresponding phase relays see the fault impedance [112]. For example, A-G fault may lead to the A-B and C-A impedances moving to the area that near to the protection characteristic zones or inside the zones as shown in fig.4-8[112].

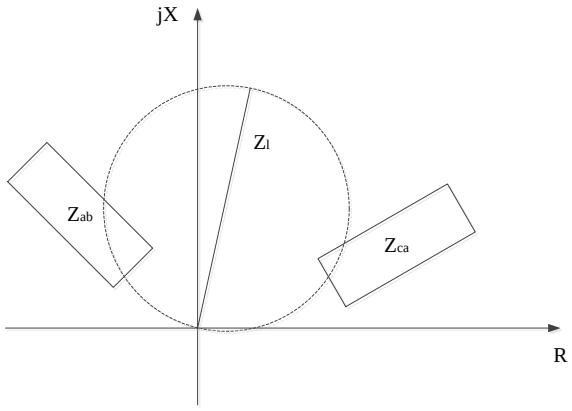

Figure 4-8 Possible A-B and C-A impedances settling areas during A-G fault

4.4.2 Impedance seen when phase-to-phase fault

When a phase-to-phase fault occurs, the phase fault voltages at fault location are equal but not zero [103]. Take phase b and c for example. At the fault location, U_{ka} = U_{kb}, the fault phase voltages are the same as equation 4.13 and 4.14. Letting $z_{ab}=z_1L_k$, then the fault impedance seen by distance relay is[103, [112]:

$$z_{bc} = \frac{U_b - U_c}{I_b - I_c} = \frac{U_{bc}}{I_b - I_c} \tag{4.21}$$

The fault impedances seen by distance relay during A-B fault and C-A fault are the same asequation4.21 as shown below.

$$z_{ab} = \frac{U_a - U_b}{I_a - I_b} = \frac{U_{ab}}{I_a - I_b} \tag{4.22}$$

$$z_{ca} = \frac{U_c - U_a}{I_c - I_a} = \frac{U_{ca}}{I_c - I_a} \tag{4.23}$$

During B-C fault, the B-G, C-G, A-B and C-A impedances may enter the protection zones or settle near to the protection zones as shown in fig.4-9 [112].

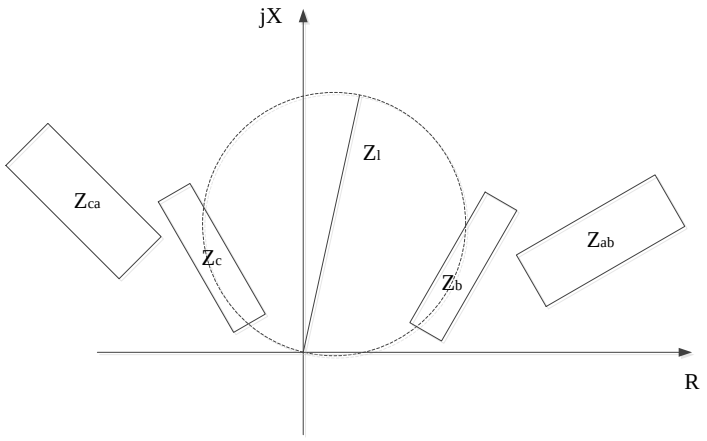

Figure 4-9 Possible B-G, C-G, A-B and C-A impedance seen by distance relay during B-C fault

4.4.3Impedance seen during phase-to-phase-to-ground fault

In the case of phase-to-phase-to-ground fault, the fault phase voltages at fault location are zero. Assuming B-C-G fault at k, then $U_{kb}=U_{kc}=0$, equation 4.14 and 4.15 becomes[103]:

$$U_b = (I_b + 3kI_0)z_1L_k \quad (4.24)$$

$$U_c = (I_c + 3kI_0)z_1L_k \quad (4.25)$$

Letting $z_{bc}=z_1L_k$, the distance relay computes fault impedance as [21, 22, 103, 106, 112]:

$$z_{bc} = \frac{U_{bc}}{I_b - I_c} \quad (4.26)$$

z_{bc} is the fault impedance seen by distance relay when there was a B-C-G fault.

Similarly, A-B-G and C-A-G fault impedance seen by distance relay are[21, 22, 103, 106, 112]:

$$z_{ab} = \frac{U_{ab}}{I_a - I_b} \quad (4.27)$$

$$z_{ca} = \frac{U_{ca}}{I_c - I_a} \quad (4.28)$$

z_{ab} and z_{ca} are the fault impedance seen by distance relay in the event of A-B-G and C-A-G fault.

During phase-to-phase-to ground fault, for example B-C-G fault, the possible A-B and C-A impedances seen by distance relay are shown in fig.4-10 [112]. Since during B-G-G fault, $I_a=0$, the A-G impedance is infinite [112].

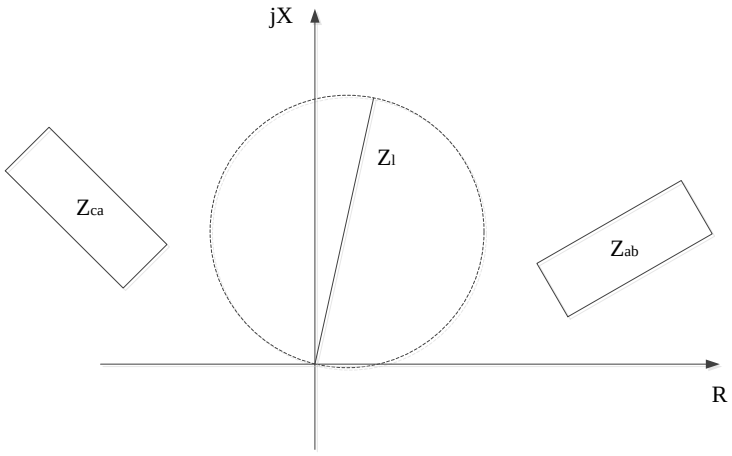

Figure 4-10 Possible A-B and C-A impedance seen by distance relay during B-C-G fault

4.4.4 Impedance seen when three phases fault

During three-phase fault or three-phases-to-ground fault, each phase voltage at fault location are equal, the simulation equals zero [103]. The fault impedance seen by distance relay can be expressed by using any phase voltage and current or phase-to-phase voltage and current.

Table 4-1 summarized the fault impedance calculating equations for each type of faults.

Fault Type	Calculating Equations
A-G	$U_a/(I_a+3kI_0)$
B-G	$U_b/(I_b+3kI_0)$
C-G	$U_c/(I_b+3kI_0)$
A-B or A-B-G	$U_{ab}/(I_a-I_b)$
B-C or B-C-G	$U_{bc}/(I_b-I_c)$
C-A or C-A-G	$U_{ca}/(I_c-I_a)$

Table 4-1 Fault impedance calculating equations for each type of faults

4.5 MHO characteristic

The Mho characteristic distance relay was first introduced in 1930s and is still the most widely used protection characteristic [113]. It uses the voltage U_r and current I_r measured at the relay location to determine the apparent impedance as shown in fig.4-11. The mho characteristic is adjusted by setting Z_{set}, the pre-set impedance along the diameter of the circle and φ the angle of displacement of the diameter from the R-axis [106, 114]. The angle φ is known as relay characteristic angle [106, 114]. The distance relay trips when fault impedance is inside the mho characteristic and does not trip if the fault impedance is outside. The mho function is directional and only operates for faults in the forward direction along the protected line.

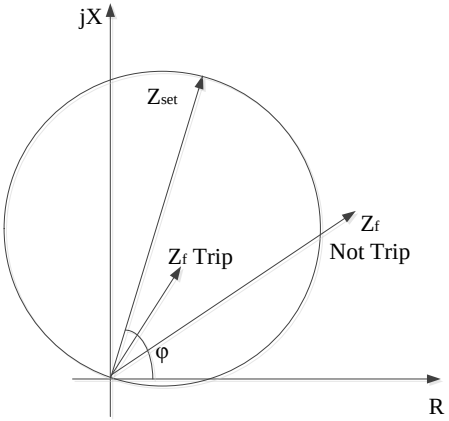

Figure 4-11 The Mho characteristic of distance relay

The mho characteristic distance relay uses an IZ signal rather than I signal, where Z is referred to as 'replica impedance' or 'mimic impedance' [115]. The replica impedance is ideally the represented equivalent of the protected line. The IZ signal is used to produce the distance relay operating signal IZ-V. The signal IZ-V and V are the two inputs for relay's comparator. The distance relay uses a phase comparator to make decisions [116]. The phase comparator compares phase angle difference between the input signals and operates when this is between pre-set limits. The phase comparator uses signal S_1 and S_2 to produce the characteristic. The signals are defined as the following [21, 112, 114, 116-118]:

$$S_1 = I_f \cdot Z_{set}\angle\varphi - V_f$$
$$S_2 = V_f \qquad (4.29)$$

Where:

S_1, S_2 are the phase comparator input signals;

V_f is the voltage applied to the distance relay;

I_f is the current applied to the distance relay;

$Z_{set}\angle\varphi$ is the setting impedance reach of the distance relay.

The phase comparator compares the angle argument of S_1 and S_2 and operates when [21, 112, 114, 116-118]:

$$-90° \leq arg\frac{S_1}{S_2} \leq 90° \qquad (4.30)$$

If the angle is less than or equal to 90°, the fault impedance Z_f lies inside the mho characteristic and the relay will trip. If the angle is greater than 90°, Z_f plots outside of mho characteristic and the relay will not trip. The mho characteristic defined by phase comparator is shown in fig.4-12 below:

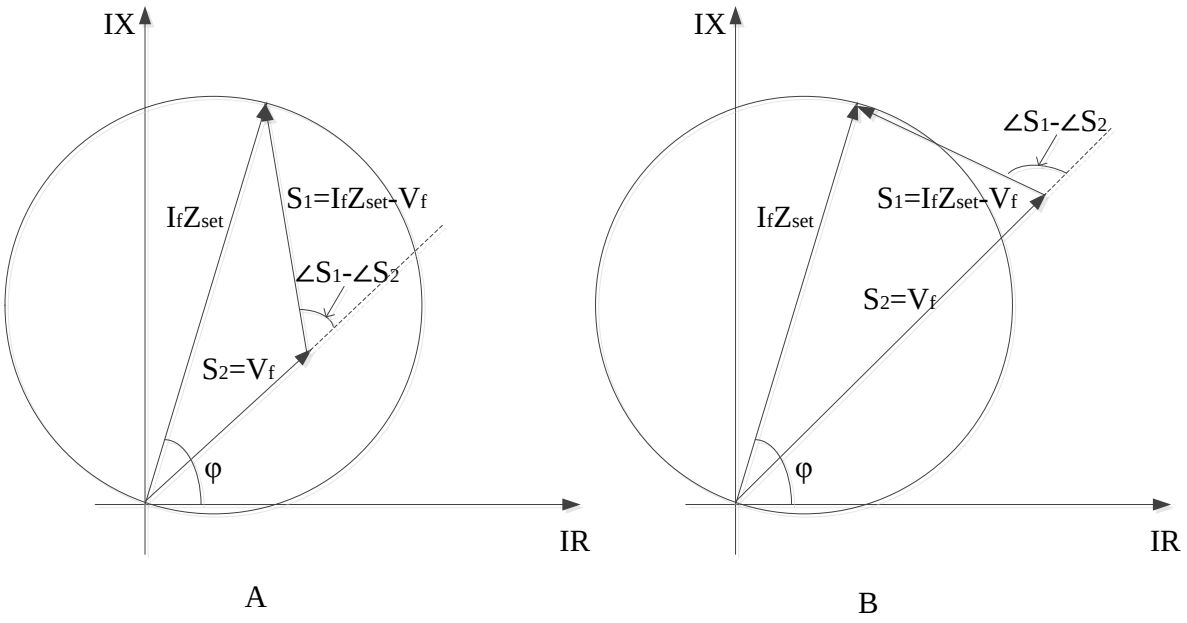

Figure 4-12 Mho characteristic defined by phase comparator

4.6 Block-average Comparator

The block average comparator is the classical comparator used in distance relays [119]. First introduced in the 1960s, it has been the basis for several successful distance relay design and is still used today [112]. The block average comparator measures the duration of polarity coincidence on both half-cycles of the input signals. Then the average value is determined in an integrating circuit. A trip signal is produced if a specified average value is maintained for more than a prescribed duration and delayed by the averaging function [120]. A detailed diagram of block average comparator is shown is fig.4-13.

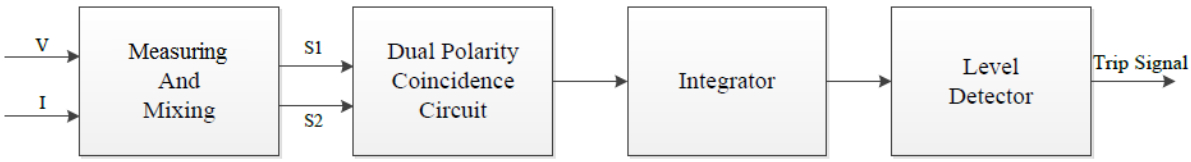

Figure 4-13 Block-average comparator

4.6.1 Basic principles of block average comparator

Two input signals S_1 and S_2 are derived from the input three phase voltage and current measured at distance relay location and processed by the mixing circuit. The S_1 and S_2 are defined as follows:

$$S_1 = I \cdot Z_{set} - V$$
$$S_2 = V \qquad (4.31)$$

Z_{set} is the replica impedance which ideally represents the line impedance of protected line. The signals used in the comparator S_1 and S_2 are on the polarities of the outputs from the mixing circuit. When the polarity of the input signal is positive, the S is positive and has a value of '1'. When the polarity of the input signal is negative or zero, S is '0'[112].

S_1 and S_2 are then input into a polarity coincidence circuit. The polarity coincidence is achieved by an 'exclusive OR' gate [112]. This compares the two input signals and generates an output pulse. When the polarity of the two signals is same, the output is positive '1'; however, when the polarity of the two signals are different, the output is '0' [119].

The generated pulse signal is then applied into an integrator, the output of which increases linearly when the input pulse is positive and decreases linearly when the input signal is zero. The outputs form the integrator increases and decreases at the same rate.

Finally the signal is input into a level detector, which by using pre-set levels provides the trip signal or the reset signal. If the input signal from the integrator ramps up beyond a pre-set trip limit, the level detector generates a trip signal. If the input

signal from the integrator falls below the pre-set reset limit, then the level detector generates a reset signal. In order to prevent the level detector output trip at twice the power system frequency, the trip value must be exceed the level which the integrator could reach in a quarter of the power frequency period [112, 119, 120]. The reset value must be the same value of distance from the trip level. An upper limit must be set in case of integrator signal increasing infinitely and must give a reasonable reset time [119].

4.6.2 The waveform in block average comparator

The block average comparator compares the phase difference of the two input signals. The comparator generates a trip signal when [112, 119, 120]:

$$-90° \leq \theta = \left(arg\frac{S_1}{S_2}\right) \leq 90° \qquad (4.32)$$

When Θ<90°, the waveforms in comparator is shown in fig.4-14 [112, 119, 120].

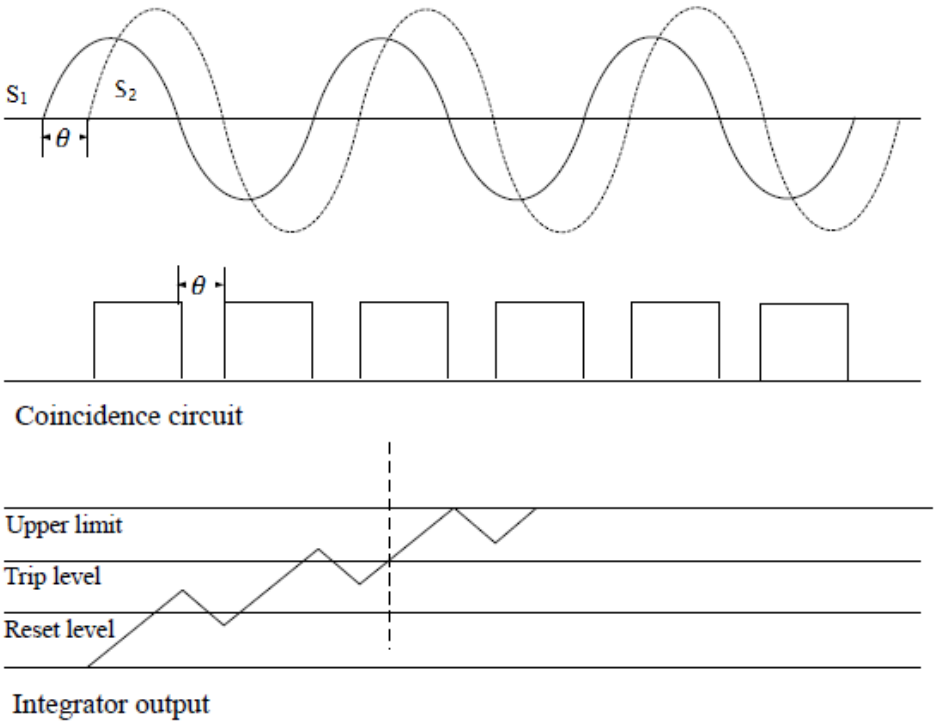

Θ < 90°

Figure 4-14 Waveforms in block average comparator when Θ<90°

When Θ<90°, the period of coincidence is greater than the period of non-coincidence. The period of the coincidence is greater than a quarter of the power frequency [112]. The ramping up period is greater than ramping down period in integrator. The output reaches the trip level in a very short period. When the phase angle is 0°, the tripping time is half a power system period, i.e.10ms [112, 121].

When Θ>90°, the waveforms in comparator is shown in fig.4-15[112, 119, 120].

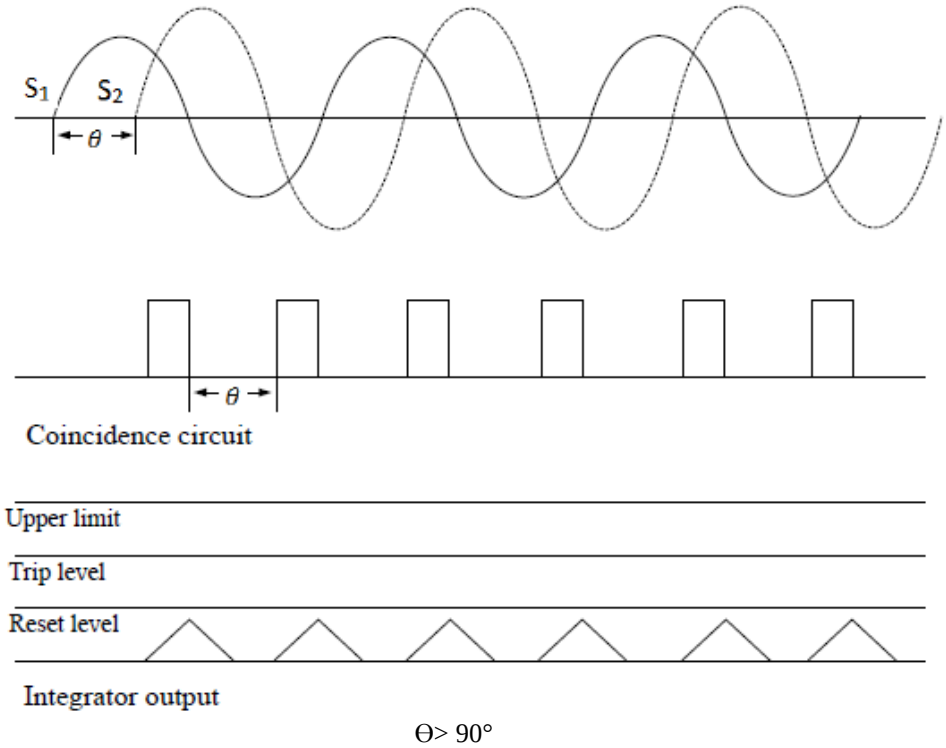

Figure 4-15 Waveforms in block average comparator when Θ>90°

When Θ>90°, the period of coincidence is less than the period of non-coincidence. The period of the coincidence is less than a quarter of the power frequency [112]. The integrator output increases during coincidence period and decreases and returns to its zero limit during non-coincidence. The pulse duration is not long enough to produce increasing linear signal. The comparator therefore restrains.

When Θ≈90°, the waveforms in comparator is shown in fig.4-16 [112, 119, 120].

When Θ≈90°, the period of the coincidence is equal to a quarter of the power frequency [112]. The integrator output ramps up during coincidence period and

ramps down during the non-coincidence period. If the phase angle is just less than 90°, the integrator output increasing duration would just exceed its decreasing period. There would be a very small increase in the integrator output signal for each power cycle and the integrator output would eventually cross the trip level [112, 119, 120].

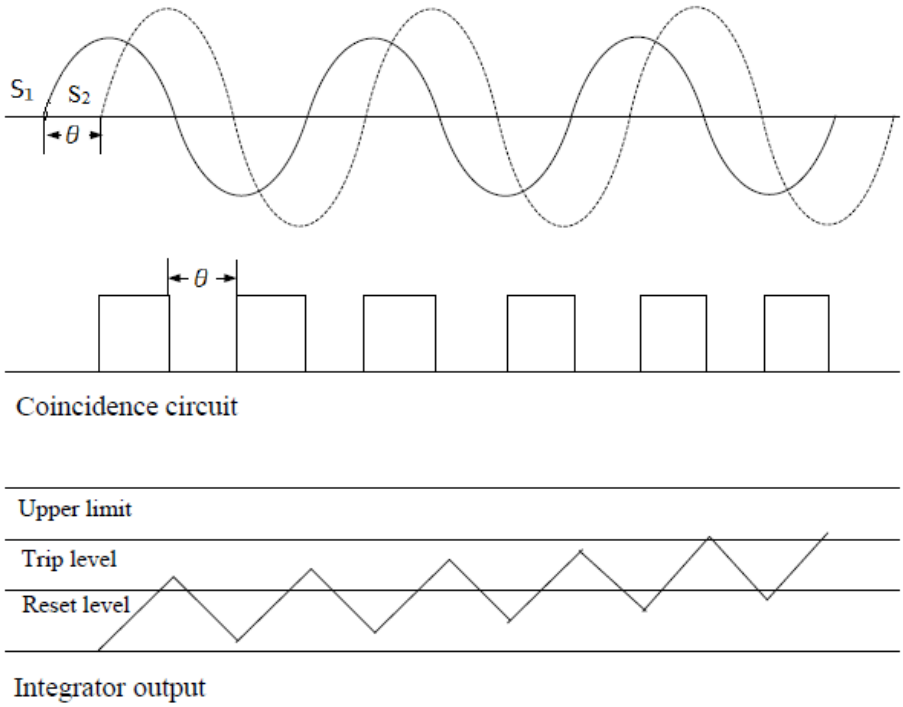

Θ≈ 90°

Figure 4-16 Waveforms in block average comparator when Θ≈90°

Because of the popularity of the Block Average relay, it has been used to demonstrate the operation of the protection for HVAC lines connected to HVDC ones.

4.7 Signal processing in distance relay

The Discrete Fourier Transformer (DFT) is the most widely used method to extract fundamental frequency component from measured voltage and current waveforms [121-125]. When the power system suffers from fault conditions, the fault voltage and current signals often contain dc components, a large amount of unwanted harmonics, high frequency oscillation quantities, etc [122-124]. These unwanted components affect the DFT accuracy and delay the DFT calculating time. The

relative error caused by these unwanted components may reach 20% from the DFT algorithm [123, 124]. The DFT algorithm may need a few cycles for decaying DC components to obtain the accurate fundamental phasors [123, 124]. Fig.4-17 shows a fault current with DC offset plotted against its unfiltered phasor magnitude [116]. Therefore, the signals need to be filtered before being used in the distance relay processor.

Low-pass anti-aliasing filters with appropriate cut-off frequency can be used to eliminate the high frequency components [122], and can remove any frequencies existing on the input signals that are greater than half the sampling frequency [110]. The steady-state power system frequency is generally 50 Hz or 60 Hz. Therefore, the low-pass filter must preserve the 50Hz or 60Hz components and reject the others. Normally the lower-pass filters used in distance protection are of third to fifth order with a cut-off frequency of 90Hz [110]. Reference [122] used low-pass filters with a cut-off frequency of 360Hz to remove the effects caused by travelling waves as well as high frequency components. In practice, the sampling rate must be at least four samples per cycle, that is, 240Hz for 60Hz system and 200Hz for 50 Hz system [110].

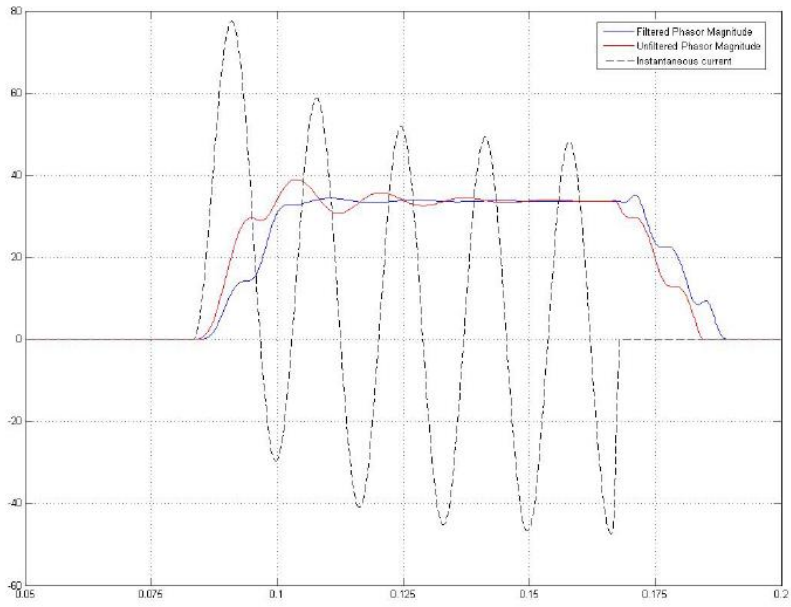

Figure 4-17 Comparing of a fault current with and without filtered phasor magnitude [116]

Low-pass filters cannot remove the dc components, therefore the DFT is used. The DFT is a digital filtering algorithm to compute the magnitude and phase at discrete

frequencies and extract wanted frequency components [110, 126]. For a sinusoidal voltage, this is represented as:

$$v(t) = V_{peak} \cdot sin(\omega t + \Theta_v) \tag{4.33}$$

The discrete fourier transform calculation of the fundamental components can be calculated as [116]:

$$V_{real} = \frac{2}{N} \cdot \sum_{k=1}^{N} \left[S_k \cdot sin\left(2\pi \frac{k}{N}\right) \right]$$
$$V_{imag} = \frac{2}{N} \cdot \sum_{k=1}^{N} \left[S_k \cdot cos\left(2\pi \frac{k}{N}\right) \right] \tag{4.34}$$

Where:

V_{real} is the real part of the fundamental V;

V_{imag} is the imaginary of the fundamental V;

S_k is the sample values of v(t);

N is the samples per cycle of sinusoidal voltage;

The fundamental components of the voltage and current could be extracted by using DFT to calculate the impedance.

4.8 Power swing to distance relay

When a power system is under its steady-state conditions, there is an equilibrium between the input mechanical torque and the output electrical torque of each of the generators that are connected to that power system [127]. Under steady-state condition, the system frequency and voltage on a 60Hz system normally varies by less than ±0.02Hz and ±5% of nominal voltage [128, 129]. All synchronous machines are operated at the same constant speed. There is a balance between the generated power and consumed power, both active and reactive.

A sudden change in the power system, such as power system transmission line fault, line switching, generator disconnection and the loss of load may result in breaking the balance and causing a system disturbance [127-129]. These disturbances can

cause oscillations in machine rotor angles and result in power flow swings. These power swings affect transmission distance relays and lead to changes in the relay measuring voltage and current. The apparent impedance seen by distance relay, may in extreme conditions enter the protection zones and cause the relay to trip rather than true fault as shown in fig.4-18 [130].

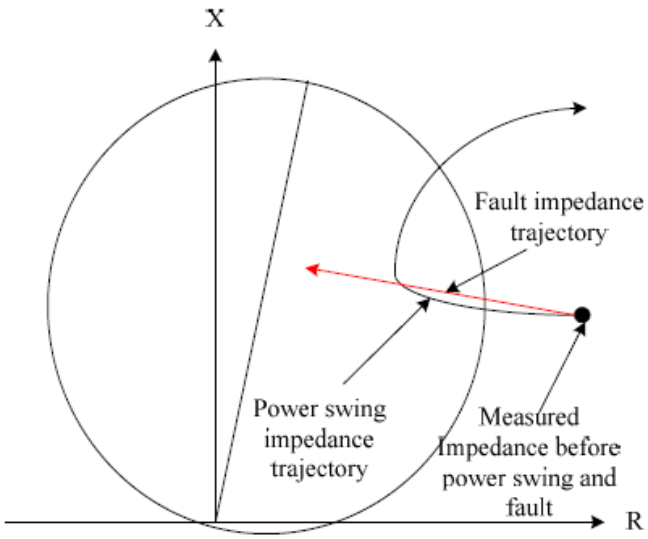

Figure 4-18 Typical fault impedance seen by distance relay during power swing [130]

Fig.4-19represents a two machine power system used to analyse the impedance seen by distance relay during power swing [127, 128, 131, 132].

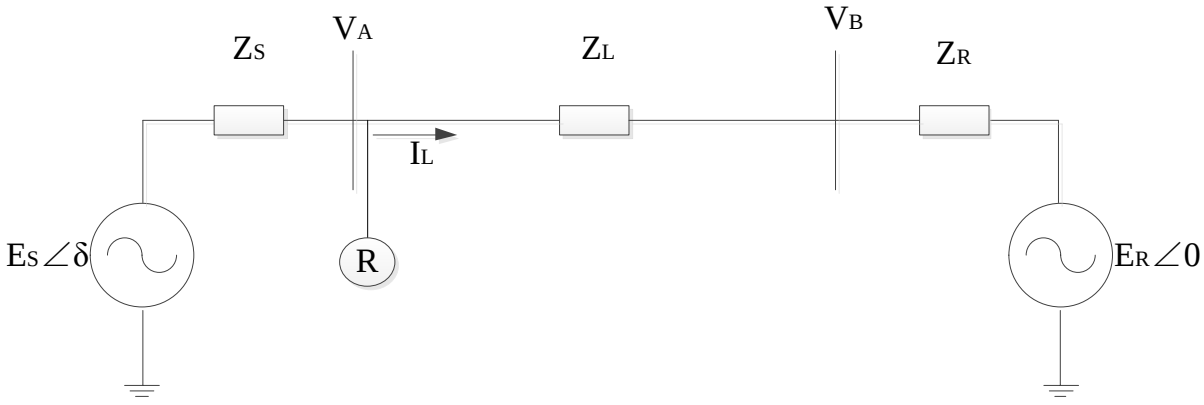

Figure 4-19 Two machine power system

E_S and E_R are the internal voltages of the two machines. Z_S and Z_R are the transient impedances. Z_L is the transmission line impedance. A distance relay is set at bus A

to protect line AB. As can be found from fig.4-19, the current at relay can be calculated as:

$$I_L = \frac{E_S\angle\delta - E_R\angle 0}{Z_T} \tag{4.35}$$

The impedance seen by relay is:

$$Z = \frac{V_A}{I_L} = \frac{E_S\angle\delta - I_L Z_S}{I_L} = \frac{E_S\angle\delta}{I_L} - Z_S \tag{4.36}$$

Combining equation 4.35 and 4.36 can get:

$$Z = \frac{E_S\angle\delta}{E_S\angle\delta - E_R\angle 0} Z_T - Z_S \tag{4.37}$$

Define:

$$k = \left|\frac{E_S}{E_R}\right| \tag{4.38}$$

Then equation 4.37 becomes:

$$Z = \left(\frac{1}{1-k\angle-\delta}\right) Z_T - Z_S \tag{4.39}$$

When k=1, equation 4.39 finally becomes:

$$Z = -Z_S + \frac{Z_T}{2}\left(1 - jcot\frac{\delta}{2}\right) \tag{4.40}$$

When δ=180°, cot(δ/2) equals 0, therefore $Z=-Z_S+Z_T/2$. Z is at the mid-point of line AB which is called the electrical centre, as shown in fig.4-20 (a) [128]. For a stable power swing, the impedance trajectory shifts direction when δ increases/decreases to maximum/minimum value [131, 132]. When k=1, the impedance trajectory is a straight line. If k≠1, the impedance trajectory follows an arc of circle as shown in fig.4-20 (b).

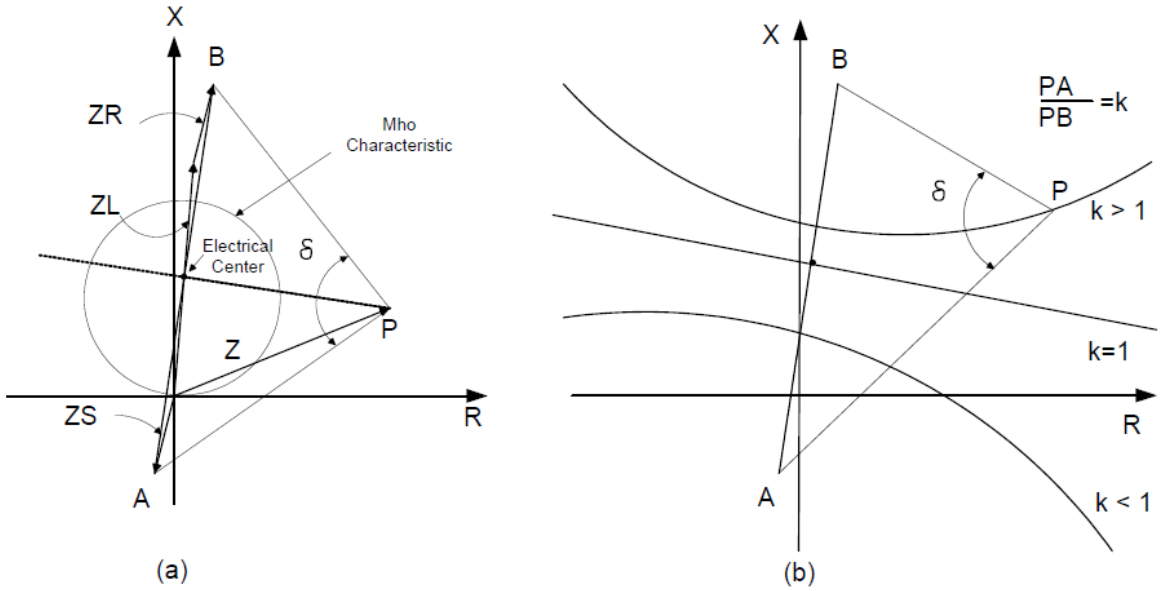

Figure 4-20 Impedance trajectories during power swing [128]

The impedances along this trajectory may pass through the protection characteristic leading to relay tripping.

4.9 Chapter Summary

This chapter first described protective relays and their objectives. It then reviewed the distance relay technologies in detail including the principle of distance relay and protection zones.

The distance relay compares the apparent impedances to the pre-set protection characteristic to determine whether a fault exists on the protected feeder or not. The distance relay trips when the fault is within the protection zones, otherwise does not trip.

The distance relay typically has three zones, normally set to 80%, 120% and 250% of the protected lines. Each protection zone is associated with time delay: 0ms for zone1, 200-500ms for zone2, and 1.0-2.5s for zone3

The calculations of single phase to ground fault, phase to phase to ground fault, phase to phase fault and three phases fault were described in detail. For single phase

to ground fault, the fault impedance is calculated by the fault phase voltage and current plus the zero-sequence current compensation. The phases fault impedance is calculated by the fault phases voltages and currents.

The Mho characteristic distance relay uses the representation impedance of the line to set the diameter of the circle and the angle of displacement of the diameter from the R-axis to create the protection zones. The Mho characteristic distance relay compares the angle between the two inputs signals, which are V and IZ-V. The distance relay operates when the angle is between -90° and 90°.

Block-average comparators are used in distance relay to measure the coincidence of the input signals. The polarity coincidence of the inputs signals causes the block-average comparators to trip when between -90° and 90°.

The measured fault voltage and current signals must be filtered before they input into the distance relay. The fault voltage and current contain the dc components, a large amount of unwanted harmonics, high frequency oscillation quantities, etc. These unwanted components may affect the distance calculating algorithms accuracy and delay the calculating time and lead to false tripping. DFT is used to obtain the fundamental phasor's information. Low-pass filters are used to remove any unwanted high frequency components. Although the relay is designed to detect fault conditions, disturbances may also cause tripping.

A sudden change, such as power system transmission line fault, line switching, generator disconnection and the loss of load in balanced power system, may result in breaking the balance and causing major system disturbances. During power system dynamic conditions, the measured voltage and current at relay location changes. These voltage and current changes may cause the apparent impedance enter the distance relay protection zones and lead to the distance relay trip. Any unwanted trip accelerates the system disturbance and may cause major blackout.

Chapter 5

HVDC Modelling and Testing

The HVDC system was studied and simulated in this chapter using MATLAB/SIMULINK.

5.1 CSC HVDC Control System

In a HVDC system, the primary functions of the dc control are to [133]:

- Control power flow between the terminals;
- Protect the equipment against the voltage/current stresses caused by faults;
- Stabilize the attached ac systems against undesirable operational mode of the dc link.

Each converter has its own local controllers. The master control communicates to each terminal and has the responsibility to coordinate the control functions of the dc link [133]. Besides the primary control functions, the HVDC control system should satisfy the following features [82, 133]:

- Limitation of the maximum DC current to protect the thyristor valves;
- Maintaining maximum DC voltage in the link to reduce transmission losses;
- Minimization of reactive power consumption by operating the converters at a low firing/extinction angle;
- Cope with steady-state and dynamic requirements of DC link.

5.1.1 Basic Control Principles

Fig.5-1 (a) presents a monopolar HVDC scheme or one pole of a bipolar HVDC link [68, 70]. The corresponding equivalent circuit and voltage profile are presented in fig.5-1 (b) and (c) respectively. The basic control principles are based on a six-pulse Garetz Bridge as discussed below.

The DC current, I_d, following from rectifier side to inverter side can be calculated as [68, 70, 82, 134]:

$$I_d = \frac{U_{d0r}\cos\alpha - U_{d0i}\cos\gamma}{R_{cr}+R_L-R_{ci}} \quad (5.1)$$

Where:

I_d is the direct current;

U_{d0r} is the ideal no-load direct voltage at the rectifier;

U_{d0i} is the ideal no-load direct voltage at the inverter;

α and γ is ignition angle at rectifier and extinction angle at inverter;

R_{cr} and $R_{ci}$is commutating resistances of rectifier and inverter respectively;

R_L is the DC line resistance.

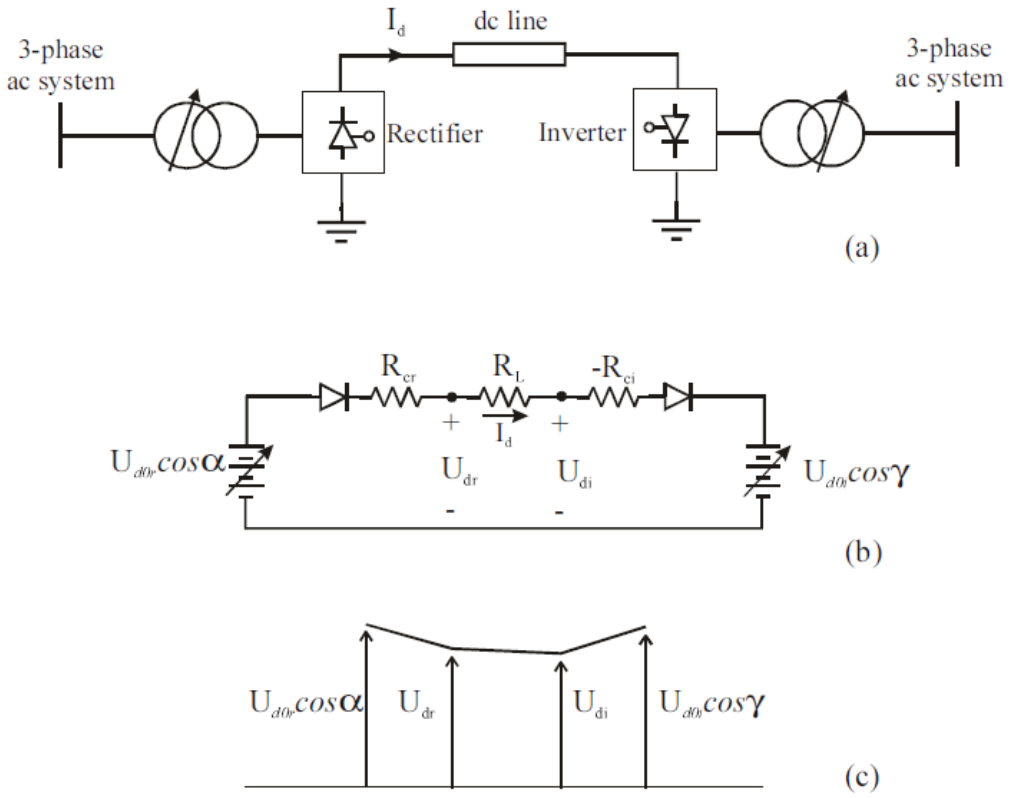

Figure 5-1 HVDC transmission link [59, 61]

(a) the HVDC scheme; (b) the equivalent circuit; (c) the voltage profile

The power transmitted at rectifier terminal is given by [68]:

$$P_{dr} = V_{dr} I_d \quad (5.2)$$

And at the inverter terminal is:

$$P_{di} = V_{di} I_d = P_{dr} - R_L I_d^2 \tag{5.3}$$

The ideal no-load DC voltage, V_{d0}, can be calculated as [68]:

$$V_{d0} = \frac{3\sqrt{2}}{\pi} E_{LL} = 1.35 E_{LL}$$

$$= \frac{3\sqrt{6}}{\pi} E_{LN} = 2.34 E_{LN}$$

$$= \frac{3\sqrt{3}}{\pi} E_m = 1.65 E_m \tag{5.4}$$

Where:

E_{LL} is the AC RMS value of Line-to-Line voltage;

E_{LN} is the AC RMS value of Line-to-Neutral voltage;

E_m is the AC Peak Value of Line-to-Neutral voltage

From equation 5.1, it is found that the only way to change the DC line current is by changing no-load voltages V_{d0r} or V_{d0i} and via changing valve angles α at rectifier or γ at inverter. A voltage change could be achieved by a converter transformer tap changer, which is usually a slow process as by a valve angle change which is very fast, normally within one-half cycle, and achieved by controlling the electronics [82, 133]. Control of the valve angle is used for rapid action and is then followed by tap changing to restore the converter quantities to their normal range [70]. Because the line and converter resistances are small and therefore, a small change in V_{d0r} or V_{d0i} results in a large change in I_d [68]. For instance, a 25% change in voltage could lead to current change as much as 100% [68].

The relations between average DC voltage when firing delay angle is equal to α, V_d, and ideal no-load voltage can be presented as [68]:

$$V_d = V_{d0} \cos \alpha \tag{5.5}$$

Since α ranges from 0° to 180°, V_d can range from V_{d0} to $-V_{d0}$. V_{d0} represents rectification while $-V_{d0}$ represents inversion [68].

The DC current I_d and ac line current RMS value I_L can be related as:

$$I_L = \frac{\sqrt{6}}{\pi} I_d = 0.78 I_d \tag{5.6}$$

5.1.2. Rectifier Operation

During the converter process, the phase currents cannot change instantly due to the inductance L_c of the ac source. There is commutation time or overlap time when transferring current from one phase to another [68, 135]. The overlap or commutation angle, μ, is in range of 15° to 25° under normal operation [68]. Fig.5-2 gives the rectifier equivalent circuit. R_{cr} is the equivalent commutating resistance.

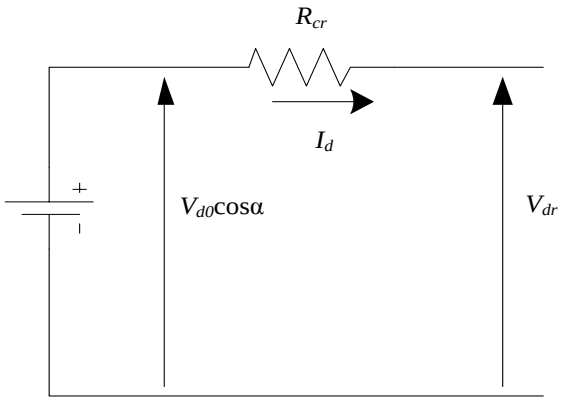

Figure 5-2 Rectifier equivalent circuit

The voltage drop caused by overlap in the rectifier is presented as:

$$\Delta V_d = R_{cr} I_d \tag{5.7}$$

R_{cr} can be calculated as:

$$R_{cr} = \frac{3}{\pi} \omega L_{cr} = \frac{3}{\pi} X_{cr} \tag{5.8}$$

Where X_c is the commutation reactance.

The voltage drop can also be represented by the corresponding overlap angle, which is [68]:

$$\Delta V = \frac{V_{d0}}{2} (\cos\alpha - \cos\delta) \tag{5.9}$$

Where:

α is the ignition delay angle;

δ is the extinction delay angle which equals α+μ.

From fig.5-2, the direct voltage output from rectifier with commutation overlap and ignition delay is represented by [57, 68, 73, 133, 135]:

$$\begin{aligned} V_d &= V_{d0}\cos\alpha - \Delta V_d \\ &= V_{d0}\cos\alpha - R_{cr}I_d \\ &= V_{d0}\frac{\cos\alpha+\cos\delta}{2} \end{aligned} \tag{5.10}$$

5.1.3. Inverter Operation

Without commutation overlap, V_d reverses when α=90°.

With overlap, $V_d = V_{d0}\cos\alpha - \Delta V_d$.

When describing the inverter, the same angles as presented in the rectifier but between 90° and 180° are used [68].

- β is the ignition advance angle which equals π-α,
- γ is the extinction advance angle which equals π-δ,
- μ is the overlap angle which equals δ-α or β-γ.

Equation 5.10 then can be described as [68, 73, 133, 136]:

$$V_d = V_{d0}\cos\gamma - R_{ci}I_d \tag{5.11}$$

Where R_{ci} is the inverter equivalent commutating resistance, which is:

$$R_{ci} = \frac{3}{\pi}\omega L_{ci} = \frac{3}{\pi}X_{ci} \tag{5.12}$$

Fig.5-3 gives the equivalent inverter circuit [68, 133].

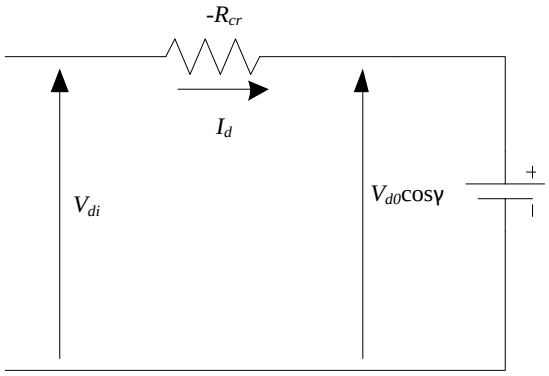

Figure 5-3 Equivalent inverter circuit

5.1.4. Power Factor

Neglecting the power loss in converter station, the ac power is equal to dc power, therefore,

$$3E_{LN}I_L \cos \Phi = V_d I_d \tag{5.13}$$

Where:

E_{LN} is the RMS value of the line-to-neutral voltage;

I_L is the RMS fundamental frequency current;

Φ is the angle where the fundamental line current lags the line-to-neutral source voltage

Combining equation 5.4, 5.10 and 5.13 gives:

$$3E_{LN}I_L \cos \Phi = \frac{3\sqrt{6}}{\pi}\frac{\cos \alpha + \cos \delta}{2} E_{LN} I_d \tag{5.14}$$

Equations 5.6 and 5.14 together can get:

$$(3E_{LN}\frac{\sqrt{6}}{\pi}I_d)\cos \Phi = (\frac{3\sqrt{6}}{\pi}E_{LN}I_d)\frac{\cos \alpha + \cos \delta}{2} \tag{5.15}$$

Hence the power factor of the fundamental wave is:

$$\cos \Phi = \frac{\cos \alpha + \cos \delta}{2} \tag{5.16}$$

From equation 5.9, 5.10 and 5.16 can get:

$$\cos \Phi = \frac{V_d}{V_{d0}} \tag{5.17}$$

The reactive power consumed by converter is then given by[73, 134]:

$$Q = P \tan \Phi \tag{5.18}$$

The power factor should be kept high to minimize reactive power consumption. To achieve a high power factor, α and γ should be kept as low as possible accepting that α has a minimum limit of 5° [68, 70]. Normally the rectifier operates at α between 15° to 20° in order to leave some room for increasing rectifier voltage to control the dc power flow [68]. The inverter's γ angle operates within an acceptable margin, typically 15° for 50Hz system and 18° for 60Hz system [68]. Normally the reactive power consumed by converters is 50%-60% of transmitted DC power [68, 73].

5.1.5. Multiple Bridge Converters

In practice, two or more bridges are connected to achieve a high direct voltage. Normally two bridges are connected in series to form a 12-pulse converter. The equivalent circuit is shown in fig.5-4 [68].

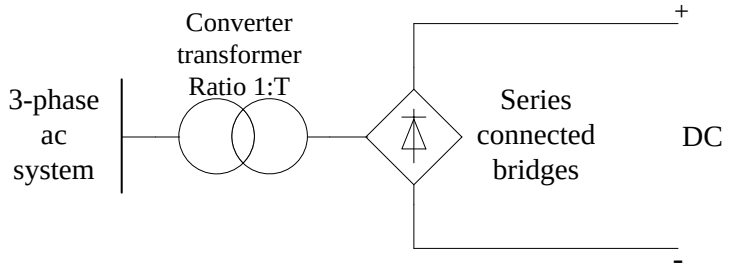

Figure 5-4 Equivalent circuit of multiple connected bridges HVDC

According to [68, 137], the ideal no-load voltage is:

$$V_{d0} = \frac{3\sqrt{2}}{\pi} N T E_{LL} \tag{5.19}$$

Where:

N is the number of connected bridges in series;

T is the converter transformer ratio

Corresponding to equation 5.10, the DC voltage is:

$$V_d = V_{d0}\cos\alpha - NR_{cr}I_d \tag{5.20}$$

at the rectifier or,

$$V_d = V_{d0}\cos\gamma - NR_{ci}I_d \tag{5.21}$$

at the inverter.

5.2Control Characteristic

The control philosophy can be analysed in Voltage-Current (V-I) coordinate diagram formed by voltage V_d and current I_d [68, 137]. Fig.5-5 shows the ideal steady state V-I characteristics measured at the rectifier where the rectifier is in CC control mode and the inverter is in CEA control mode. The operating point E is the intersection between the rectifier characteristic (CC) and the inverter characteristic (CEA). The voltage drop is due to line resistance.

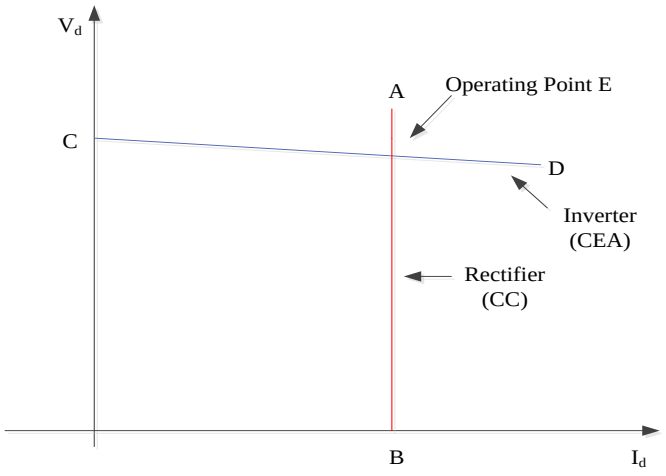

Figure 5-5 Ideal V-I characteristics

From fig.5-1 (b), if the rectifier maintains constant current, and the direct voltage is:

$$V_d = V_{d0i}\cos\gamma + (R_L - R_{ci})I_d \tag{5.22}$$

If $R_{ci} > R_L$, the characteristic, as shown in fig.5-5, has a small negative slope due to voltage drop across the line. The operating point has to satisfy both the rectifier and inverter.

The actual control characteristic is shown in fig.5-6 [68, 70, 133]. In actual operation, the rectifier keeps a constant current (CC) by varying α as shown in fig.5-6 AB. The inverter operates in a constant extinction angle mode (CEA) to maintain voltage as shown in fig.5-6. The normal operating point E in fig.5-6 is an intersection between the rectifier characteristic (CC) and the inverter characteristic (CEA).

Under normal operation, the rectifier variesα to keep the current constant (CC control mode). When α is hitting its minimum limitation, the direct voltage cannot increase further. Then the rectifier changes to a constant ignition angle mode (CIA). In fig.5-6, AB represents the CC mode and FA represents the CIA mode. Similarly, the inverter maintains direct voltage under a constant extinction angle mode (CEA) during normal operation.

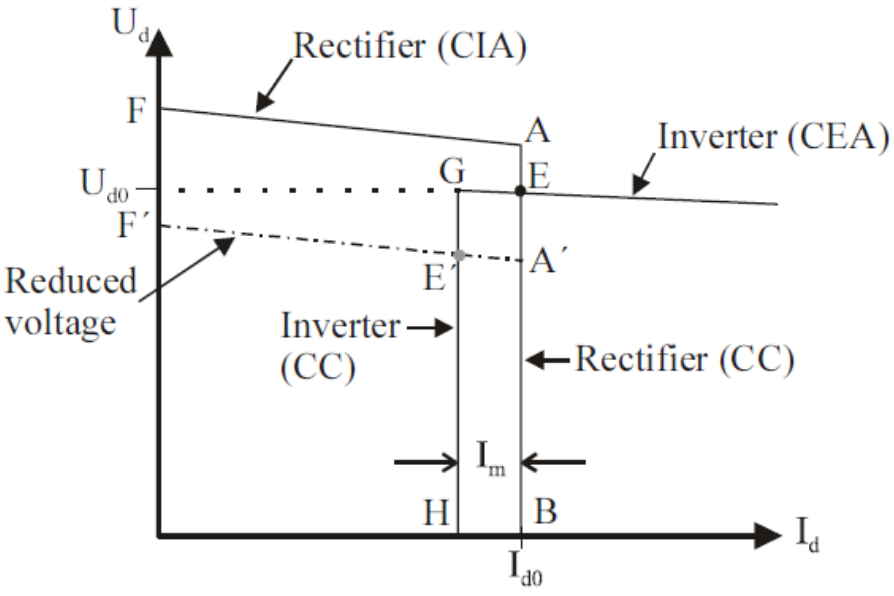

Figure 5-6 Actual operation characteristic [59, 61, 125]

The inverter CEA characteristic intersects the rectifier characteristic at E during normal operation. However, the inverter CEA characteristic does not intersect the rectifier characteristic when the voltage decreases, shown as F'A' in fig.5-6. Therefore, the inverter is also provided with a current controller. The inverter current

controller is set at a lower value than that set in the rectifier. Under the situation that the voltage is decreasing, the operating point E may not reach the point as shown in fig.5-6 F'A'. In this situation, the inverter changes from a constant current mode to a controlled current mode as shown in fig.5-6 GH. Thus the inverter control characteristic has two modes: CEA and CC.

There is current margin I_m, as shown in fig.5-6 which presents the different current order between the rectifier and the inverter: normally I_m is 10% -15% of the rated direct current [68, 70, 73, 82, 133]. At a reduced voltage situation, the rectifier shifts to voltage control. The new operating point is then represented as point E' in fig.5-6.

The control characteristic can be summarised in the following stages. Under steady-state operation, when there is a voltage drop on the rectifier side of the ac bus, FA moves down to F'A'. The operating point changes from E to E'. The inverter shifts to current control while the rectifier controls voltage. The current transmitted would be reduced to 0.9 pu due to the current margin. The power transmission would be maintained to 0.9 pu of its original value.

HVDC systems are required to be able to reverse the power flow, which means both converters should be able to operate either as a rectifier or an inverter [70, 73]. Fig.5-7 shows the combined rectifier-inverter characteristics. Fig.5-7 (a) shows the power flow from converter 1 to converter 2 while (b) shows the power flow from converter 2 to converter 1.

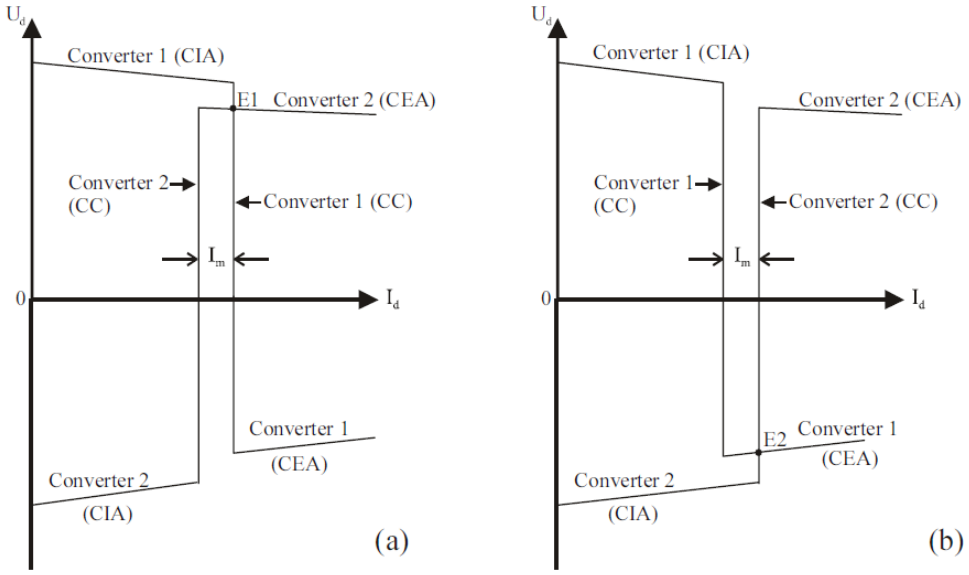

Figure 5-7 Combined rectifier-inverter characteristics [61, 63]

5.3 Current Order

There are three current limits that need to be considered in an HVDC control system. They are: maximum current limits, minimum current limits and Voltage Dependent Current Order Limit (VDCOL) [68, 70, 73, 133, 137, 138].

5.3.1. Maximum Current Limits

The allowed maximum current is limited to 1.2 to 1.3 times normal full-load current I_d. If the current is higher than the maximum current value will lead to the damaging of the converter valves.

5.3.2. Minimum Current Limits

If the current is too low it may result in the current becoming discontinuous. It is unacceptable due to high voltage induced in transformer windings and dc reactors caused by their inherent inductance and a high rate of current changes. Low values of direct current will also cause small overlaps and extra stress on the valves.

5.3.3. Voltage Dependent Current Order Limit (VDCOL)

Under low voltage conditions, it is difficult to maintain the rated direct current and power. Voltage drops will lead to an increase in current. When the voltage at one converter drops over 0.3 pu, the reactive power demand will increase due to a higher α or γ needed to control the current. Voltage drops can also result in commutation failure and voltage instability. The VDCOL is used to prevent such issues. VDCOL limits the maximum allowable direct current when the voltage drops below a specified value based on piecewise-linear characteristic [68]. Fig.5-8 gives the VDCOL characteristic through the converter V-I characteristic diagram. VDCOL could be a function of either the dc voltage or the ac commutating voltage.

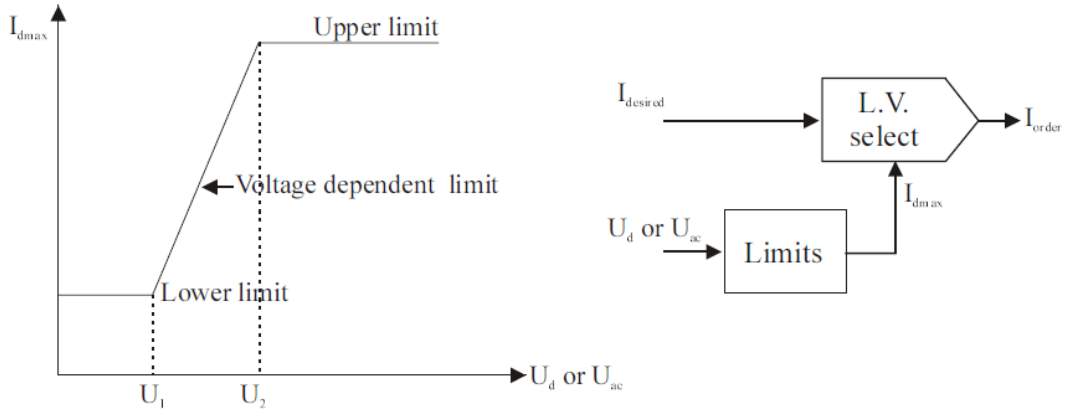

Figure 5-8 VDCOL characteristic [68]

The HVDC control system characteristic combining with VDCOL, CC, CEA and CIA characteristics can be presented in fig.5-9.

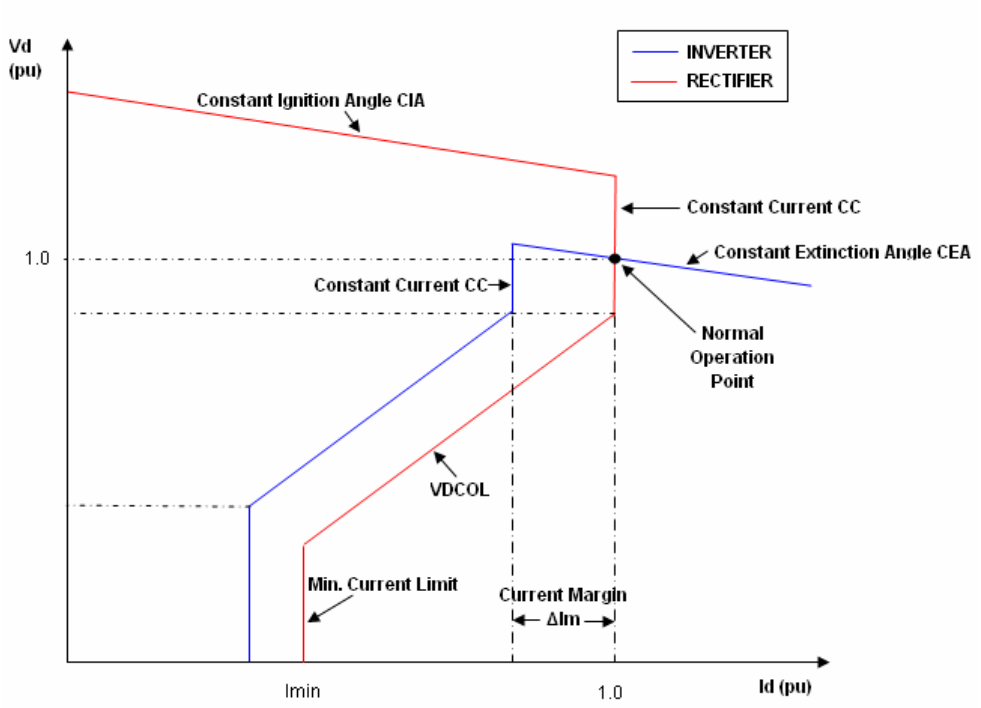

Figure 5-9 Combine HVDC control characteristic [128]

5.4 AC and DC Interaction

The strength of the AC-DC system is expressed by the Short-Circuit Ratio (SCR). It is defined as [68, 73, 138-142]:

$$SCR = \frac{short-circuit MVA of ac system}{dc rated power} \tag{5.23}$$

According to [73, 138], three levels of system strength could be defined by SCR value:

- Strong system when SCR>3,
- Weak system when SCR is between 2-3,
- Very weak system when SCR<2

When considering the reactive power compensation, the Effective Short Circuit Ratio (ESCR) is used, where [73, 138, 140, 142]:

$$ESCR = \frac{S-Q_c}{P_{dc}} \tag{5.24}$$

Where:

S is the short-circuit MVA of ac system;

Q_c is the reactive compensation for HVDC system;

P_{dc} is the rated dc power.

Then the system strength levels are listed as:

- Very strong system when ESCR>5,
- Strong system when ESCR ranges from 2.5 – 5,
- Weak system when ESCR ranges from 1.5- 2.5,
- Very strong system when ESCR<1.5.

A weak AC-DC system may have potential problems including harmonic resonance, voltage instability and frequent commutation failures.

5.5 Response to Fault Conditions

5.5.1 Rectifier side ac fault

A fault at rectifier side will result in decreasing rectifier voltage and current. The current regulator in the rectifier reduces the value of α, to restore current. When α is at the α_{min} limit, the rectifier then switches to CIA control mode and transfers the current control to the inverter [68]. VDCOL will take part when the voltage drops low to regulate the current and power. If a three-phase fault is close to the rectifier, the dc system may shut down until the fault is cleared [68, 73]. An unbalanced fault does not usually cause shut down of dc link.

5.5.2 Inverter side ac fault

If the fault causes a small voltage dip at the inverter, the rectifier CC control and inverter CEA control respond to voltage dip and increase the voltage. If the voltage dip is significant, the reduction may lead to commutation failure at the inverter. For

example, a voltage reduction from 0.15pu to 0.1pu will cause commutation failure when the inverter operated at γ of 18° [68]. The rectifier decreases the direct voltage to match the reduction in the inverter voltage. An extremely low voltage condition caused by an ac fault will lead to commutation failures.

5.6 HVDC system modelling

5.6.1 Simulating Software

The simulation work is done using MATLAB. MATLAB provides highly efficient programming tools for scientific research, engineering design and the other subjects that need valid numerical calculation [143]. MATLAB contains scientific calculation, automatic control, signal processing, neural networks, image processing, etc. It incorporates a large number of domain specific toolboxes such as fuzzy logic toolbox, neural network toolbox, control toolbox, real-time workshop, etc [144]. SIMULINK is an interactive tool for modelling, simulating, and analysing dynamic systems in MATLAB [143]. Its special component library contains Communications Block set, DSP Block set, Sim Power Systems, Neutral Network Block set and etc [145]. Within these it provides basic blocks from its built-in blocks library, which include continuous, discrete, nonlinear etc., for users to build specific systems. SIMULINK has some features that include modularization, overload, encapsulation, programme facing the structure diagram, and visualization [143]. These features make MATLAB/SIMULINK more efficient, reliable and more attractive for power systems-related research.

The power system block (PSB) allows power system simulation in MATLAB. It targets the three-phase power system simulation[145]. PSB provides users the commonly used electrical models which include electrical sources, elements, power electronics, machines, connectors, measurements, extras, demos and powergui [144]. These models can be used directly to build up the target systems that users want and added to a required system for measurement and test.

5.6.2 HVDC modelling and study

Kundur [68] describes a two area system consists an HVDC interconnection and an HVAC interconnection which is also discussed by Klein etc. [146] as shown in fig.5-10. The details of the two area system are shown in Appendix. A.

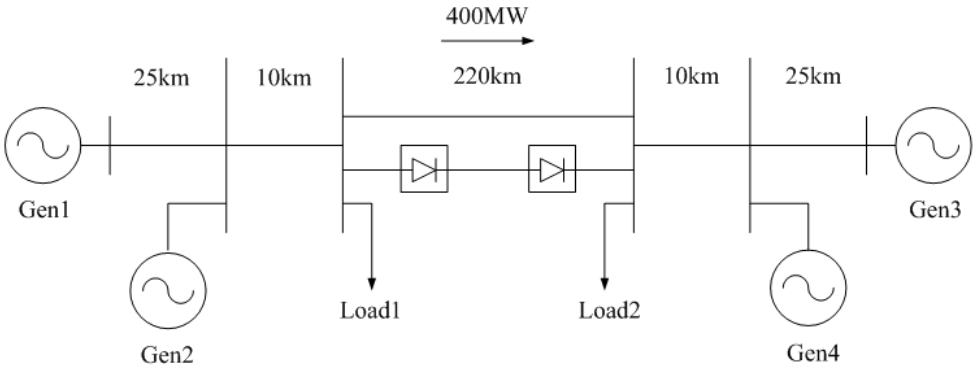

Figure 5-10 The Kundur's two area power system [68]m

This HVDC link is a 200 MW monopolar dc link with a voltage rating of 56kV and a current rating of 3600 A. The dc line resistance is 1.5 Ω and inductance is 100 mH. The commutating reactance is 0.57 Ω associated with each converter. A smoothing reactor is used at each end of the line with the value of 50 mH. Reactive power support is 125 MVAr at both the rectifier and the inverter side.

Under normal operation, the rectifier controls the current while the inverter controls voltage. The ignition delay angle α is limited between 5° to 180° at the rectifier. The extinction advance angle γ is limited between 17° to 70° at the inverter. Under normal conditions, the inverter is on constant extinction angle (CEA) control represented as:

$$\cos\alpha = \frac{6X_c I_d}{\pi V_{d0}} - \cos\gamma \qquad (5.25)$$

Current order is limited by the VDCOL function shown in fig.5-11 below.

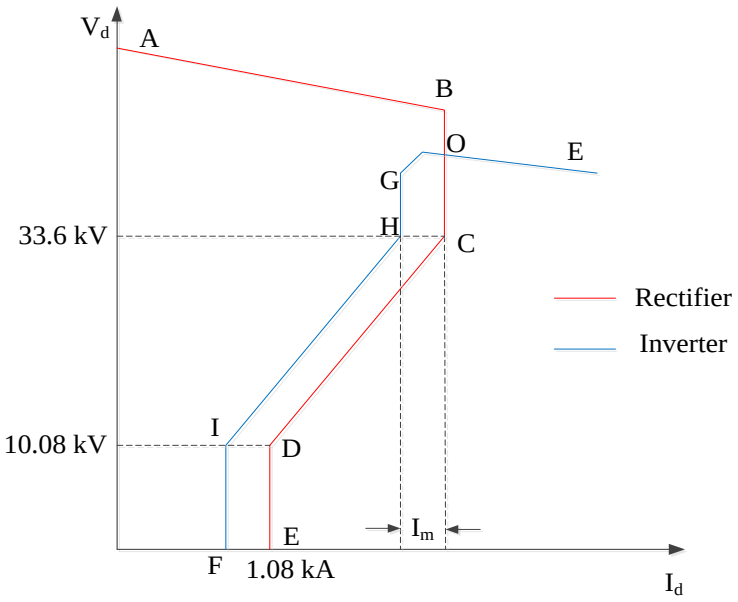

Figure 5-11VDCOL function

From fig.5-11, AB represents rectifier CIA control. BC represents rectifier CC control. CDE represents VDCOL function in rectifier. OE represents inverter CEA control. GH represents inverter CC control. HIF represents the inverter VDCOL function. I_m presents the current margin, which is set to 0.36 kA.

The HVDC link has been simulated in MATLAB/SIMULINK based on the HVDC demo from [147, 148]. The HVDC link connects a 230 kV, 9000 MVA ac system to an infinite bus as shown in fig.5-12. The modelled system was based on the HVDC example in [68]. The AC line parameters are shown in table.5-1 [68]. System frequency was 60 Hz.

r_1	x_1
0.053Ω/km	0.531 Ω/km

Table 5-1 AC Line Parameters [68]

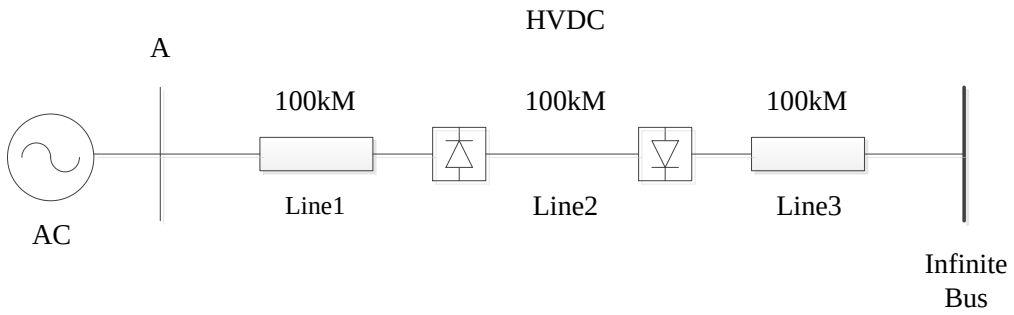

Figure 5-12 Modelled system

The results from a series of simulation tests are shown in figures 5-13 to 5-19. The DC voltage and current were measured in pu value and displayed against the time axis.

5.6.3 HVDC Link Operated in Steady-state

Fig.5-13 shows the steady-state dc voltage and current. At t=0.02s the HVDC link was started by ramping the reference current. The DC voltage and current then started to build. The HVDC link began charging. At t=0.4s the reference current ramped to 1 pu (3.6kA). The DC current reached 1 pu at t=0.6s and reached steady-state at t=1.2s. DC voltage went steady-state at around t=1.0s. The system was simulated for 3 seconds. DC voltage and current are measured at the rectifier.

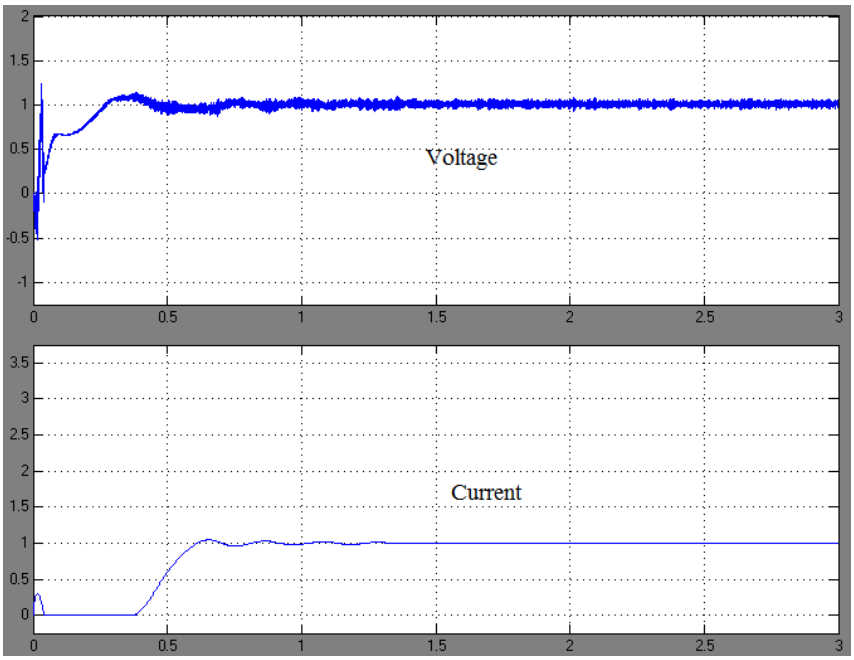

Figure 5-13Steady-state DC voltage and current in pu

5.6.4 HVDC Response to DC Line Fault

The response to a DC line fault which occurred at 50km from 1.5s-1.6s, is shown in fig.5-14 and 5-15.The DC voltage and current are measured at the rectifier.

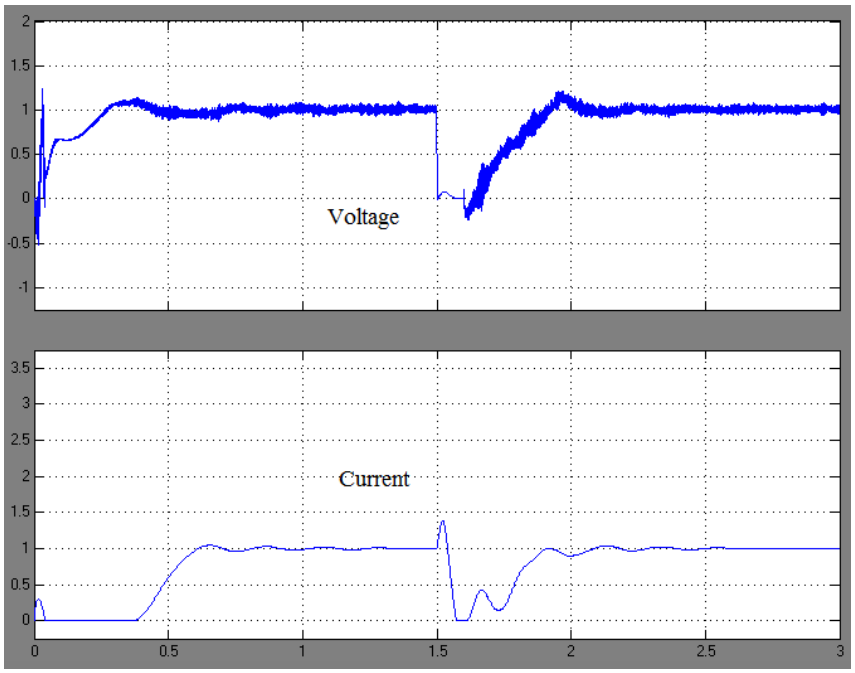

Figure 5-14 DC voltage and current response to a DC line fault at 50km from 1.5s-1.6s

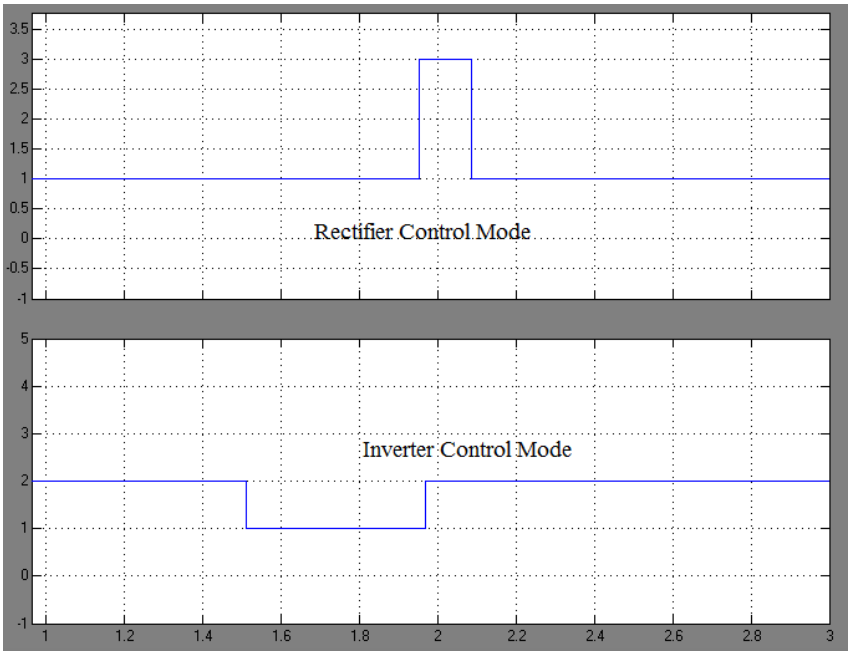

Figure 5-15 Rectifier and Inverter control mode during the DC line fault at 50km from 1.5s-1.6s

As shown in fig.5-14, at t=1.5s, the DC line voltage sudden decreased to zero. This corresponds to the inverter changing to CC control mode and attempting to maintain the DC power, as also seen in fig.5-15. There was a sudden increase in DC current due the converter operations. The current decreased to zero as the valves were blocked due to the fault.

At t=1.6s, the fault cleared. The DC voltage and current increased to the rated power. At around t=2.0s, the DC voltage was restored to its rated value. The inverter changed back to voltage control mode at around t=1.9s while the rectifier changed to CIA mode giving a higher converter voltage. The rectifier changed back to normal current control mode at t=2.1s. Both the DC voltage and current were at the steady-stable state at t=2.5s.

5.6.5 HVDC Response to Three-phase-to-ground Fault at Rectifier Side

A three-phase-to-ground fault at the start point along the line from 1.5s to 1.6s on the rectifier side ac line at the start point, produced the response shown in fig.5-16 and 5-17. The DC voltage and current are measured at the rectifier.

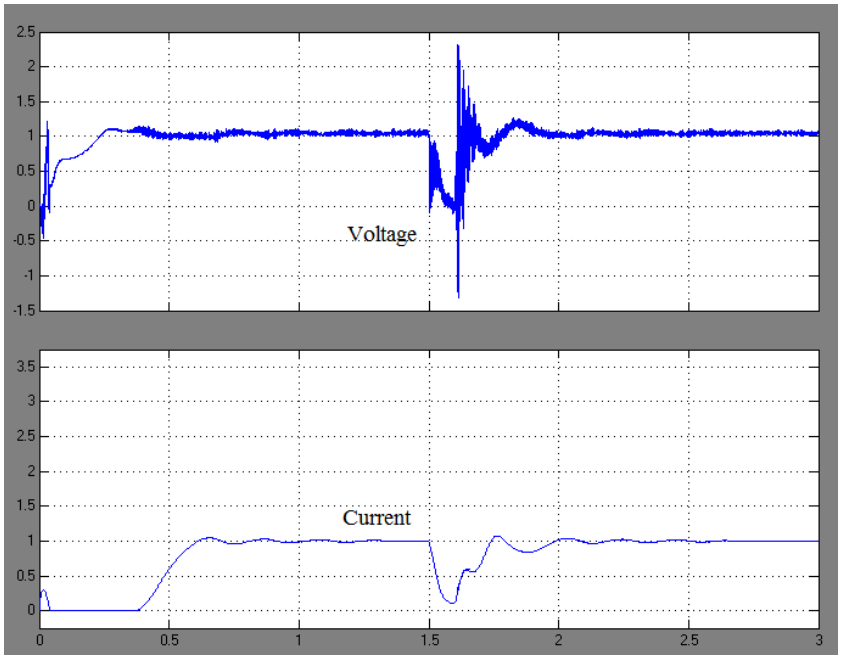

Figure 5-16 DC voltage and current when rectifier side AC three-phase-to-ground fault from 1.5s-1.6s

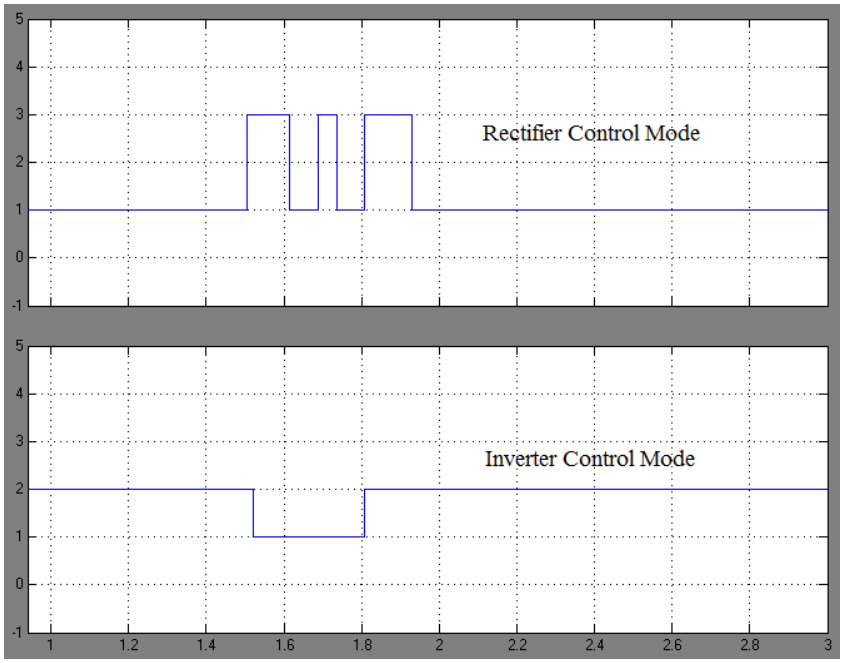

Figure 5-17 Converter control mode during rectifier side AC three-phase-to-ground fault from 1.5s-1.6s

As can be seen from fig.5-16 and 5-17, at t=1.5s when the three-phase-to-ground fault occurred, there was no input voltage or current for the conversion process. The rectifier changed from control mode 1 (CC) to control mode 3 (CIA) and the inverter changed from control mode 2 (Voltage Control) to control mode 1 (CC) and attempted to maintain the DC voltage and current. However, the DC voltage and current decreased to 0.

At t=1.6s the fault was cleared. The conversion process was restored. The rectifier kept CIA control to restore dc voltage. The inverter maintained CC mode to restore the DC current order. At around t=1.8s, the DC power was restored to the pre-fault level. The inverter then changed back to voltage control mode. The rectifier kept CIA mode to ensure that the DC voltage level was restored. Around t=1.9s, the rectifier changed back to CC mode. At around t=2.2s, the DC link was stable.

5.6.6 HVDC Response to Three-phase-to-ground Fault at Inverter Side

When a three-phase-to-ground fault occurred from 1.5s-1.6s on the inverter side ac line at the end, the response was shown in fig.5-18 and 5-19.The DC voltage and current were measured at the rectifier.

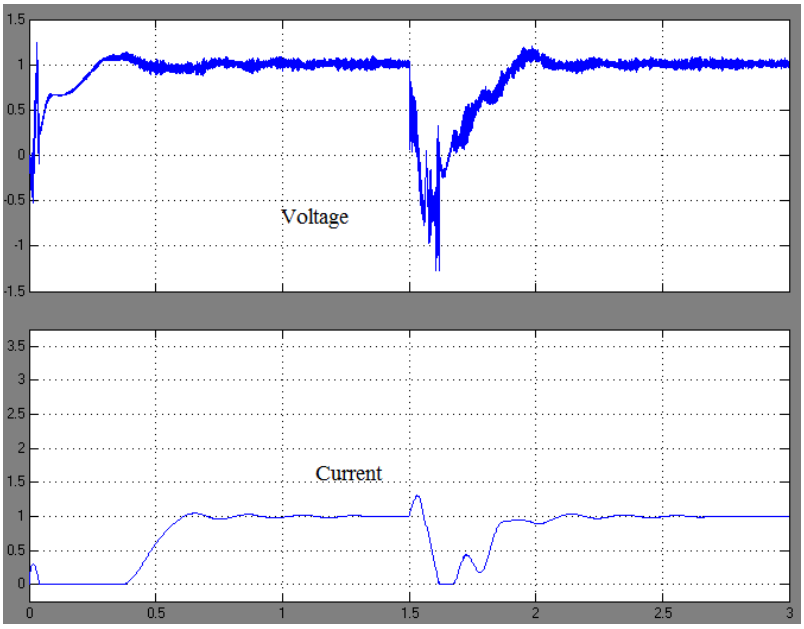

Figure 5-18 DC voltage and current when inverter side AC three-phase-to-ground fault from 1.5s-1.6s

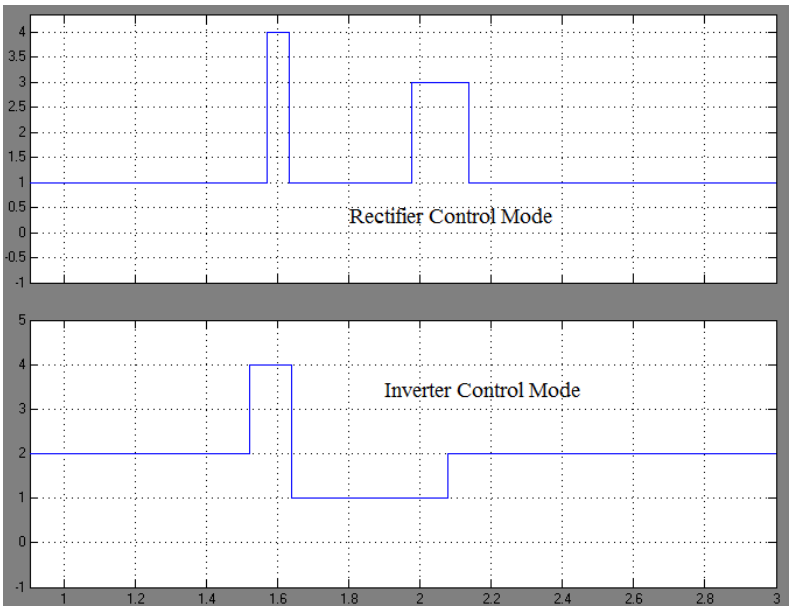

Figure 5-19 Rectifier and Inverter control mode during inverter side AC three-phase-to-ground fault from 1.5s-1.6s

At t=1.5s, after the fault occurred, the DC voltage suddenly decreased to a negative value. The DC current suddenly increased to maintain DC power. Both rectifier and inverter changed to maximum α control mode then. The presence of the fault caused the conversion to be reversed. DC current then decreased to zero.

At t=1.6s, the fault was cleared. Both rectifier and inverter changed to current control mode to restore the voltage and current, and the DC voltage and current increased. The rectifier changed to CIA mode to restore DC line voltage at around t=1.9s. At around t=2.1s, the inverter changed back to voltage control mode. The rectifier changed back to the current control mode at around t=2.15s. The DC link was stable after t=2.5s.

5.7 Chapter Summary

The HVDC interconnection is connected to the AC system by converter transformers associated in the converter stations. The converter stations are installed at both ends of the HVDC terminal. Both converters could operate as a rectifier or an inverter.

The converter stations perform the ac/dc/ac conversion and control the dc power flow through the HVDC link. The dc voltage at any point of the dc line and the dc current along the dc line are controlled by controlling the converter internal voltages $V_{d0}\cos\alpha$ or $V_{d0}\cos\gamma$. This is achieved by varying firing angle.

Under normal operation, the rectifier is under constant current (CC) control and inverter is under constant extinction angle (CEA) control. The HVDC control system has maximum current limitation, minimum current limitation and VDCOL control in case there is an internal dc line fault or a fault on ac system.

During DC line fault, the rectifier current increases while the inverter current decreases. The rectifier current control reduces the voltage and restores the current to its normal value. The inverter changes its control mode from CEA control to CC control to maintain the current.

Under the situation that a fault on the ac network causes an ac voltage reduction on the rectifier side, the rectifier firing angle decreases until hits the α_{min} limit then the rectifier switches to α_{min} control. At this point, the inverter assumes the current control.

Under the situation the fault causes an ac voltage drop in ac system at inverter side, the DC voltage in inverter decreases. This decreasing the inverter DC voltage will lead to a reduction of rectifier direct voltage.

A simple HVDC link from Kundur's two area system was simulated and studied in this chapter [68]. The HVDC response to the fault at both side of the HVDC terminal on ac lines were studied as well as the dc line fault. The tested results were compared with previous works and were proofed that the modelled HVDC link worked as expected. In the following chapters, the HVDC link's impacts on the distance relay will be investigated.

Chapter 6

Distance Relay Modelling and Testing

6.1 Modelling Distance Relay

6.1.1 Measuring and mixing circuit

The distance relay uses IZ and V to determine whether or not a fault exists in a section of the power system, where Z is the replica impedance that is ideally equal to the protected transmission line. Voltage Transformers (VT) and Current Transformers (CT) are used to obtain a replica of the primary voltages and currents with transformer ratios defining the secondary voltages and currents. VTs and CTs are modelled using the ideal transformers from SIMULINK with the ratios of 500kV/110V and 2000A/1A. Fig.6-1 shows the block diagram of the current measuring and mixing circuit as well as the zero-sequence current compensation circuit.

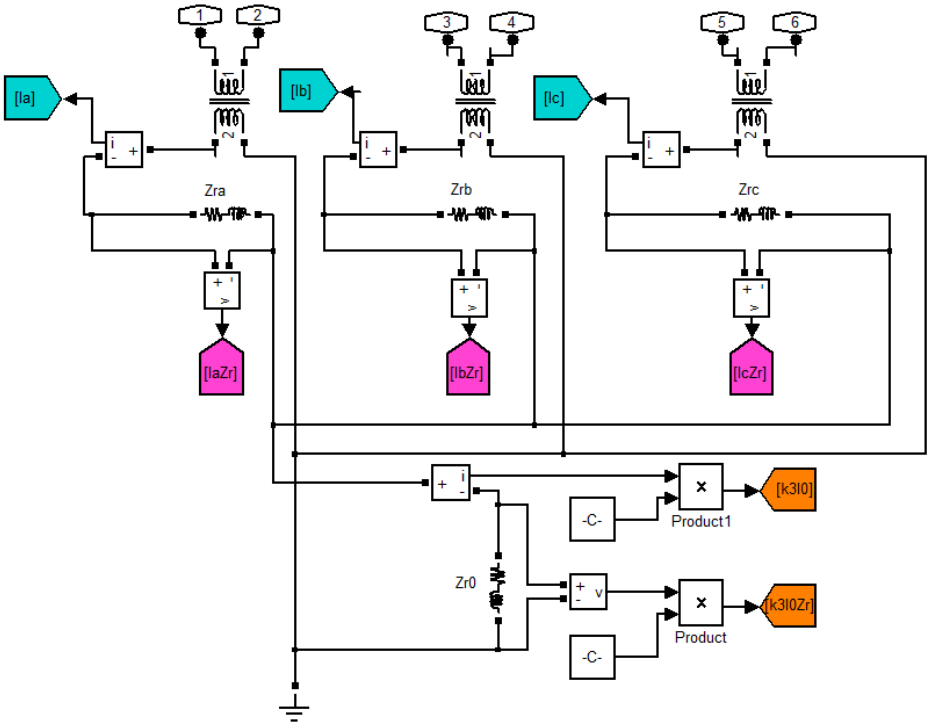

Figure 6-1 Current measuring, mixing circuit and zero-sequence current compensation circuit for a distance relay

The connectors 1 and 2 in the primary of CT connect to transmission line A phase to measure the phase a current. The phase a secondary current is measured by a

current transformer. The positive output of CT secondary winding is connected to the replica impedance to produce IZ_r. A voltage measurement block is used to measure $V=IZ_r$. The negative output of CT secondary winding is connected to ground. Similarly to connectors 3,4 and 5,6. Connectors 3 and 4 are connected to the transmission line B phase to export phase b current. Connectors 5 and 6 are connected to the transmission line C phase to export phase c current. The phase b and c secondary currents are measured by current transformers. The a, b and c phase currents from the replica impedances are connected together to produce $3*I_0$. Then the current is put through neutral replica impedance to generate $3*I_0*Z_{rn}$. A voltage measurement is used to measure $V_n=3I_0Z_{rn}$. The neutral compensation constant value, equals to $(Z_0-Z_1)/3Z_1$, is used together with V_n to produce $k*3*I_0*Z_{rn}$.

The voltage measuring circuit is shown in fig.6-2. Connectors 7, 8 and 9 are connected to transmission line A, B and C phase to measure phase a, b and c voltage separately. The secondary windings of the VTs are connected to voltage measurement directly to measure secondary voltages.

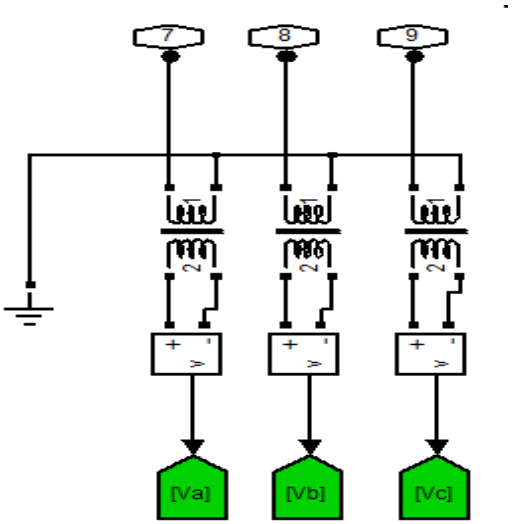

Figure 6-2 Voltage measuring circuit

The measured secondary voltages and currents are passed to the Goto block. The Goto block can pass its inputs to its corresponding From blocks [147, 148]. The inputs can be any data type. The From and Goto block can pass a signal from one block to another without actually connecting them [147, 148].

6.1.2 Simulation of Block-average Comparator

MATLAB logical blocks have been used to simulate the block-average comparator. Fig.6-3 shows the modelled block-average comparator.

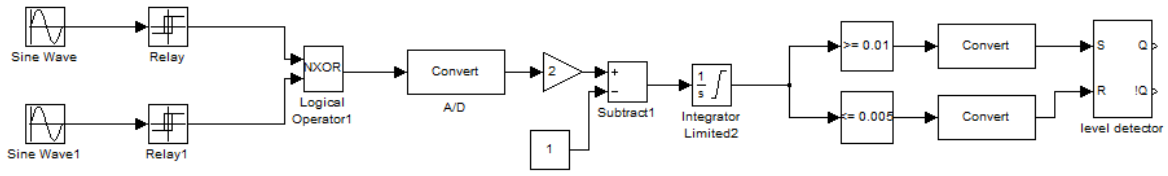

Figure 6-3 Modelled block-average comparator

The Relay block was used to converter sine wave to square wave for comparison in coincidence circuit. This allows its output to switch between two specified values which are set as '1' and '0'. A logical operation block 'NXOR' was used to simulate the coincidence circuit. It outputs a positive pulse when the two input signals are of the same polarity and negative pulse when the two input signals are of the different polarity. This is shown in fig.6-4

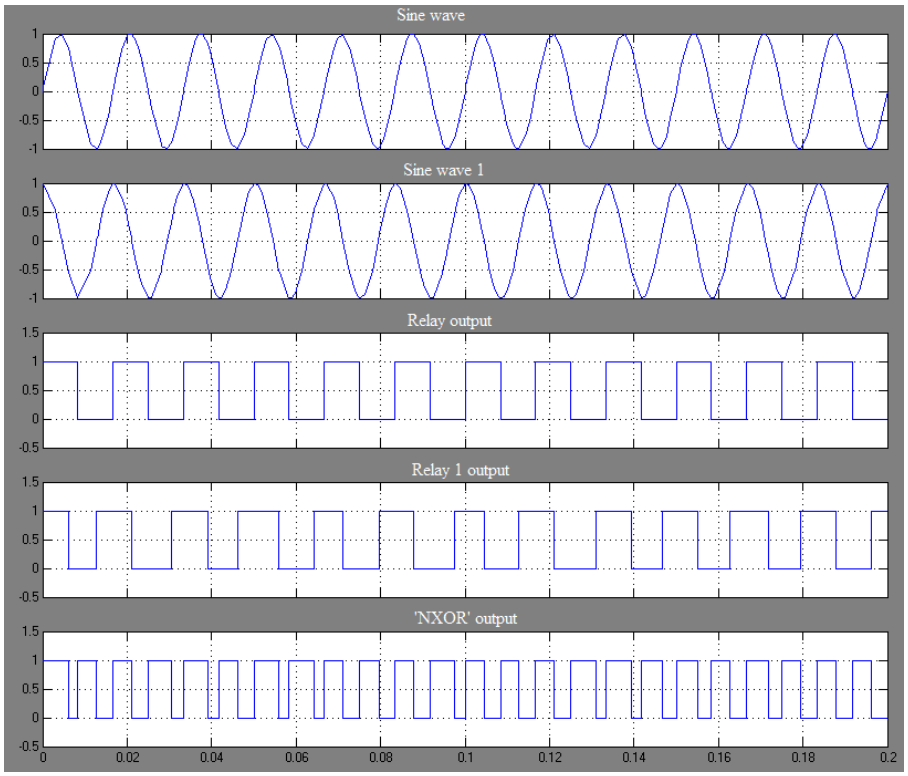

Figure 6-4 Outputs of relay and 'NXOR' block

In fig.6-4, two sine waves @60Hz but 90° different phase angles were used to simulate the power system voltage or current. Simulation duration was 0.2s.

A converter block was used as analogue to digital convertor. An integrator block was used to detect polarity difference and generate trip or reset output signals. The integrator block outputs an increasing linearize when inputting pulse is positive and falling at the same rate when inputting pulse is negative. The integrator's up-limit was set at 0.015 to give a quick response to input pulses. The trip level would be 0.01 and reset level would be 0.005.

The level detector was simulated using the S-R Flip-Flop block. It has two inputs, S and R, and two outputs, Q and !Q. S stands for Set and R stands for Reset[148]. The truth logic of the block is shown in table.6-1 below [148]:

S	R	Q	!Q
0	0	Q_{n-1}	$!Q_{n-1}$
1	0	1	0
0	1	0	1
1	1	0	0

Table 6-1The truth logic of S-R Flip-Flop block [140]

The input signals to S and R were filtered by comparing to trip level (≥0.01) and reset level (≤0.005). When S is 1 and R is 0, the flip-flop goes to the set state (Q is 1). When S is 0 and R is 1, the flip-flop goes to the reset state (Q is 0). When both S and R are 0, the flip-flop stays in the previous state (Qn-1 and !Qn-1). When both S and R are 1, the flip-flop outputs 0.

The block-average comparator compares the phase difference of inputs signals and generates trip signals when -90°≤Θ≤90°. The modelled comparator was tested when Θ=90°, -90°≤Θ≤90° and Θ>90° separately.

6.1.2.1 Trip (when -90°≤Θ≤90°)

For Θ between any angle from -90° to 90°, the block-average comparator trips. Θ=45° was tested. Results are shown in fig.6-5 and fig.6-6.

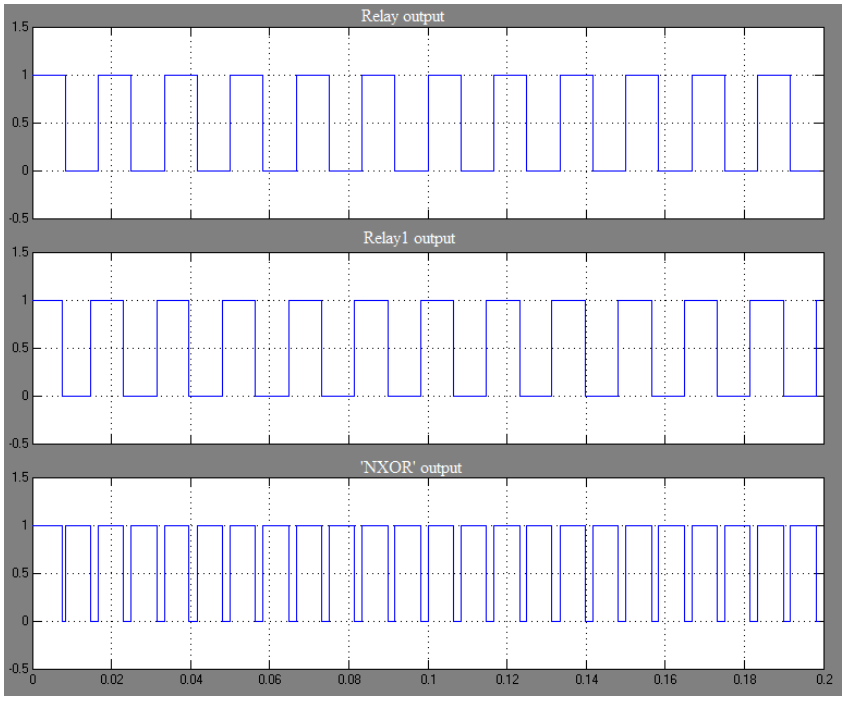

Figure 6-5 Coincidence circuit output

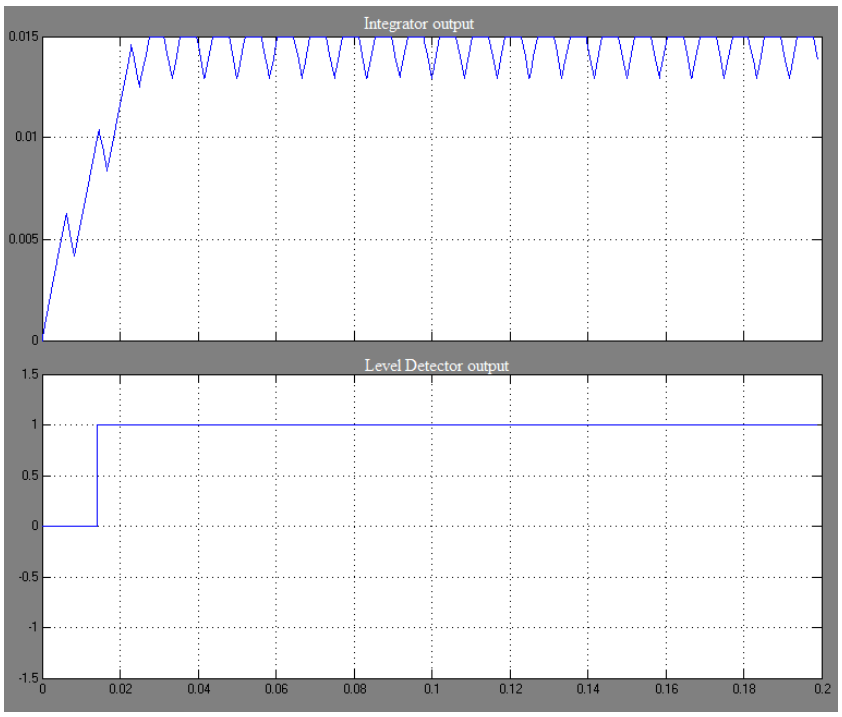

Figure 6-6 Integrator output and trip signal

Fig.6-5 shows the coincidence circuit output while fig.6-6 shows the integrator output and trip signal. The trip level is set at 0.01. As can be seen from the fig.6-6, when integrator pulse increased upper than 0.01, level detector gave a trip signal immediately.

6.1.2.2Restrain (when Θ>90° and Θ <-90°)

The block-average comparator will restrain not trip when Θ>90° and Θ<-90°. A test with Θ=120° was simulated. Results are shown in fig.6-7 and fig.6-8.

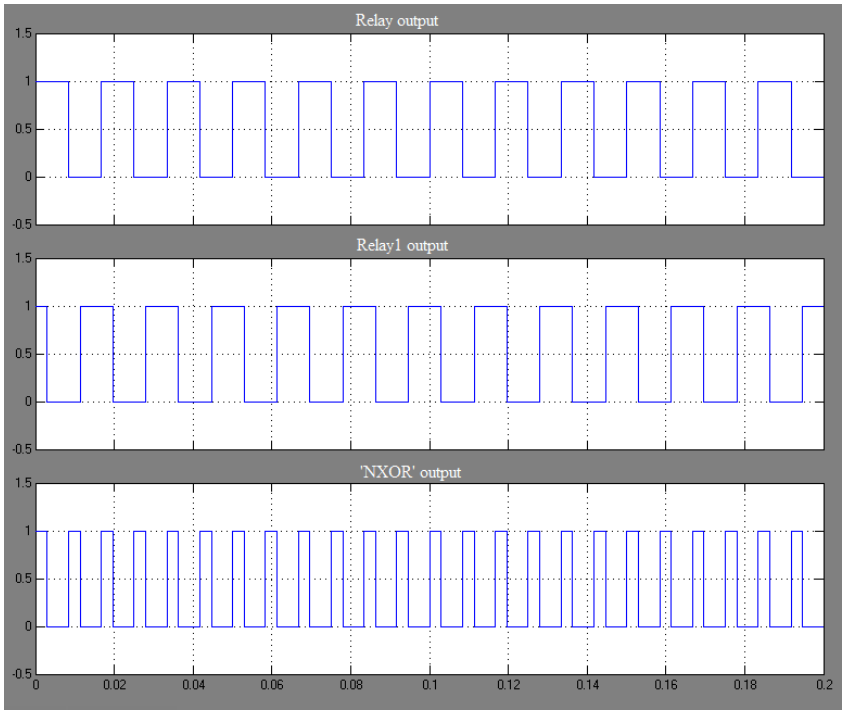

Figure 6-7 Coincidence circuit output

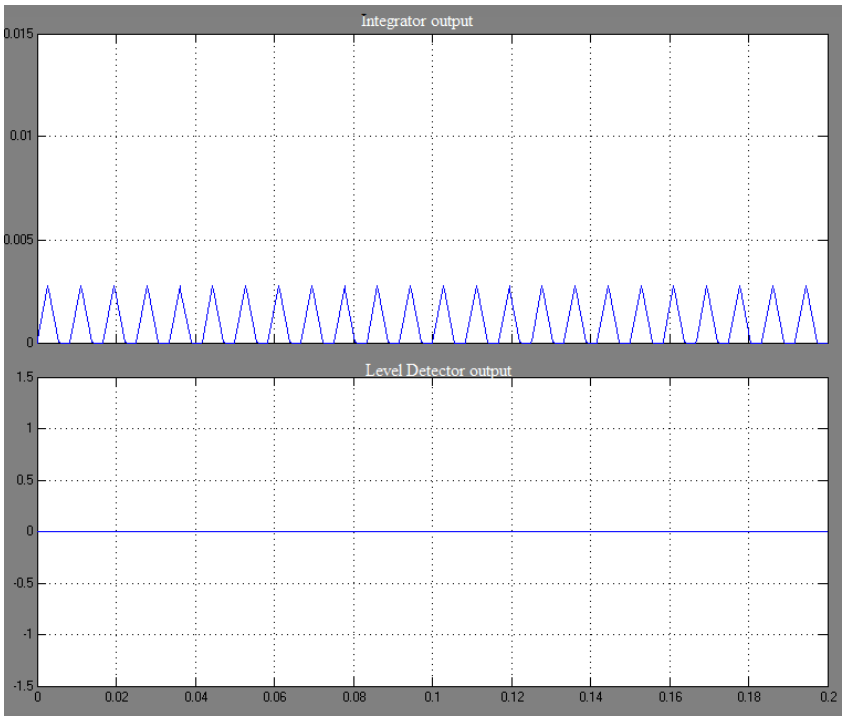

Figure 6-8 Integrator output and trip signal

As can be seen from fig.6-7 and fig.6-8, there was not enough polarity coincidence time for integrator pulse to climb. The increasing time was shorter than decreasing time. The integrator pulse stayed below reset level. Level detector did not trip.

6.1.2.3 Boundary Fault (Θ≈90°)

When the two input sine waves are at 90 degrees different phase angles, it is the boundary of the trip characteristic. The periods of the different polarity between the two sine waves were same. The output of the integrator will cross the trip level in infinite time. Level detector gave a trip signal. Results are shown in fig.6-9 and fig.6-10.

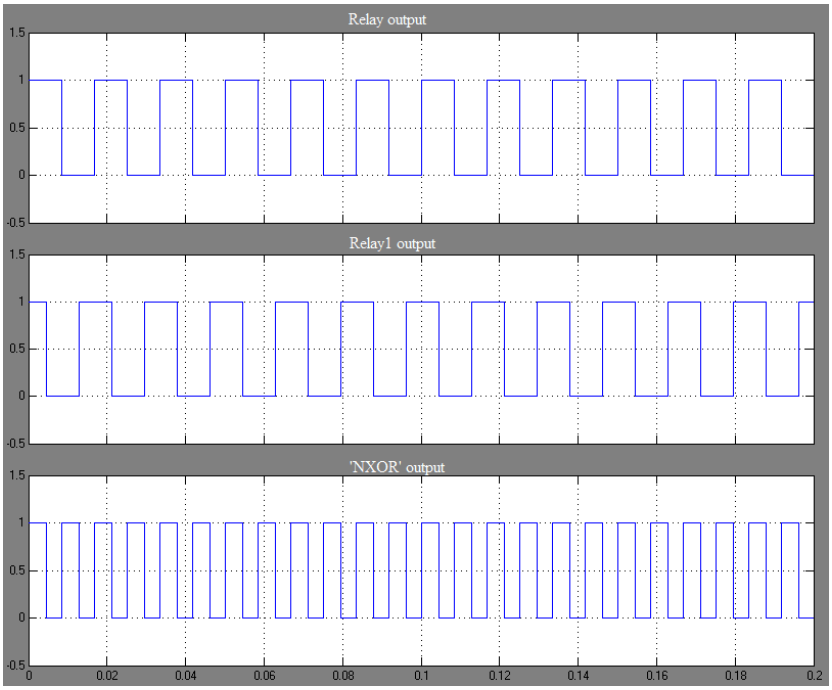

Figure 6-9 Coincidence circuit output

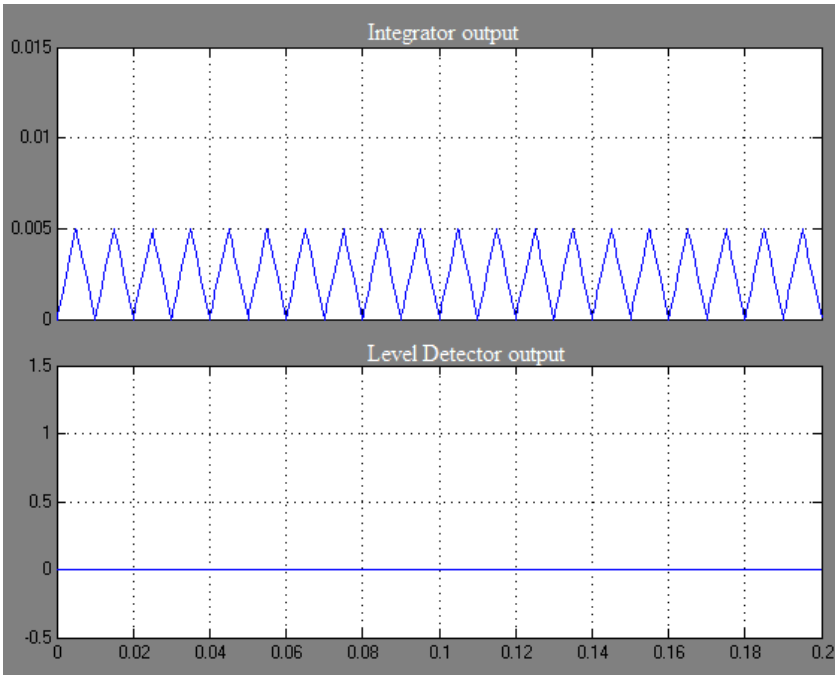

Figure 6-10 Integrator output and trip signal

The trip time characteristics of the block-average comparator based relay could be achieved by testing different phase angles between -90 º to 90 º randomly. Table 6-2 gives the tested phase angles and corresponding tripping time.

Phase angles (degree)	Tripping time (ms)
0 º	10
±15 º	11.7
±30 º	13.3
±45 º	15.0
±60 º	16.7
±70 º	25.6
±75 º	35.0
±80 º	45.5
±85 º	95.0

Table 6-2 Tested phase angles and corresponding tripping time

According to the tested phase angles and corresponding tripping time, the tripping time characteristic from the simulation is drawn in fig.6-11.

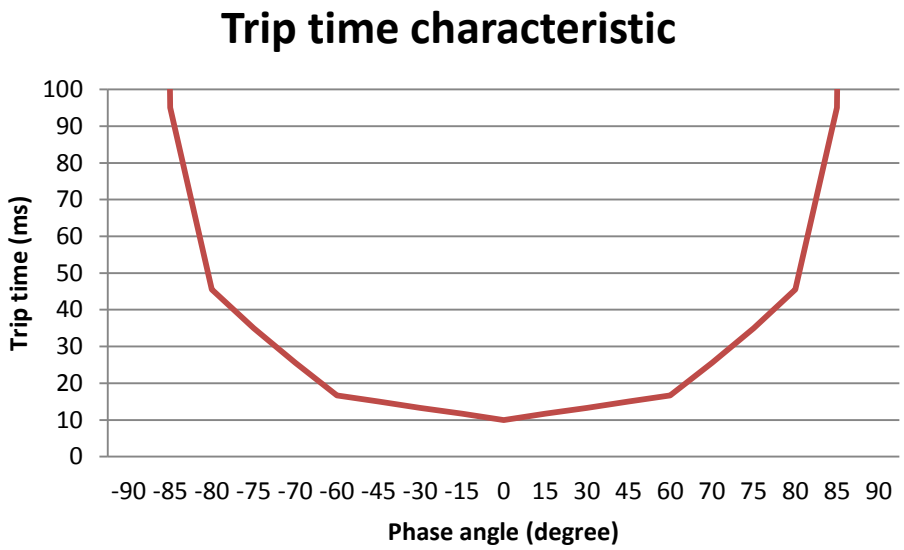

Figure 6-11 Trip time characteristics from simulation studies

6.1.3 Zones setting

The distance relay has three zones to protect the transmission lines, normally are:

- Zone1: 80% of the protected line with no time delay;
- Zone2: 120% of the protected line with time delay of 200ms;
- Zone3: 250% of the protected line with time delay of 500ms.

For zone1 simulated in MATLAB/SIMULINK using block-average comparator is shown in fig.6-12:

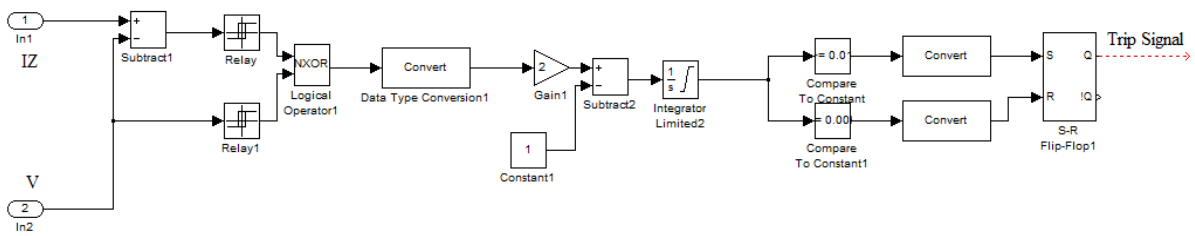

Figure 6-12 Zone1 protection

The connector 1 and 2 are the IZ and V from measuring circuits. A subtraction block was used to produce IZ-V signal.

Zone2 and Zone3 were performed by multiplying IZ with a constant value to adjust the protecting characteristic reach based on zone1 protection. The simulation block diagram for the distance relay's three zones of protection is shown in fig.6-13. Zone2 had 200ms time delay and Zone3 had 500ms time delay. The scope module was used to monitor the trip signal.

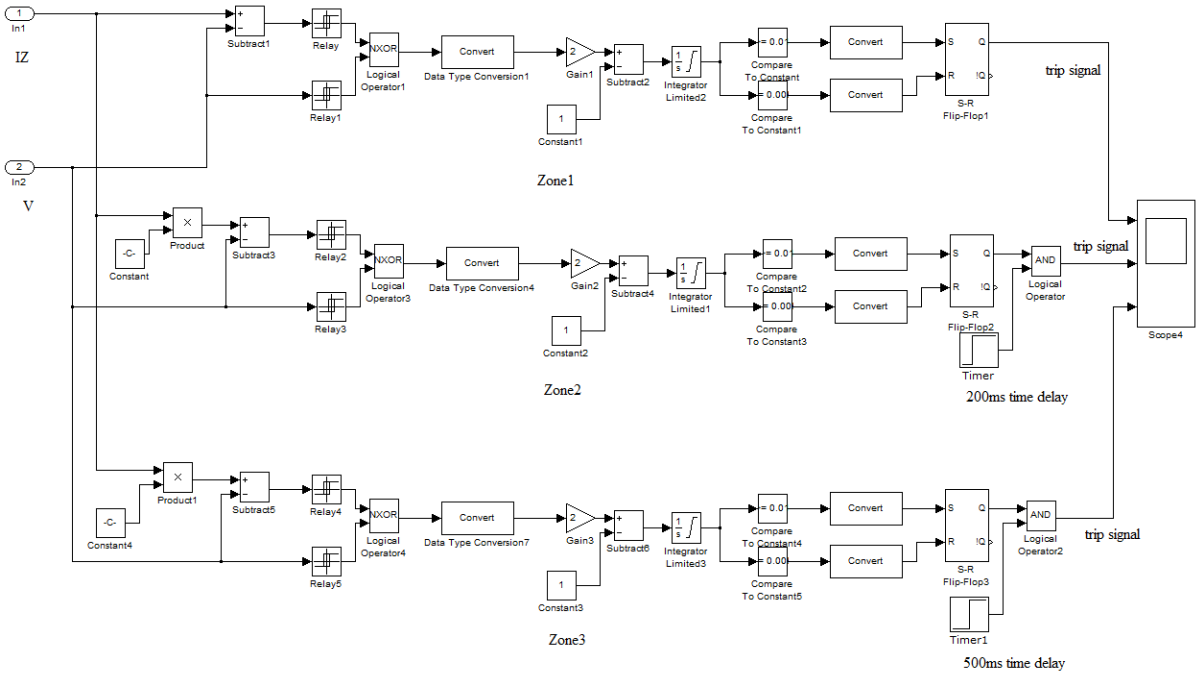

Figure 6-13 Block-average comparator distance relay three zones protection

6.1.4 Impedance trajectory plot circuit

The impedance seen by the relay was calculated by current and voltage signals. The I and V signals were put through a digital filter to remove unwanted high frequency components. The digital filter was performed by a 2nd order low-pass filter with cut-off frequency of 360Hz [110]. Then the signal was put through A/D converter which was performed by a Quantizer block. The Quantizer block passes its input signal through a stair-step function and use round-to-nearest method to produce a symmetric output about zero [110]. The sampled signal was input to DFT (Discrete Fourier Transformer) to remove DC offset and calculate the phasors values of the input signal. The output of DFT was input through the apparent impedance

computing algorithm and determine the apparent impedance seen at the relay point. The modelled circuit is shown in fig.6-14.

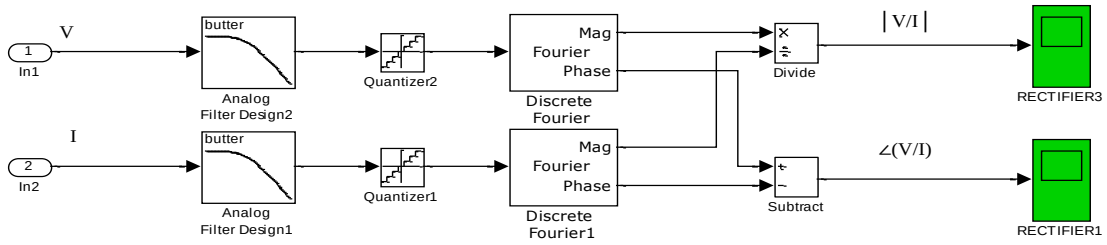

Figure 6-14 Modelled impedance trajectory circuit

The magnitude outputs of two DFTs were passed through a divide block to produce magnitude value of V/I. The phase outputs of DFTs were passed through a subtract block to produce the phase angle argument of V and I. The magnitude value and phase angle argument were stored in workspace in MATLAB for computing algorithm to compute the impedance and plot the impedance trajectory.

6.1.5 Modelled distance relay arrangement

For phase-to-ground faults, the fault impedance measured by the distance relay is:

$$z_m = \frac{U}{I+3kI_0} \tag{6.1}$$

For phase-to-phase faults, the fault impedance measured by the distance relay is:

$$z_m = \frac{U_{LL}}{I_{LL}} \tag{6.2}$$

Based on the simulation used for the block-average comparator, IZ and V were used for comparison. Fig.6-15 shows the simulated distance protection.

For single phase to ground faults, the voltage and current were taken from the Goto block. The Add blocks were used to produce $I+3kI_0$ signal. The voltage and current signal were put through the block-average comparators A-N, B-N and C-N. For phases faults, the subtract blocks were used to produce the phase voltages and currents. The phase voltages and currents were put through the block-average comparators A-B, B-C and C-A.

Similarly to the impedance trajectory plotting circuits, the impedance trajectory plotting circuits use V and I to compute the impedance. For single phase to ground faults, the plotting circuits used V and $I+3kI_0$ for computing. For phase to phase faults, the plotting circuits use phase voltage V_{LL} and current I_{LL} to compute the impedance.

The flow diagram used for the distance relay decision making process is shown in fig.6-16.

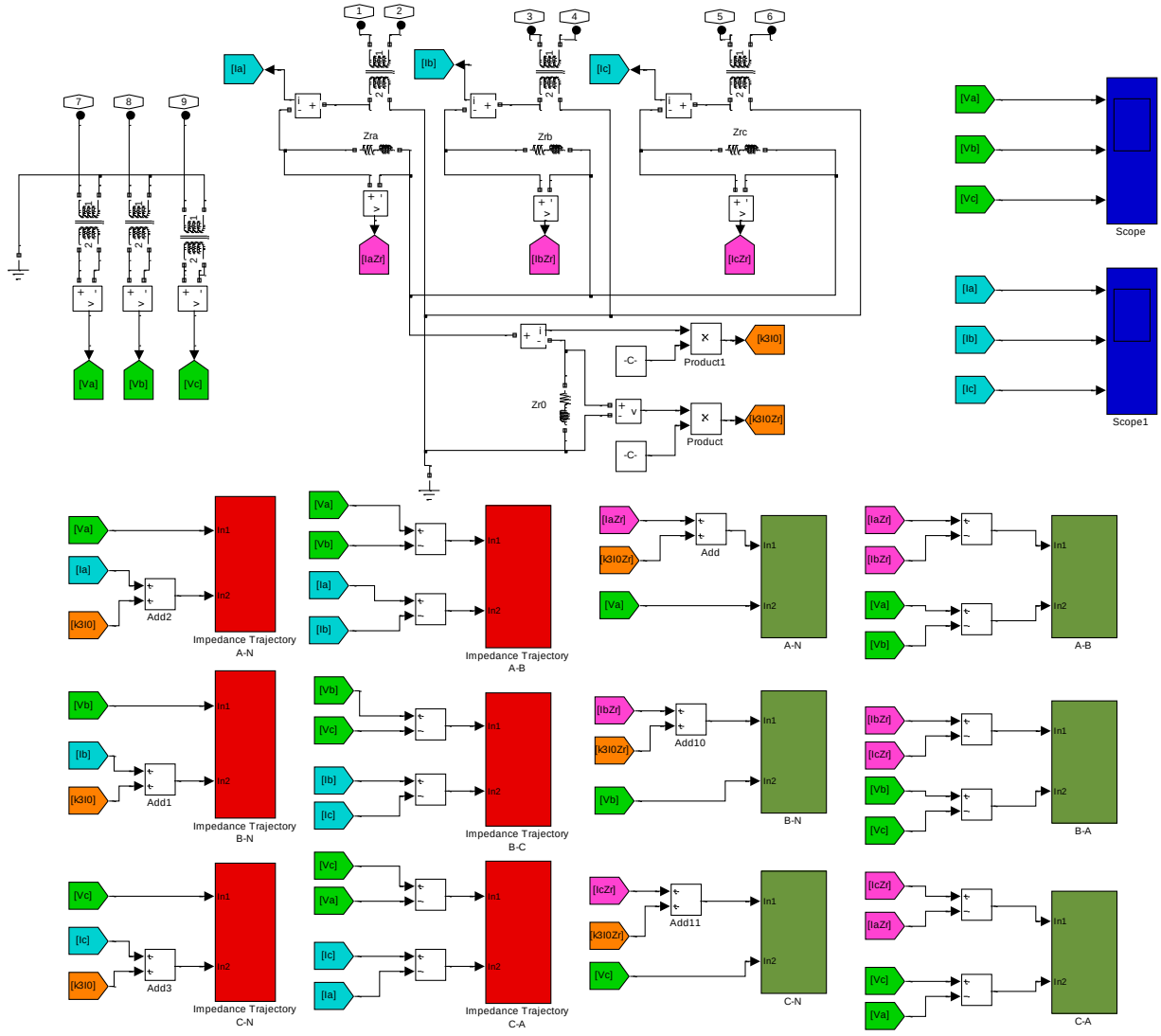

Figure 6-15 Simulated distance protection

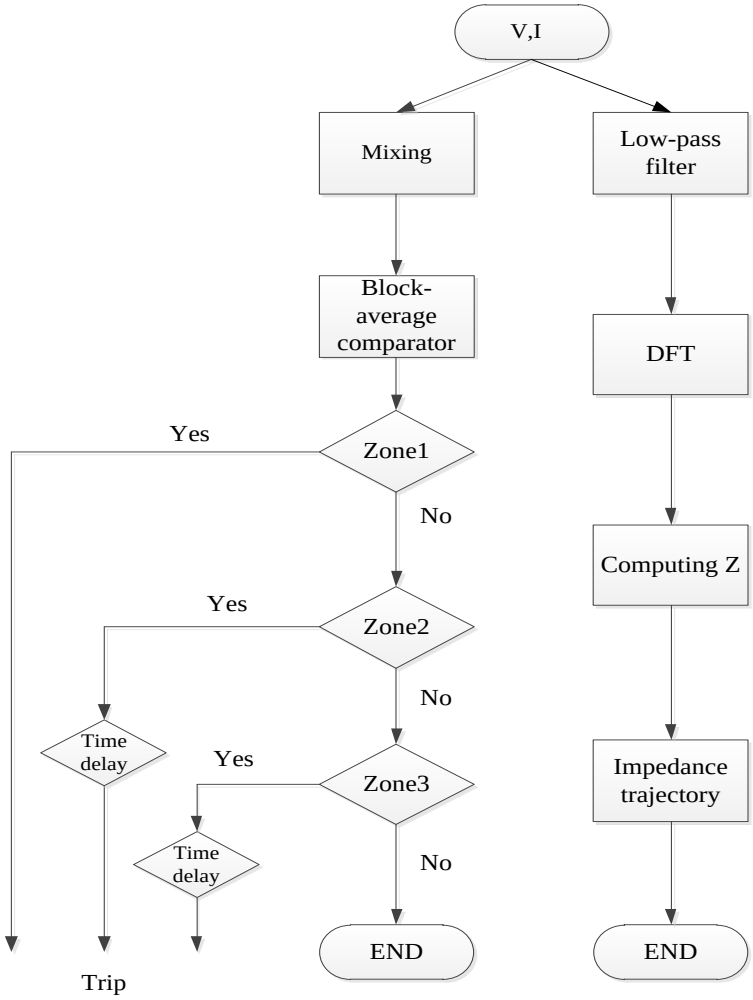

Figure 6-16 Distance relay decision making process to show relay tripping and the impedance trajectory

6.2 Test distance relay

In order to validate the modelled distance relay, it was tested in a simple power system as shown in fig.6-17 below. The details are shown in Appendix. B.

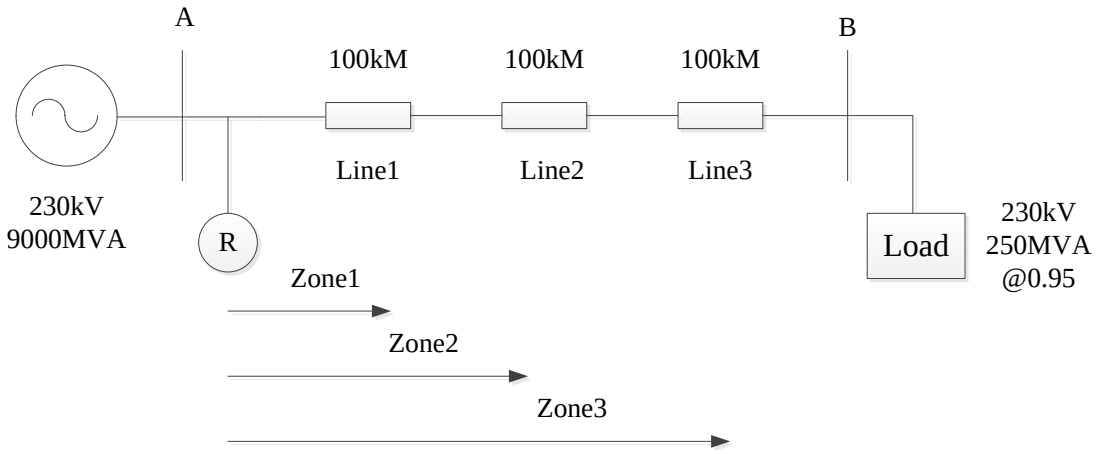

Figure 6-17 A simple power system

The modelled power system was taken from Kundur's two area system [68]. A 230kV, 9000MVA power system connected to a 230kV, 250MVA local load through three 100kM transmission lines. The distance relay was located at busbar A to protect line1. Zone1 was set to 80% of the line1. Zone2 was set to 120% of the line1. Zone3 was set to 250% of the line1. Time delay for zone1, zone2 and zone3 were 0ms, 200ms and 500ms respectively.

Transmission line parameters is shown in table.6-3 below [68].

Positive-sequence		Zero-sequence	
r_1	x_1	r_0	x_0
0.053Ω/km	0.531 Ω/km	1.638 Ω/km	2.312 Ω/km

Table 6-3 Transmission line parameters

To test the distance relay, different types of faults were applied including A-G, B-G, C-G, A-B, B-A, C-A, A-B-G, B-A-G, C-A-G, A-B-C and A-B-C-G. These were applied into the power system at different locations at 50km (zone1), 100km (zone2), 200km (zone3) and 280km (outside of protection area) respectively. The fault duration was between 1.2s-2.0s. The simulation time was 2.0s.

6.2.1 Faults in Zone1

6.2.1.1Single phase to ground fault at 50km

To test the distance relay response to single phase to ground fault covered by zone1 protection, an A-G fault was applied to the system at 50km on line1 from 1.2s-2.0s. Fig.6-18 shows the A-G fault impedance trajectory as seen by the relay.

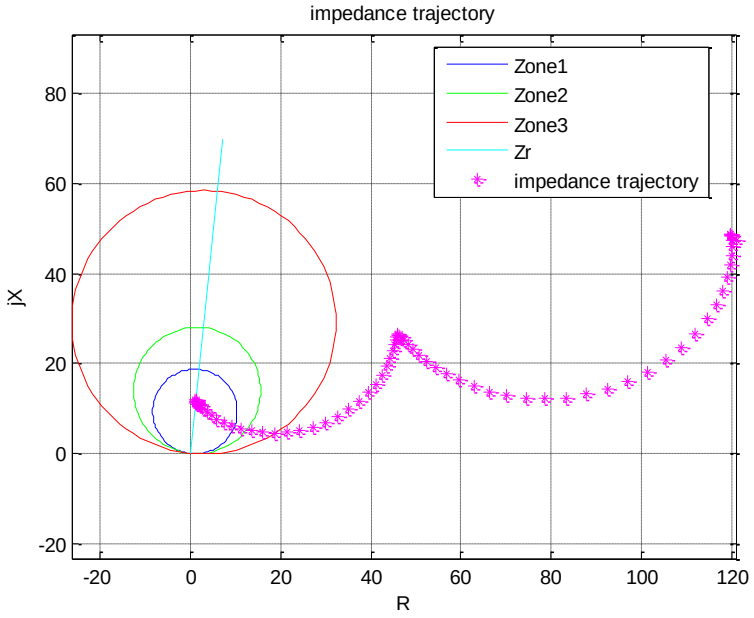

Figure 6-18 A-G fault impedance trajectory during A-G fault

As can be seen from the fig.6-18, the fault impedance locus hit at the protected line in zone1 area. The block-average comparator output is shown in fig.6-19. Fig.6-19 shows the A-G distance protection block-average comparator output crossed the trip level (0.01) in a very short time after fault occurred. Fig.6-20 gives the distance relay trip signal. Zone1 tripped at 1.21s, 10ms after fault occurred. Zone2 tripped at 1.4s, 200ms after fault occurred. Zone3 tripped at 1.7s, 500ms after fault occurred.

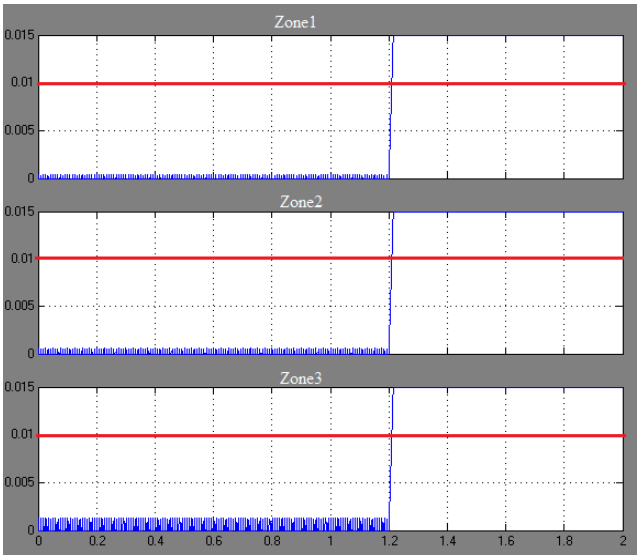

Figure 6-19 Block-average comparator output

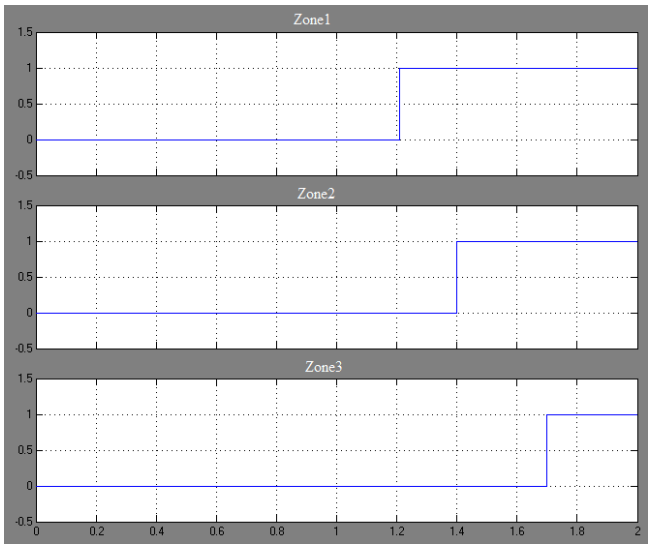

Figure 6-20 Distance relay trip signals

The B-G, C-G, A-B, B-A, C-A fault impedance trajectories are shown in fig.6-21.

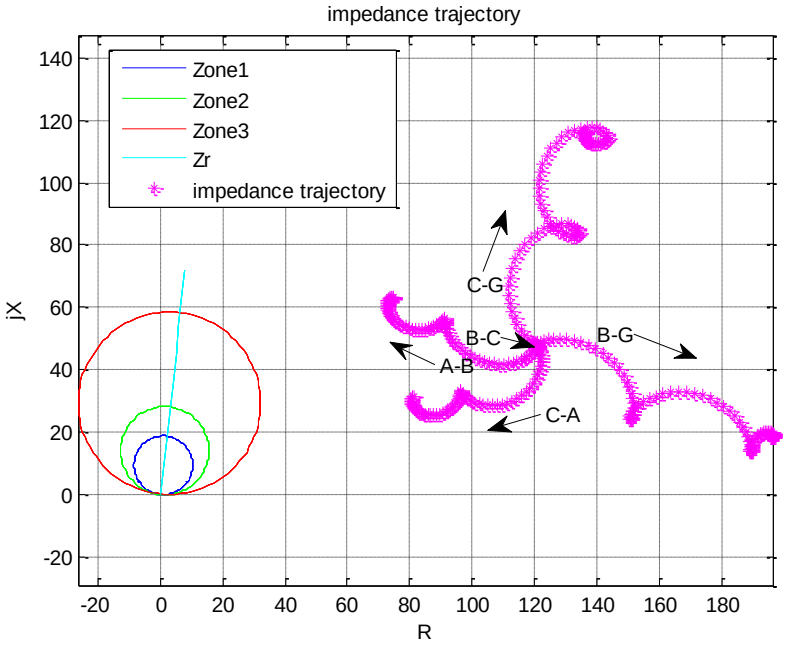

Figure 6-21 B-G, C-G, A-B, B-A, C-A fault impedance trajectories

The B-G, C-G, A-B, B-A, C-A fault impedance trajectories did not enter the protection zones, and therefore the B-G, C-G, A-B, B-A, C-A distance protection comparators did not trip.

For B-G and C-G fault, the results are similar to the A-G fault. The results are shown in appendix C.1 and C.2.

6.2.1.2 Phase to phase fault at 50km

To study distance relay response to phase to phase fault, an A-B fault was injected into the power system on 50km at line1 to test phase-phase protection. The fault was from 1.2s to 2.0s. Fig.6-22 gives the A-B fault impedance trajectory. The fault impedance entered the protection zone1 characteristic after fault occurred. The A-B protection block-average comparator output is shown in fig.6-23. The block-average comparator output crossed the trip boundary after fault occurred in a short time. The trip signal is shown in fig.6-24. Zone1 tripped 10ms after the fault occurred. Zone2 tripped 200ms after the fault occurred. Zone3 tripped 500ms after the fault occurred.

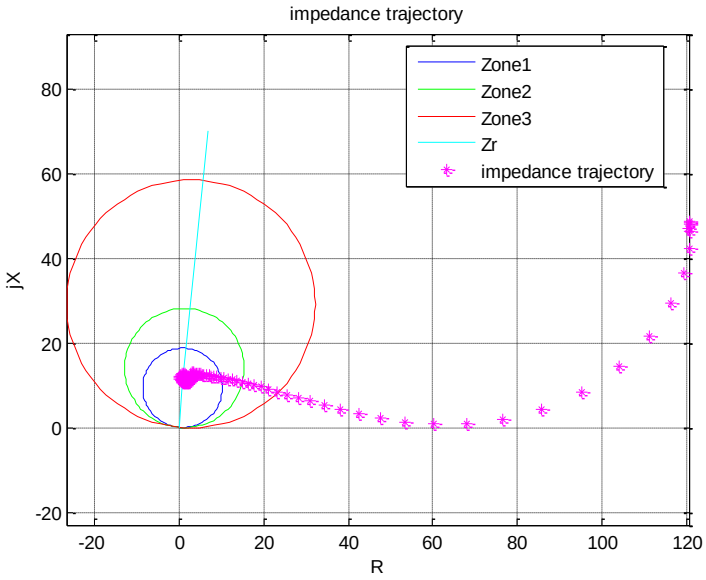

Figure 6-22 A-B fault impedance trajectory

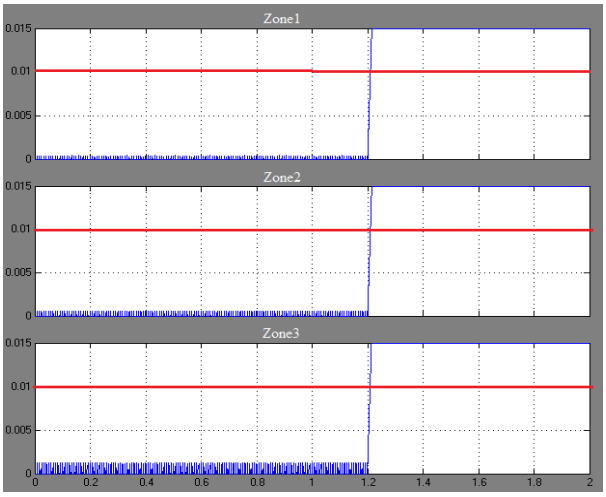

Figure 6-23 Block-average comparator output

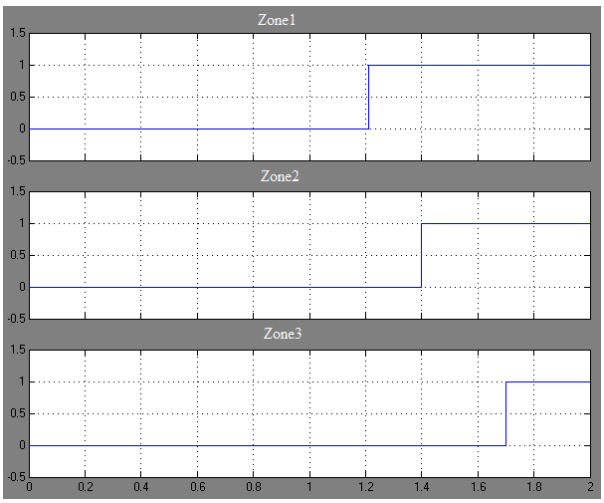

Figure 6-24 Distance relay trip signals

The A-G, B-G, C-G, B-C and C-A impedance trajectories are shown in fig.6-25. The A-G, B-G fault impedance trajectories entered protection zone1 protection characteristics. The B-C and C-A fault impedance trajectories entered protection zone3 near the boundary. The A-G, B-G, B-C and C-A protection block-average comparator outputs are shown in fig.6-26 (a), (b), (c) and (d) respectively. As can be seen from fig.6-26, the A-G, B-G protection block-average comparator zone1 outputs crossed the trip level 50ms and 170ms after the fault. B-C protection block-average comparator output did not trip. The C-A protection block-average comparator zone3 output did trip 100ms after the fault.

The trip signals are given in fig.6-27 (a), (b), (c) and (d). Fig.6-27 (a) shows the A-G protection trip signal. As can be seen from fig.6-27 (a), A-G protection Zone1 tripped 50ms after fault occurred. A-G zone2 and zone3 tripped 200ms and 500ms after the fault respectively. Fig.6-27 (b) shows the B-G protection trip signal. Zone1 tripped 170ms after fault occurred. Zone2 and zone3 tripped 200ms and 500ms after the fault. Fig.6-27 (c) gives the B-C protection trip signal. There was no trip signal from B-C protection. Fig.6-27 (d) shows the C-A protection signal. As can be seen from fig.6-27 (d) that the C-A protection zone3 tripped 500ms after the fault.

The A-B protection responded to fault rapidly, about 10ms after the fault.

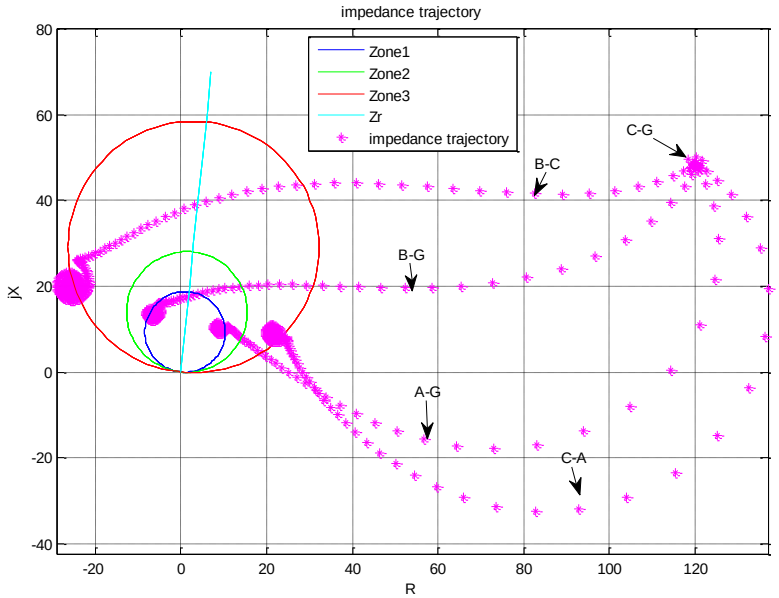

Figure 6-25 A-G, B-G, C-G, B-C and C-A impedance trajectories

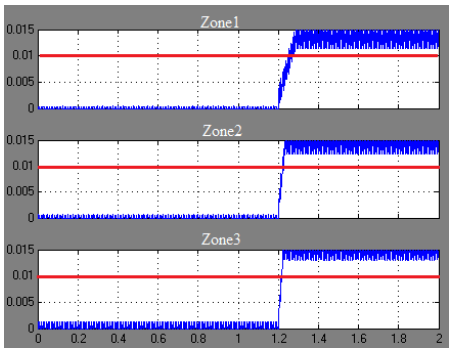

(a) A-G block-average comparator output

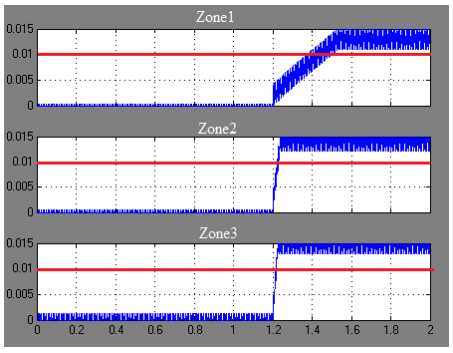

(b) B-G block-average comparator output

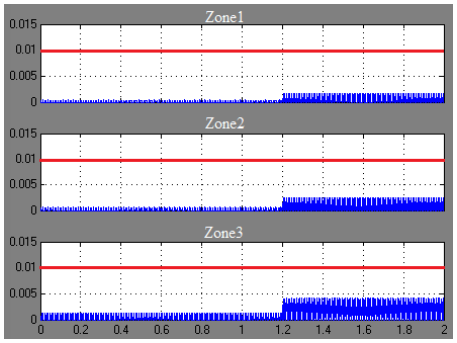

(c) B-C block-average comparator output

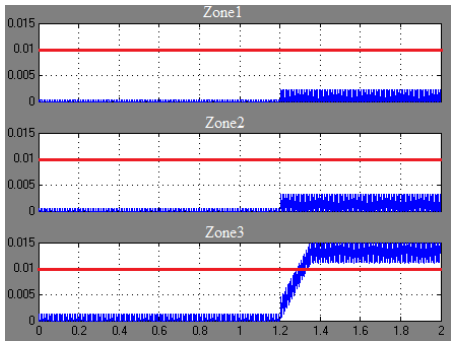

(d) C-A block-average comparator output

Figure 6-26 The Block-average comparator outputs

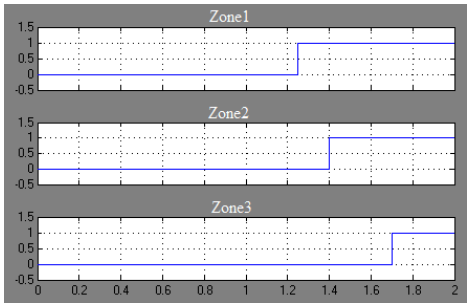

(a) A-G relay trip signals

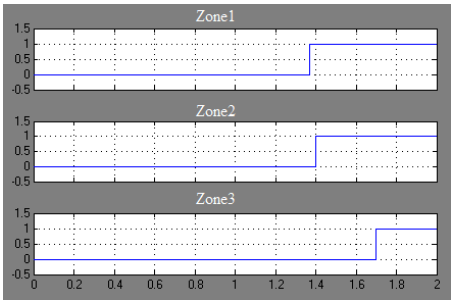

(b) B-G relay trip signals

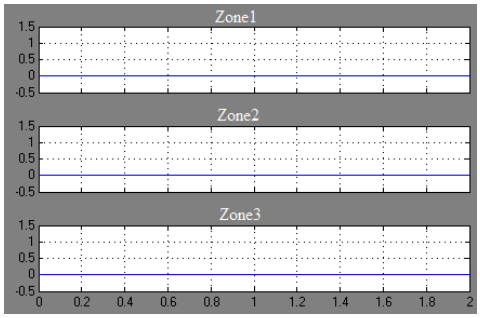

(c) B-C relay trip signals

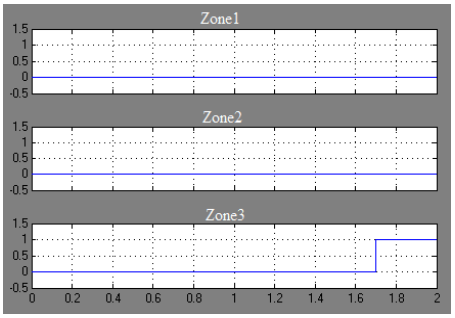

(d) C-A trip signals

Figure 6-27 Distance relay trip signals

The responses to B-C and C-A fault are similar to the A-B fault. Results are shown in appendix C.3 and C.4.

6.2.1.3 Phase to phase to ground fault at 50km

To study the distance relay response to phase to phase to ground fault, a B-C-G fault was applied to line1 at 50km. The fault was applied after 1.2s and maintained until 2.0s. The B-G, C-G and B-C fault impedance trajectories are shown in fig.6-28. The B-G, C-G and B-C fault impedance trajectories all entered the zone1 characteristic tripping the relay. Fig.6-29 gives the B-G, C-G and B-C block-average comparator outputs in (a), (b) and (c) respectively. All outputs crossed the zone1 trip level 10ms after fault occurred.

Fig.6-30 (a), (b) and (c) gives the distance relay trip signals from B-G, C-G and B-C protection respectively. The B-G protection zone1 tripped at 1.21s, 10ms after fault occurred. The C-G protection zone1 and B-C protection zone1 tripped at the same time. All protection zone2 and zone3 tripped at 200ms and 500ms after the fault respectively.

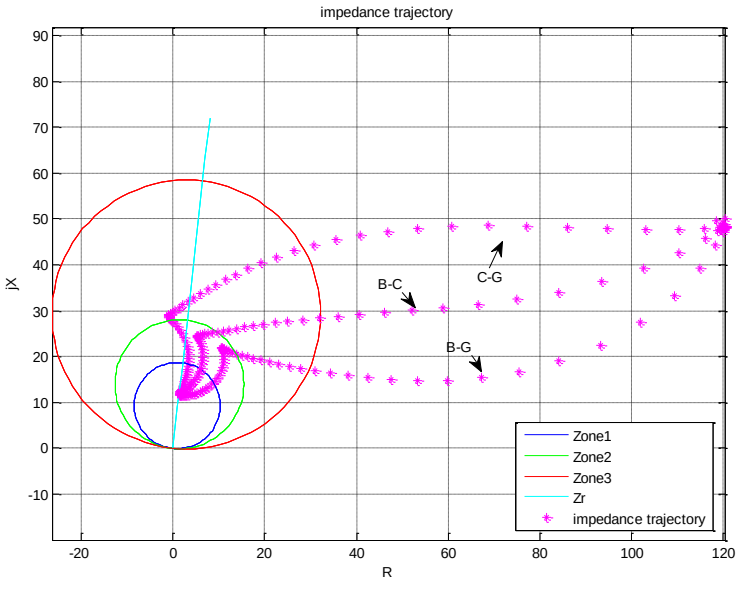

Figure 6-28 B-G, C-G and B-C fault impedance trajectories

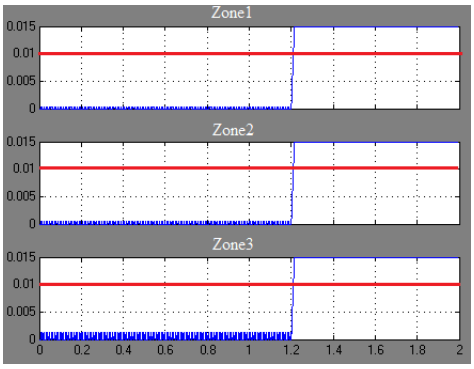

(a) B-G block-average comparator output

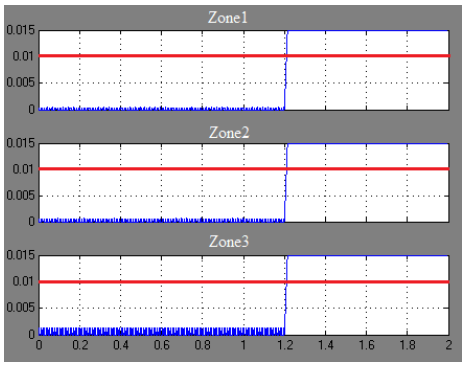

(b) C-G block-average comparator output

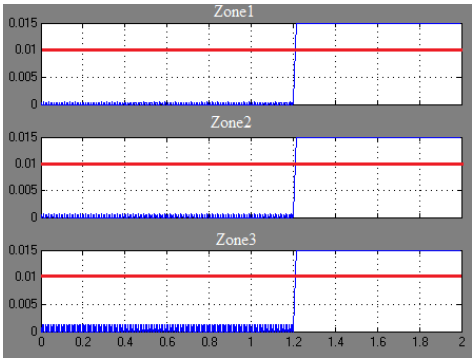

(c) B-C block-average comparator output

Figure 6-29 B-G, C-G and B-C block-average comparator outputs

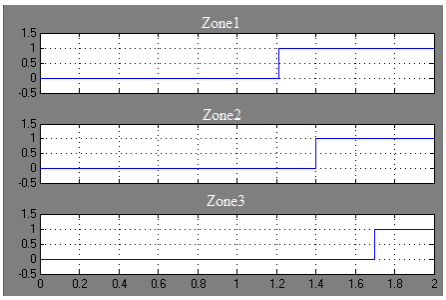

(a) B-G relay trip signals

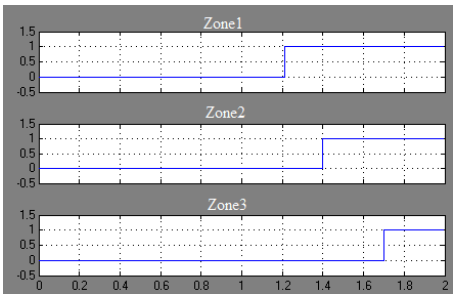

(b) C-G relay trip signals

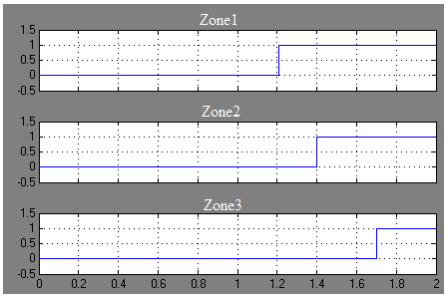

(c) B-C relay trip signals

Figure 6-30 B-G, C-G and B-C protection trip signals

Fig.6-31 shows the A-G, A-B and C-A fault impedance trajectories. The C-A and A-B impedance trajectories entered the protection zone3 characteristic. Although the C-A impedance trajectory entered the zone3 boundary, it did not cause the comparator to trip. This is a feature of the comparator filtering action and demonstrated that it was a boundary fault with an expected very high tripping time. Fig.6-32 (a), (b) and (c) gives the A-G, A-B and C-A protection block-average comparators' outputs respectively. The A-B protection zone3 block-average comparator output tripped after 100ms. Fig.6-33 (a), (b) and (c) gives the A-G, A-B and C-A protection trip signals. A-B zone3 tripped at 500ms after fault occurred.

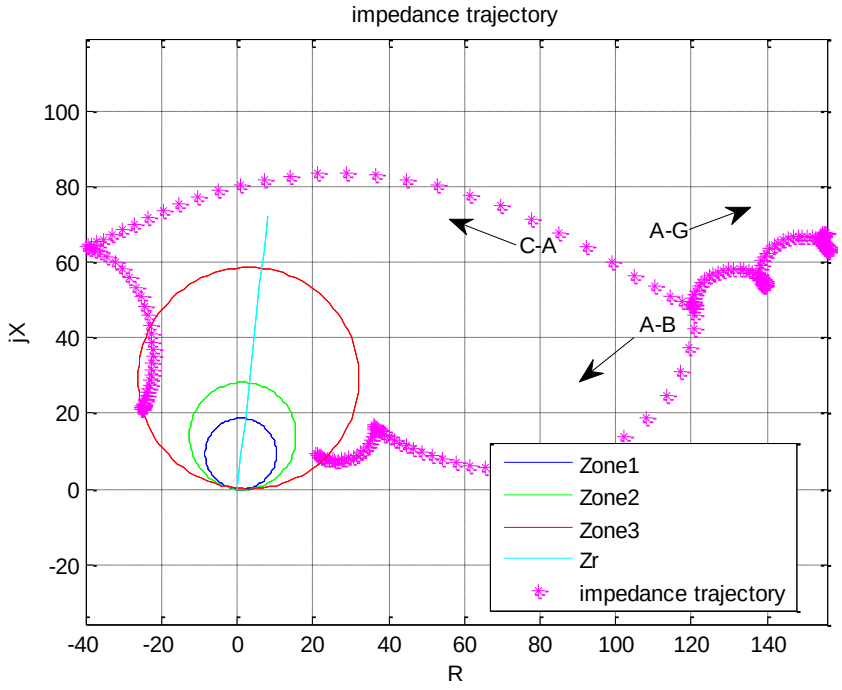

Figure 6-31 A-G, A-B and C-A fault impedance trajectories

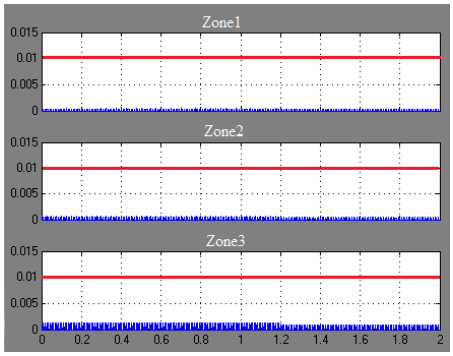

(a) A-G block-average comparator output

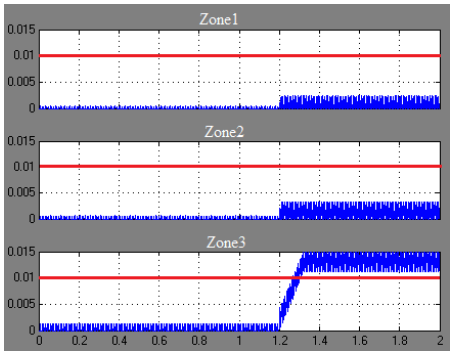

(b) A-B block-average comparator output

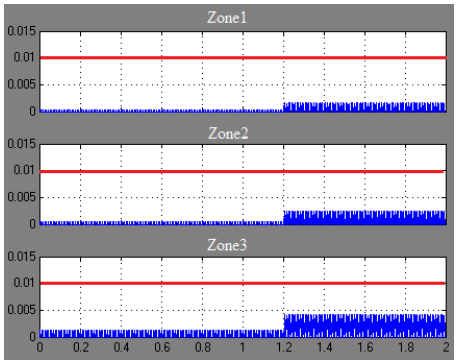

(c) C-A block-average comparator output

Figure 6-32 A-G, A-B and C-A block-average comparator outputs

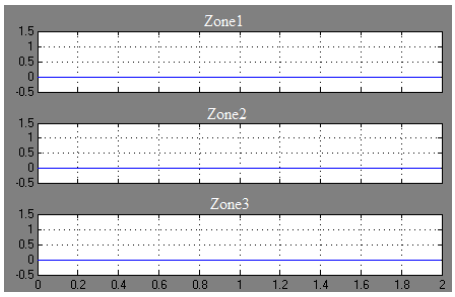

(a) A-G relay trip signals

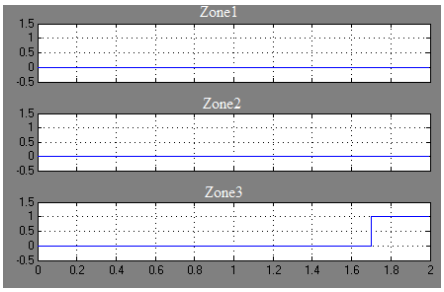

(b) A-B relay trip signals

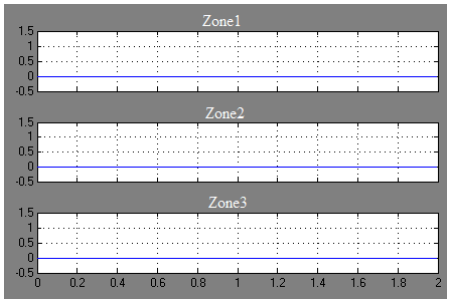

(c) C-A relay trip signals

Figure 6-33 A-G, A-B and C-A relay trip signals

For A-B-G and C-A-G faults, the results are similar to the B-C-G fault. Results are shown in appendix C.5 and C.6.

6.2.1.4 Three-phase fault

For a balanced three-phase fault, only the positive sequence currents are considered, and both the zero-sequence and negative sequence current are zero. The fault impedance measured by distance relay is from the relay point to the fault location. All relays are required to and did trip. A three-phase fault was applied to the power system on line1 at 50km. The fault impedance trajectories are shown in fig.6-34. This shown that all impedance trajectories entered the protection zone1 characteristic. The block-average comparators' outputs are shown in fig.6-35 where (a), (b), (c), (d), (e), (f) present the A-G, B-G, C-G, A-B, B-C, C-A comparators' outputs respectively. The trip signals are shown in fig.6-36. All relay zone1 protection tripped 10ms after fault.

The results of three-phase to ground comparators are similar to those of the phase-to-phase comparators.

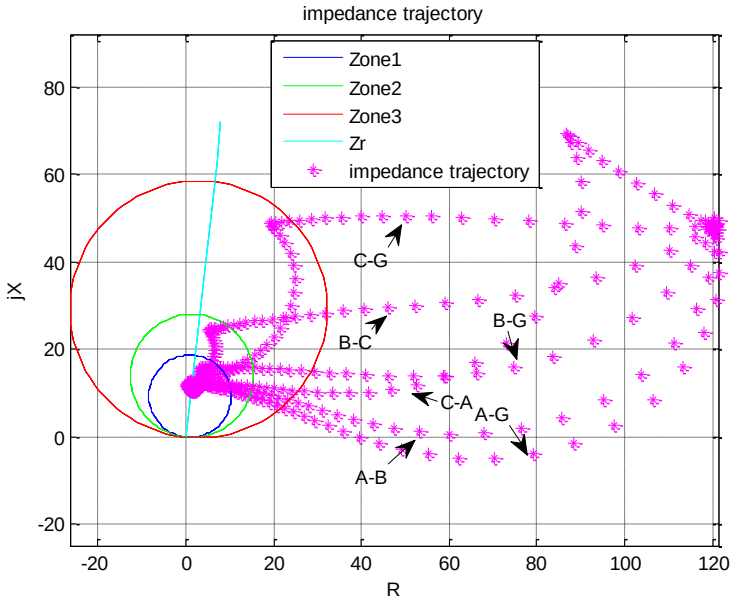

Figure 6-34 A-G, B-G, C-G, A-B, B-C, C-A fault impedance trajectories

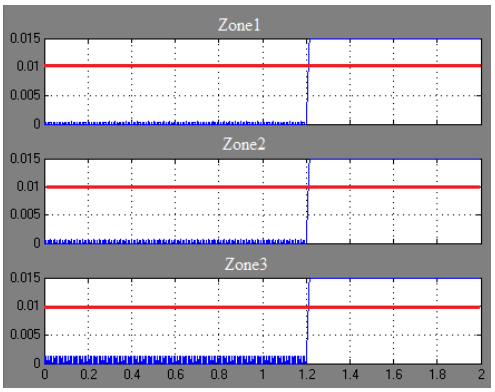

(a) A-G block-average comparator output

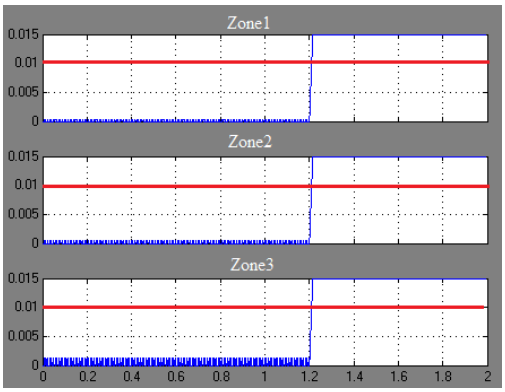

(b) B-G block-average comparator output

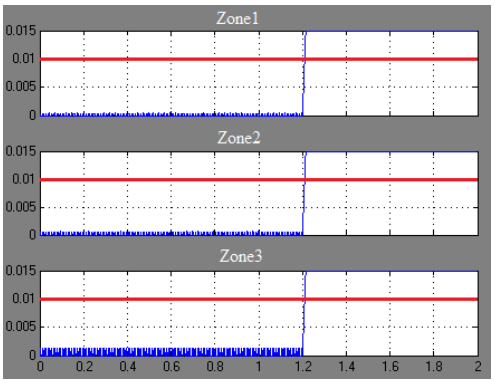

(c) C-G block-average comparator output

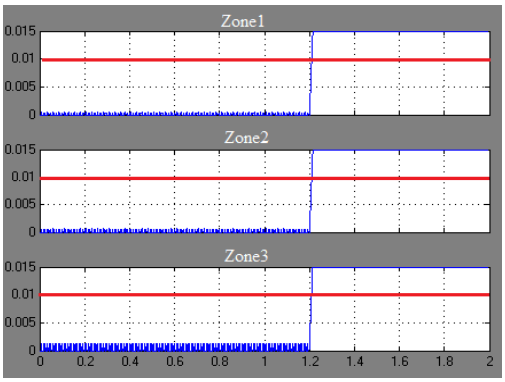

(d) A-B block-average comparator output

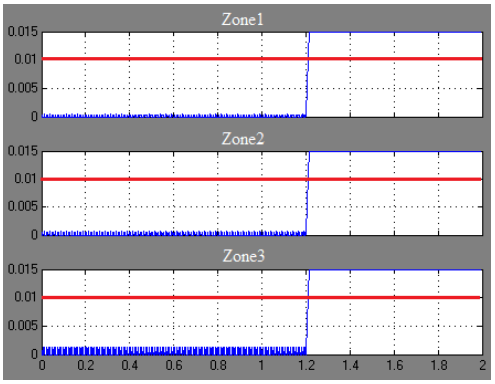

(e) B-C block-average comparator output

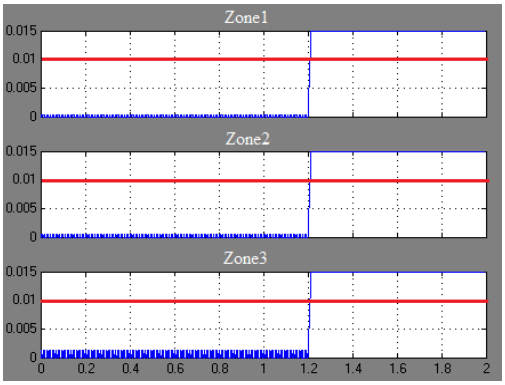

(f) C-A block-average comparator output

Figure 6-35 The block-average comparators' outputs

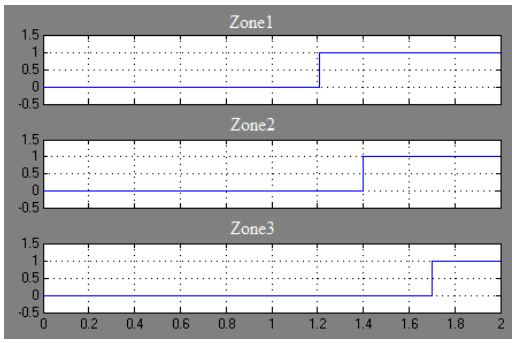

(a) A-G relay trip signals

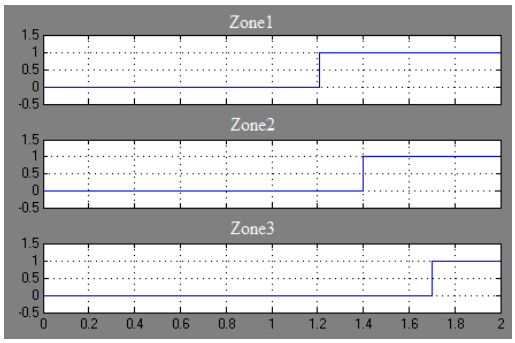

(b) B-G relay trip signals

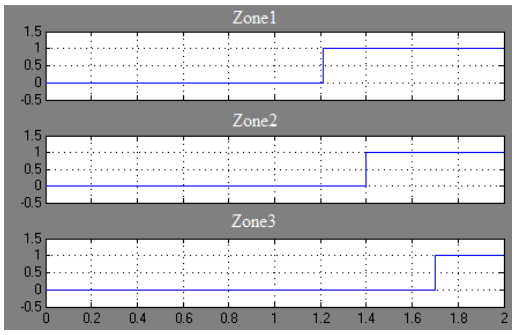

(c) C-G relay trip signals

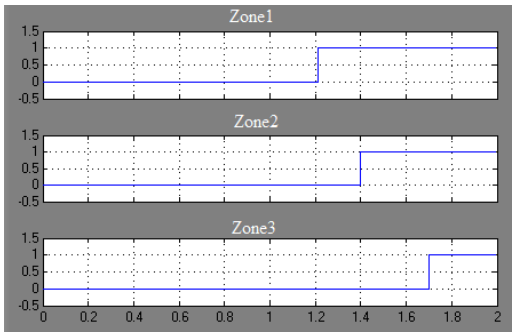

(d) A-B relay trip signals

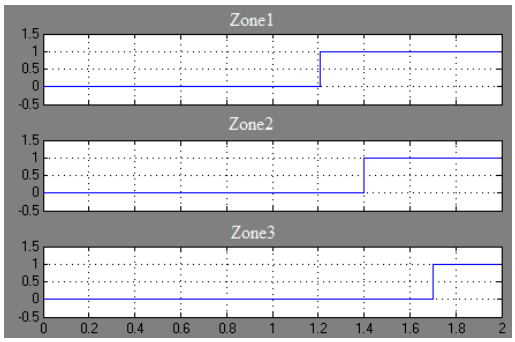

(e) B-C relay trip signals

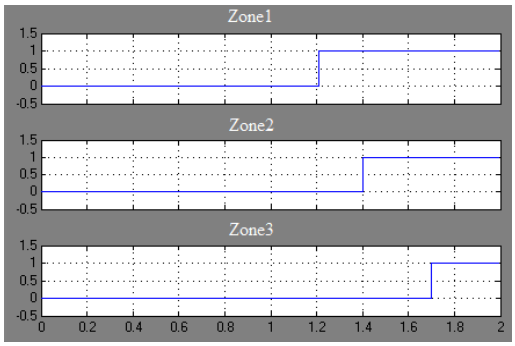

(f) C-A relay trip signals

Figure 6-36 Distance relay trip signals

6.2.2 Faults in Zone2

When fault occur in zone2 area, it is not covered by zone1 protections and the zone1 protection will not trip.

6.2.2.1 Single phase to ground fault

An A-G fault was applied to power system on line1 at 100km from 1.2s to 2.0s. A fault at 100km was covered by zone2 (120%) but not covered by zone1 (80%). The A-G fault impedance trajectory is shown in fig.6-37. The fault impedance trajectory entered the protection zone2 characteristic and settled on the protected line at 100km. Fig.6-38 shows the A-G clock-average comparator output. The zone2 and zone3 output crossed the trip level after fault occurred. Zone1 was not because the fault location was out of its reach. Fig.6-39 shows the relay trip signal. Zone2 tripped 200ms after fault and zone3 tripped 500ms after fault.

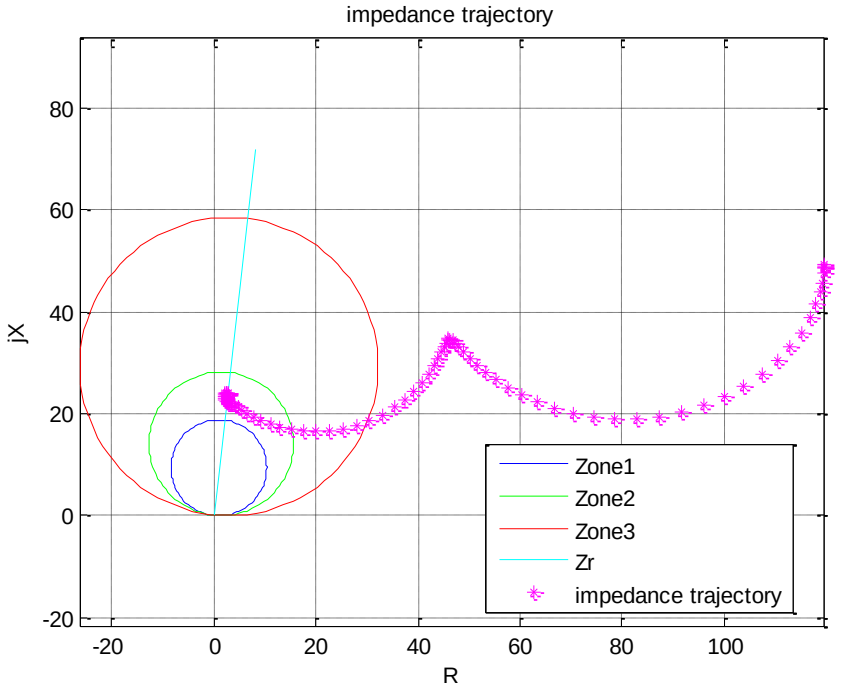

Figure 6-37 A-G fault impedance trajectory

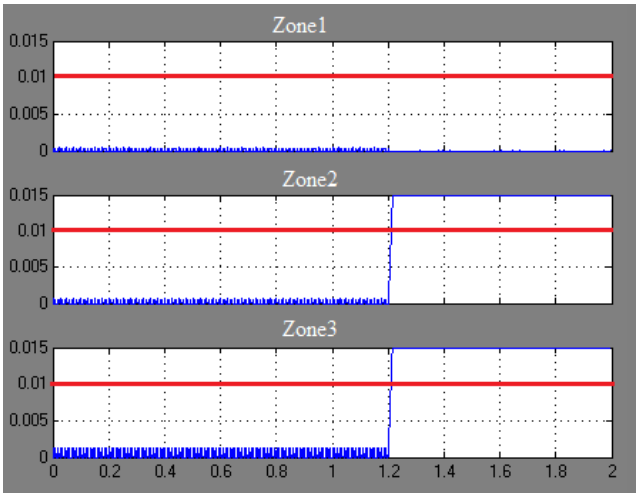

Figure 6-38 A-G block-average comparator output

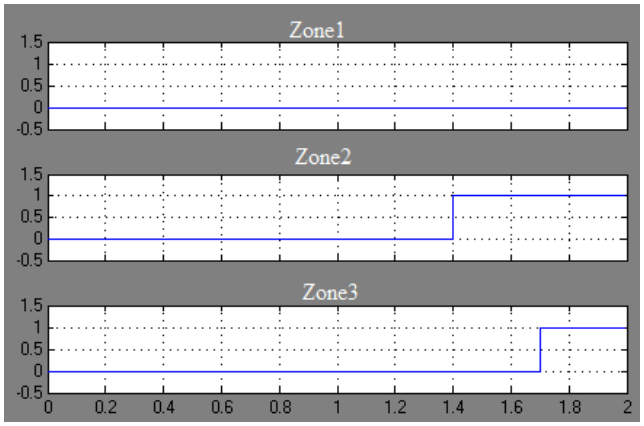

Figure 6-39 A-G relay trip signals

Fig.6-40 shows the B-G, C-G, A-B, B-C, C-A impedance trajectories. None of the impedance trajectories entered the protection characteristics.

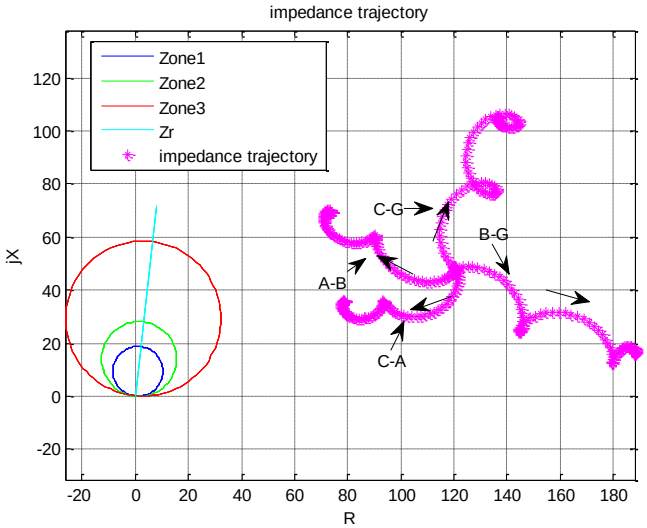

Figure 6-40 B-G, C-G, A-B, B-C, C-A impedance trajectories

The results of B-G and C-G fault at 100km are similar to A-G fault. Results are shown in appendix D.1 and D.2.

6.2.2.2 Phase to phase fault at 100km

An A-B fault was applied to power system on line1 at 100km from. The fault location was out of zone1 reach but covered by zone2 and zone3. The A-B fault impedance trajectory is shown in fig.6-41. The impedance locus entered the protection zone2 characteristic and settled on the protected line at 100km. The A-B block-average comparator output is shown in fig.6-42. The zone1 output did not trip. The zone2 and zone3 outputs both tripped. Fig.6-43 gives the trip signal. Zone2 tripped 200ms after fault and zone3 tripped 500ms after fault.

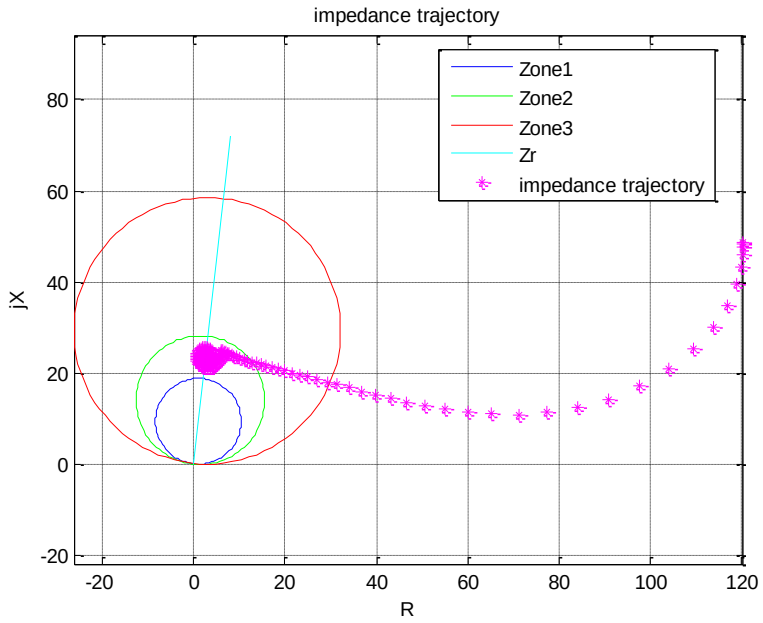

Figure 6-41 A-B fault impedance trajectory

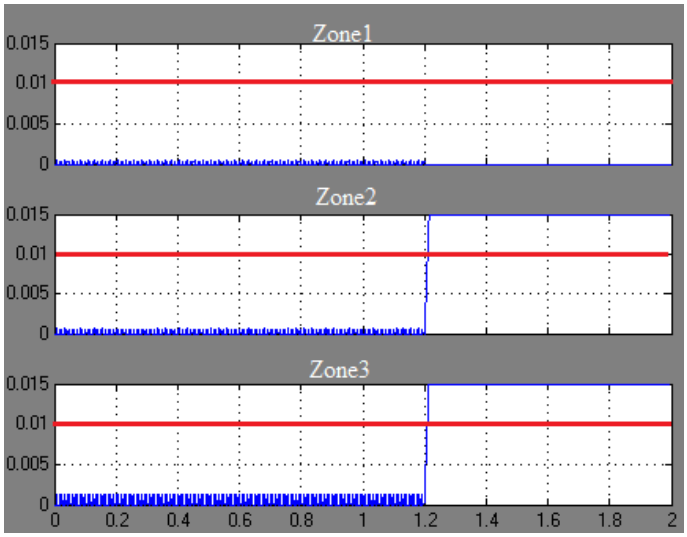

Figure 6-42 A-B block-average comparator output

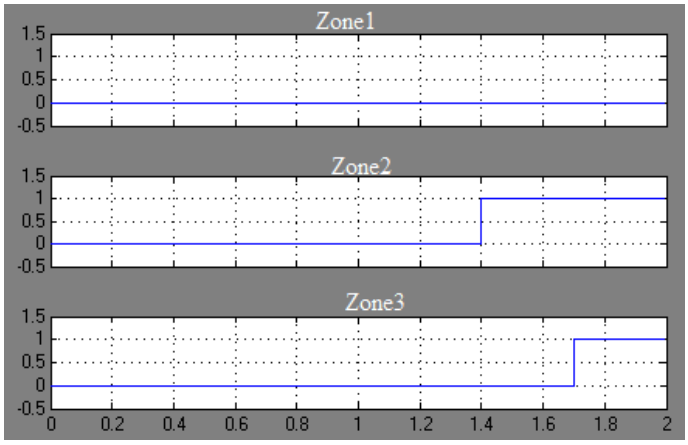

Figure 6-43 A-B relay trip signals

Fig.6-44 shows the A-G, B-G, C-G, B-C and C-A impedance trajectories. The A-G and B-G impedance trajectories entered the protection zone3 characteristic and were expected to result in tripping. The C-G, B-C and C-A impedance trajectories did not enter protection zones. Fig.6-45 gives the A-G, B-G comparators' outputs and A-G, B-G trip signals in (a), (b), (c), (d) respectively. The A-G, B-G zone3 tripped 500ms after the fault.

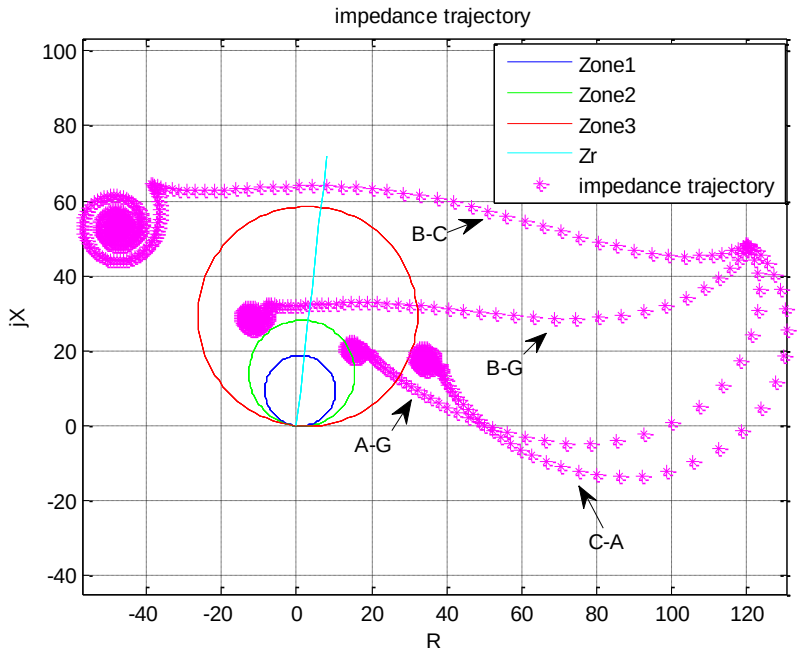

Figure 6-44 A-G, B-G, C-G, B-A, C-A fault impedance trajectories

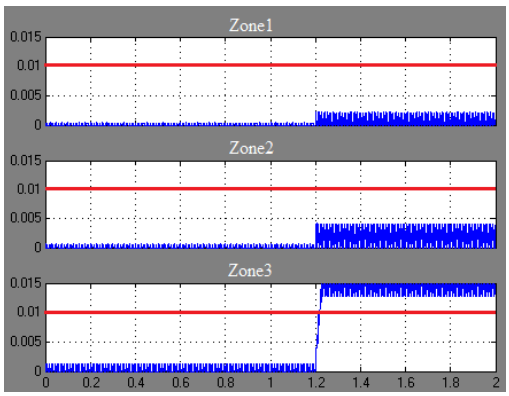

(a) A-G block-average comparator output

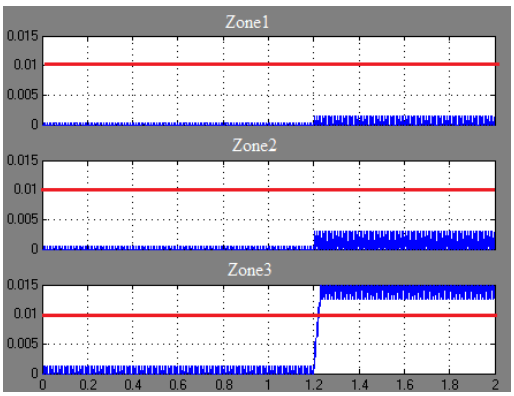

(b) B-G block-average comparator output

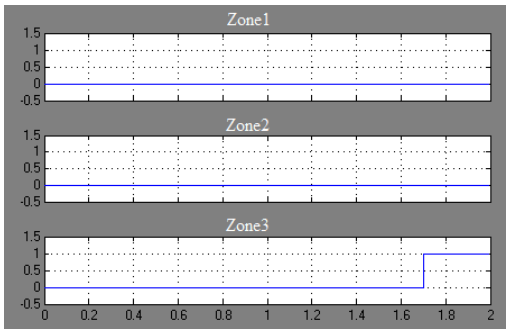

(c) A-G relay trip signals

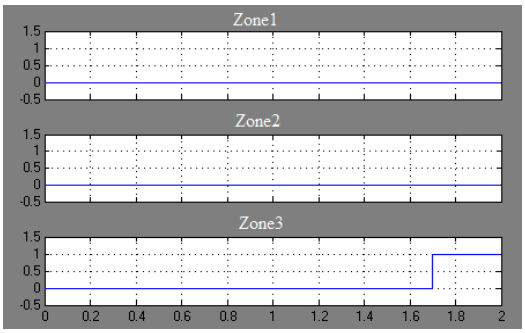

(d) B-G relay trip signals

Figure 6-45 A-G, B-G comparators' outputs and trip signals

The results of B-C and C-A faults are similar to A-B fault. Results are shown in appendix D.3 and D.4.

6.2.2.3 Phase to phase to ground fault

A B-C-G fault was applied to the power system on line1 at 100km from 1.2s to 2.0s. Fig.6-46 shows the B-G, C-G and B-C fault impedance trajectories. All three impedance trajectories entered the zone2 characteristic and settled on the protection line at 100km. Fig.6-47 (a), (b), (c) give the B-G, C-G and B-C block-average comparators' outputs respectively. All comparators zone2 and zone3 outputs tripped. Fig.6-48 (a), (b), (c) show the B-G, C-G and B-C trip signals. B-G, C-G and B-C protection zone2 tripped 200ms after fault and zone3 tripped 500ms after fault.

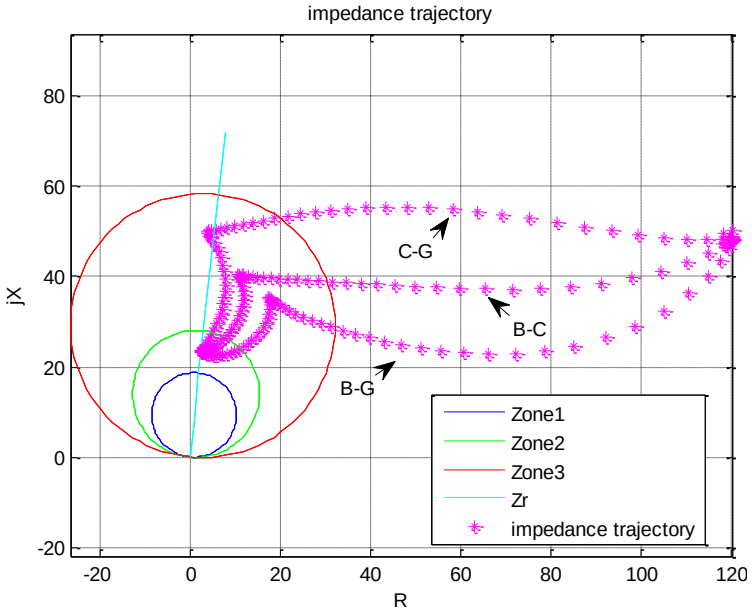

Figure 6-46 B-G, C-G, B-C fault impedance trajectories

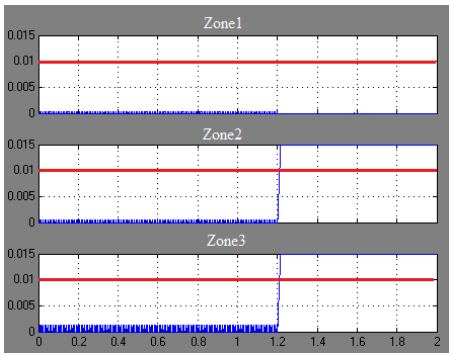

(a) B-G block-average comparator output

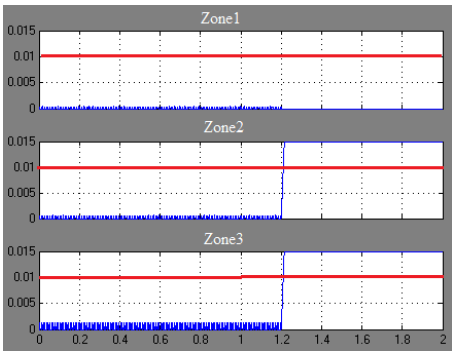

(b) C-G block-average comparator output

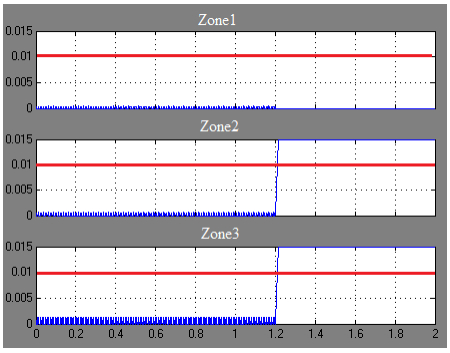

(c) B-C block-average comparator output

Figure 6-47 B-G, C-G, B-C block-average comparators' outputs

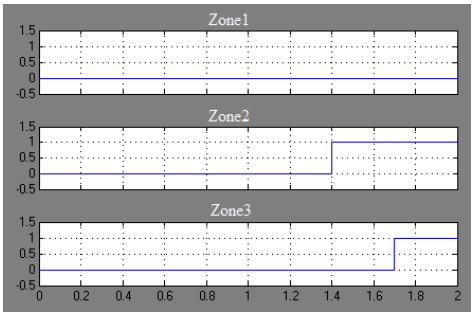

(a) B-G relay trip signals

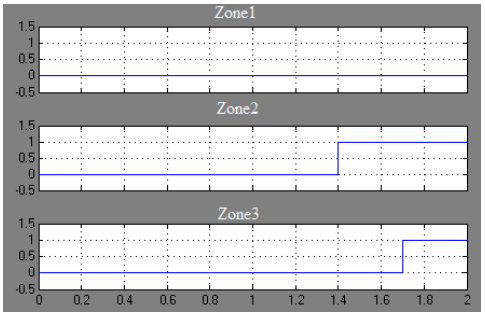

(b) C-G relay trip signals

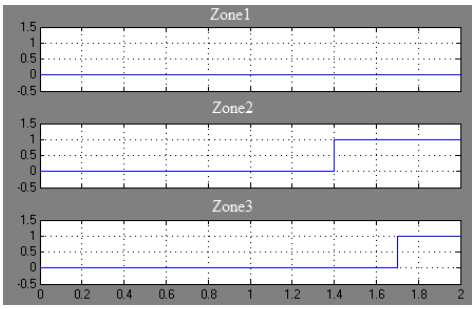

(c) B-C relay trip signals

Figure 6-48 B-G, C-G, B-C relay trip signals

Fig.6-49 gives the A-G, A-B, C-A impedance trajectories. None of these three impedance trajectories entered the protection zones.

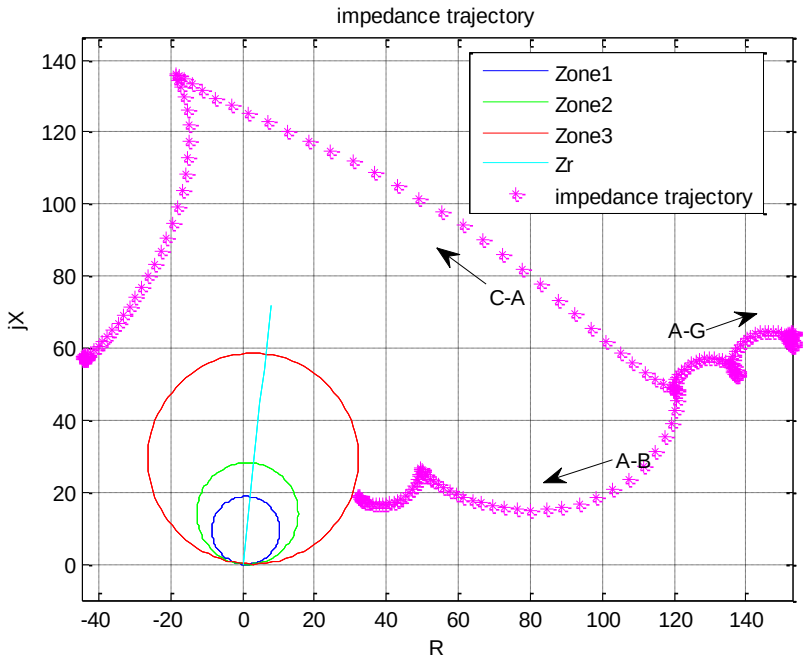

Figure 6-49 A-G, A-B, C-A impedance trajectories

Results of A-B-G, C-A-G faults are similar to B-C-G fault and shown in appendix D.5 and D.6.

6.2.2.4 Three phase fault at 100km

A three-phase fault was applied to the power system on line1 at 100km. The fault impedance trajectories are shown in fig.6-50. All impedance trajectories entered the protection zone2 characteristic. Fig.6-51 (a), (b), (c), (d), (e), (f) show the A-G, B-G, C-G, A-B, B-A, C-A block-average comparators' responses. All zone2 and zone3 block-average comparators tripped. Fig.6-52 (a), (b), (c), (d), (e), (f) show the A-G, B-G, C-G, A-B, B-A, C-A trip signals. All protection zone2 tripped 200ms after fault and zone3 tripped 500ms after fault.

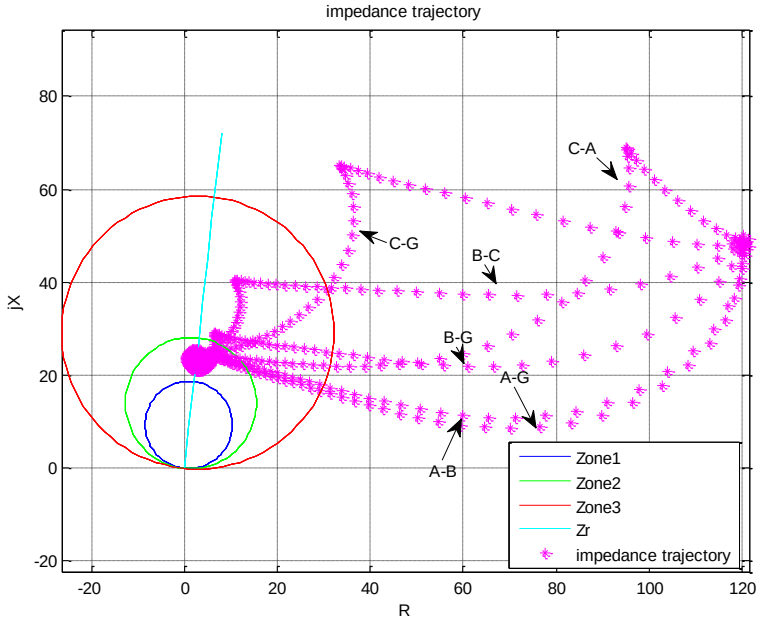

Figure 6-50 A-G, B-G, C-G, A-B, B-A, C-A fault impedance trajectories

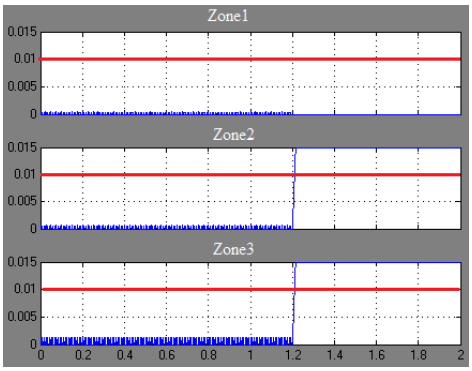

(a) A-G block-average comparator output

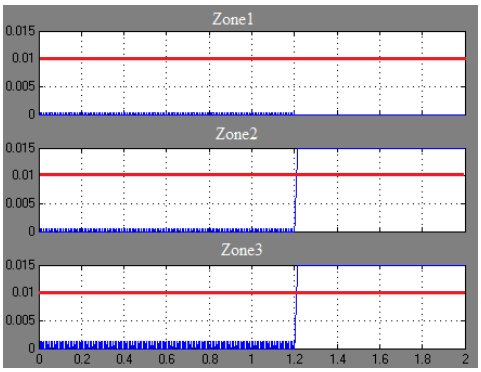

(b) B-G block-average comparator output

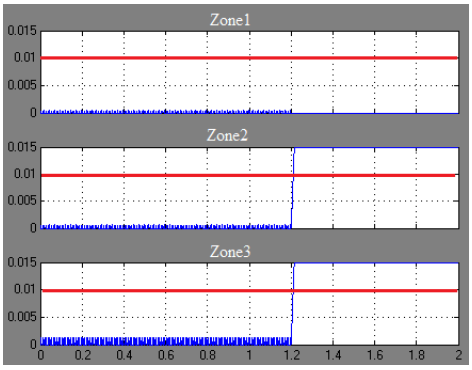

(c) C-G block-average comparator output

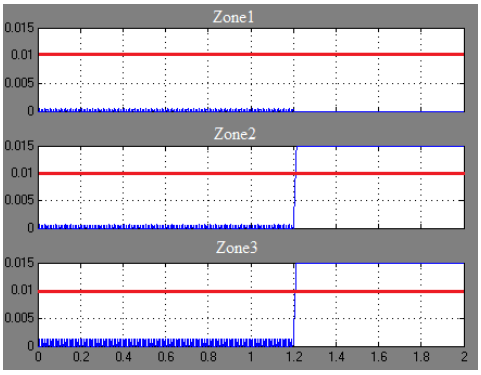

(d) A-B block-average comparator output

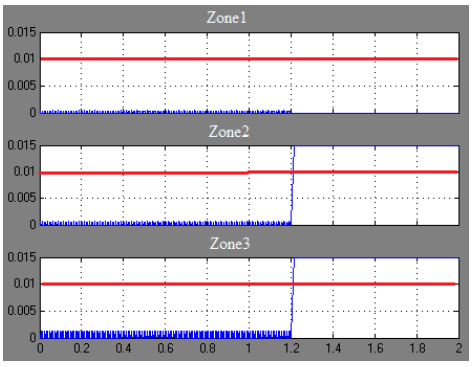

(e) B-C block-average comparator output

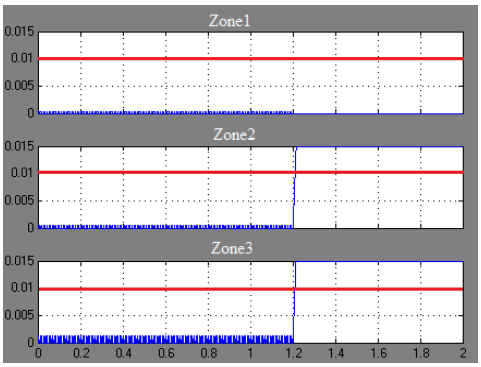

(f) C-A block-average comparator output

Figure 6-51 A-G, B-G, C-G, A-B, B-A, C-A block-average comparators' outputs

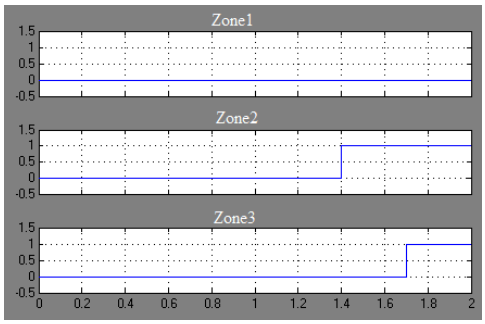

(a) A-G relay trip signals

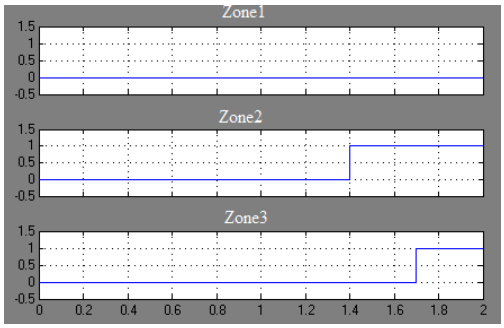

(b) B-G relay trip signals

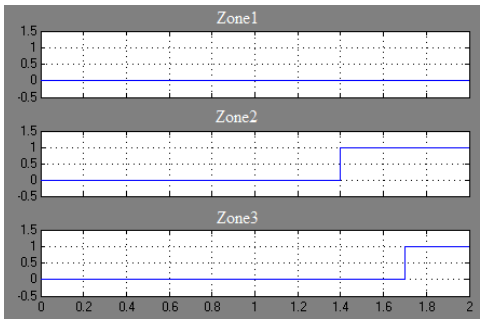

(c) C-G relay trip signals

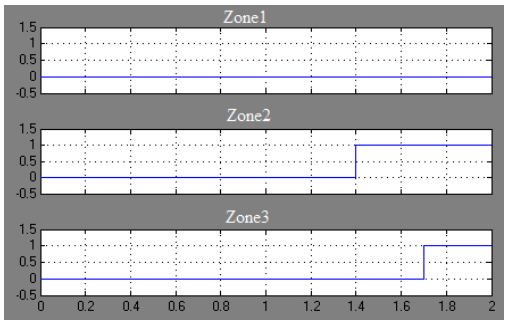

(d) A-B relay trip signals

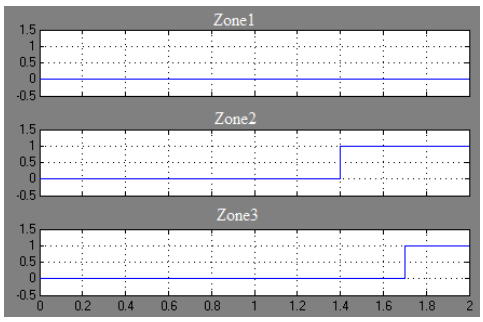

(e) B-C relay trip signals

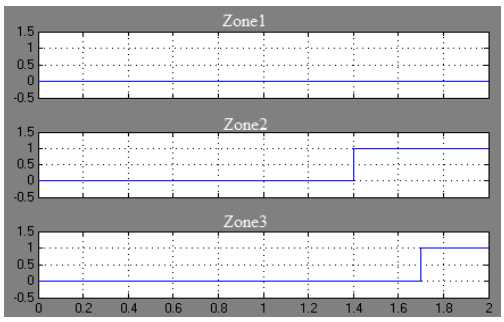

(f) C-A relay trip signals

Figure 6-52 A-G, B-G, C-G, A-B, B-A, C-A relay trip signals

6.2.3 Faults in Zone3

When a fault occurs at zone3 area, it is not covered by zone1 and zone2 protection and these should not trip.

6.2.3.1 Single phase to ground fault at 200km

An A-G fault was applied to the power system on line2 at 200km. The fault was out of zone1 and zone2 reach. Zone3 protection covered the fault and was expected to trip when fault occurred.

Fig.6-53 shows the A-G fault impedance trajectory. The A-G fault impedance trajectory entered the protection zone3 characteristic and settled at the fault point on the line. Fig.6-54 shows the A-G block-average comparator output. Fig.6-55 shows the A-G trip signal. Zone3 tripped 500ms after fault.

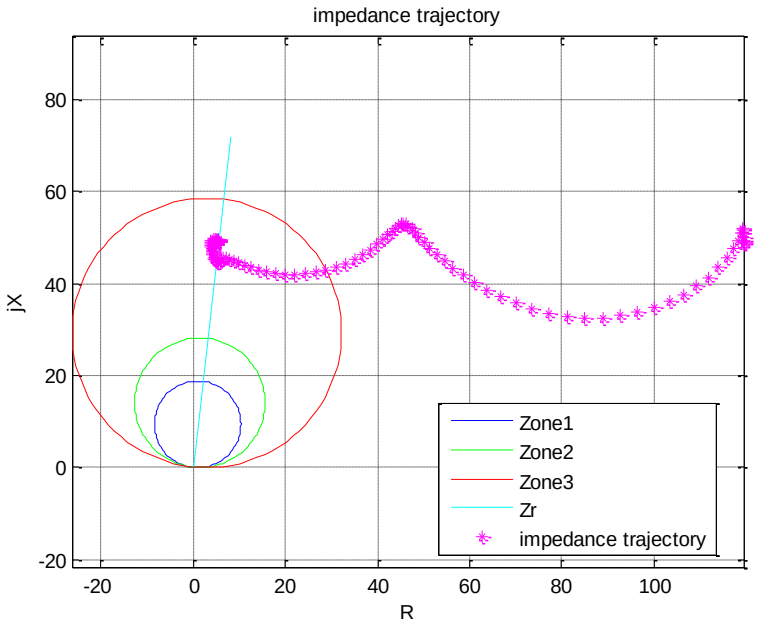

Figure 6-53 A-G fault impedance trajectory

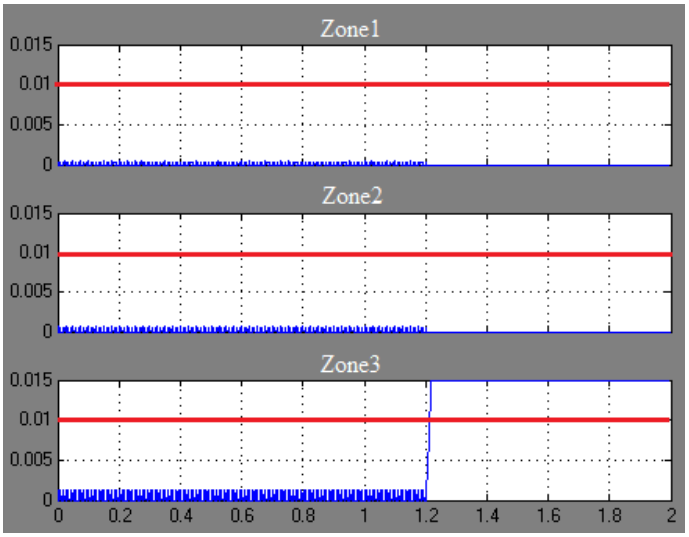

Figure 6-54 A-G block-average comparator output

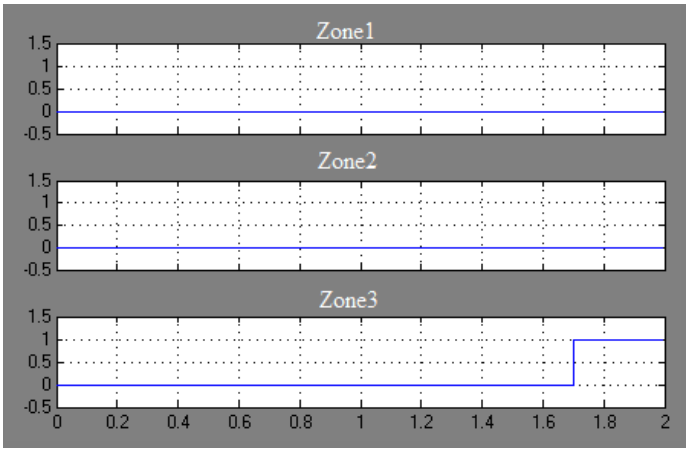

Figure 6-55 A-G relay trip signals

The B-G, C-G, A-B, B-A, C-A fault impedance trajectories are shown in fig.6-56. As can be seen from the fig.6-56, no impedance trajectories entered the protection zones.

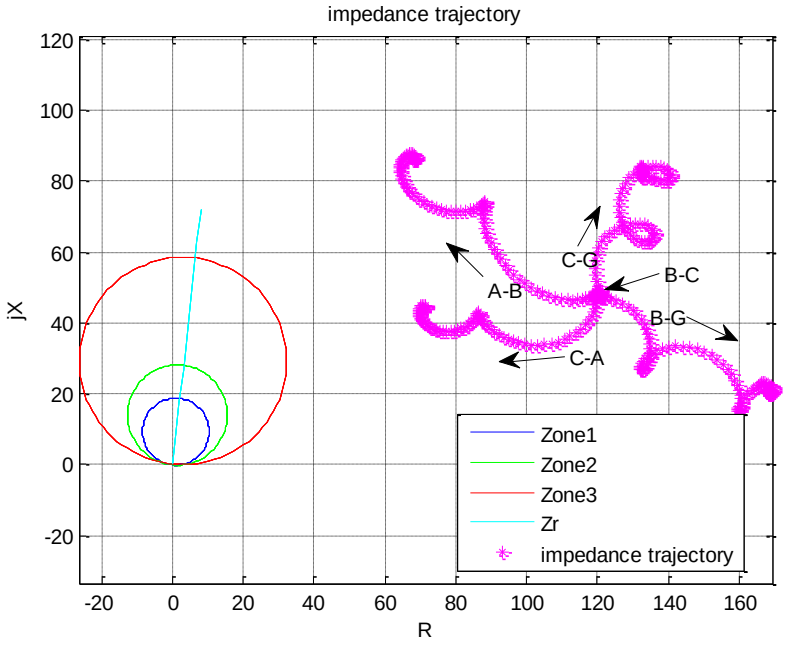

Figure 6-56 B-G, C-G, A-B, B-A, C-A fault impedance trajectories

The results of B-G and C-G faults are similar to A-G fault and shown in the appendix E.1 and E.2.

6.2.3.2 Phase to phase fault at 200km

An A-B fault was applied to the power system on line2 at 200km. The fault was covered by the A-B zone3 protection. The A-B fault impedance trajectory is shown in fig.6-57. The impedance locus entered the protection zone3 characteristic. Fig.6-58 shows the A-B block-average comparator output. Only zone3 output tripped. The trip signal is given in fig.6-59. A-B zone3 tripped 500ms after fault.

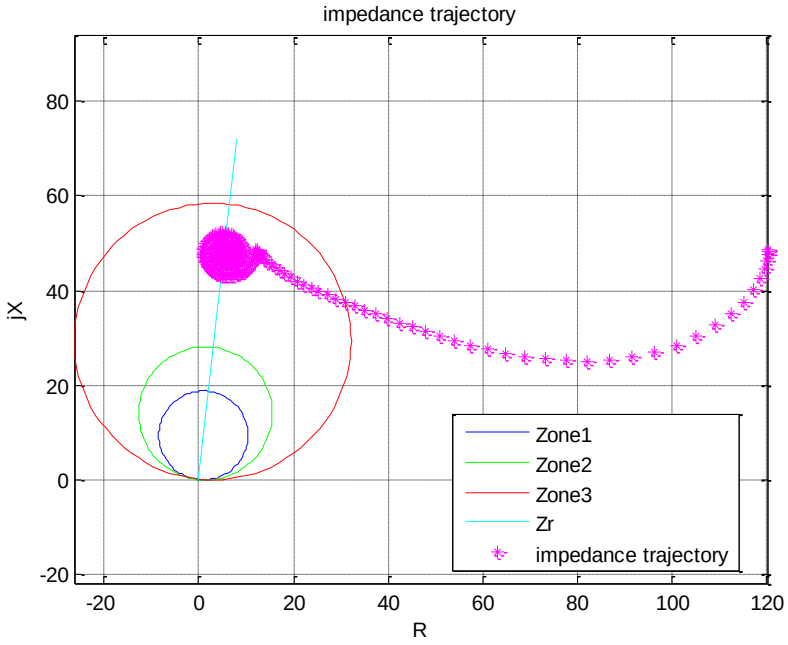

Figure 6-57 A-B fault impedance trajectory

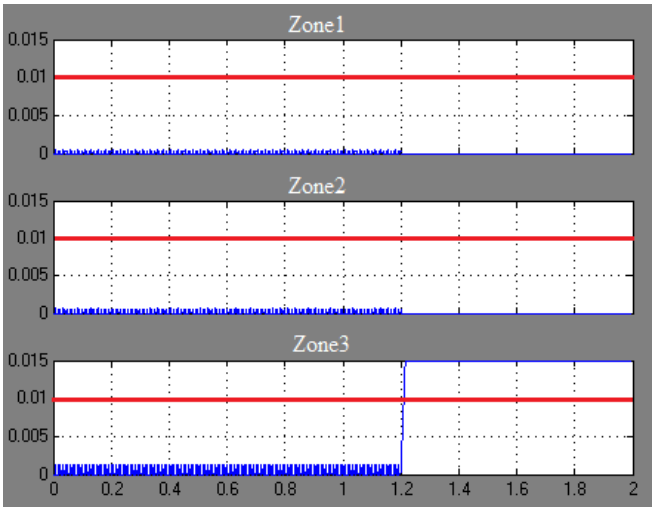

Figure 6-58 A-B block-average comparator output

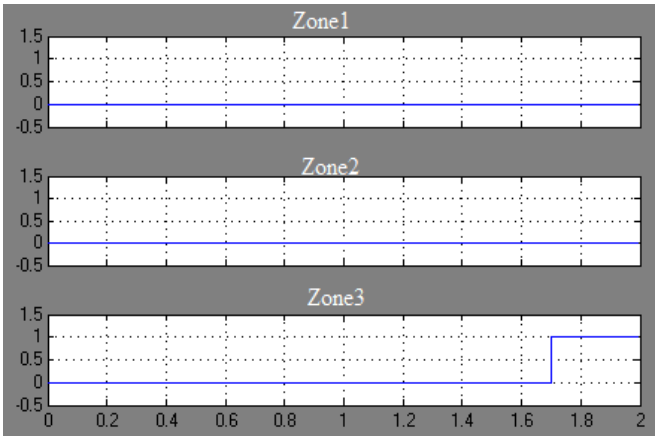

Figure 6-59 A-B relay trip signals

The A-G, B-G, C-G, B-C, C-A impedance trajectories are shown in fig.6-60. As can be seen from the fig.6-60, only A-G impedance trajectories entered the protection zone3 characteristic. Fig.6-61 (a) and (b) show the A-G block-average comparator output and A-G protection trip signals.

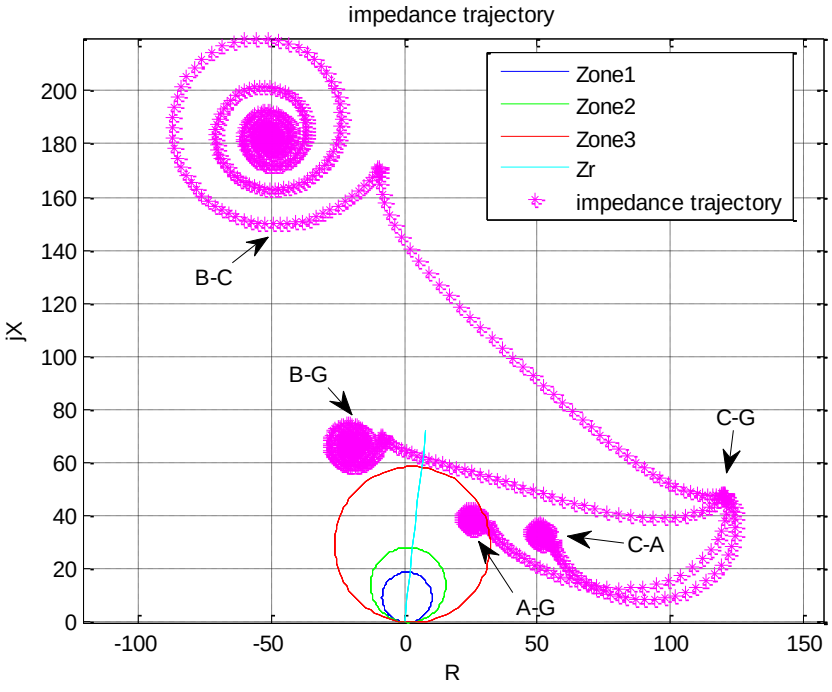

Figure 6-60 A-G, B-G, C-G, B-C, C-A impedance trajectories

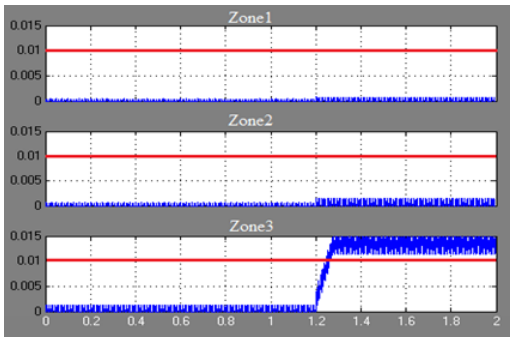

(a) A-G block-average comparator output

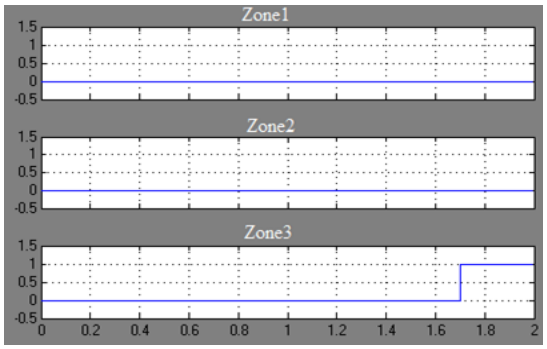

(b) A-G relay trip signals

Figure 6-61 A-G block-average comparator output and trip signals

The results of B-C and C-A faults are similar to A-B fault. Results are shown in appendix E.3 and E.4.

6.2.3.3 Phase to phase to ground fault at 200km

A B-C-G fault was applied to the power system on line2 at 200km. Fig.6-62 shows the B-G, C-G and B-C fault impedance trajectories. All three impedance trajectories entered protection zone3 characteristic and settled on the protection line at 200km. Fig.6-63 (a), (b), (c) show the B-G, C-G and B-C block-average comparators' outputs. All three comparators' zone3 outputs tripped. Fig.6-64 (a), (b), (c) show the B-G, C-G and B-C trip signals. All three relay zone3 tripped at 500ms after fault.

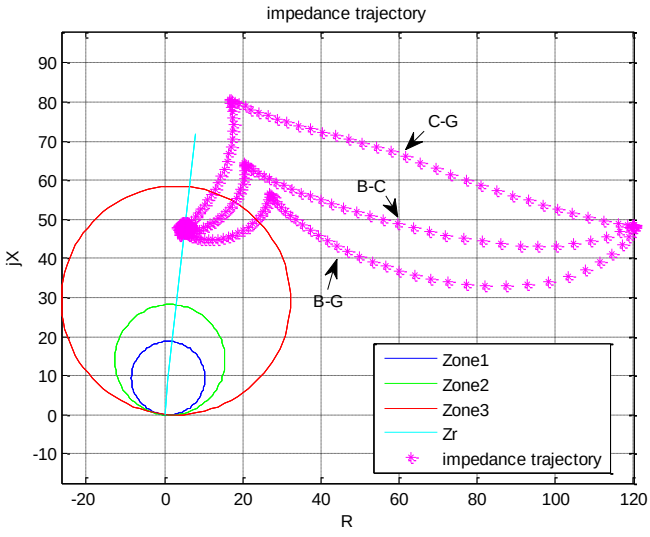

Figure 6-62 B-G, C-G and B-C fault impedance trajectories

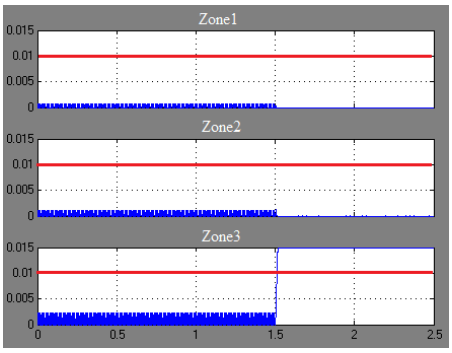

(a) B-G block-average comparator output

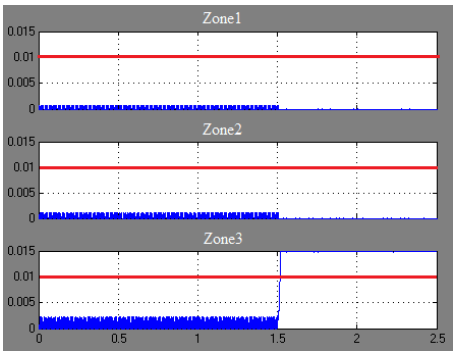

(b) C-G block-average comparator output

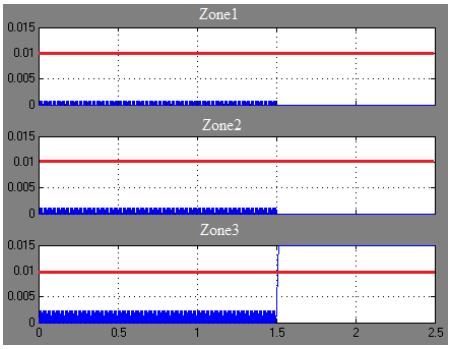

(c) B-C block-average comparator output

Figure 6-63 B-G, C-G and B-C block-average comparators' outputs

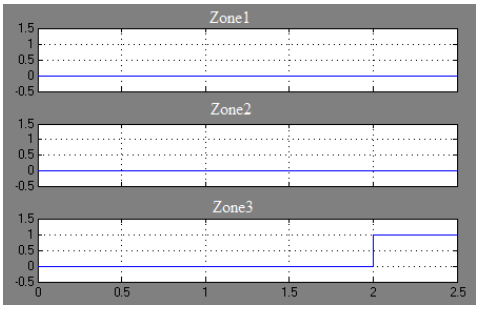

(a) B-G relay trip signals

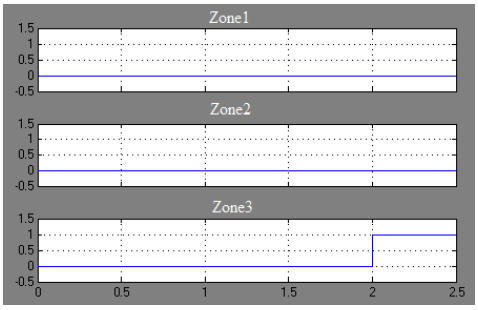

(b) C-G relay trip signals

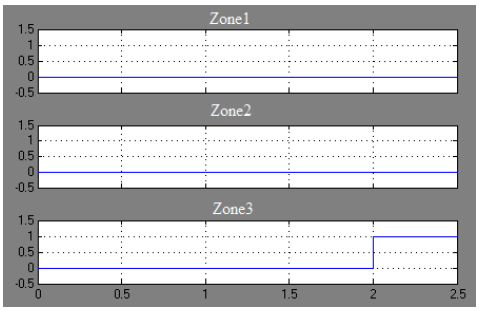

(c) B-C relay trip signals

Figure 6-64 B-G, C-G and B-C relay trip signals

The A-G, A-B and C-A impedance trajectories are shown in fig.6-65. None of these impedance trajectories entered the protection zones.

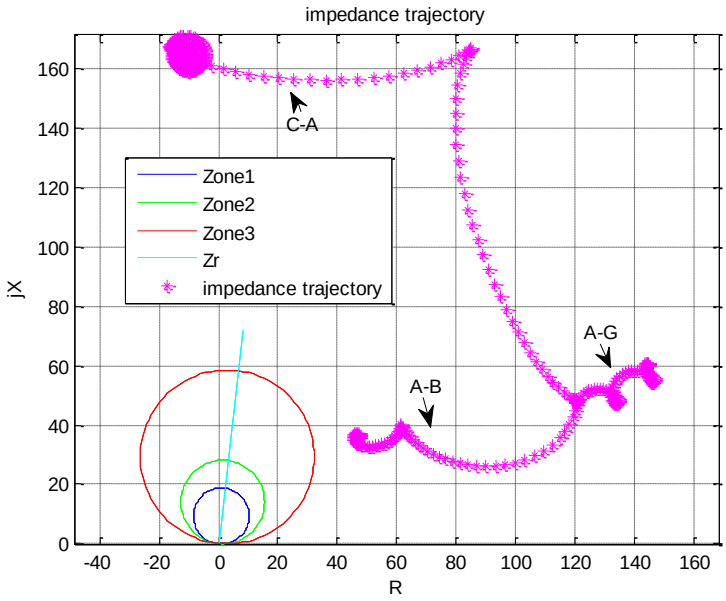

Figure 6-65 A-G, A-B and C-A impedance trajectories

The results of A-B-G, C-A-G faults are similar to B-C-G fault and shown in appendix E.5 and E.6.

6.2.3.4 Three-phase at 200km

A three-phase fault was applied to the power system on line2 at 200km. The fault impedance trajectories are shown in fig.6-66. All fault impedance trajectories entered the protection zone3 characteristic. Fig.6-67 (a), (b), (c), (d), (e), (f) show the A-G, B-G, C-G, A-B, B-A, C-A block-average comparators' outputs. All zone3 outputs crossed the trip level after fault. Fig.6-68 (a), (b), (c), (d), (e), (f) show the A-G, B-G, C-G, A-B, B-A, C-A protection trip signals. The relay's zone3 protection tripped 500ms after fault.

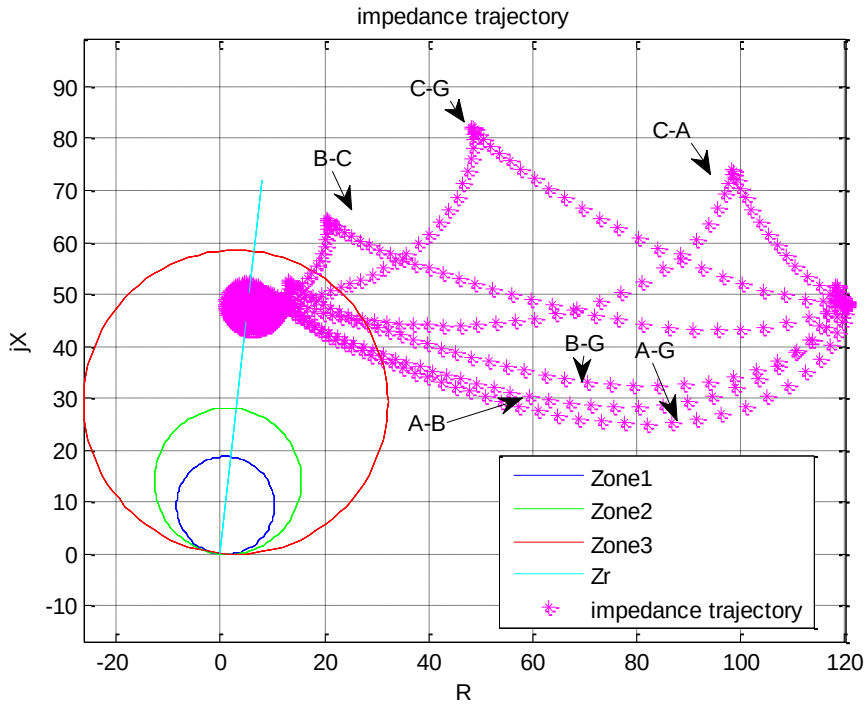

Figure 6-66 A-G, B-G, C-G, A-B, B-A, C-A fault impedance trajectories

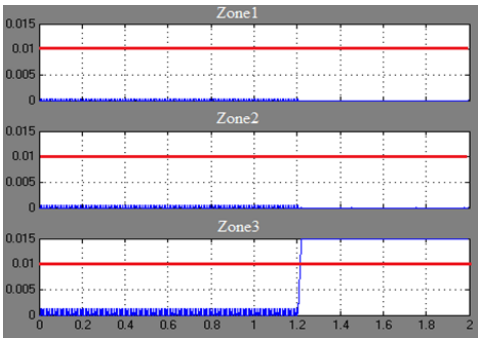

(a) A-G block-average comparator output

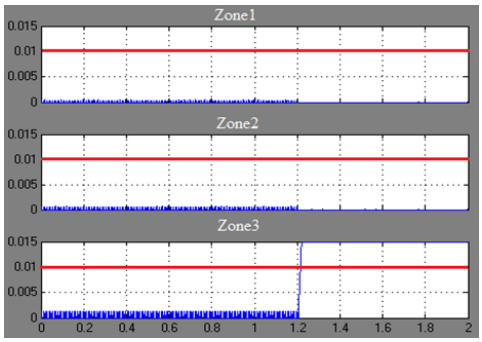

(b) B-G block-average comparator output

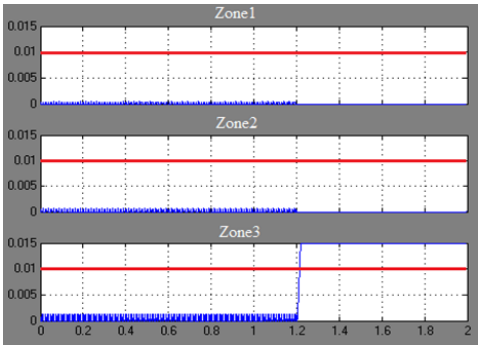

(c) C-G block-average comparator output

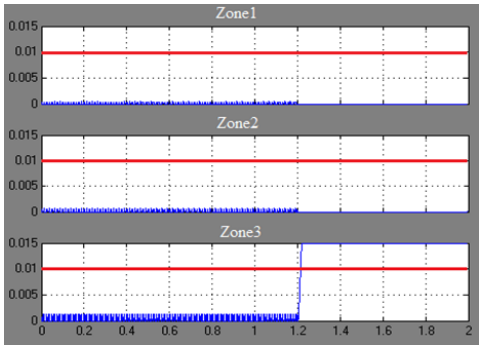

(d) A-B block-average comparator output

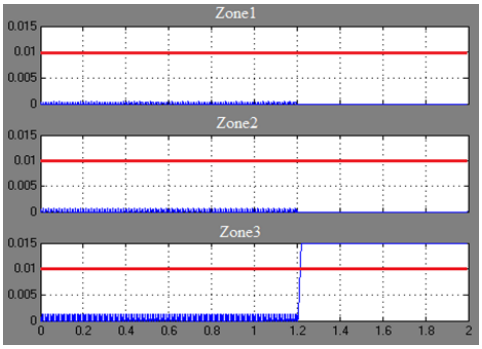

(e) B-C block-average comparator output

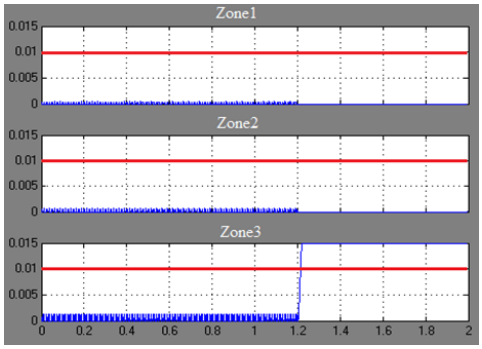

(f) C-A block-average comparator output

Figure 6-67 A-G, B-G, C-G, A-B, B-A, C-A block-average comparators' outputs

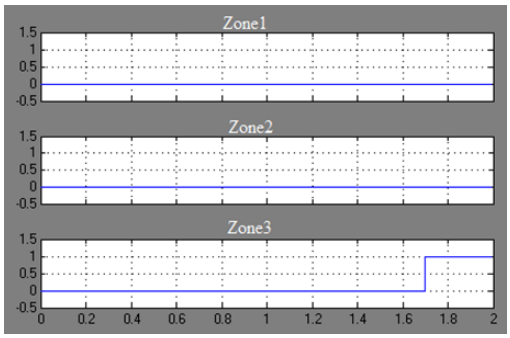

(a) A-G relay trip signals

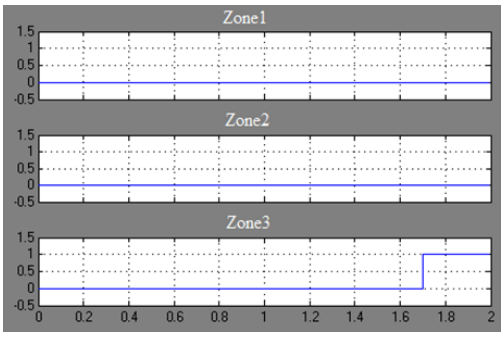

(b) B-G relay trip signals

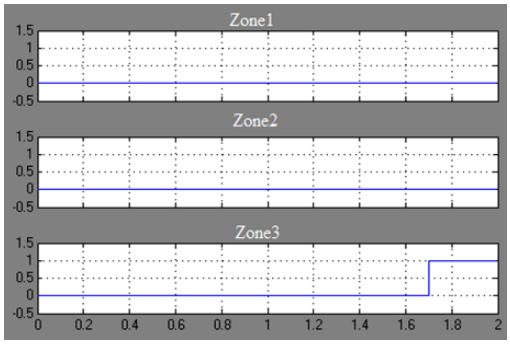

(c) C-G relay trip signals

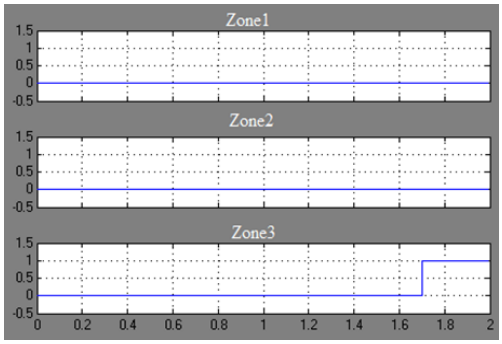

(d) A-B relay trip signals

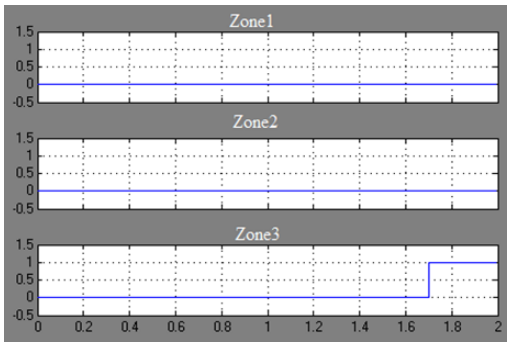

(e) B-C relay trip signals

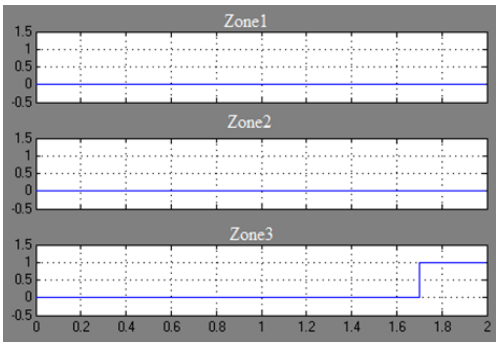

(f) C-A relay trip signals

Figure 6-68 A-G, B-G, C-G, A-B, B-A, C-A relay trip signals

6.2.4 Faults out protection zones

The three-phase fault is the worst fault in the power system. All relays are required to operation during three phase fault. In order to test the distance relay's response to faults outside of its protecting zones, a three-phase fault was applied to the power system on line3 at 280km. The fault was outside of the distance relay's protection zones. The fault impedance trajectories are shown in fig.6-69. None of the

impedance trajectories entered the protection zones. They all settled on the protected line at 280km. There was no tripping in response to this fault.

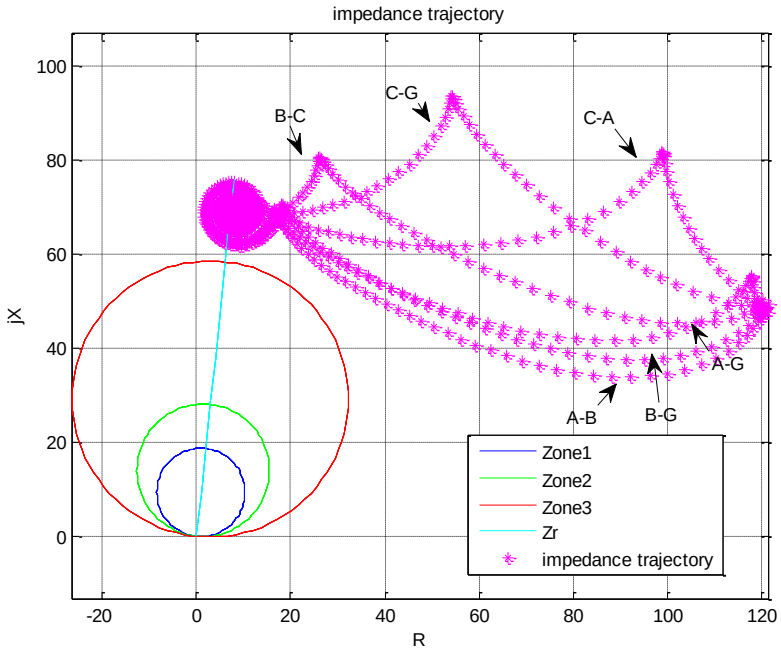

Figure 6-69 A-G, B-G, C-G, A-B, B-A, C-A fault impedance trajectories

6.3 Chapter Summary

This chapter introduced the modelled distance relay and explained how the relay would respond to a selection of fault conditions. The simulation work was carried on in MATLAB/SIMULINK. The modelled distance relay used the Mho characteristic.

The interface between the distance relay and the protected ac lines was performed by ideal current transformers and voltage transformers.

The current signals from CT were input to replica impedance circuits to generate IZ signals. The IZ signals were mixed with the V signals for block-average comparators to compare and generate trip signals when there was a fault. Different zones settings were achieved by changing z_r.

In order to plot the impedance trajectories, the measured voltage and current signals were filtered by low-pass filters to remove the unwanted high frequency components. The filtered signals were then input into DFT circuits to extract fundamental phasor

information. The outputs of the DFT were finally processed by the impedance computing algorithm and plot the apparent impedance.

The modelled distance relay was tested using a simple AC power system based on the Kundur's two areas system [68]. Different types of faults at different locations within distance relay protection zones and outside the protection zones were tested and studied. The distance relay block-average comparator outputs during faults were studied as well as the fault impedance trajectories. The results of the distance relay operations were compared with previous researcher's work and the distance relay were proofed worked as expected.

The modelled distance relay response to faults when the protected feeders containing HVDC lines will be investigated in the following chapter.

Chapter 7

The HVAC/HVDC Impacts on Distance Relay under fault conditions

In this chapter, the response of distance relay to fault conditions on a network containing both HVDC and HVAC lines were investigated

7.1 The impact of HVAC/HVDC circuit on distance relay during fault conditions

To investigate the HVDC interconnection impact on distance relay during fault conditions, the previous simulated HVDC-HVAC interconnection system was studied when it was protected by set distance relay at busbar A. The modelled power system was developed from the system modelled by Kundur [68] and as shown in fig.7-1.

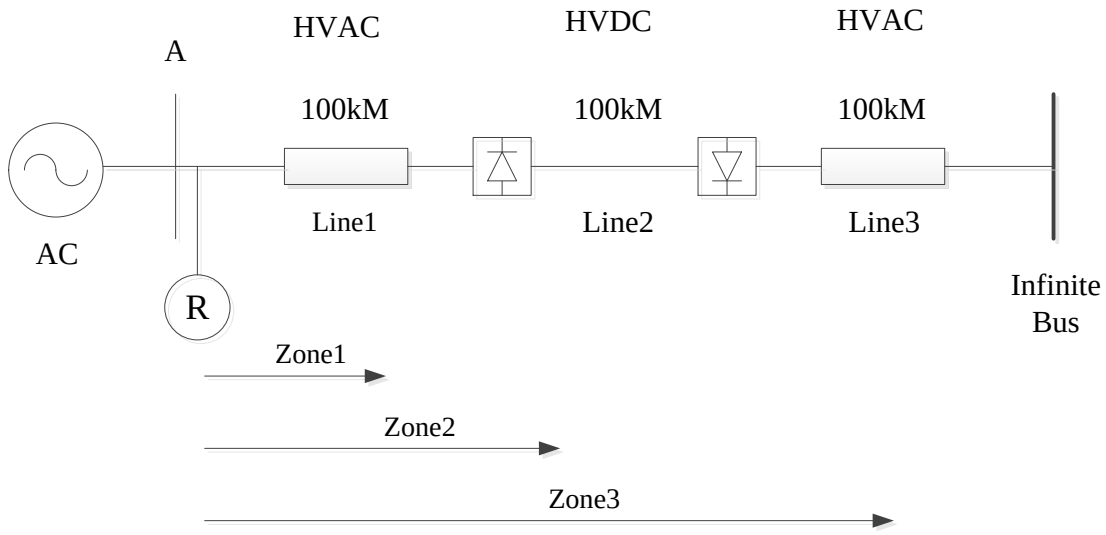

Figure 7-1 Modelled HVDC interconnection system

A 230kV, 9000MVA ac system was connected to 230kV infinite bus through two 100km HVAC transmission lines and 100km HVDC link. The HVDC link had a rated voltage and current of 56kV and 3.6kA respectively. The DC line resistance was 1.5Ω and inductance is 100mH. A smoothing reactor of 50mH was used at each end of the line. The converter transformers were modelled as ideal transformers.

The responses were compared to a simple HVAC interconnection system as shown in fig.7-2. These two systems were set up under similar conditions. The details of the model are shown in Appendix. F

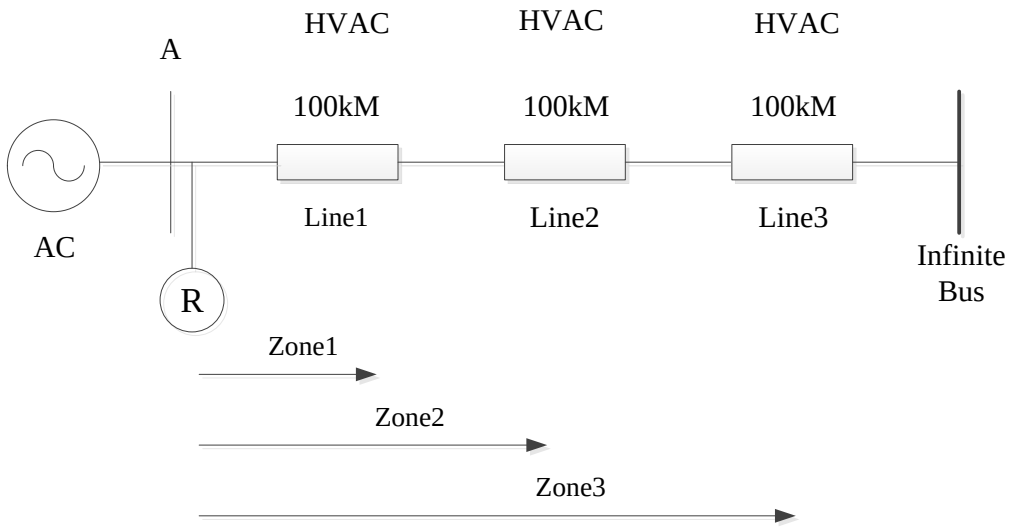

Figure 7-2 The comparing HVAC system

The AC line parameters are shown in table.7-1 [68].

Positive-sequence		Zero-sequence	
r_1	x_1	r_0	x_0
0.053Ω/km	0.531 Ω/km	1.638 Ω/km	2.312 Ω/km

Table 7-1 AC line parameters [68]

The distance relay was located at busbar A to protected line1. Zone1 was set to 80% of line1, Zone2 to 120% of line1 and Zone3 to 250% of line1. The time delays for zone1, zone2 and zone3 were 0ms, 200ms and 500ms respectively. The simulation duration was 2.5s. The fault duration was from 1.5s to 2.5s.

The study was carried out by applying different types of faults at different locations into HVAC/HVDC system and HVAC system to investigate the distance relay's response. The distance relay's response to faults on the HVAC/HVDC system was compared to similar faults on the HVAC system.

7.1.1 Protection response to fault in zone1

7.1.1.1 Protection response to A-G fault at 50km on line1

An A-G fault was injected into both power systems at 50km on line1. The fault was covered by distance relay zone1 protection. Fig.7-3 (a), (b) shows the HVAC/HVDC and HVAC A-G fault impedance trajectories respectively. Both fault impedance trajectories entered the protection zone1 characteristic. Fig.7-4 (a), (b) gives the A-G block-average comparator outputs in HVAC/HVDC and HVAC systems respectively. Both comparators tripped. Fig.7-5 (a), (b) gives the distance relay zone1 trip signals in both HVAC/HVDC system and HVAC system. Fig.7-5 (a) presents distance relay A-G trip signal in the HVAC/HVDC system. The distance relay zone1tripped 11ms after fault. Zone2 and Zone3 tripped 200ms after fault and 500ms after fault. Fig.7-5 (b) shows the distance relay A-G trip signal in HVAC system. The distance relay zone1 tripped 10ms after fault. Zone2 and zone3 tripped 200ms after fault and 500ms after fault respectively.

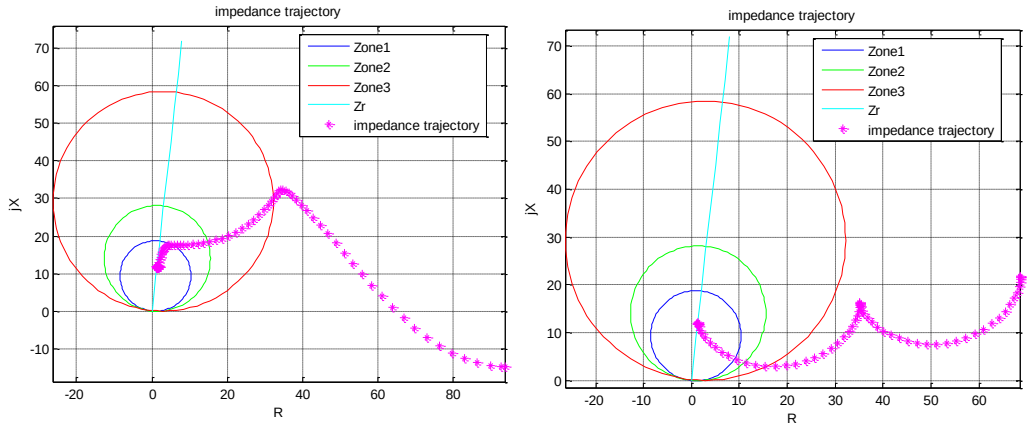

(a) HVAC/HVDC (b) HVAC

Figure 7-3 Fault impedance trajectories

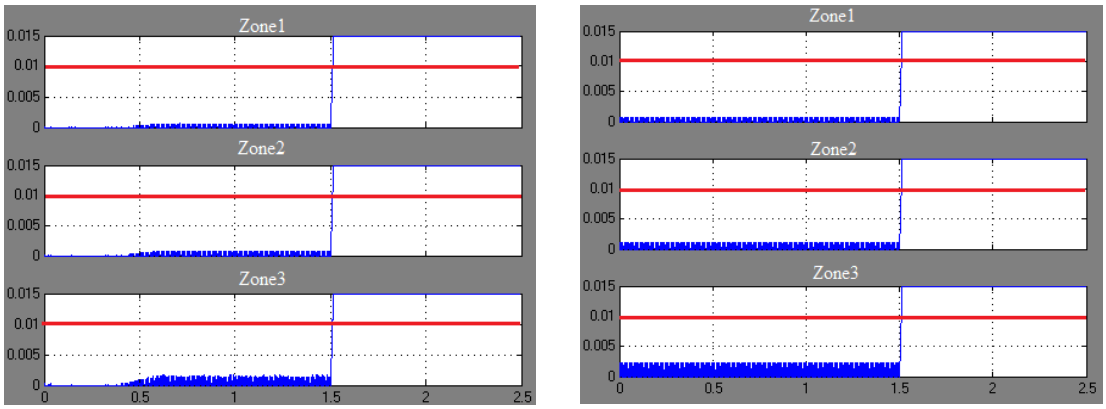

(a) HVAC/HVDC (b) HVAC

Figure 7-4 A-G block-average comparator output

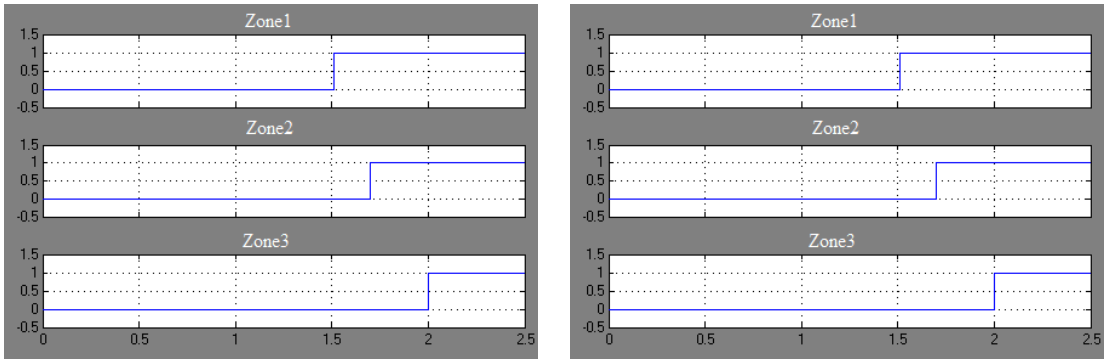

(a) HVAC/HVDC (b) HVAC

Figure 7-5 Distance relay A-G trip signals

7.1.1.2 Protection response to A-B-G fault at 50km on line1

The A-B-G fault was applied to both the HVDC system and HVAC system at 50km on line1. The fault duration was from 1.5s to 2.5s. The fault was covered by distance relay zone1 protection. The A-G, B-G and A-B protection responded to the fault. Fig.7-6 (a), (b) give the A-G, B-G, A-B fault impedance trajectories in HVAC/HVDC system and HVAC system respectively. All the impedance trajectories entered the protection zone1 characteristic. Distance relays tripped for the faults. Fig.7-7 (a), (b), (c) show the distance relay A-G, B-G, A-B block-average comparators' outputs in HVAC/HVDC system. All zone1, zone2 and zone3 outputs crossed the trip level. Fig.7-8 (a), (b), (c) give the distance relay A-G, B-G and A-B trip signals in HVAC/HVDC system. As can be seen from fig.7-8, the zone1

protection tripped 10ms after fault. Zone2 and zone3 protection tripped at 200ms after fault and 500ms after fault.

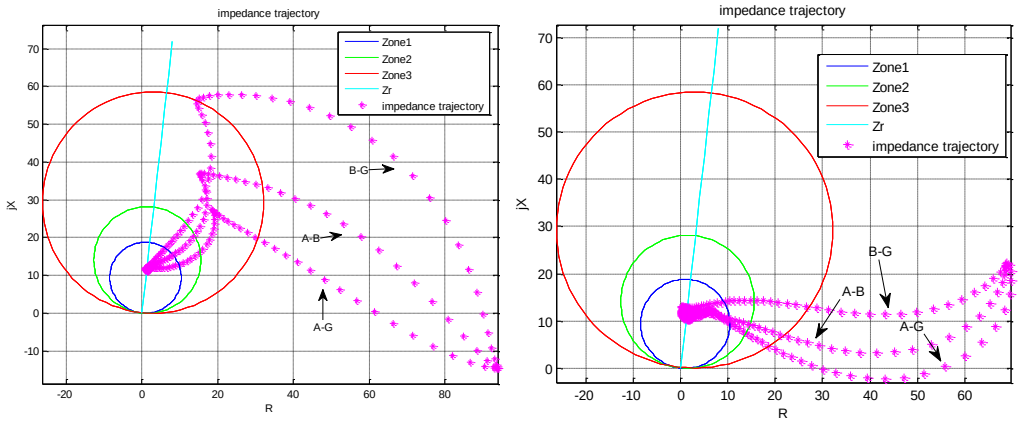

(a) HVAC/HVDC (b) HVAC

Figure 7-6 A-G, B-G, A-B fault impedance trajectories

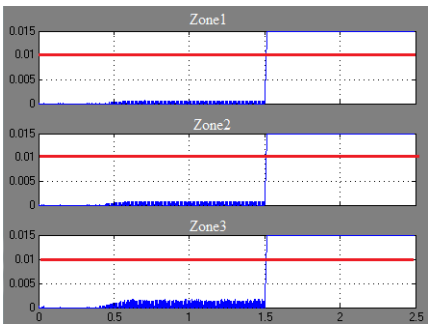

(a) A-G block-average comparator output

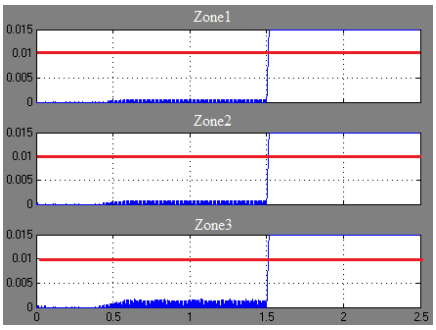

(b) B-G block-average comparator output

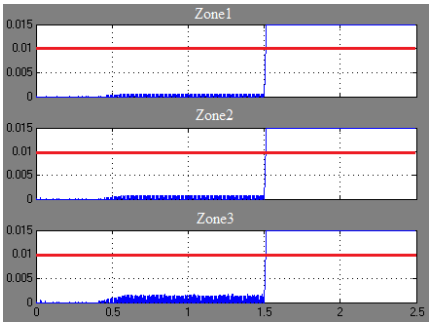

(c) A-B block-average comparator output

Figure 7-7 A-G, B-G, A-B block-average comparators' outputs for the HVAC/HVDC transmission system

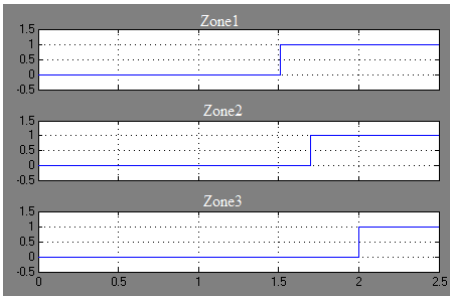

(a) A-G relay trip signals

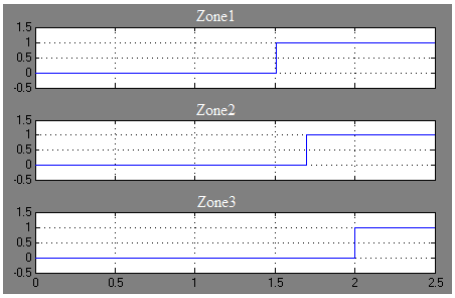

(b) B-G relay trip signals

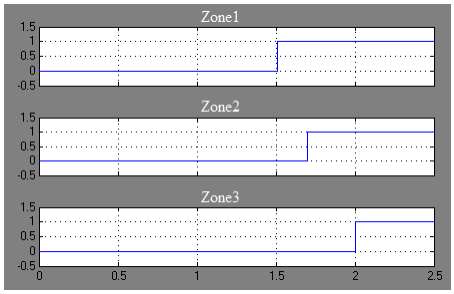

(c) A-B relay trip signals

Figure 7-8 A-G, B-G, A-B trip signals for the HVAC/HVDC transmission system

Fig.7-9 (a), (b), (c) give the distance relay A-G, B-G, A-B block-average comparators' outputs in HVAC system. All the comparators tripped as expected. Fig.7-10 (a), (b), (c) show the distance relay A-G, B-G, A-B trip signals in HVAC system. The zone1 protection tripped 10ms after fault, zone2 protection tripped 200ms after fault and zone3 protection tripped 500ms after fault respectively.

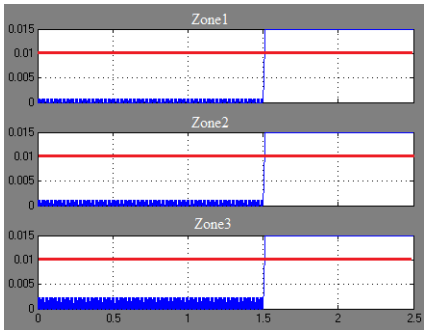

(a) A-G block-average comparator output

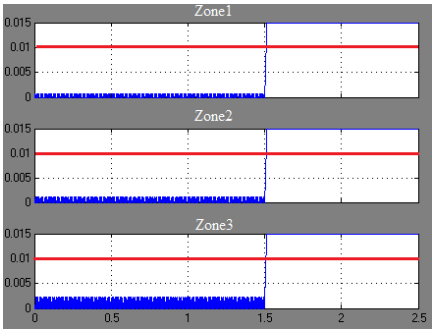

(b) B-G block-average comparator output

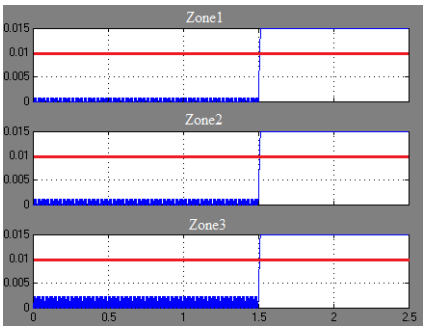

(c) A-B block-average comparator output

Figure 7-9 A-G, B-G, A-B block-average comparators' outputs for HVAC transmission system

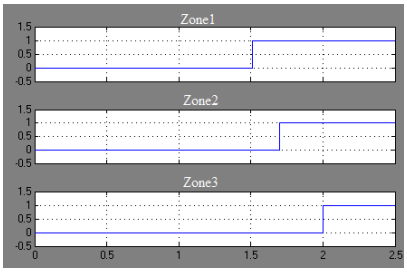

(a) A-G relay trip signals

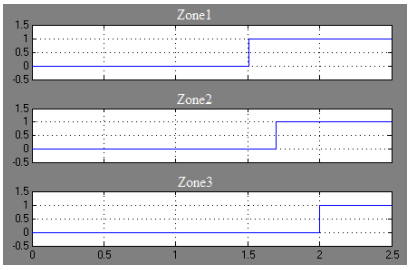

(b) B-G relay trip signals

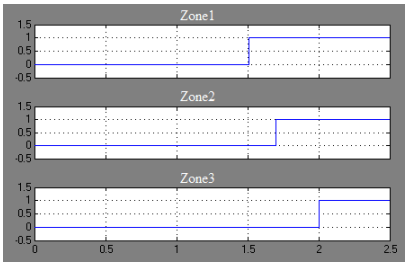

(c) A-B relay trip signals

Figure 7-10 Distance relay trip signals for HVAC transmission system

From the results above, it is apparent that when fault occurred in zone1 area, the distance relays in both HVAC/HVDC system and HVAC system tripped as expected.

7.1.2 Protection response to fault in zone2

For a line to ground fault on the HVDC line as shown in fig.7-11 below, the connected ac system experiences the fault current and voltage in each phase. The distance relay including A-G, B-G, C-G, A-B, B-C, C-A protection which is set to protect the ac transmission line, will all detect the fault voltage and current. Due to HVDC converter station control strategy, the fault impedances seen by the array of distance relay comparators will be similar.

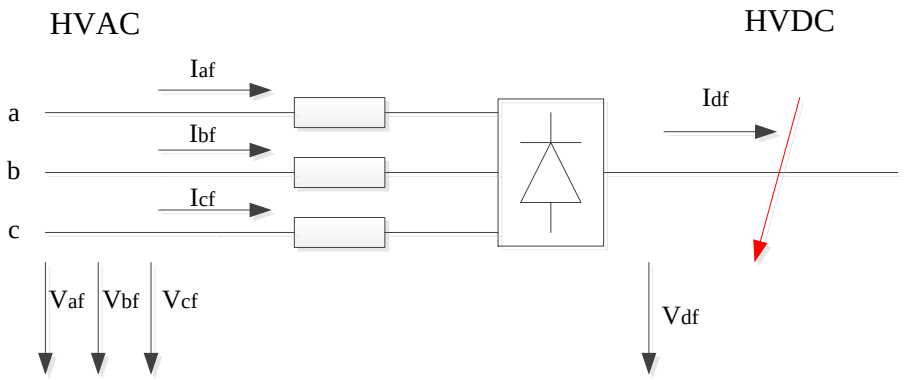

Figure 7-11 Fault on DC line

A DC line to ground fault was injected into the system on DC line at 10km from the converter station. The fault location therefore was 110km from the distance relay and covered by distance relay zone2 protection. The A-G, B-G, C-G, A-B, B-C, C-A fault impedance trajectories are shown in fig.7-12 (a), (b), (c), (d), (e), (f). As can be found in fig.7-12, the impedance trajectories were similar.

Considering the phase A-G fault impedance trajectory, the fault impedance trajectory started from the steady point and circled the protection characteristic zones. The fault impedance was higher than the set impedance and did not enter the protection zones. There was no possibility to trip since the fault impedance trajectory did not enter the protection zones during the fault. The fault impedance trajectory finally settled in negative reactance area at about -275Ω reactive after a few cycles.

This negative reactive impedance indicated that there was huge reactive power in the system, which was absorbed by HVDC converter station. The B-G, C-G, A-B, B-C, C-A fault impedance trajectories were similar. Fig.7-13 (a), (b), (c), (d), (e), (f) show the A-G, B-G, C-G, A-B, B-C, C-A block-average comparators' outputs. Since there was no fault impedance entering the protection zones, none of the comparator tripped. Fig.7-14 (a), (b), (c), (d), (e), (f) give the distance relay trip signals. There were no trips given that the HVDC link limited the values of fault voltage and current.

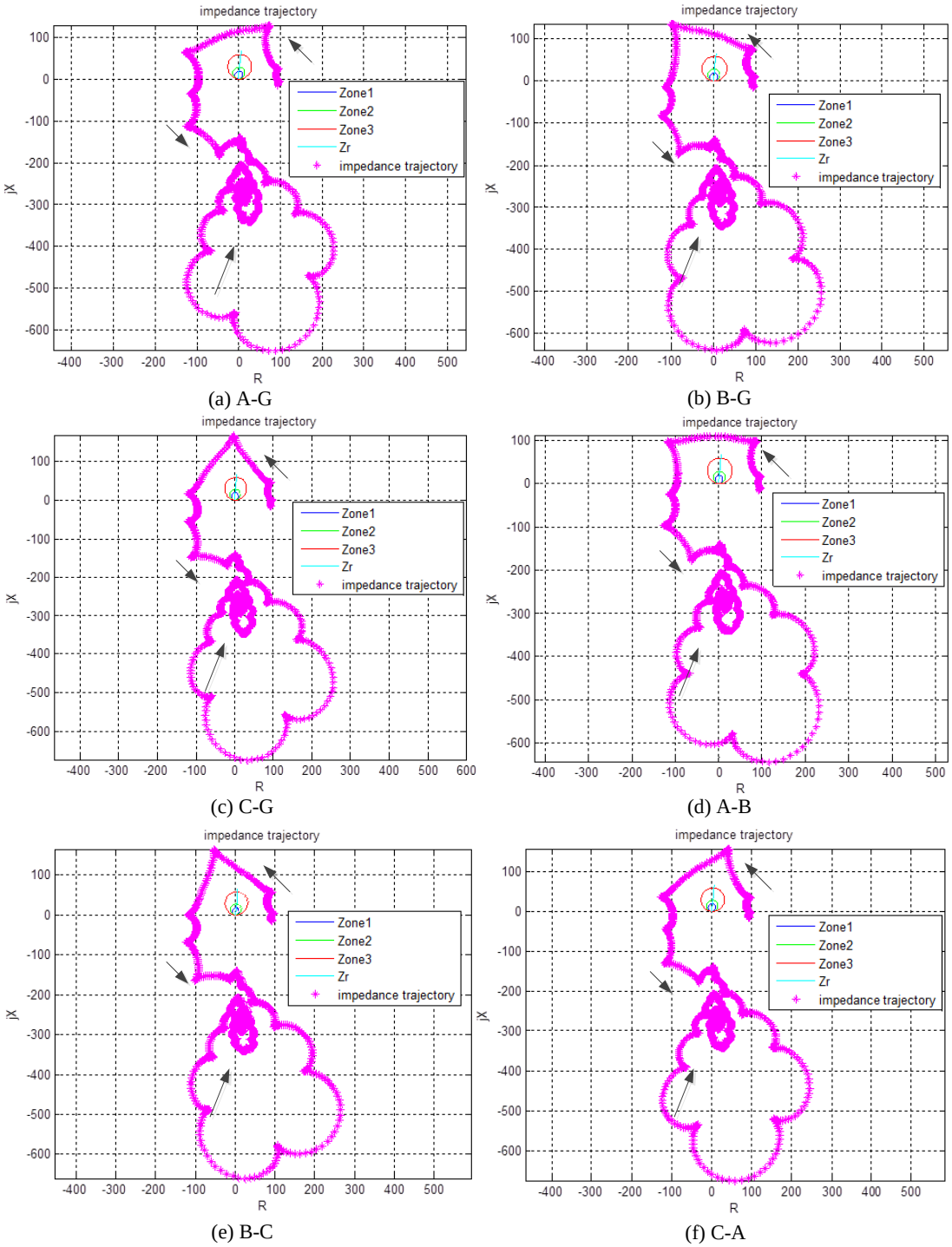

(a) A-G (b) B-G

(c) C-G (d) A-B

(e) B-C (f) C-A

Figure 7-12 The A-G, B-G, C-G, A-B, B-C, C-A fault impedance trajectories for a zone2 fault in the HVAC/HVDC transmission system

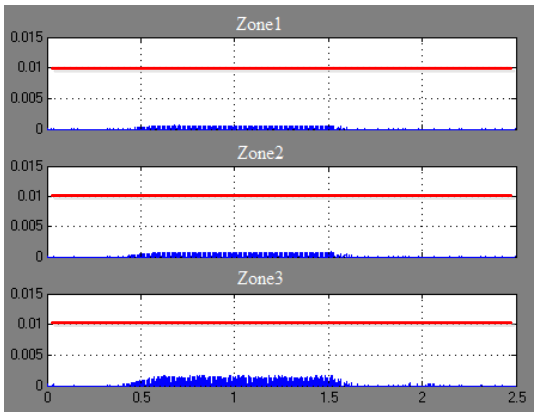

(a) A-G block-average comparator output

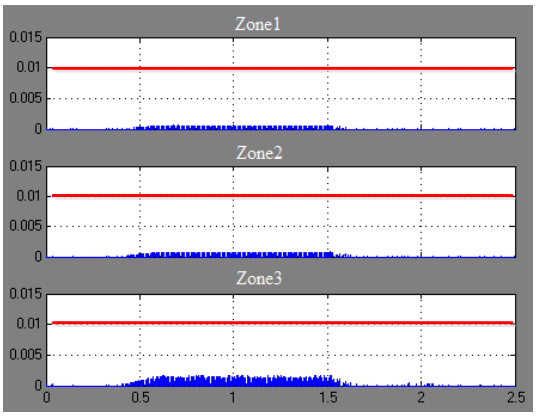

(b) B-G block-average comparator output

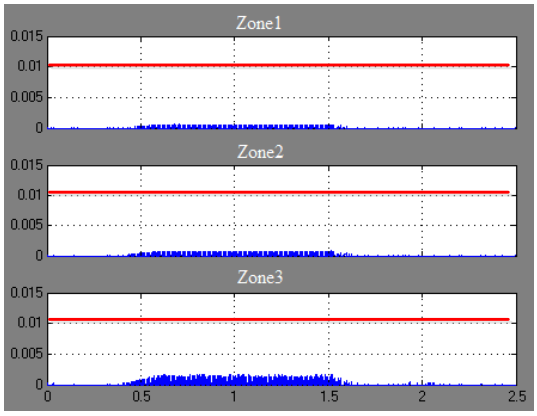

(c) C-G block-average comparator output

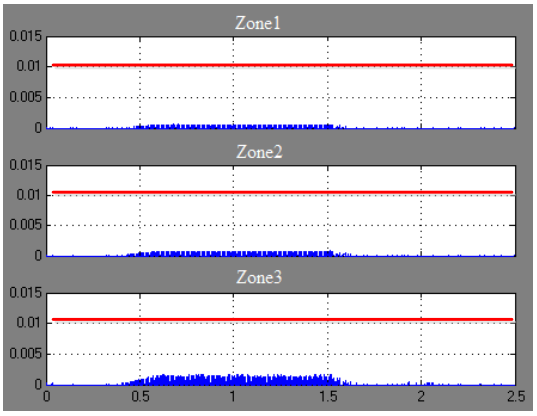

(d) A-B block-average comparator output

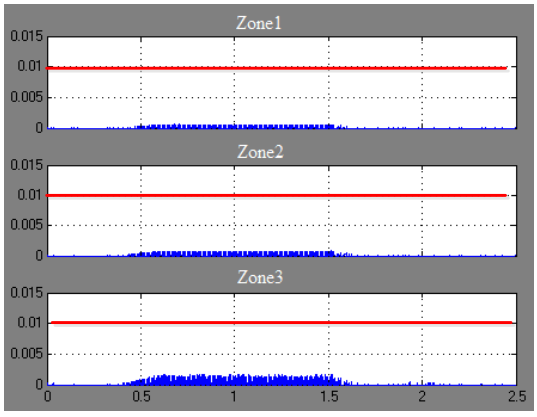

(e) B-C block-average comparator output

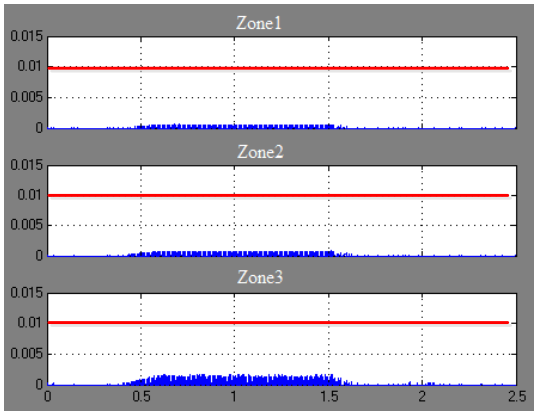

(f) C-A block-average comparator output

Figure 7-13 A-G, B-G, C-G, A-B, B-C, C-A block-average comparators' outputs for a zone2 fault in the HVAC/HVDC transmission system

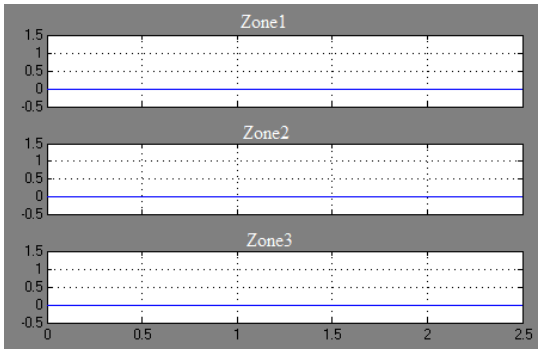

(a) A-G relay trip signals

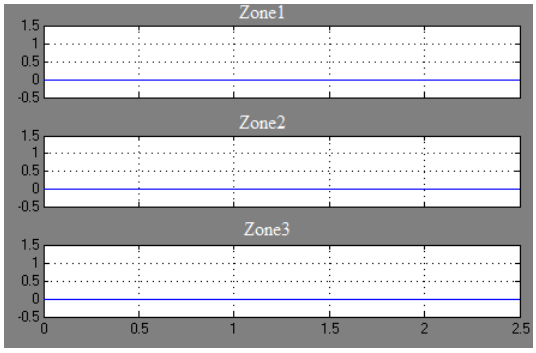

(b) B-G relay trip signals

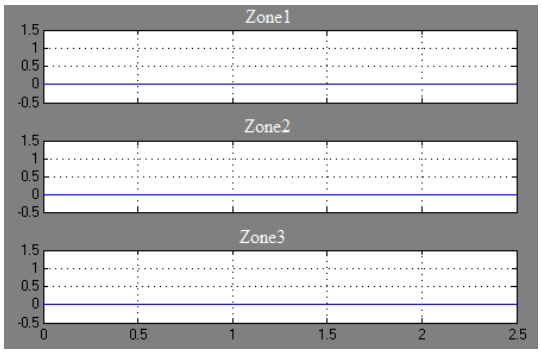

(c) C-G relay trip signals

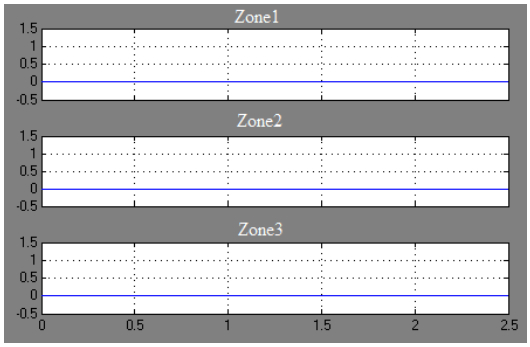

(d) A-B relay trip signals

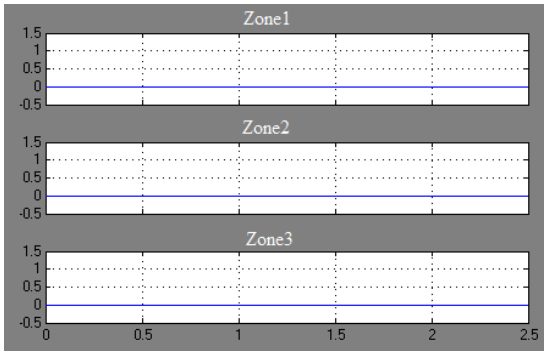

(d) B-C relay trip signals

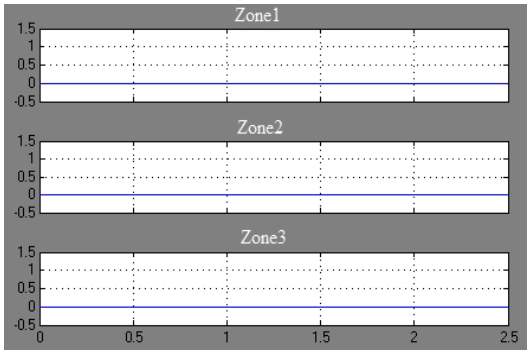

(f) C-A relay trip signals

Figure 7-14 Distance relay trip signals for a zone2 fault in the HVAC/HVDC transmission system

For comparison, an A-B-C-G fault was applied to the HVAC system on line2 at 10km, the similar location to that applied to the HVAC/HVDC system. The fault was covered by distance relay zone2 protection. Fig.7-15 gives the fault impedance trajectories, and shows that all the fault impedance trajectories entered the protection zone2 characteristic and settled at set impedance at 110km. Fig.7-16 (a), (b), (c),

(d), (e), (f) show the A-G, B-G, C-G, A-B, B-C, C-A block-average comparators' outputs. All zone2 and zone3 comparators' outputs tripped after fault. Fig.7-17 shows the distance relay trip signals, illustrating that zone2 tripped 200ms after fault. Zone3 tripped 500ms after fault.

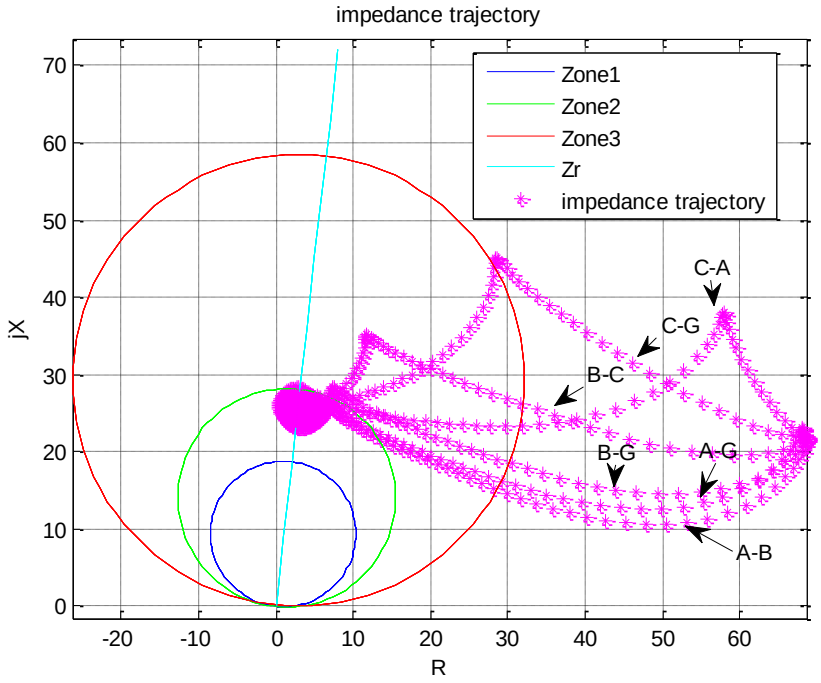

Figure 7-15 Fault impedance trajectories for a zone2 fault in the HVAC transmission system

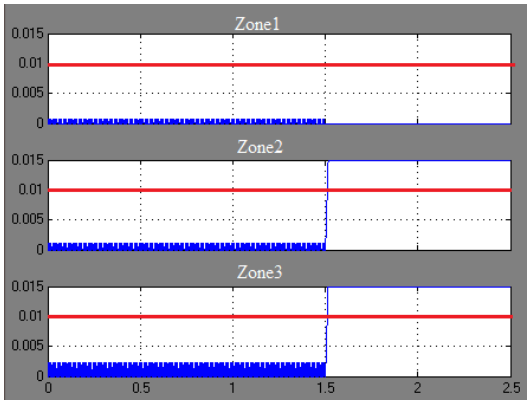

(a) A-G block-average comparator output

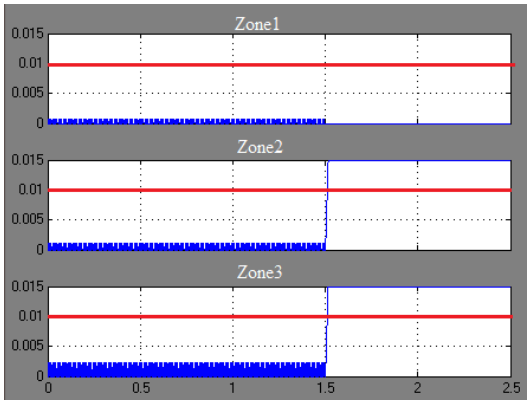

(b) B-G block-average comparator output

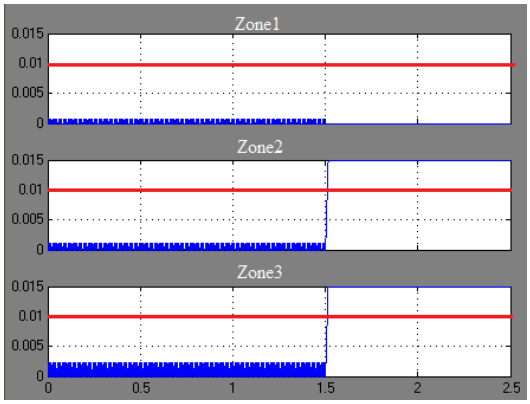

(c) C-G block-average comparator output

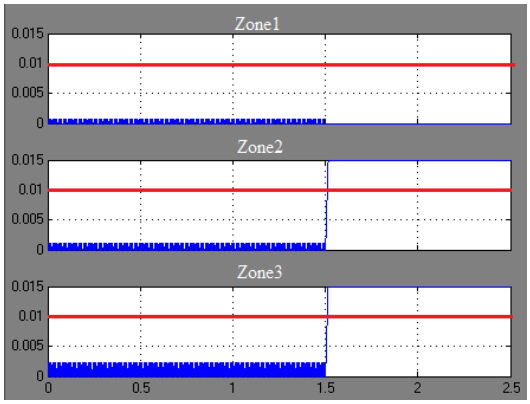

(d) A-B block-average comparator output

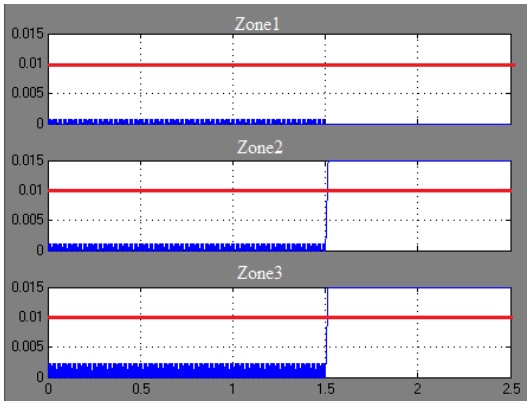

(e) B-C block-average comparator output

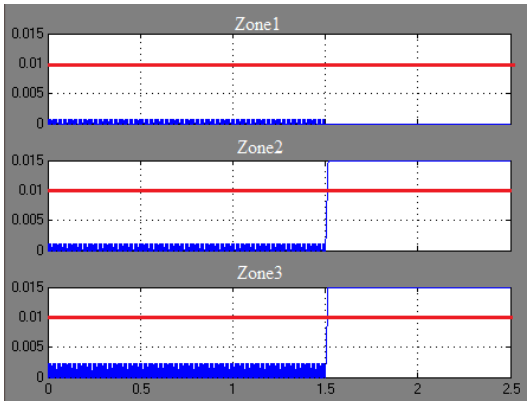

(f) C-A block-average comparator output

Figure 7-16 A-G, B-G, C-G, A-B, B-C, C-A block-average comparators' outputs for a zone2 fault in the HVAC transmission system

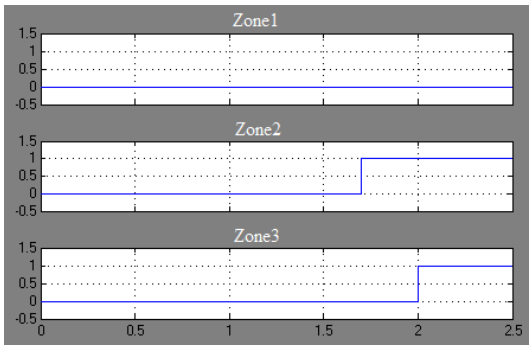

(a) A-G relay trip signals

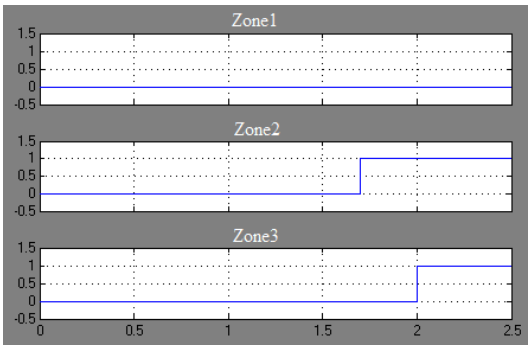

(b) B-G relay trip signals

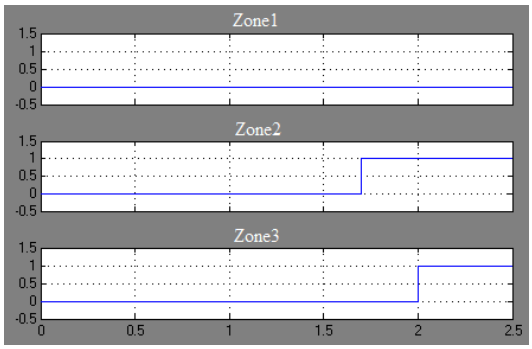

(c) C-G relay trip signals

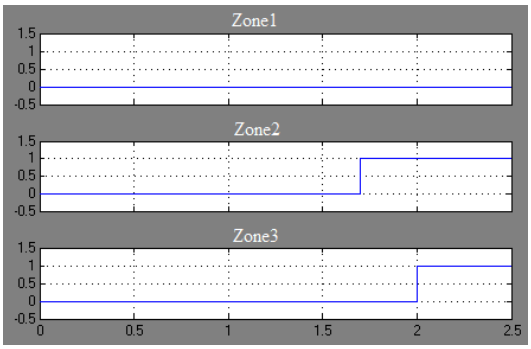

(d) A-B relay trip signals

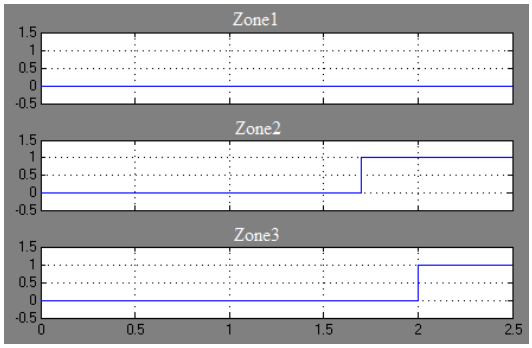

(d) B-C relay trip signals

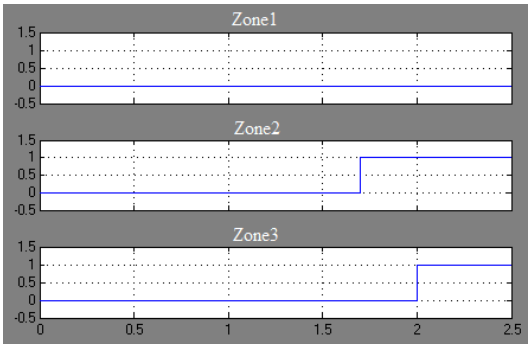

(f) C-A relay trip signals

Figure 7-17 Distance relay trip signals for a zone2 fault in the HVAC transmission system

From the results above it has been demonstrated that when a fault occurred on HVDC line of the HVAC/HVDC network, although it was covered by distance relay zone2 protection, the distance relay did not trip. In comparison, when a fault occurred on HVAC line at the same location on the HVAC system, the distance relay tripped as expected.

For the fault on HVDC line all of distance relay comparators detected the fault current and voltage. The fault impedances seen by distance relay when fault occurred on HVDC line were similar.

7.1.3 Protection response to fault in zone3

7.1.3.1 Protection response to fault on DC line at 50km

A DC line to ground fault was applied to the HVDC/HVAC system on the HVDC line at 50km from the converter station. The fault location was 150km from the distance relay, and therefore for an AC network would be covered by distance relay zone3 protection. The distance relay A-G, B-G, C-G, A-B, B-C, C-A protections' fault impedance trajectories are shown in fig.7-18 (a), (b), (c), (d), (e), (f), and show that all the fault impedance trajectories are similar to each other. The fault impedance trajectories started from a steady point and circled the protection zones. The fault impedances were higher than the set impedance. None of the fault impedance trajectories entered the protection zones and therefore there were no trips. The impedance trajectories settled in negative reactance area at about -275Ω reactive after a few cycles. The negative reactance was due to the HVDC converter station absorbing reactive power during fault. Fig.7-19 (a), (b), (c), (d), (e), (f) show the A-G, B-G, C-G, A-B, B-C, C-A block-average comparators' outputs. None of the comparator tripped. There were no trip signals output from distance relay as in fig.7-20.

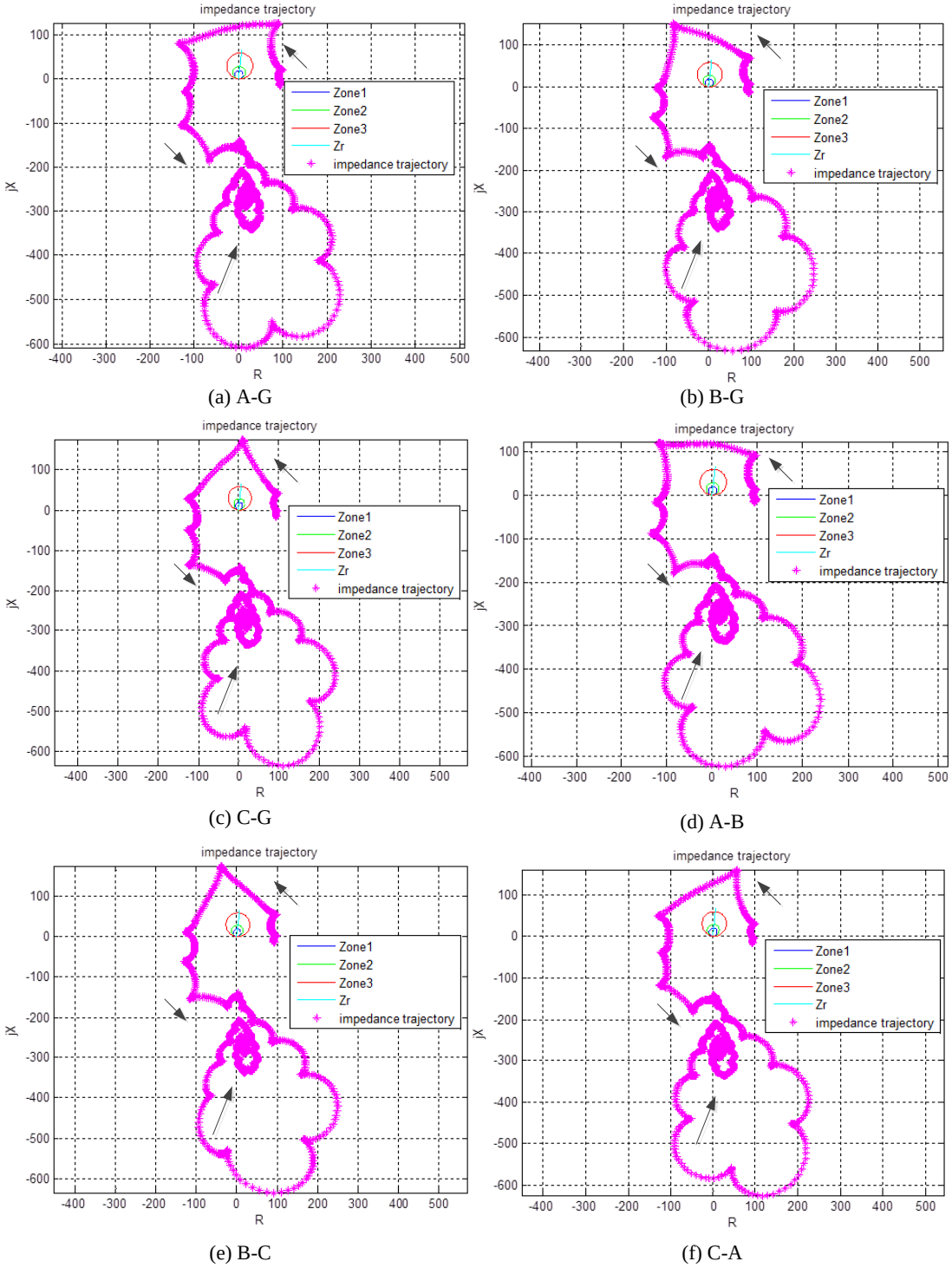

(a) A-G (b) B-G

(c) C-G (d) A-B

(e) B-C (f) C-A

Figure 7-18 A-G, B-G, C-G, A-B, B-C, C-A fault impedance trajectories for a fault at 50km along the DC line in the HVAC/HVDC transmission system

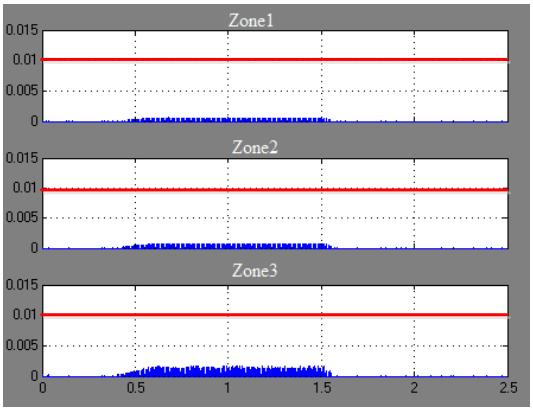

(a) A-G block-average comparator output

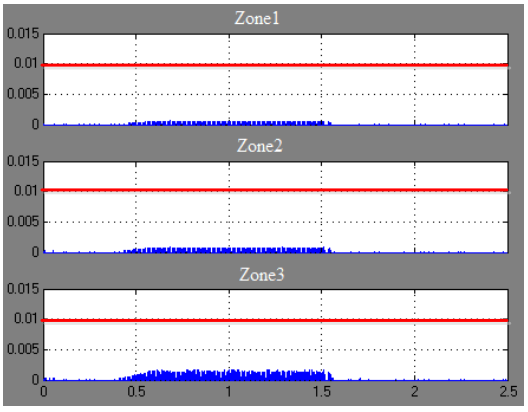

(b) B-G block-average comparator output

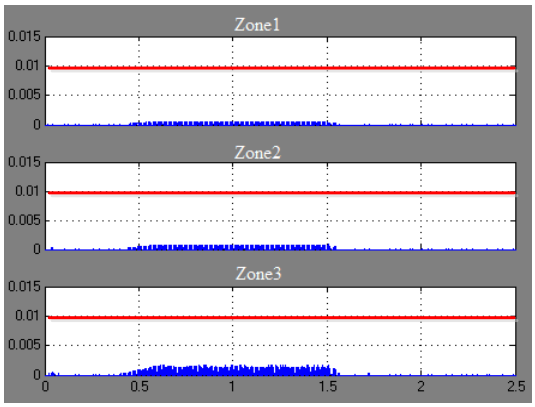

(c) C-G block-average comparator output

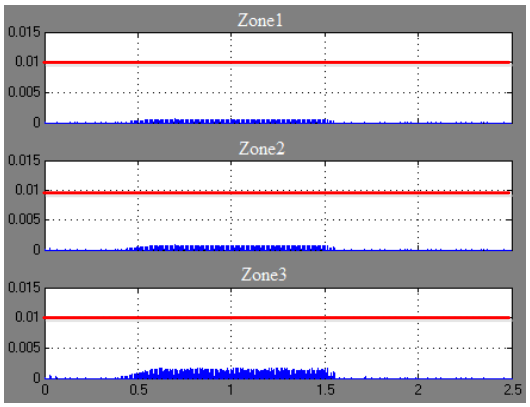

(d) A-B block-average comparator output

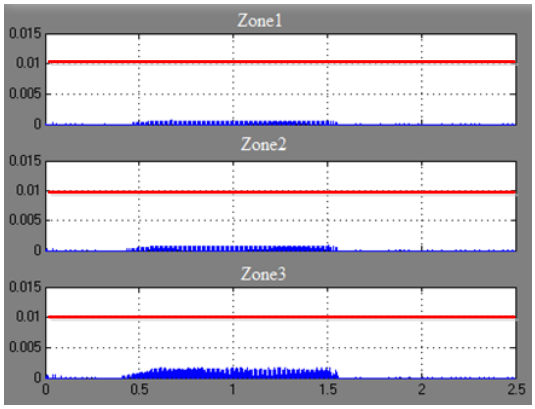

(e) B-C block-average comparator output

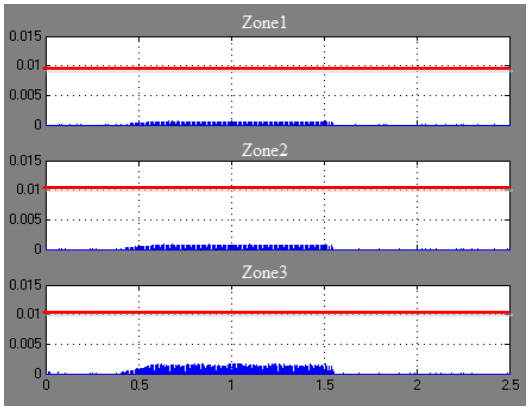

(f) C-A block-average comparator output

Figure 7-19 A-G, B-G, C-G, A-B, B-C, C-A block-average comparators' outputsa fault at 50km along the DC line in the HVAC/HVDC transmission system

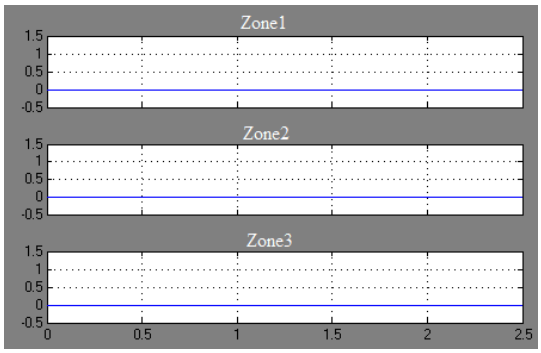

(a) A-G relay trip signals

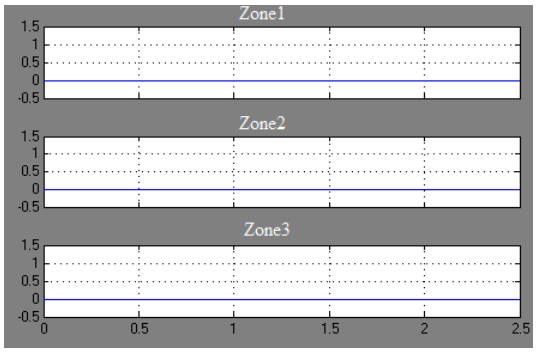

(b) B-G relay trip signals

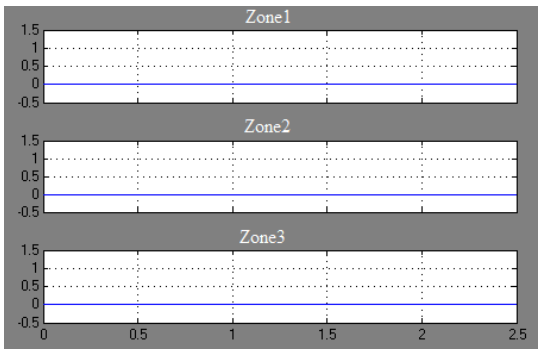

(c) C-G relay trip signals

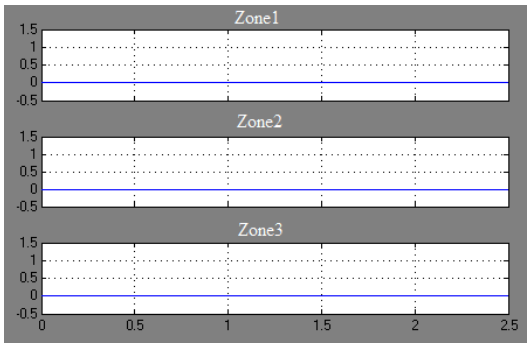

(d) A-B relay trip signals

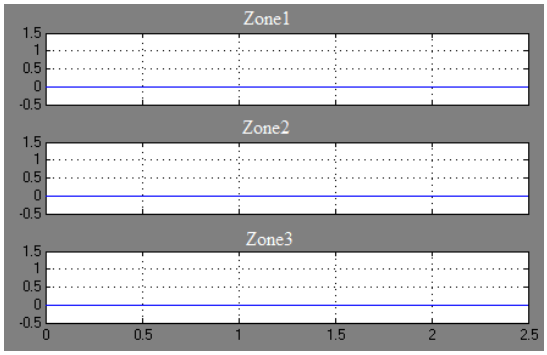

(d) B-C relay trip signals

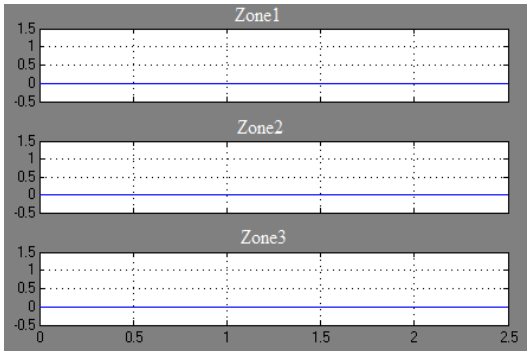

(f) C-A relay trip signals

Figure 7-20 Distance relay trip signals a fault at 50km along the DC line in the HVAC/HVDC transmission system

As a comparison, a A-B-C-G fault was injected into the HVAC system on line2 at 50km. The fault was detected by all distance relay protections. The fault location was 150km from distance relay and covered by distance relay zone3 protection. Fig.7-21 gives the fault impedance trajectories. All the fault impedance entered the protection zone3 characteristic and settled on the fault impedance at 150km. Fig.7-

22 (a), (b), (c), (d), (e), (f) show the A-G, B-G, C-G, A-B, B-C, C-A block-average comparators' outputs. All zone3 comparators tripped. Fig.7-23 gives the distance relay trip signals and demonstrates that all zone3 protections tripped 500ms after fault.

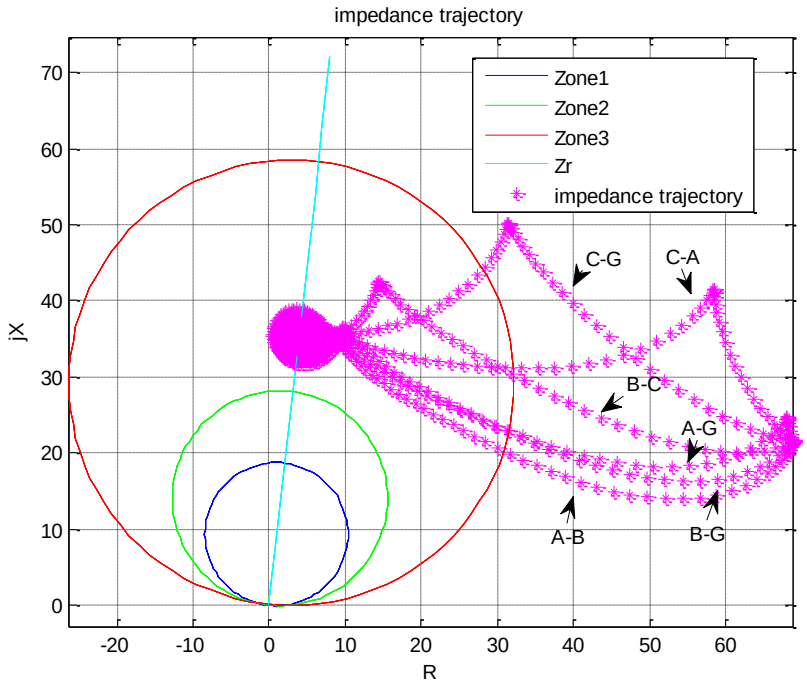

Figure 7-21 Fault impedance trajectories for a fault 150km from the relay point in the HVAC transmission system

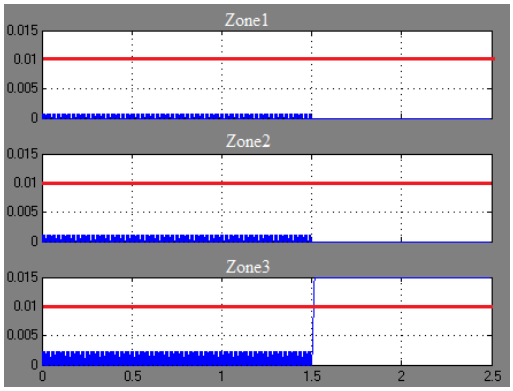

(a) A-G block-average comparator output

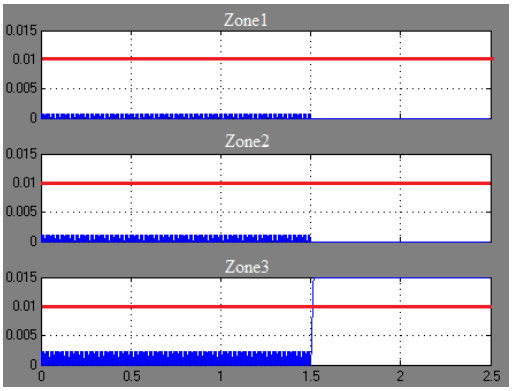

(b) B-G block-average comparator output

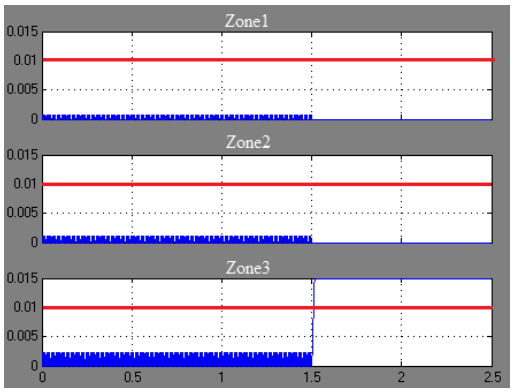

(c) C-G block-average comparator output

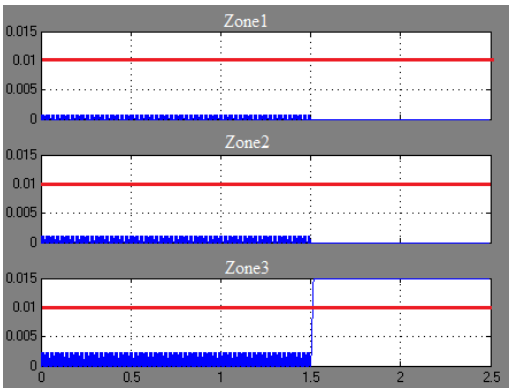

(d) A-B block-average comparator output

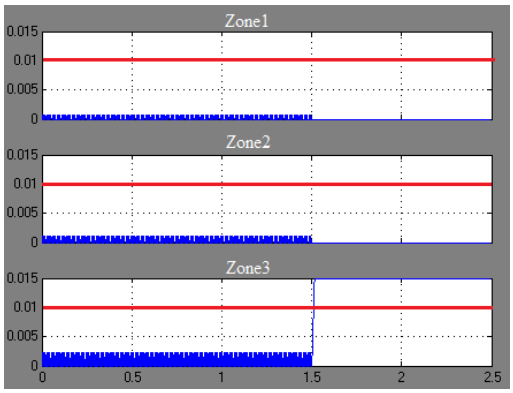

(e) B-C block-average comparator output

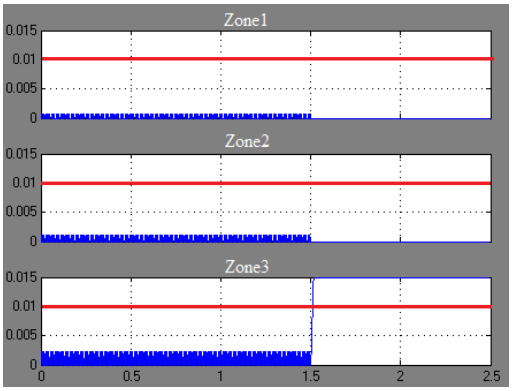

(f) C-A block-average comparator output

Figure 7-22 A-G, B-G, C-G, A-B, B-C, C-A block-average comparators' outputs for a fault 150km from the relay point in the HVAC transmission system

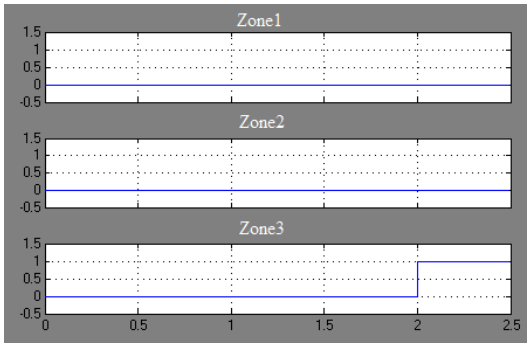

(a) A-G relay trip signals

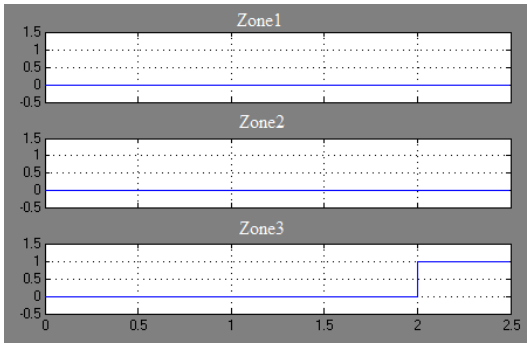

(b) B-G relay trip signals

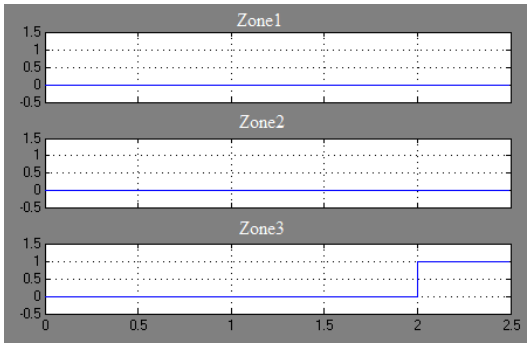

(c) C-G relay trip signals

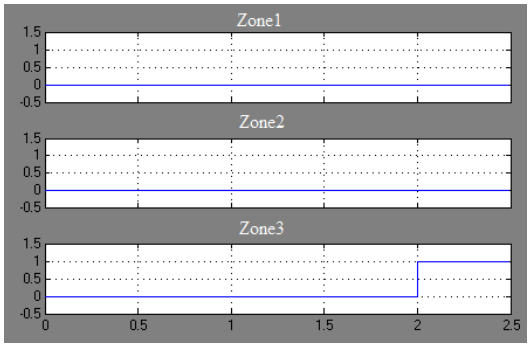

(d) A-B relay trip signals

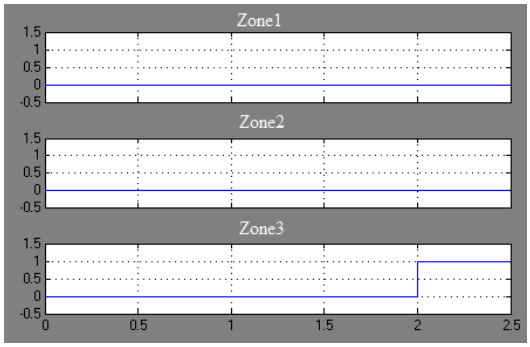

(e) B-C relay trip signals

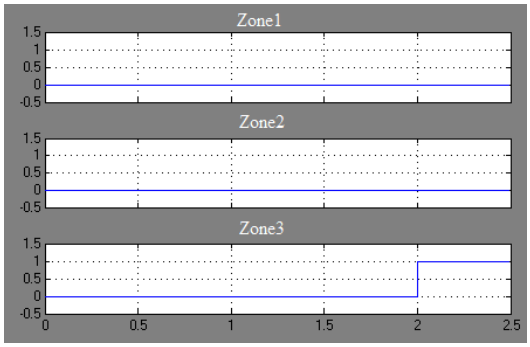

(f) C-A relay trip signals

Figure 7-23 Distance relay trip signals for a fault 150km from the relay point in the HVAC transmission system

From the results above, when fault occurred in zone3 area in the HVAC/HVDC system the distance relay did not trip while in the HVAC system the distance relay tripped. The fault impedances seen by distance relay in the HVAC/HVDC system were similar when the fault occurred in zone2 and zone3 areas. The fault locations

on DC line did not contribute to the distance relay protection response. The fault impedances started from the pre-fault load impedance, circled the distance relay protection zones and finally settled at a high impedance negative reactance point. This was a result of the reactive power absorbed by the HVDC converter stations during faults. The faults in the HVAC/HVDC system on DC line in protection zones did not cause distance relay trips. However, when faults occurred in the HVAC system at the same locations, the distance relay tripped.

7.1.3.2 Protection response to faults in HVAC/HVDC system on ac line beyond HVDC interconnection

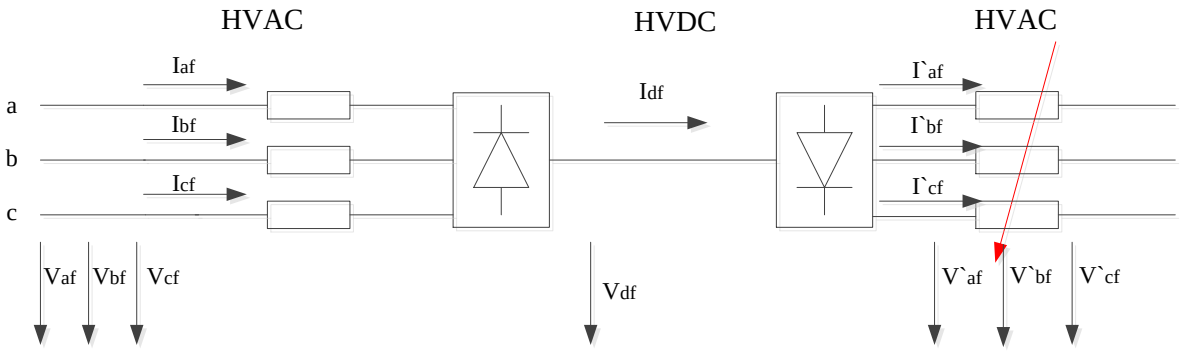

Figure 7-24 Fault beyond DC link

When the fault occurs beyond the dc links on the ac line as shown in fig.7-24, the protection at the feeder substation will see both fault voltage and current. Because the dc link does not contain three phase voltage and current elements, a single phase to ground fault, for example, an A-G fault occurs beyond the dc link on ac line, all of the comparators in the distance relay will see the fault. The dc link can regulate the fault voltage and current so the distance relay will not trip. In comparison, if an A-G fault occurs in HVAC system, the distance relay's A-G comparators will detect the fault.

7.1.3.2.1 Protection response to A-G fault at 200km on line3

An A-G fault was applied to the HVAC/HVDC system on line3 at 200km from the relay. The fault would be expected to be covered by distance relay zone3 protection. Fig.7-25 (a), (b), (c), (d), (e), (f) show the A-G, B-G, C-G, A-B, B-C, C-A fault impedance trajectories and show that a similar response, albeit modified by the shift

in the post-fault waveforms. The fault impedance trajectories started from steady points defined by the pre-fault load and moved around the distance relay protection zones. No fault impedances trajectories entered the protection zones. There were no trips. The fault impedances finally settled at a high value of negative reactance in several cycles. This was attributed to the HVDC converter station absorbing reactive power during fault. Fig.7-26 (a), (b), (c), (d), (e), (f) show the A-G, B-G, C-G, A-B, B-C, C-A block-average comparators' outputs. No tripping occurred. Fig.7-27 gives the distance relay trip signals.

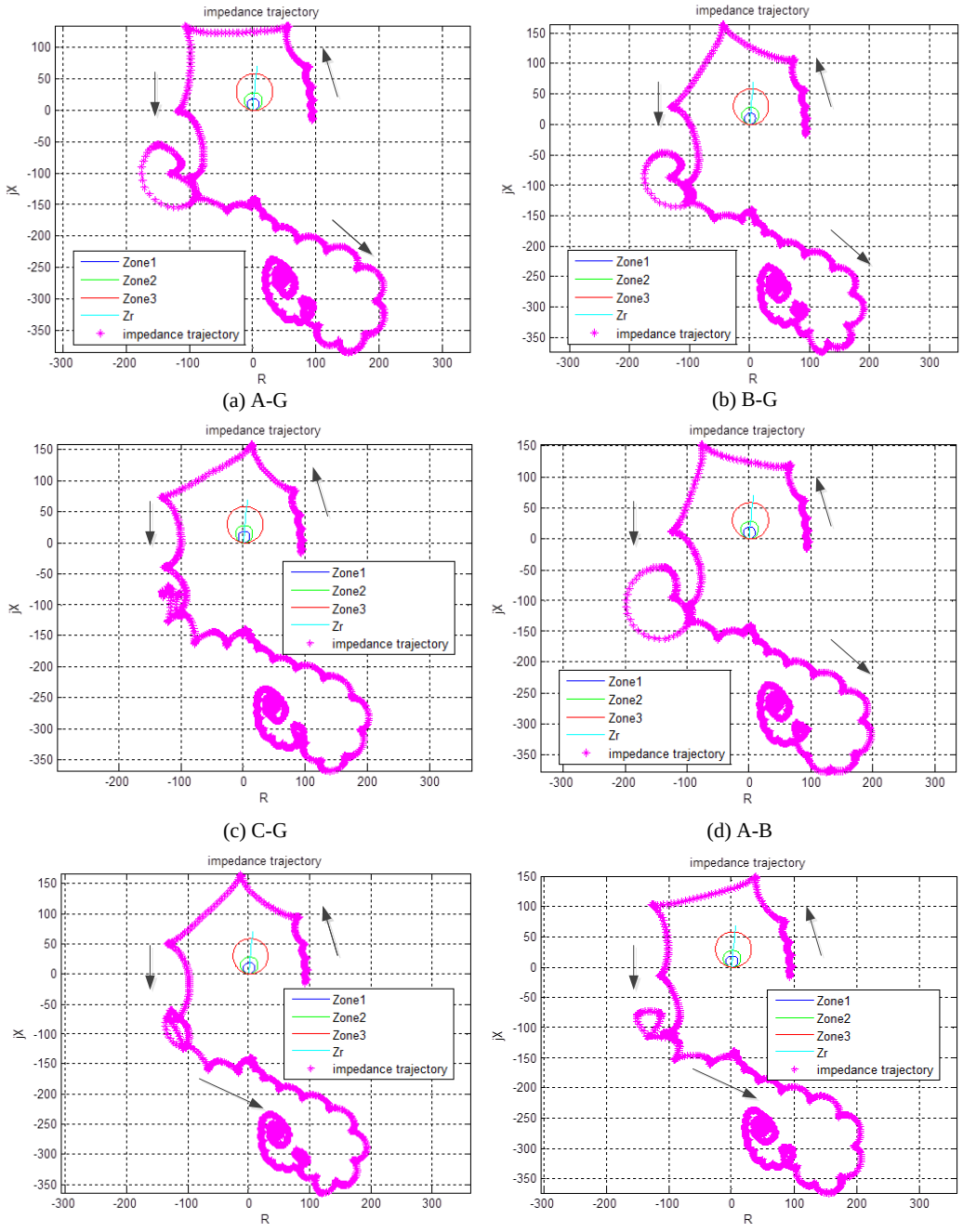

(a) A-G (b) B-G

(c) C-G (d) A-B

(e) B-C (f) C-A

Figure 7-25 A-G, B-G, C-G, A-B, B-C, C-A fault impedance trajectories for an A-G fault on the HVAC line beyond the DC link in the HVAC/HVDC transmission system

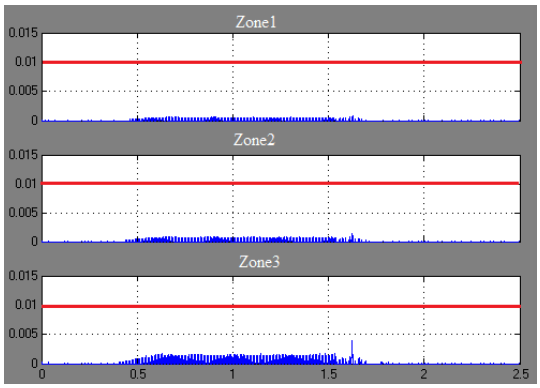

(a) A-G block-average comparator output

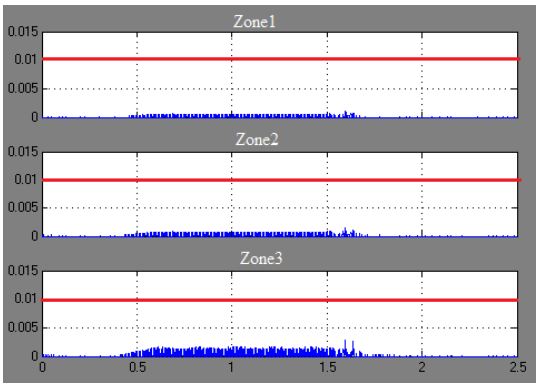

(b) B-G block-average comparator output

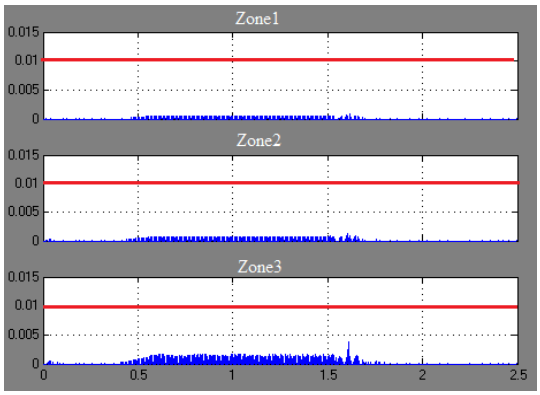

(c) C-G block-average comparator output

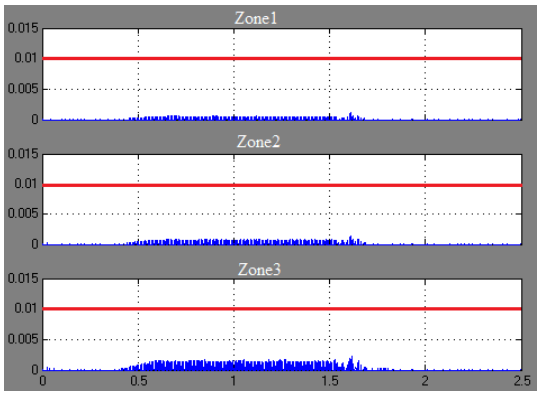

(d) A-B block-average comparator output

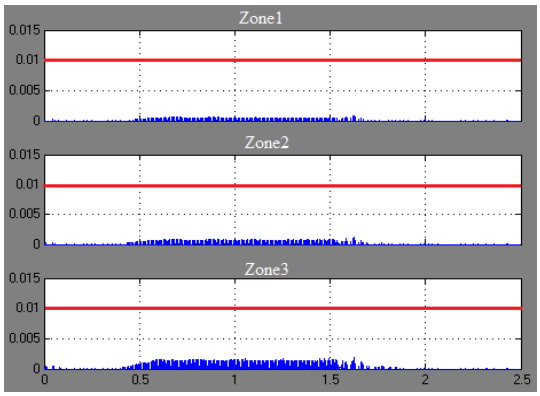

(e) B-C block-average comparator output

(f) C-A block-average comparator output

Figure 7-26 A-G, B-G, C-G, A-B, B-C, C-A block-average comparators' outputsfor an A-G fault on the HVAC line beyond the DC link in the HVAC/HVDC transmission system

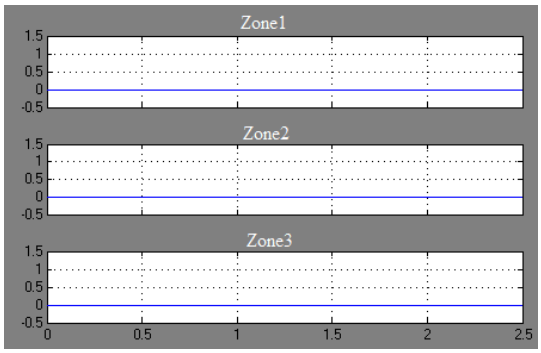

(a) A-G relay trip signals

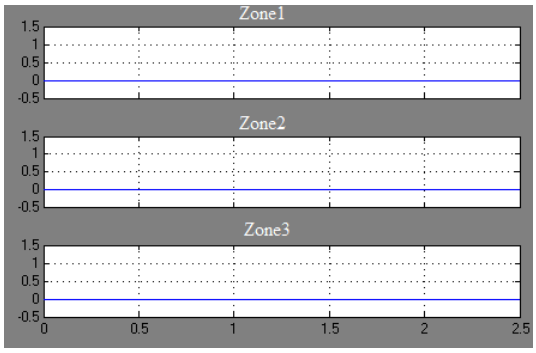

(b) B-G relay trip signals

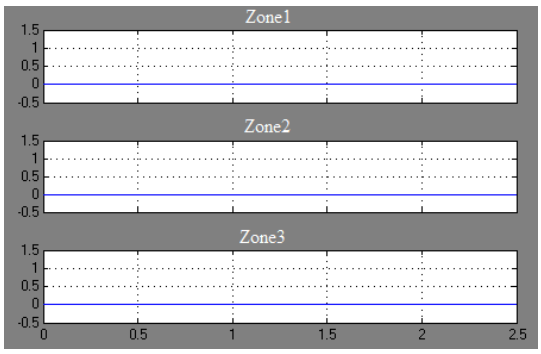

(c) C-G relay trip signals

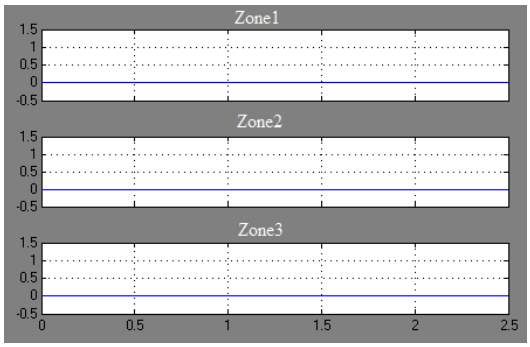

(d) A-B relay trip signals

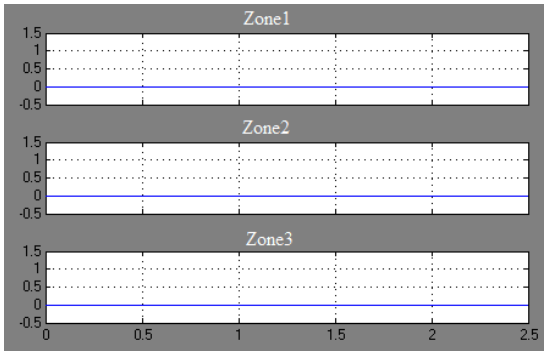

(d) B-C relay trip signals

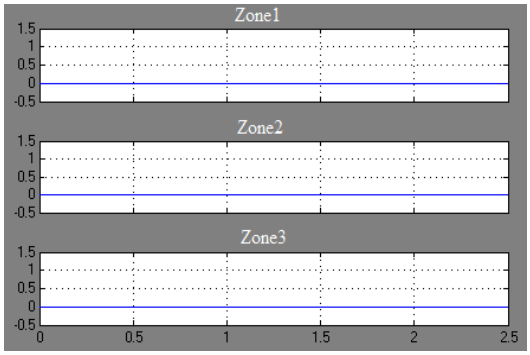

(f) C-A relay trip signals

Figure 7-27 Distance relay trip signals for an A-G fault on the HVAC line beyond the DC link in the HVAC/HVDC transmission system

To provide a comparison, an A-G fault was applied to the HVAC system on line3 at 200km from the relay point. The fault was covered by distance relay zone3 protection. Fig.7-28 (a) shows the A-G fault impedance trajectory. The fault impedance entered the protection zone3 characteristic after a few cycles and settled on the fault impedance at 200km. Fig.7-28 (b) shows the A-G block-average

comparator outputs. Fig.7-28 (c) shows the trip signal, highlighting that zone3 tripped 500ms after fault.

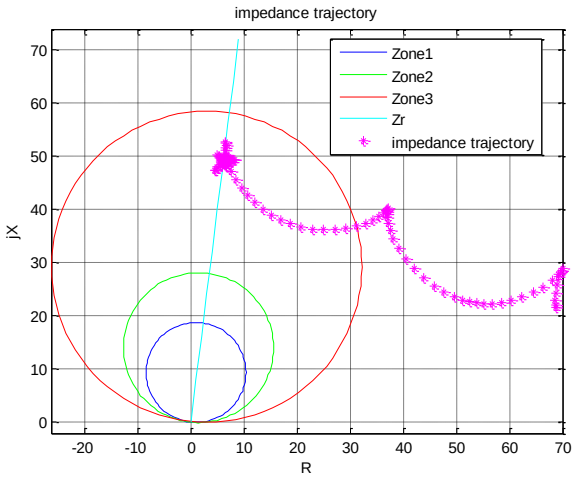

(a) A-G fault
impedance trajectory

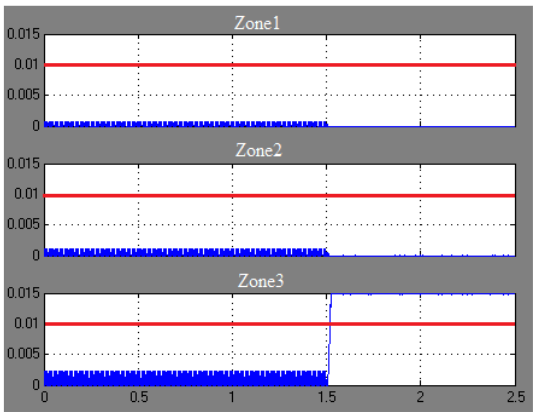

(b) A-G block-average
comparator output

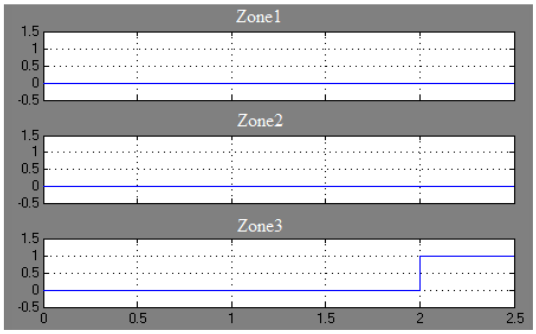

(c) A-G relay trip signals

Figure 7-28 A-G fault on line3 in HVAC system 200km from the relay point on the HVAC system

7.1.3.2.2 Protection response to A-B-G fault at 200km on line3

When an A-B-G fault was applied to the AC power system on the transmission line in zone3 area, the distance A-G, B-G, A-B protection were expected to respond to the fault. The fault impedances seen by A-G, B-G, A-B relay should enter the protection zone3 characteristic and settle at the fault impedance. The C-G, B-C, C-A relay will see fault impedances since they will be influenced by the fault voltages and currents.

When the A-B-G fault occurs in HVDC/HVAC system on the ac line beyond DC link, the distance relay protection will experience fault voltages and currents, but due to the influence of the converter stations they are not expected to trip.

An A-B-G fault was applied to the HVAC/HVDC system on line3 at 200km from the relay point. The fault was covered by distance relay zone3 protection. Fig.7-29 (a), (b), (c), (d), (e), (f) show the A-G, B-G, C-G, A-B, B-C, C-A fault impedance trajectories. The distance relay all protections responded to the fault. The A-G, B-G, C-G, A-B, B-C, C-A fault impedances were similar to each other. All the fault impedance trajectories started from the pre-fault load impedances, circled the distance relay protection zones and settled at a high value of negative reactance. Because the fault impedances trajectories did not enter the trip characteristics, there were no trips. The post-fault impedance settled in negative reactance area was attributed to the HVDC converter stations absorbing the reactive power during fault. Fig.7-30 (a), (b), (c), (d), (e), (f) show the A-G, B-G, C-G, A-B, B-C, C-A block-average comparators' outputs. None of the comparators tripped. Fig.7-31 shows the distance relay trip signals with no tripping signals.

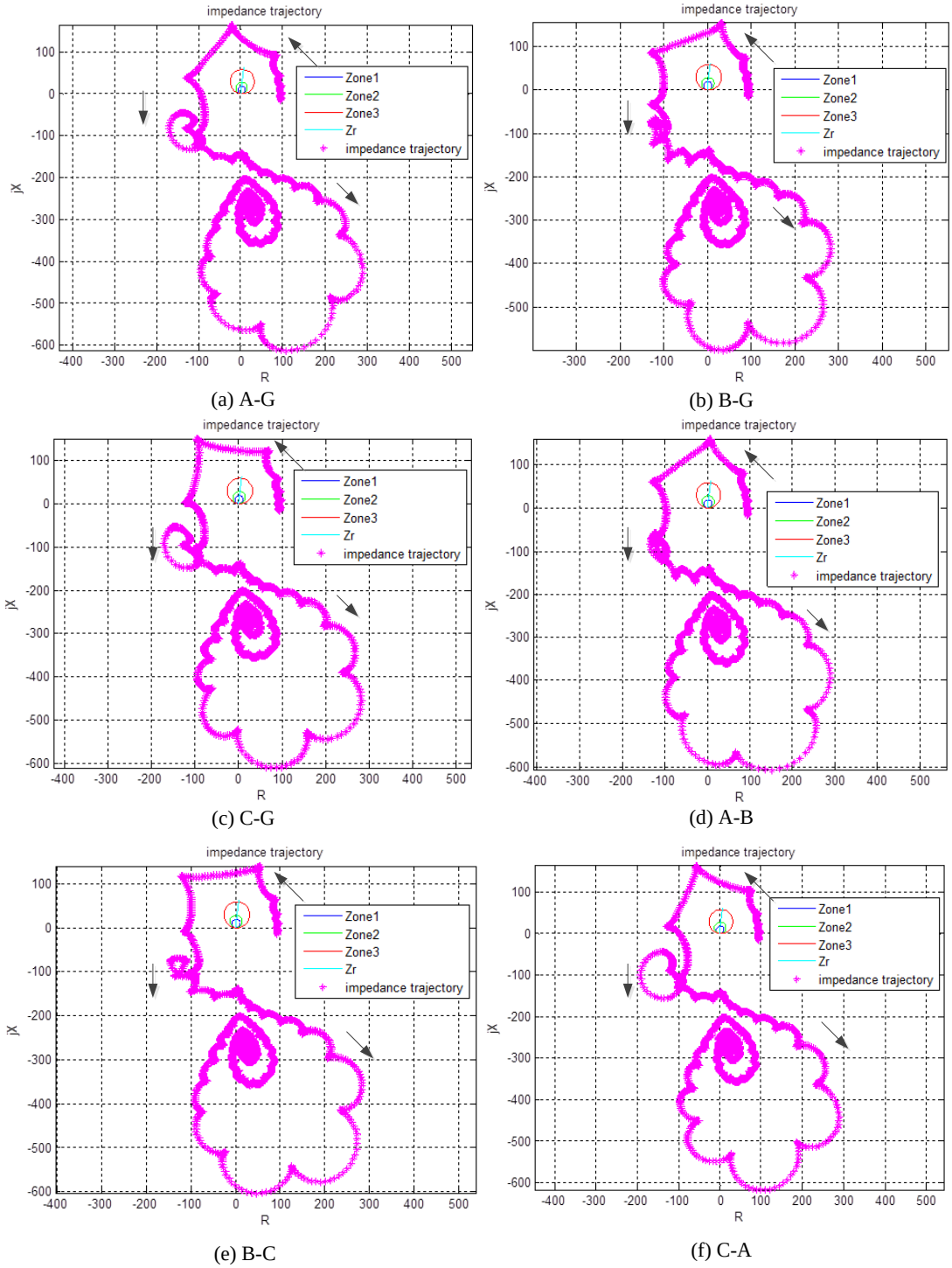

(a) A-G (b) B-G

(c) C-G (d) A-B

(e) B-C (f) C-A

Figure 7-29 A-G, B-G, C-G, A-B, B-C, C-A fault impedance trajectories for fault at 200km from the relay point on the HVAC/HVDC transmission system

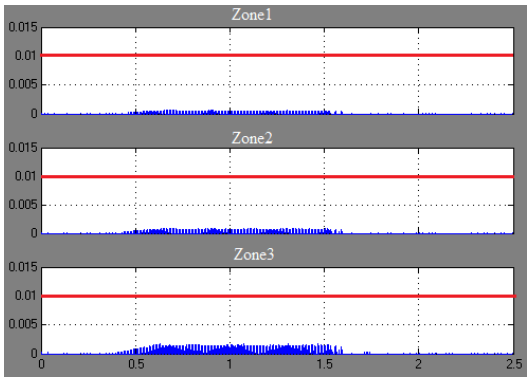

(a) A-G block-average comparator output

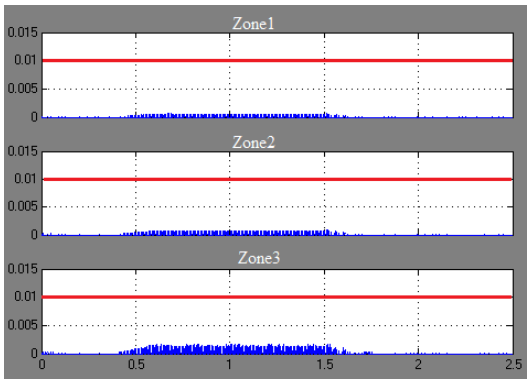

(b) B-G block-average comparator output

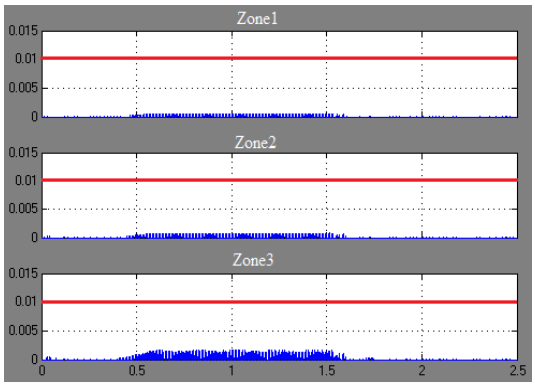

(c) C-G block-average comparator output

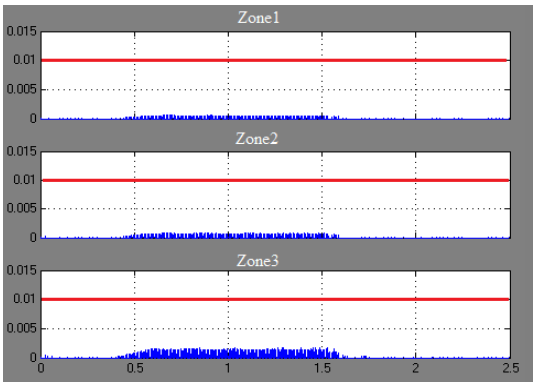

(d) A-B block-average comparator output

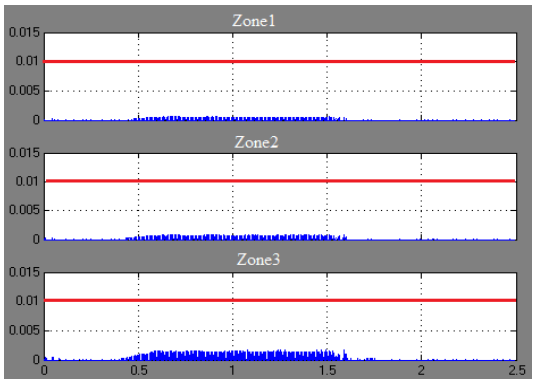

(e) B-C block-average comparator output

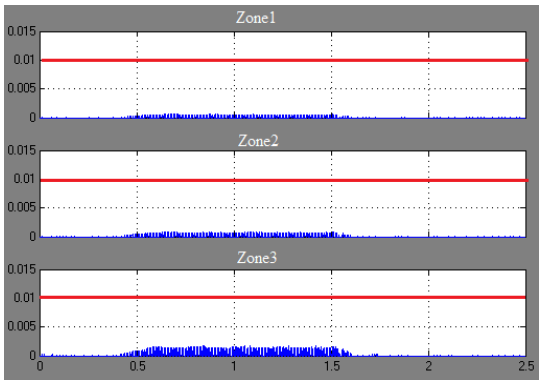

(f) C-A block-average comparator output

Figure 7-30 A-G, B-G, C-G, A-B, B-C, C-A block-average comparators' outputs for fault at 200km from the relay point on the HVAC/HVDC transmission system

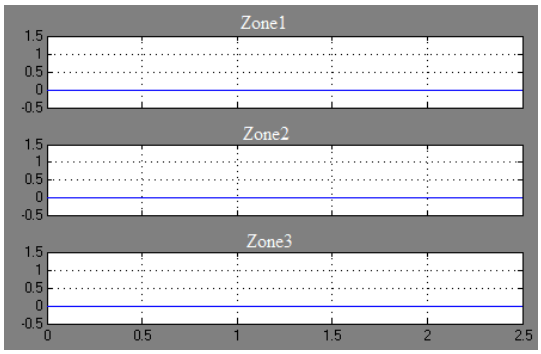

(a) A-G relay trip signals

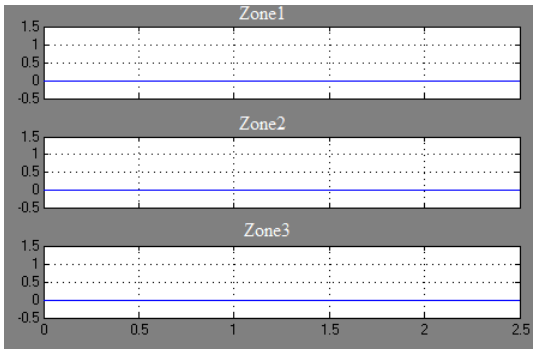

(b) B-G relay trip signals

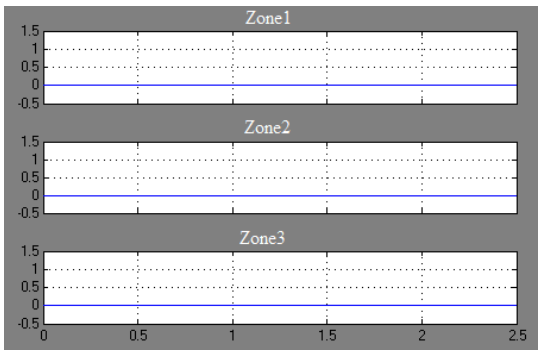

(c) C-G relay trip signals

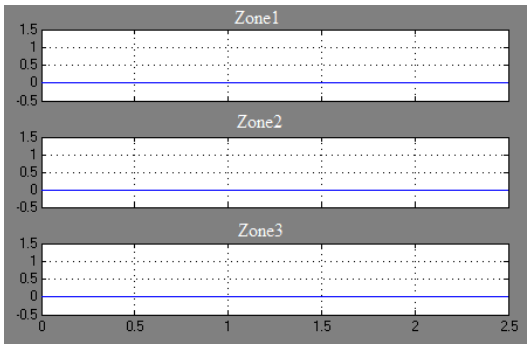

(d) A-B relay trip signals

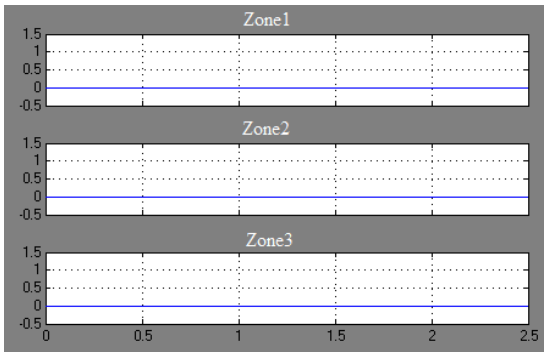

(d) B-C relay trip signals

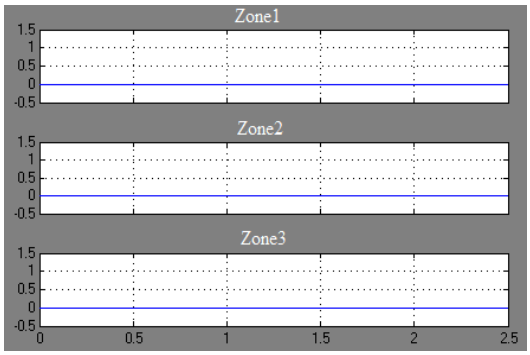

(f) C-A relay trip signals

Figure 7-31 Distance relay trip signals for fault at 200km from the relay point on the HVAC/HVDC transmission system

For a comparison, an A-B-G fault was applied to the HVAC system on line3 at 200km. The fault was detected by A-G, B-G and A-B zone3 protections. The A-G,

B-G, A-B fault impedances seen by distance relay are shown in fig.7-32, and show that the A-G, B-G, A-B fault impedances entered the distance relay zone3 characteristic and settled on the fault impedance at 200km after a few cycles. Fig.7-33 (a), (b), (c) show the A-G, B-G, A-B block-average comparators' outputs, and reveal that zone3 outputs crossed the trip level in few cycles. Fig.7-34 gives the distance relay A-G, B-G, A-B protection trip signals. The distance relay A-G, B-G, A-B zone3 protection tripped 500ms after fault.

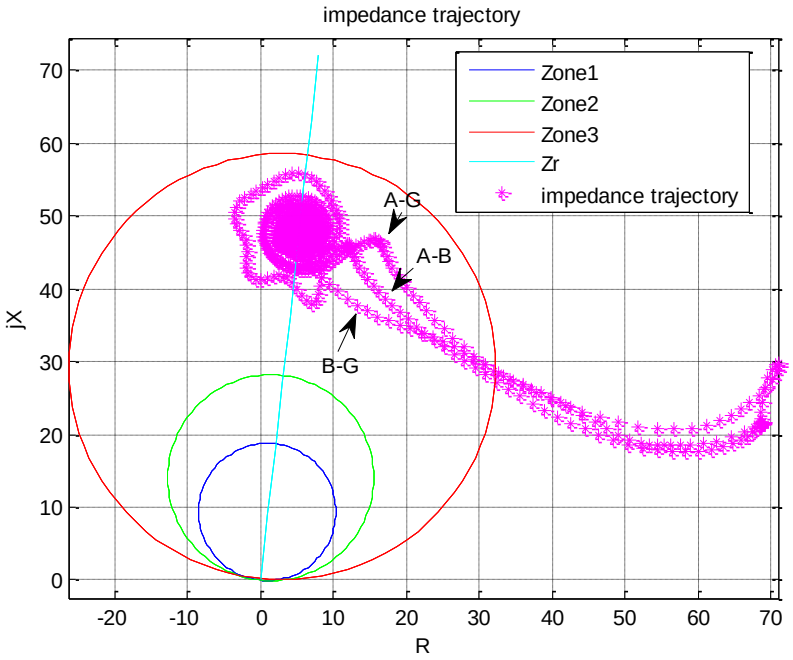

Figure 7-32 A-G, B-G, A-B fault impedance trajectories for fault at 200km from the relay point on the HVAC transmission system

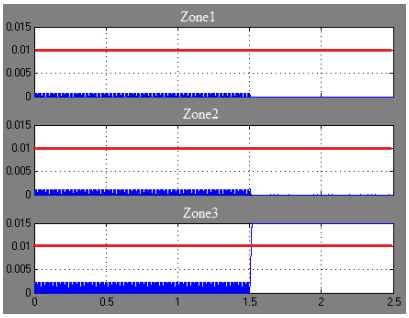

(a) A-G block-average comparator output

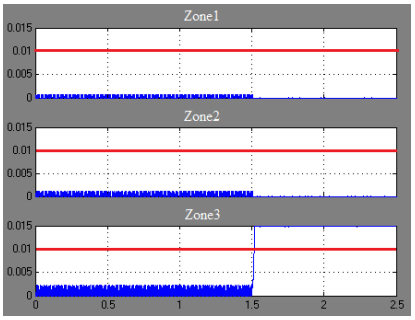

(b) B-G block-average comparator output

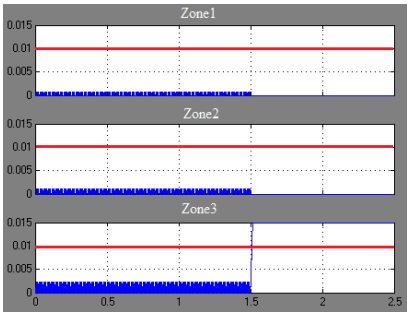

(c) A-B block-average comparator output

Figure 7-33 A-G, B-G, A-B block-average comparators' outputs for fault at 200km from the relay point on the HVAC transmission system

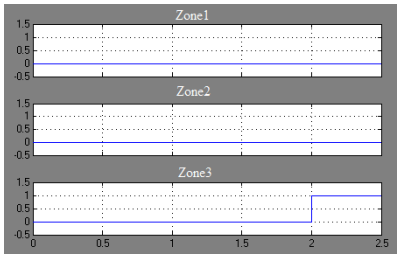

(a) A-G relay trip signals

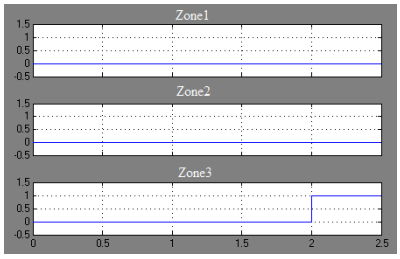

(b) B-G relay trip signals

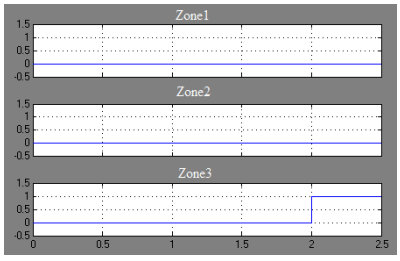

(c) A-B relay trip signals

Figure 7-34 Distance relay A-G, B-G, A-B protection trip signals for fault at 200km from the relay point on the HVAC transmission system

From the results above, it has been shown that when fault occurred on ac line beyond the DC link, the distance relay did not trip for the fault. The dc link effectively isolated the faults on the other side of it. All distance relay protections detected the fault no matter the fault type. The fault impedances seen by the distance relay protection were similar to each other. In the comparison with the HVAC system, the similar faults at same locations caused the distance relay to trip.

Comparing the fault impedances when the fault occurred on ac line beyond the dc link with the fault impedances when fault was on the dc link, it was shown that they all were similar. All the fault impedances started from steady points corresponding to the pre-fault load impedance, circled the distance relay protection zones and settled at a highly reactive impedance. All the fault impedances were outside the trip characteristics. There were no possibilities to trip. The post-fault negative reactive impedance was attributed to HVDC converter stations absorbing reactive power during the faults.

7.1.4 Protection response to fault out of protection zones

An A-B-C-G fault was applied to the HVAC/HVDC system on line3, 280km from the relay point. The fault was therefore outside the distance relay protection zones. Fig.7-35 (a), (b), (c), (d), (e), (f)show the A-G, B-G, C-G, A-B, B-C, C-A fault impedance trajectories, these were all similar to each other with minor differences associated with the different phase signals used. Comparing the fault impedance trajectories when the fault was inside protection zones on dc line and beyond dc link, the fault impedance trajectory was outside of the distance relay protection zones and there were no trips.

Fig.7-36 shows the fault impedance trajectories when an A-B-C-G fault was applied to the HVAC system on line3 at 280km from the relay point. None of these fault impedances entered the protection zones. The trajectories started from the pro-fault load impedances and settled at the post-fault impedance.

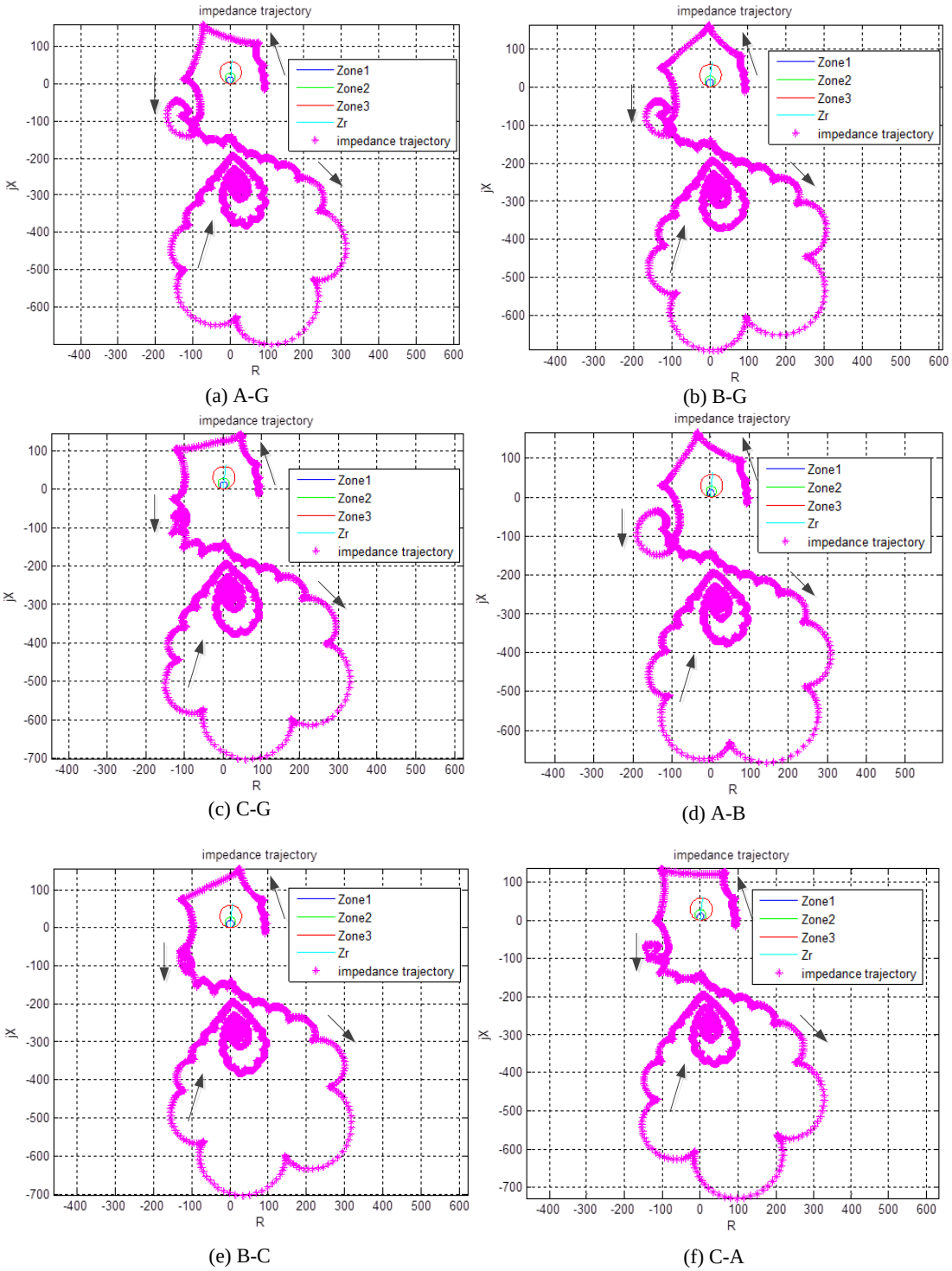

(a) A-G (b) B-G

(c) C-G (d) A-B

(e) B-C (f) C-A

Figure 7-35 A-G, B-G, C-G, A-B, B-C, C-A fault impedance trajectories for fault at 280km from relay point on the HVAC/HVDC transmission system

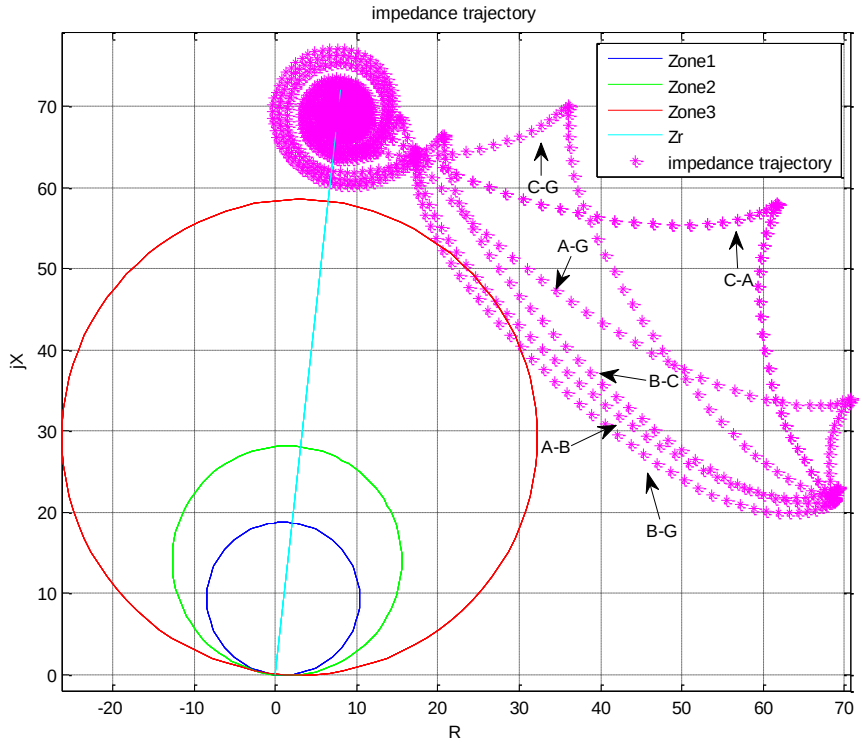

Figure 7-36 Fault impedance trajectories for fault at 280km from relay point on the HVAC transmission system

7.2 Chapter Summary

The modelled distance relay response to faults when the protected high voltage transmission system contained a HVDC link was investigated in this chapter. In comparison, the response to faults on a similar HVAC system was simulated as well.

In both HVAC/HVDC and HVAC interconnection systems, the faults located in the zone1 area all caused the distance relay zone1 to trip as expected. The distance relay detected the fault impedance and tripped within a few cycles. The fault impedances seen by distance relay in the two systems were similar.

In HVAC/HVDC system, when the fault was located in zone2 area on ac line, the distance relay detected the fault and tripped in the same manner as the fault in HVAC system at that location. When fault occurred on the dc line within zone2 and zone3 area, the distance relay did not trip.

For HVAC/HVDC system, when the fault occurred beyond dc terminal on ac line covered by zone3 protection, the distance relay did detect the fault and there were impedance trajectories but there were no tripping since none of the impedance trajectories entered the protection characteristics. In comparison, when the same fault occurred in HVAC system at the same location, the distance relay tripped.

The distance relays did not trip in both HVAC/HVDC and HVAC systems when faults located outside of the protection zones.

Chapter 8

The HVAC/HVDC Impacts on Distance Relay during Power Swing

In this chapter, the impact of the inclusion of HVDC lines in HVAC network on the performance of a distance relay during transient conditions is investigated

8.1 The impact of HVAC/HVDC circuit on distance relay during power swing

Several large scale blackouts have been caused by the operation of the distance relay's remote back protection (zone3). This has resulted in cascading failures and domino effects. The distance relay zone3 protection can cover a very large area. During the steady state the power system is balanced and there is a match between generated power and consumed power. Any change in the power system - load change, transmission line faults, line switching and generator disconnection - can break the balance and result in major changes in power system voltages and currents. Such changes may lead to the measured impedances as seen by distance relay entering the protection zone3 characteristic. The distance relay zone3 will then trip in this situation as if there had been a fault.

8.2 Distance relay operation in one generator system

Distance relay operation has been investigated for HVAC networks which includes HVDC links during transient conditions. The investigation involved simulation work carried out in MATLAB/SIMULINK. In order to investigate the distance relay operation, a power system was simulated as shown in fig.8-1. The simulated power system was based on two area power systems as described by Kundur [68]. The system was used to investigate inter-area oscillations [68, 149, 150].

The model involved a 230kV, 9000MVA power system connected to a 230kV 900MVA load through two 100kM ac transmission lines and a 100kM HVDC link. The load included a local 20kV, 900MVA power station. The power station connected through a 20/230kV, 900MVA power transformer T and 10km ac line. The distance relay was located at busbar A to protect the ac line1. The distance relay zone1 was set to 80% of line1. Zone2 and zone3 was set to 120% and 250% of the line1. Time delays for zone1, zone2 and zone3 were 0ms, 200ms and 500ms

respectively. The AC transmission line parameters were set at the same levels as previous simulated power systems in section 7.1.

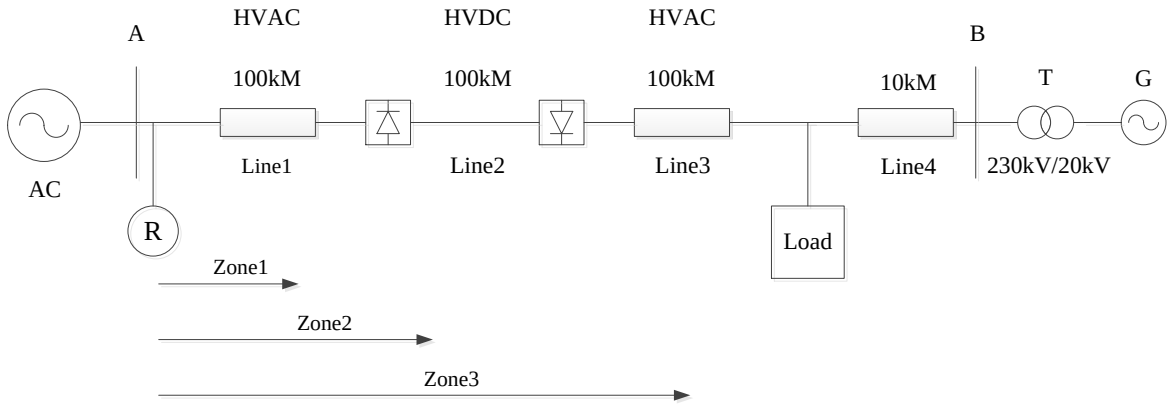

Figure 8-1 Simulated HVAC/HVDC power system

For comparison purposes, a similar network was also modelled, which was an ac system connected to the load through three 100km ac lines. The simulated HVAC power system is shown in fig.8-2 below.

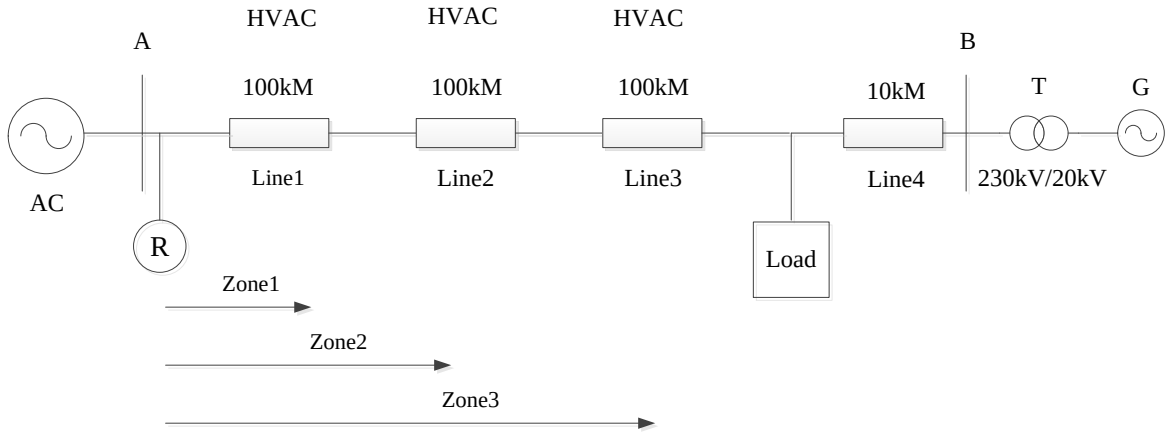

Figure 8-2 Simulated HVAC power system

The two power systems were used similar parameters models and the simulation duration was 4 seconds. Simulations results are shown in following sections. The details of the models are shown in Appendix. F.

Fig.8-3 (a) and (b) give the pre-fault impedance seen by distance relay in HVAC/HVDC system and HVAC system respectively. The impedance seen in HVAC/HVDC system was in negative reactance was due to the HVDC converter stations absorbing reactive power.

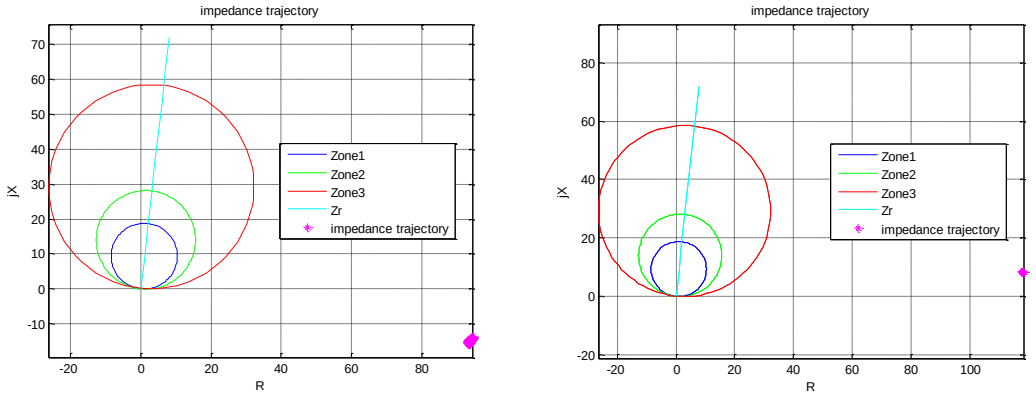

(a) Pre-fault load impedance seen by distance relay in HVAC/HVDC system

(b) Pre-fault load impedance seen by distance relay in HVAC system

Figure 8-3 Pre-fault impedance seen by distance relay for the HVAC/HVDC and HVAC networks

8.2.1 Protection response to an A-G fault on line3 at 300km from the relay location.

An A-G fault was applied to HVAC/HVDC power system on line3 at 300km.The HVDC control strategies, after fault, maintained the power system stable and no power swing occurred. The HVDC link prevented the power swing acting as a filter against such a disturbance. The A-G fault impedance trajectory is shown in fig.8-4. The fault impedance started from pre-fault load impedance and circled the distance relay protection zones for a few cycles. The impedance trajectory was outside the protection characteristics and did not enter the protection zones and therefore prevented the distance relay from tripping. The fault impedance presented irregularities during HVDC control strategies, although after removal of the fault, the impedance reverted to the pre-fault value. The fault impedance did not enter the protection zones with other distance relay protections having similar fault impedance.

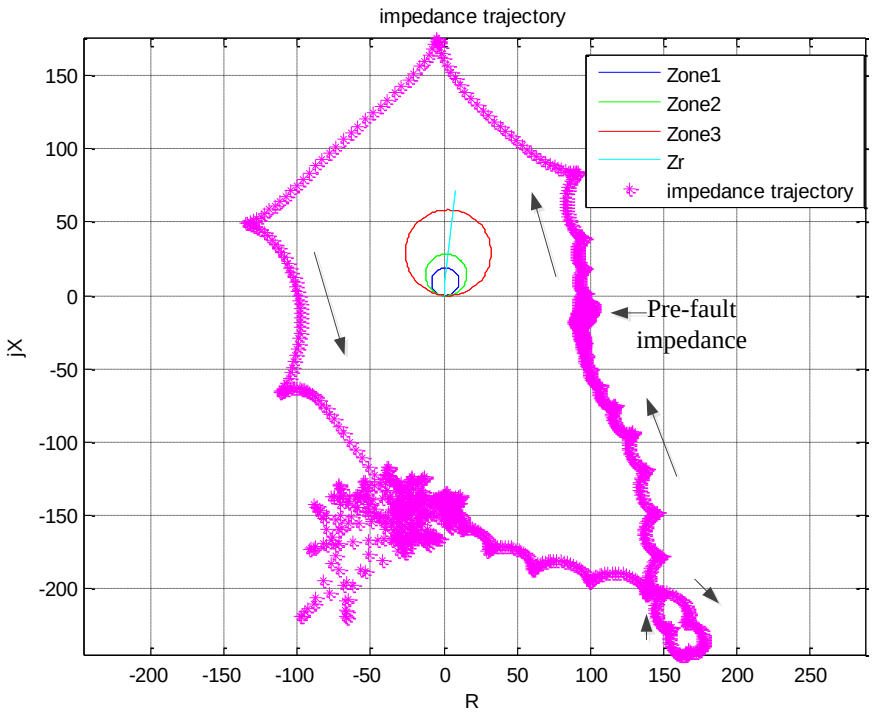

Figure 8-4 The response to an A-G fault at 300km from the relay point on the HVAC/HVDC network

In comparison, similar fault was applied to the HVAC system on line3 at 300km from the relay location. The fault caused power swing in the system. The A-G fault impedance trajectory as seen by distance relay is shown in fig.8-5.

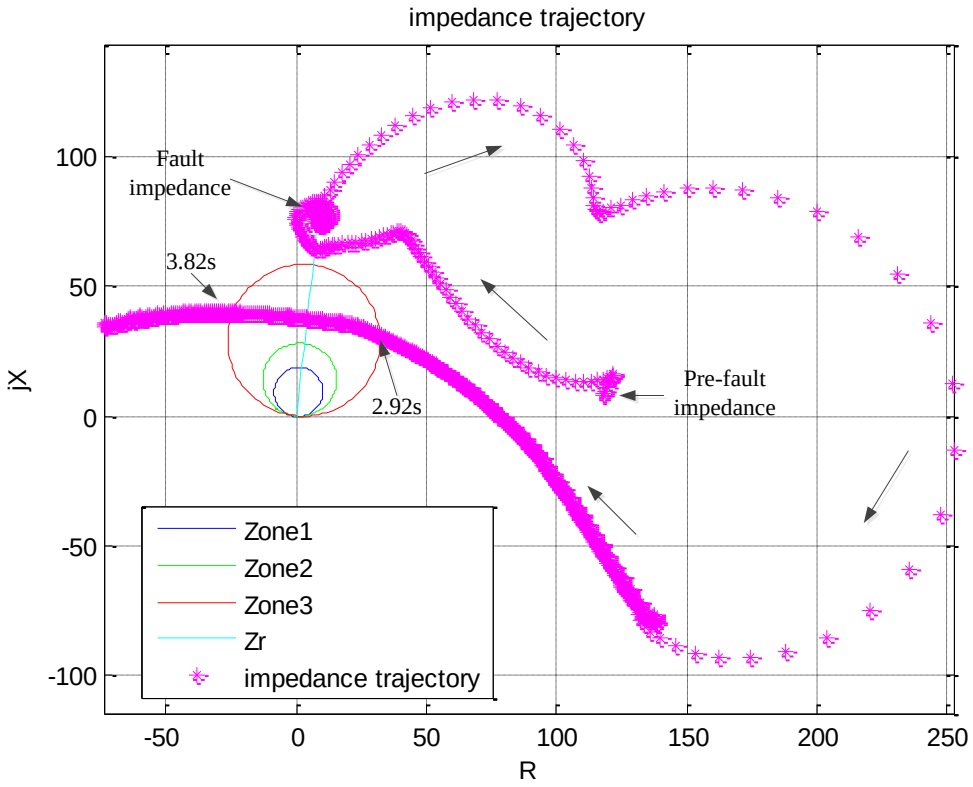

Figure 8-5The A-G fault impedance trajectory in response to a fault at 300km from the relay point on the HVAC network

As can be seen from fig.8-5, the A-G fault impedance trajectory first started from the pre-fault impedance, then moved to the fault impedance corresponding to a fault at 300km. When fault removed, power swing occurred in the system. After power swing occurred, the A-G fault impedance entered the distance relay zone3 protection characteristic at 2.92s and left the protection characteristic at 3.92s. The duration that impedance trajectory stayed inside protection zone3 was 900ms. The distance relay's A-G zone3 comparator's output is given in fig.8-6. The zone3 output crossed the trip level as per the distance relay trip signal is given in fig.8-7. Distance relay A-G zone3 protection tripped at 3.42s, corresponding to 2.92s+500ms time delay and reset at 3.82s when the fault impedance exited the zone3 characteristic. The power system fault did not cause distance relay to trip; however, the power swing did.

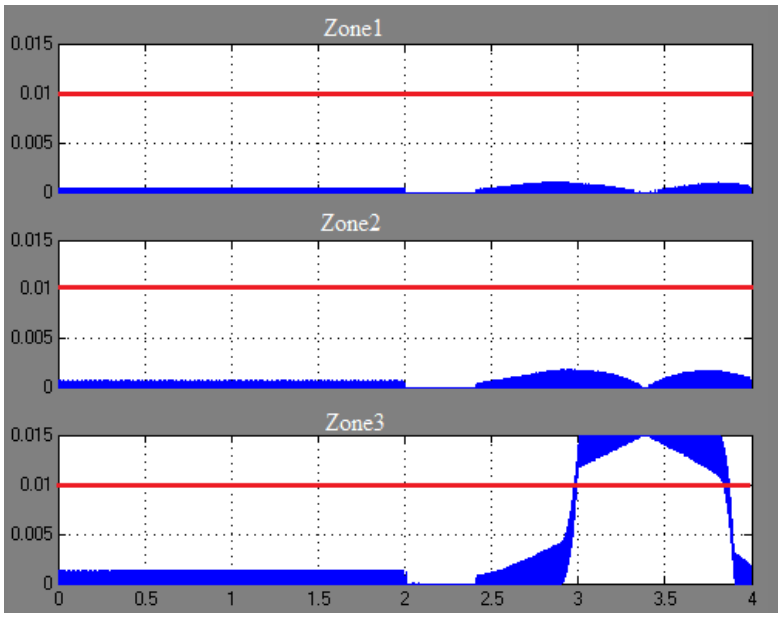

Figure 8-6 The A-G comparator output for the fault and subsequent power swing

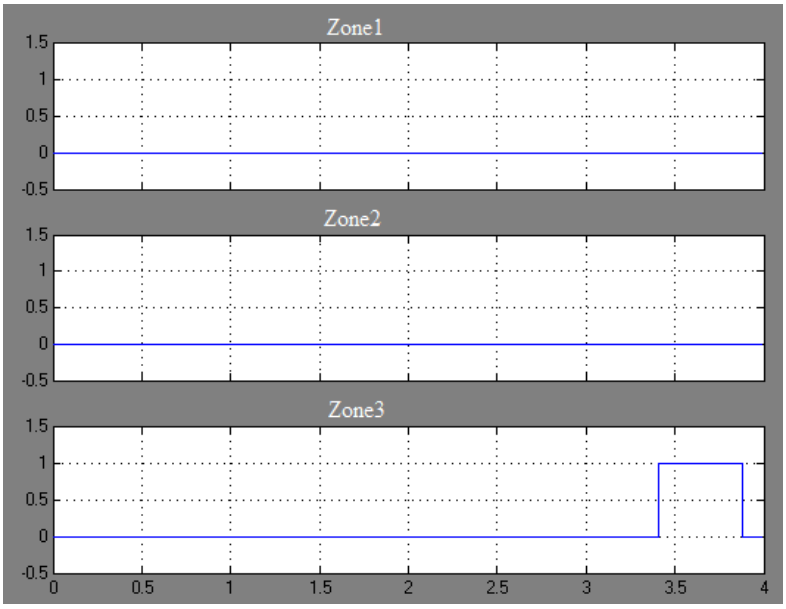

Figure 8-7 Distance relay trip signal for the fault and subsequent power swing

8.2.2 Protection response to an A-B-C-G fault on line3 at 300kmfrom relay location

The response to an A-B-C-G fault was simulated in the HVAC/HVDC system on line3 at 300km. The HVDC converter station affected the voltages and currents during the fault. After removal of the fault, the system maintained a stable state and the power swing did not occur. The HVDC link acted as a ‘firewall’ against the

power swing. All the distance relay protection had similar fault impedance trajectories. The response of the A-G fault impedance is shown in fig.8-8. The fault impedance trajectory circled the distance relay protection zones measurement starting at the pre-fault load impedance. The irregular part was caused by the HVDC converter stations control strategies. After removal of the fault, the fault impedance settled back to the steady point. The fault impedance did not enter the protection zones, so there was no trip.

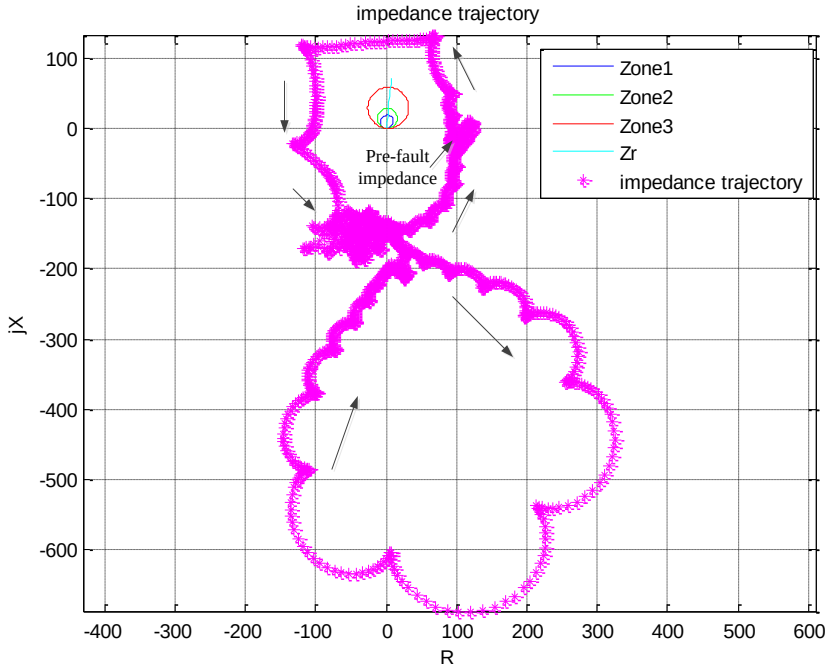

Figure 8-8 The response to an A-G fault following a fault at 300km on the HVAC/HVDC system

The same fault was applied in the HVAC system. After the fault was removed, a power swing occurred. All distance relay protection detected the fault and the fault impedances seen by distance relay comparators were similar. Fig.8-9shows the A-G fault impedance trajectory, which started at the pre-fault load impedance and settled on the fault impedance on the line during the fault. When the power swing occurred, the fault impedance followed a complex trajectory and entered the distance relay zone3 characteristic at 2.49s and exited at 2.95s. The duration was 0.46s which was shorter than zone3 time delay of 500ms. The distance relay zone3 protection therefore did not trip. Although in this case the power swing did not cause tripping,

it had the potential to cause distance relay zone3 trip. Fig.8-10 (a), (b) show the distance relay A-G block-average comparator output and relay trip signal. As can be seen from fig.8-10 (a), the A-G block-average comparator zone3 output crossed the trip level when fault impedance entered the zone3 characteristic and reset after fault impedance left the zone3 characteristic. The duration was shorter that zone3 time delay, therefore the distance relay did not trip.

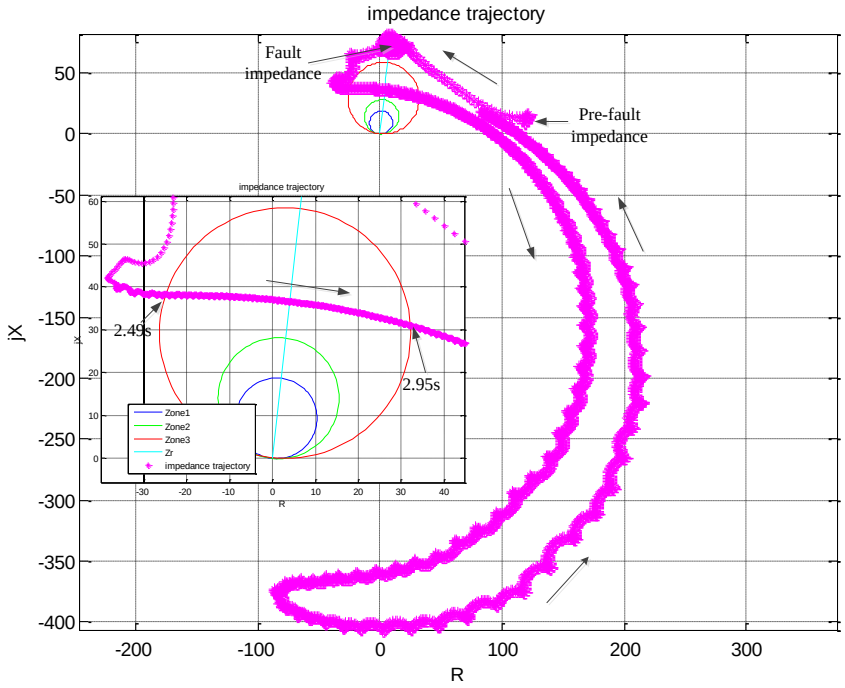

Figure 8-9 The response to an A-G fault impedance trajectory for a 300km fault from the relay point on the HVAC transmission system

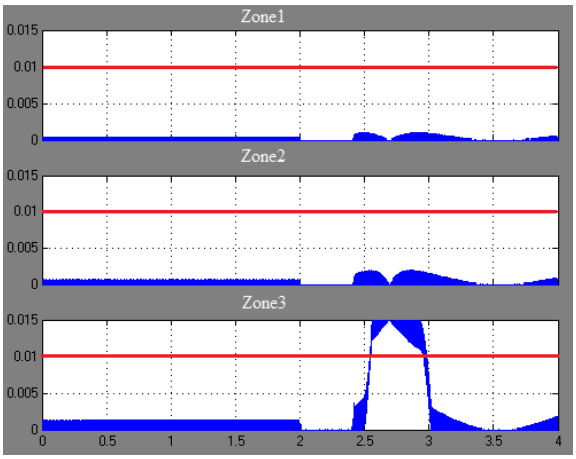

(a) A-G block-average comparator output

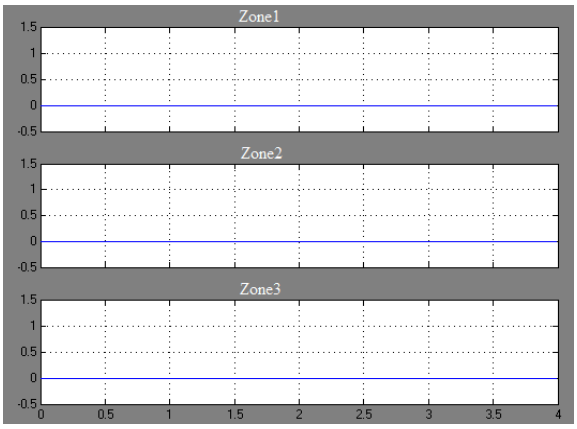

(b) A-G relay trip signals

Figure 8-10 The A-G block-average comparator output and relay trip signals for a 300km fault from the relay point on the HVAC transmission system

8.2.3 Protection response to load changes

Sudden load changes can result in power swings occurring in AC networks. This was demonstrated in a serious of simulation studies which examined the response of distance protection to these events. The distance relay's response to load changes condition in the HVAC/HVDC system was investigated. The load disconnection caused sudden changes in system voltages and currents. The HVDC converter stations adjusted the voltages and currents. The power system finally maintained a stable state and the power swing did not occur. The HVDC link effectively acted as

a ‘firewall’ against the power swing. The apparent impedances seen by all distance relay protections were similar, and the A-G comparator’s apparent impedance trajectory is shown in fig.8-11. It circled the protection zones in a counter-clockwise direction from the pre-fault load impedance. The apparent impedance presented irregularities due to the HVDC converter stations control strategies. The apparent impedance returned the pre-fault load point when the system stabilised. The apparent impedance did not enter the protection zones, and therefore the distance relay did not trip due to the changes to the load.

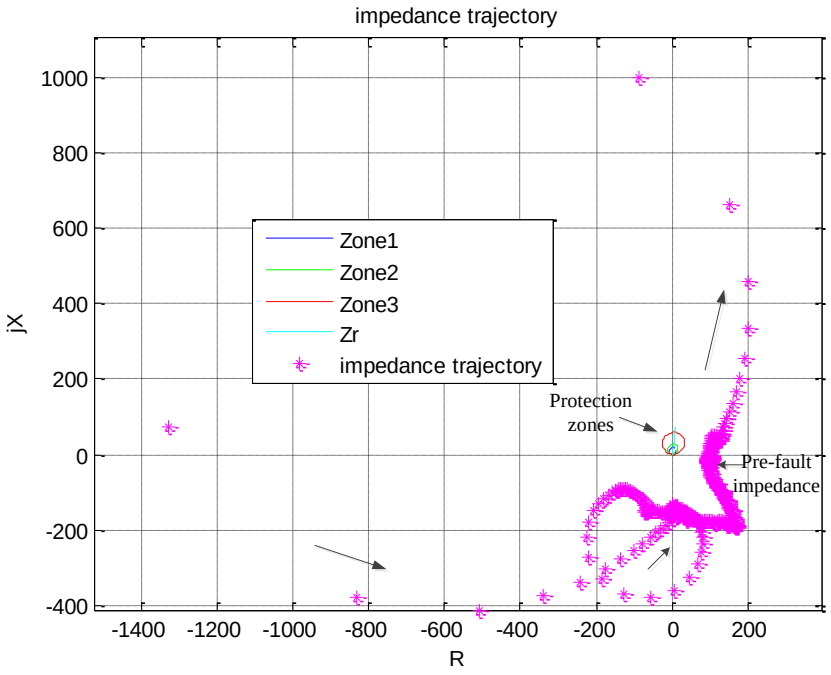

Figure 8-11 The impedance trajectory of the A-G comparator seen by distance relay to a sudden load change on the HVDC/HVAC system

The same situation was simulated in the HVAC system. All of the distance relay protections detected the power swing. The apparent impedances seen by the distance relay protections were similar. Fig.8-12 shows the A-G impedance seen by distance relay, and shows that the apparent impedance circled the distance relay protection zones. The apparent impedance went in a clockwise direction from the pre-fault load point and entered the protection zone3 characteristic at 2.7s. At 3.16s, the apparent impedance left the zone3 characteristic. This amounts to a total duration of 460ms

inside zone3, which was shorter than the zone3 time delay and hence would not result in tripping.

The apparent impedance left the zone3 characteristic in a counter-clockwise direction and re-entered the zone3 characteristic a second time at 3.81s and remained there until the end of simulation. The durations when the apparent impedance was inside the zone3 characteristic were shorter than the zone3 time delays and the distance relay did not trip.

Fig.8-13 (a) and (b) show the response of the distance relay's A-G block-average comparator outputs and distance relay trip signal. As can be seen in fig.8-13 (a), the zone3 output crossed the trip level when apparent impedance entered the zone3 characteristic for the first time. The block-average comparator zone3 output decreased below re-set level after the apparent impedance left the zone3 characteristic. The block-average comparator zone3 output crossed the trip level second time when the apparent impedance entered the zone3 characteristic a second time. The durations were all shorter than the zone3 time delay, therefore distance relay did not trip, as shown in fig.8-13 (b).

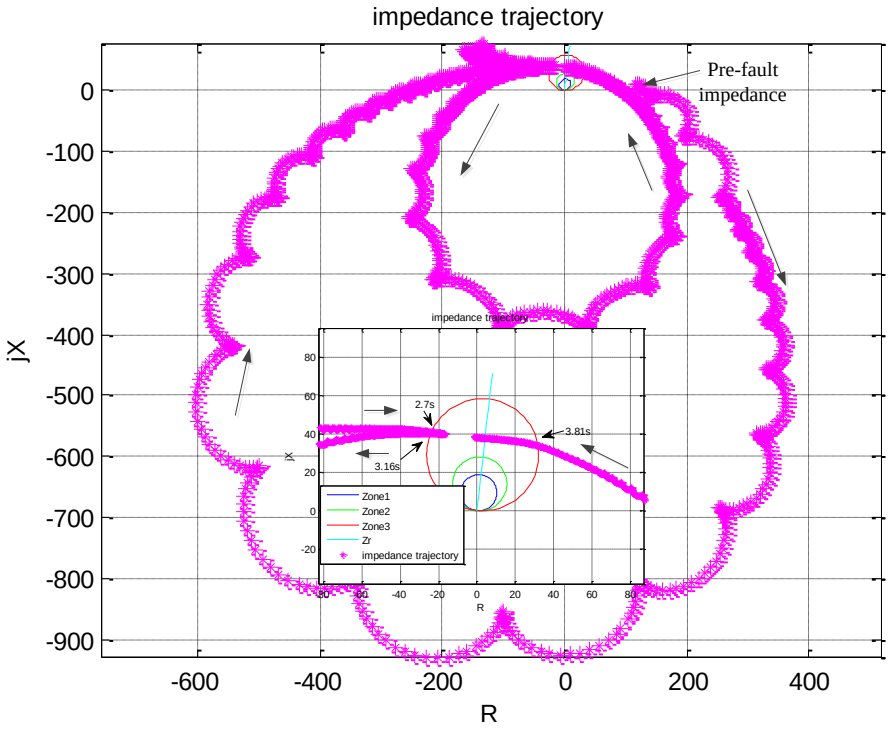

Figure 8-12 The impedance trajectory of A-G comparator seen by distance relay to a sudden load change on the HVAC system

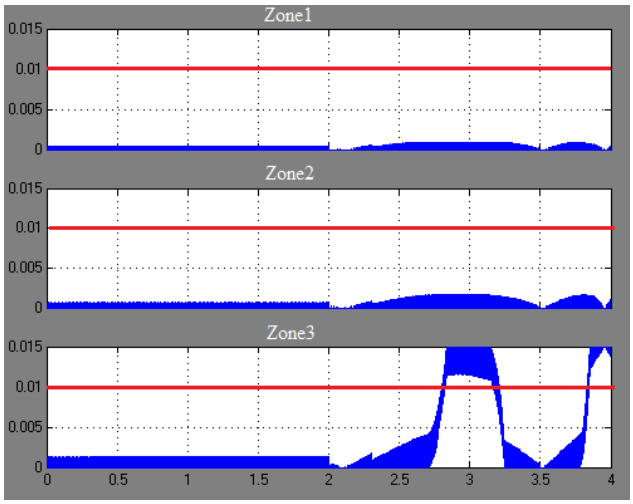

(a) A-G block-average comparator output

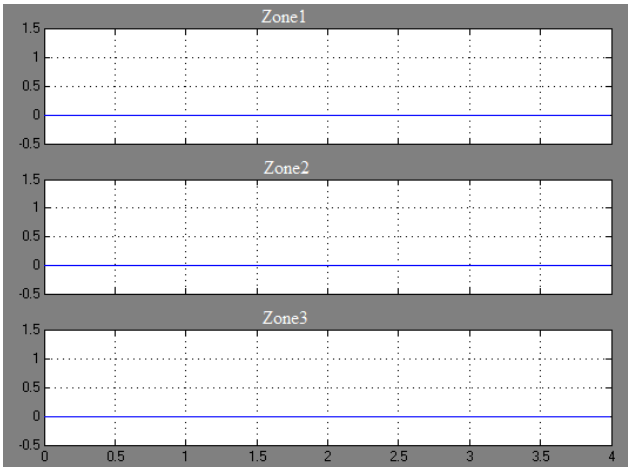

(b) A-G relay trip signals

Figure 8-13 The A-G block-average comparator output and relay trip signals for a sudden load change on the HVAC system

8.3Distance relay response to disturbances in two generators system

In the previous section, the load scheme included a small generator to examine the system's behaviours to network disturbances. In this section, the systems behaviours of the two generators of a similar size in the sources and loads networks were investigated.

The power system was simulated based on two areas power system described by Kundur [68] as shown in fig.8-14 (a) and (b). Fig.8-14 (a) presents the power system with a HVDC interconnection while fig.8-14 (b) shows the power system with

HVAC interconnection. Two 20kV, 900MVA generators G1 and G2 were connected to the power system through two 20/230kV, 900MVA power transformers T1 and T2. The generators were connected to two local loads through two 10kM AC transmission lines, line1 and line5. Load 1 was 230kV, 500MVA and Load 2 was 230kV, 1000MVA. In fig.8-14 (a), the loads were connected by two 100kM AC transmission lines, line2 and line4 and one 100kM HVDC link line3. In fig.8-14 (b), the loads were connected by three 100kM AC transmission lines: line2, line3 and line4. The distance relay was located at busbar B to protect line2. Zone1 was set to 80% of the line2, zone2 was set to 120% of line2, and zone3 was set to 250% of line2. The time delays set for zone1, zone2 and zone3 were 0ms, 200ms and 500ms respectively. The power generators' parameters are as previously used for the simulated generator in section 8.2. The details of the models are shown in Appendix. F.

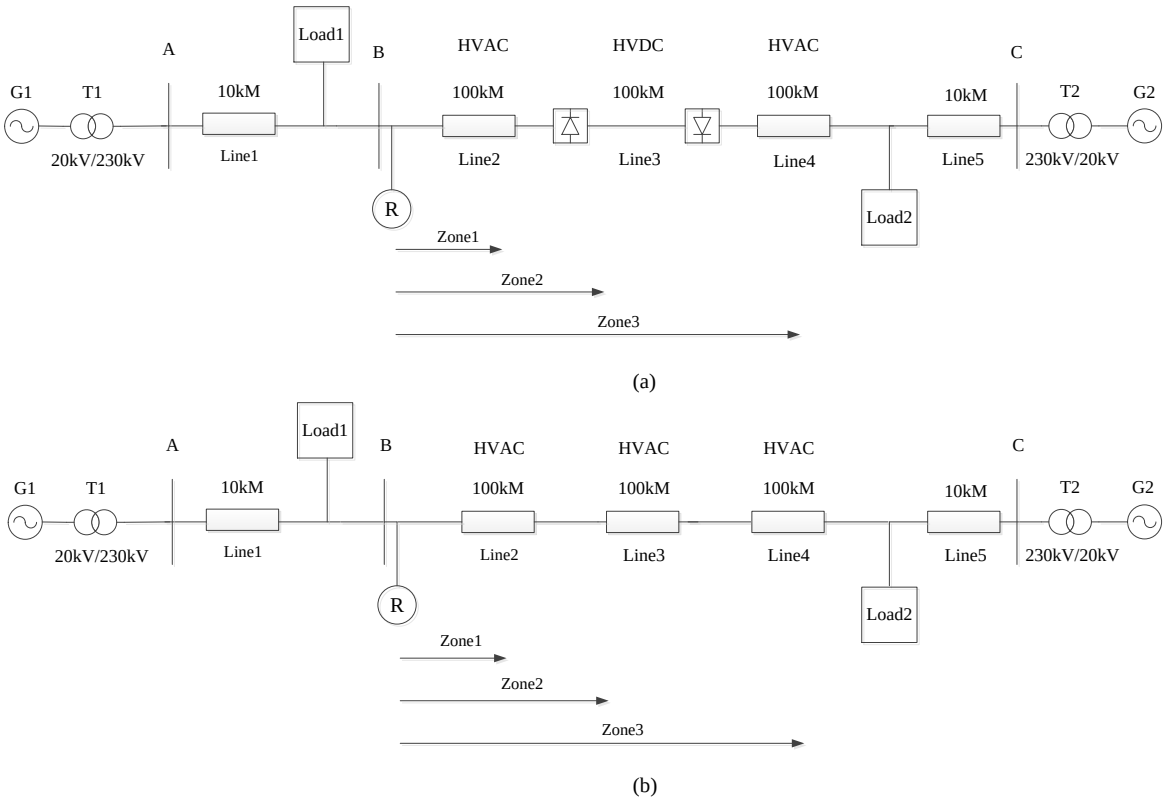

Figure 8-14 Simulated power systems

Fig.8-15 (a) and (b) show the pre-fault impedance seen by distance relay in the HVAC/HVDC system and the HVAC system respectively. The impedance seen in

the HVAC/HVDC system had negative reactance was due to the HVDC converter station absorbing reactive power.

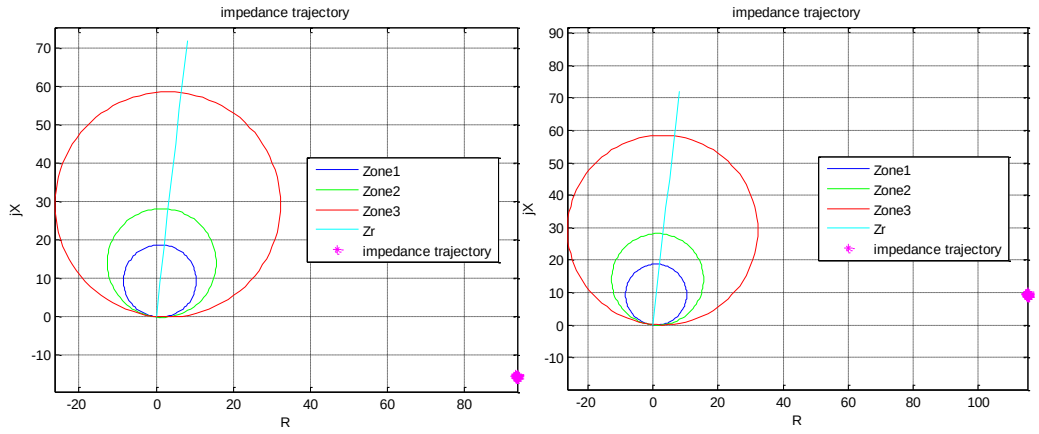

(a) Steady impedance seen by distance relay in HVAC/HVDC system

(b) Steady impedance seen by distance relay in HVAC system

Figure 8-15 Pre-fault impedance seen by distance relay for the HVAC/HVDC and HVAC networks

8.3.1 Protection response to load1 disconnected and reconnection

The distance relay's response to a load change condition in the HVAC/HVDC system was investigated. The sudden load change caused changes in power system voltages and currents, but due to the HVDC converter control functions, the power swing did not occur when load 1 was disconnected and reconnected. The power system maintained a stable state. The HVDC link effectively acted as a 'firewall' against the power swing. All of the distance relay protection detected the variations in the voltages and currents during load change. The apparent impedances as seen by all distance relay protections were similar. The A-G apparent impedance is shown in fig.8-16, starting at the pre-fault load impedance and followed a series of circles during the load change. When the power system returned to the stable state, the apparent impedance returned back to the pre-fault load impedance. The apparent impedance did not enter the protection zones and distance relay did not trip.

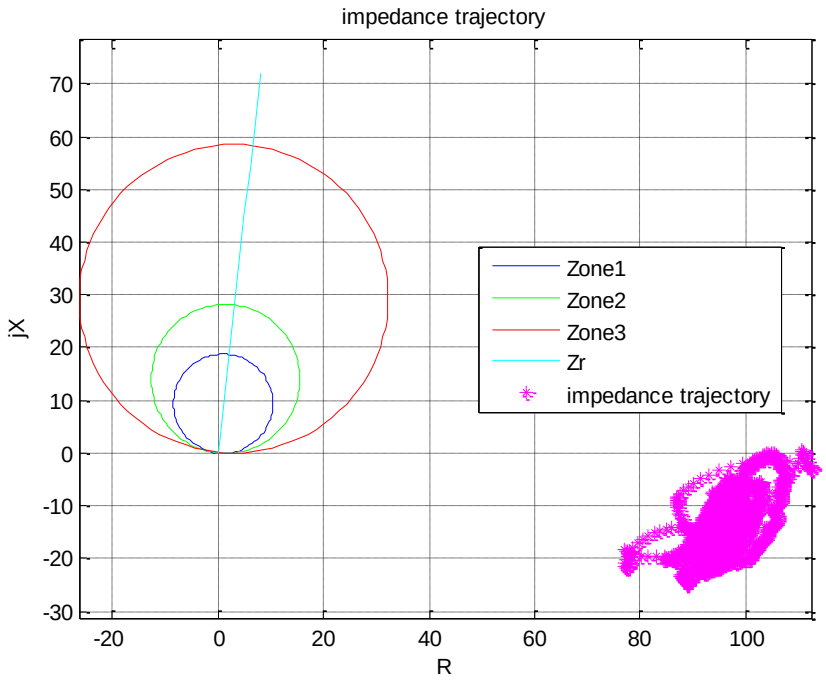

Figure 8-16 The impedance trajectory of A-G comparator seen by distance relay for sudden load changes on the HVAC/HVDC system

For comparison, the same condition was simulated in HVAC system. Sudden changes in load can cause the power swing occurred in HVAC power systems. All the distance relay protections detected the power swing. The apparent impedances seen by the distance relay protections were similar. Fig.8-17 shows the A-G impedance trajectory, which started at the pre-fault load impedance and moved towards the distance relay protection zones during the power swing. After 2.6s, the apparent impedance entered the protection zone3 characteristic, and then moved back leaving the trip characteristic. After 3.7s, the apparent impedance moved out the zone3 characteristic. The duration that apparent impedance stayed inside protection zone3 characteristic was 1.1s, which was long enough to cause a zone3 trip. Fig.8-18 (a), (b) show the distance relay's A-G protection block-average comparator output and trip signal. The block-average comparator zone3 output crossed the trip level at about 2.6s when apparent impedance entered the protection zone3 characteristic and fall below the reset level at 3.75s. The trip signal was given at 3.1s, 2.6s+500ms time delay. The trip signal was reset after 3.75s when comparator output returned back to reset level. Although there were no faults, the distance relay tripped due to the power swing.

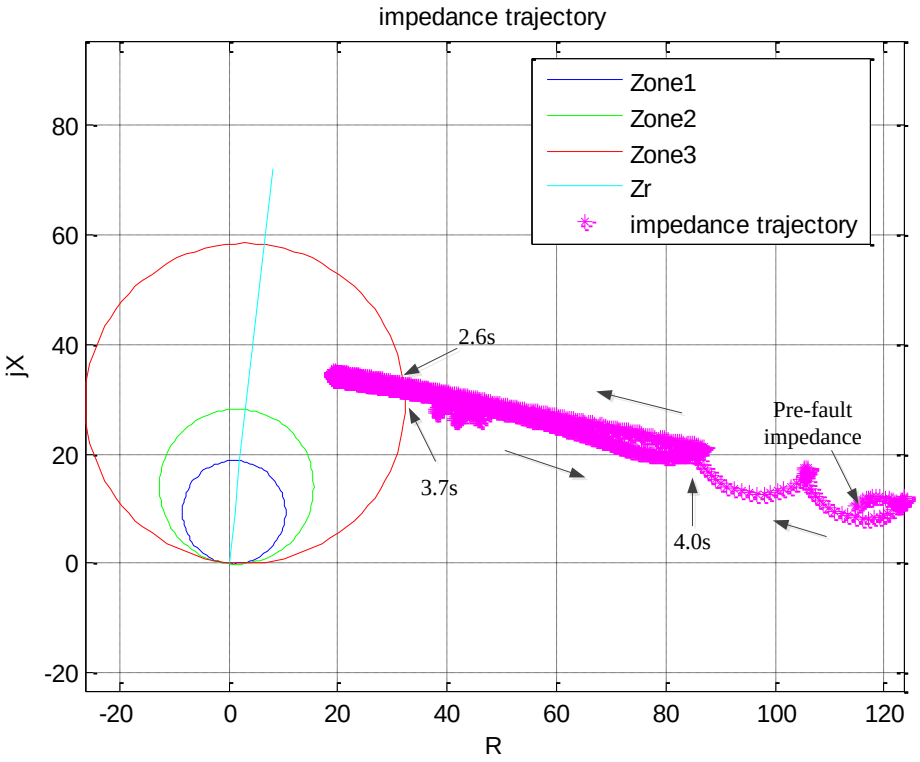

Figure 8-17 The impedance trajectory of A-G comparator seen by distance relay for sudden load changes on the HVAC system

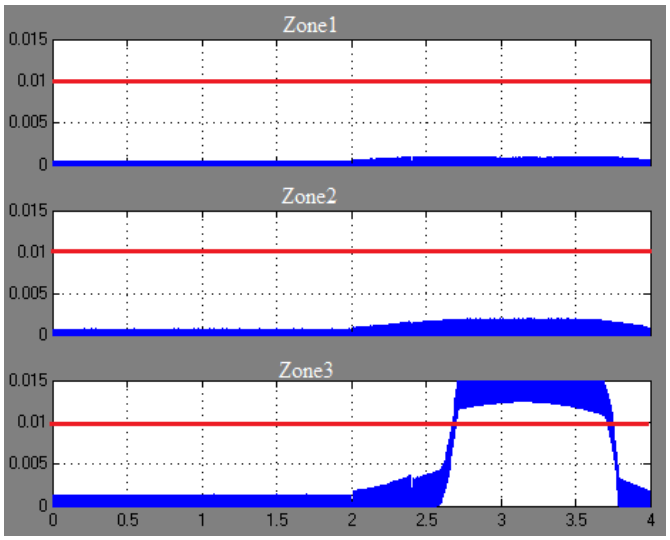

(a) A-G block-average comparator output

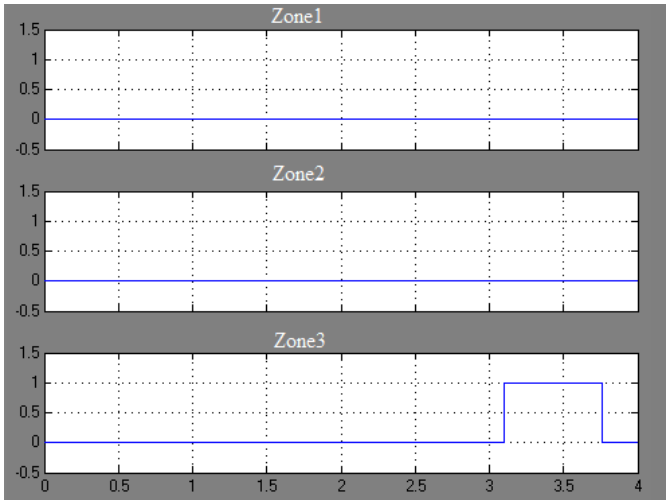

(b) A-G relay trip signals

Figure 8-18 A-G block-average comparator output and relay trip signals for sudden load changes on the HVAC system

8.3.2 Protection response to load2 disconnected and reconnected

The load2 was disconnected and reconnected in the HVAC/HVDC system in order to investigate the distance relay response to the load change. The load change resulted in voltage and current changes in the power system, but the HVDC control strategies ensured that the variations in the voltage and current did not result in a trip impedance. The HVDC link effectively acted as a 'firewall' against the power swing.

All the distance relay protections detected the voltage and current changes, and the apparent impedances seen by all distance relay protections were similar. The A-G apparent impedance trajectory is shown in fig.8-19. The apparent impedance started at the pre-fault impedance and circled in a clockwise direction. The apparent impedance returned to this pre-fault impedance when the power system returned to a stable state. The apparent impedance did not enter the distance relay protection zones, thus the distance relay did not trip.

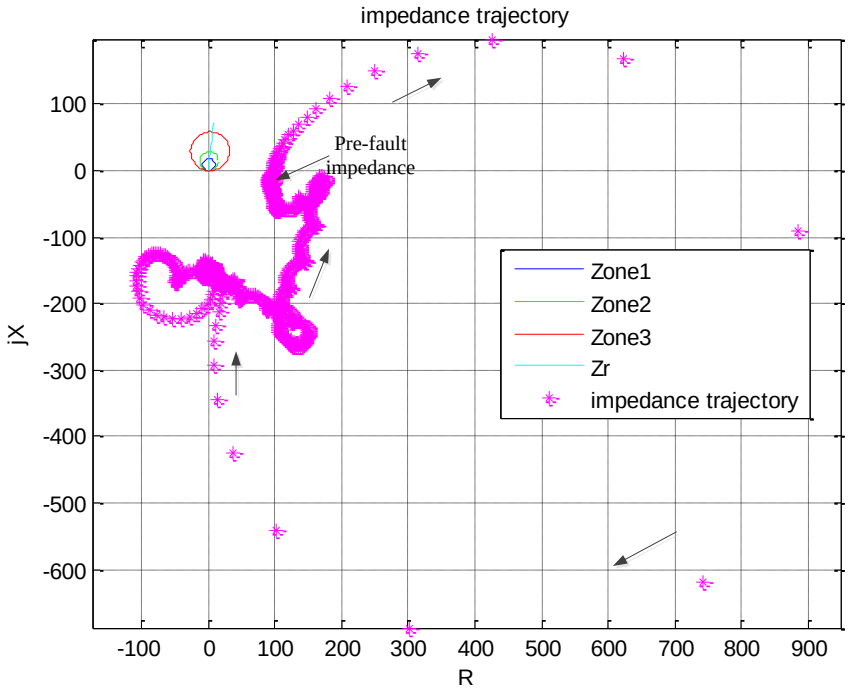

Figure 8-19 The impedance trajectory of A-G comparator seen by distance relay for a sudden load change on the HVAC/HVDC system

For comparison, the same situation was simulated in the HVAC system. This change to the load was important at the load end the HVAC transmission system. The load change caused the two generators to struggle with each other and a power swing occurred. All the distance relay protections detected the swing voltages and currents. The apparent impedances seen by the different distance relay protections were the similar. The A-G apparent impedance is shown in fig.8-20 (a) and (b). Fig.8-20 (a) shows the overview of the A-G impedance trajectory and fig.8-20 (b) shows the A-G impedance trajectory that inside the protection zone3 characteristic. The impedance trajectory started at the pre-fault load impedance and circled the trip

characteristic in a clockwise direction. The apparent impedance changed its direction before it entered the protection zones. Following that the apparent impedance circled in a counter-clockwise direction. After 3.23s the apparent impedance entered the protection zone3 characteristic. It moved out of the characteristic after 3.63s. The apparent impedance continued circling the protection zones in a counter-clockwise direction and stopped when simulation ended. The duration that apparent impedance stayed inside the protection zone3 characteristic was 400ms, which was shorter than zone3 time delay and would not cause the zone3 to trip. Fig.8-21 (a) and (b) show the distance relay A-G protection's block-average comparator output and trip signals. The A-G block-average comparator zone3 output crossed the trip level when apparent impedance entered the zone3 characteristic. The output returned below reset level when apparent impedance moved out of zone3 characteristic. Because the duration that apparent impedance stayed inside protection zone3 was shorter than the zone3 time delay, the distance relay did not trip.

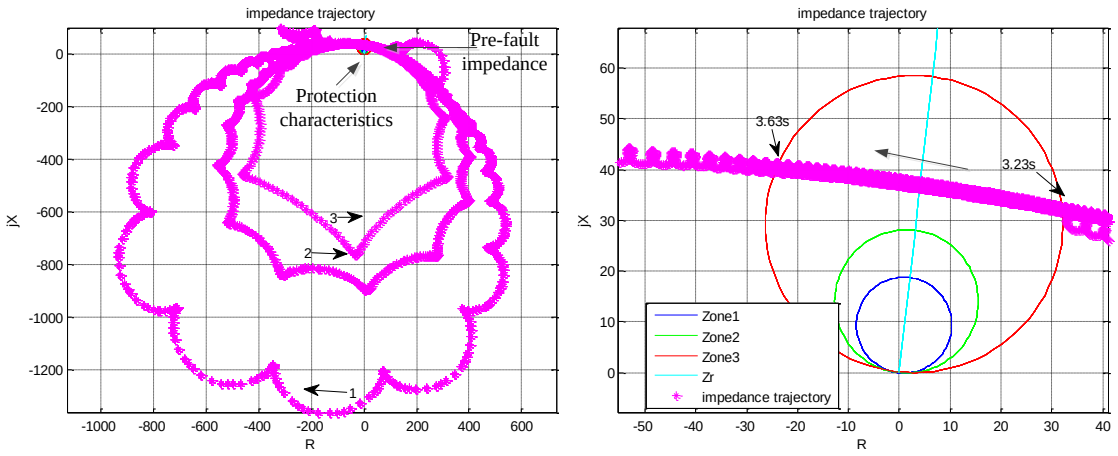

(a) Overview of the A-G impedance trajectory

(b) Impedance trajectory inside protection zone3 characteristic

Figure 8-20 The impedance trajectory of A-G comparator seen by distance relay for a sudden load change on the HVAC system

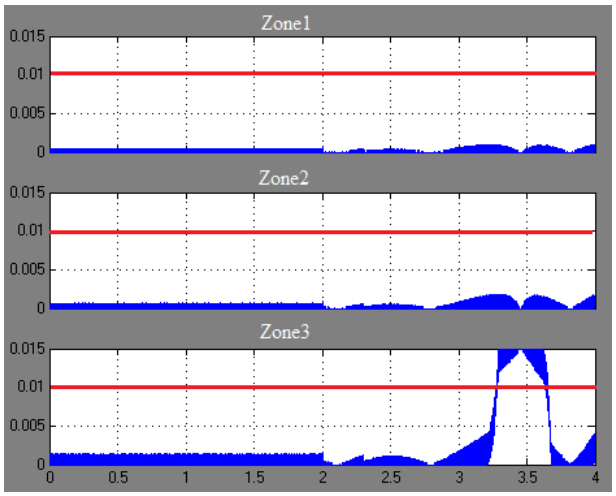

(a) A-G block-average comparator output

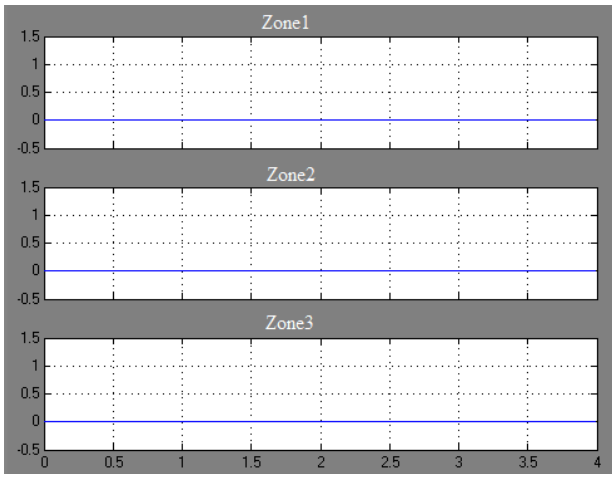

(b) A-G relay trip signals

Figure 8-21 The A-G block-average comparator output and relay trip signals for a sudden load change on the HVAC system

8.3.3 Protection response to an A-B-C-G fault on line5 at 5kM

An A-B-C-G fault was applied to the HVAC/HVDC system at the mid-point of line5. The fault caused the power system voltages and currents to change as dictated by the HVDC system. The HVDC control strategies regulated the fault voltage and current and a power swing did not occur. The HVDC link effectively acted as a 'firewall' against the power swing. The distance relay detected the changes in the fault voltage and current, and the fault impedances seen by all of the distance relay protections were similar. The A-G fault impedance trajectory is shown in fig.8-22. The fault

impedance circled the protection zones in a counter-clockwise direction. When the power system returned to a stable state, the fault impedance trajectory returned to the pre-fault point. The fault impedance did not enter the protection zones and distance relay did not trip.

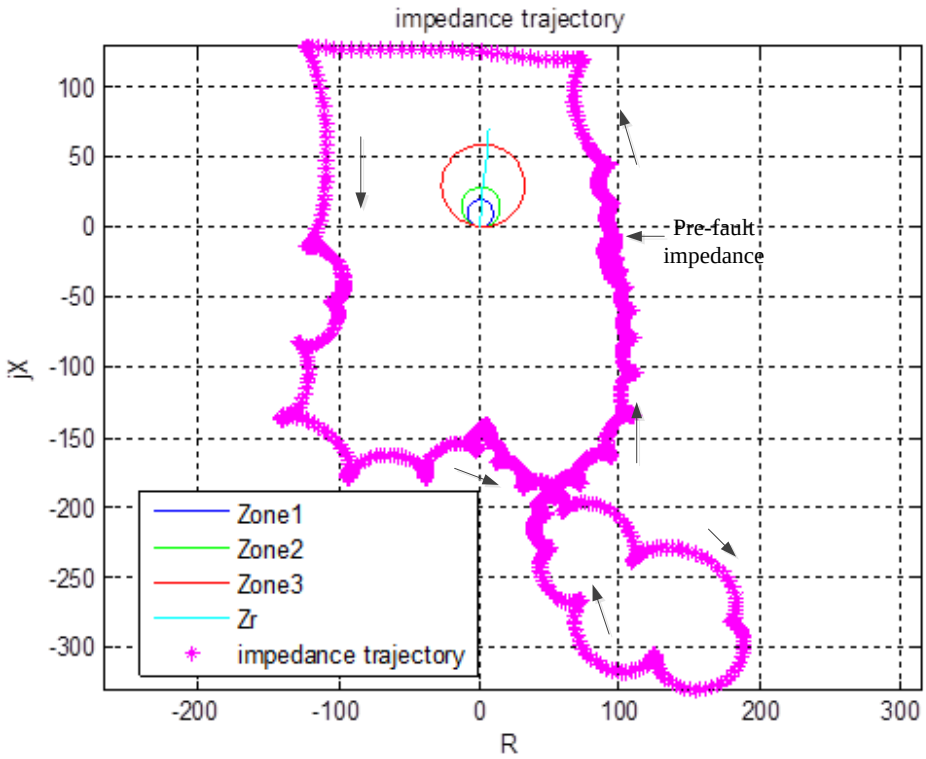

Figure 8-22 The impedance trajectory of A-G comparator seen by distance relay for an A-B-C-G fault on 305km from the relay point on the HVAC/HVDC system

For comparison, the same situation was simulated in the HVAC system. A power swing occurred after the fault was removed. When fault occurred on line5, the distance relay detected a fault. The fault impedances seen by all of the comparators in the distance relay were similar. The A-G fault impedance is shown in fig.8-23 (a) and (b). Fig.8-23 (a) shows the overview of the A-G impedance trajectory and fig.8-23 (b) shows the A-G impedance trajectory that settled on the fault impedance and inside the protection zone3 characteristic. The impedance trajectory first moved towards to fault impedance and settled at the equivalent to 305km from the relay. When power swing occurred, the fault impedance moved from this fault impedance and began to move in a circular manner in a clockwise direction. The seen impedance entered the protection zone3 characteristic at 3.15s and left it at 3.9s. The duration

that apparent impedance stayed inside protection zone3 characteristic was 750ms, which was greater than zone3 time delay and therefore would result in a trip. The fig.8-24 (a) and (b) show the distance relay A-G protection block-average comparator output and trip signal. The comparator output crossed the trip level after fault impedance entered the protection zone3 characteristic after 3.2s. Due to zone3 time delay, the distance relay zone3 tripped after 3.7s. The distance relay did not trip because of the fault but tripped in response to the power swing.

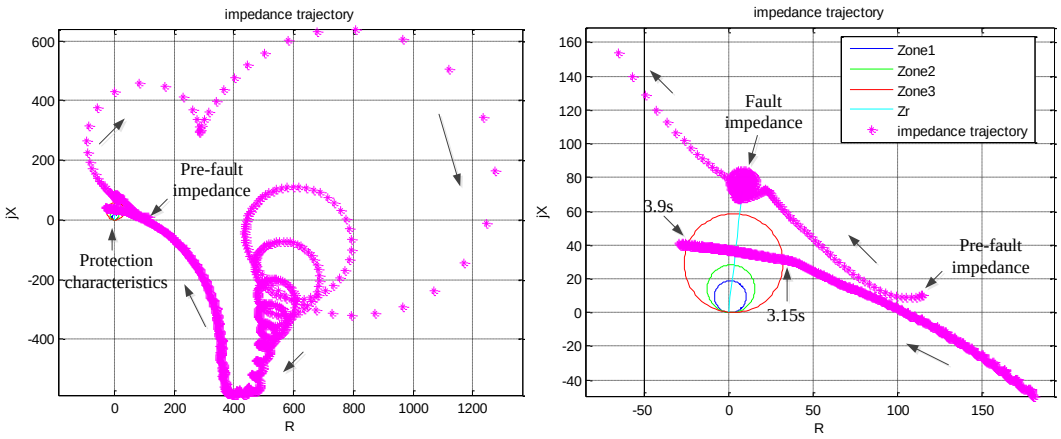

(a) Overview of the A-G impedance trajectory

(b) A-G impedance trajectory started from the pre-fault point to fault impedance and inside the protection zone3 characteristic

Figure 8-23 The impedance trajectory of A-G comparator seen by distance relay for an A-B-C-G fault on 305km from the relay point on the HVAC system

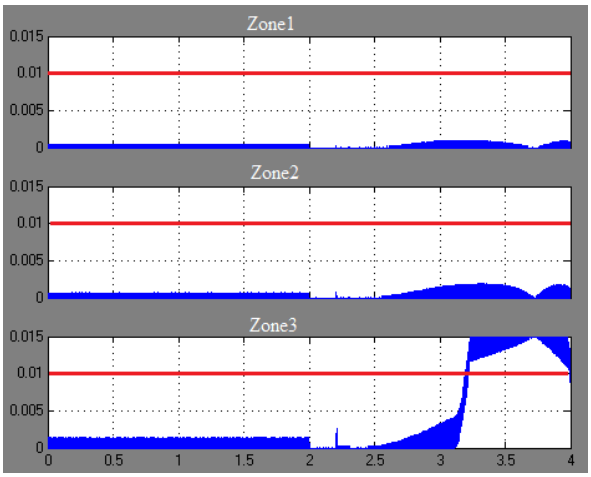

(a) A-G block-average comparator output

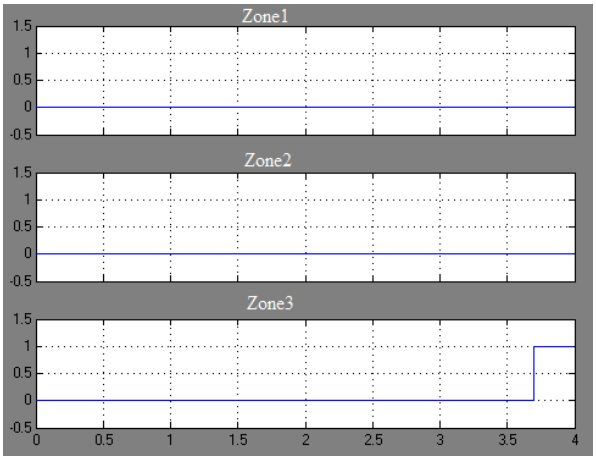

(b) A-G relay trip signals

Figure 8-24 The A-G block-average comparator output and relay trip signals for an A-B-C-G fault at 305km from the relay point on the HVAC system

8.3.4 Protection response to an A-B-C-G fault at load2

An A-B-C-G fault was applied to the HVAC/HVDC system at load 2. The fault resulted in HVDC control actions to affect the fault voltages and currents. Following the fault, a power swing did not occur. Again the HVDC link acted as a 'firewall' against the power swing.

The distance relay detected the fault voltage and current, and the fault impedances seen by all distance relay protections were similar. A-G fault impedance trajectory

is shown in fig.8-25. The impedance trajectory did not enter the protection zones, and hence the distance relay had no possibility to trip.

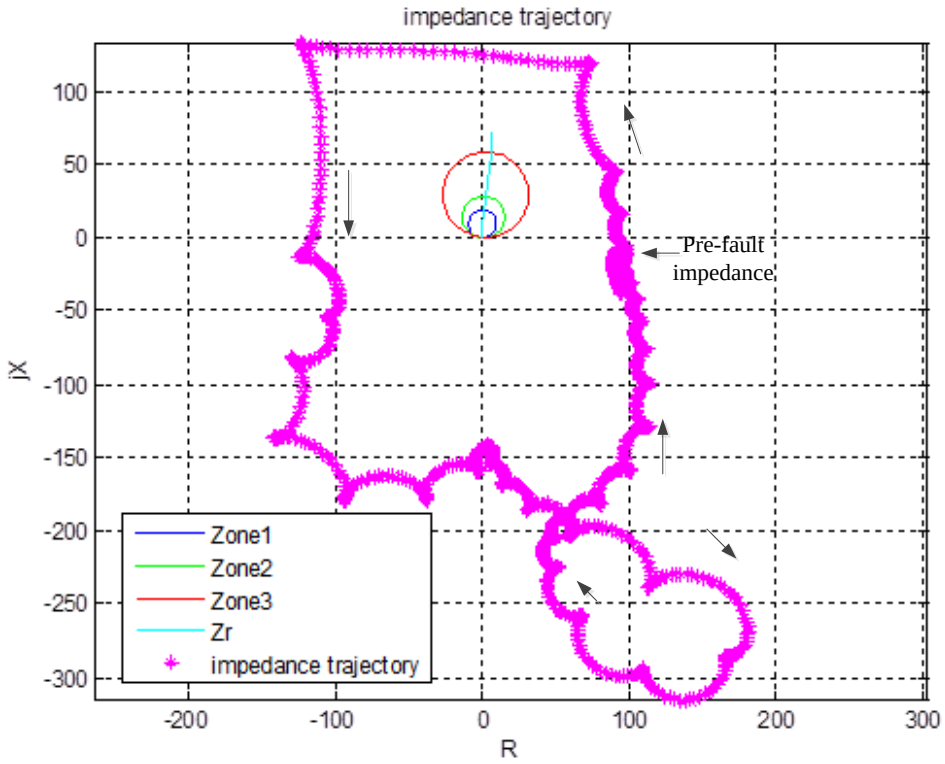

Figure 8-25 The impedance trajectory of A-G comparator seen by distance relay for an A-B-C-G fault on 300km from the relay point on the HVAC/HVDC system

For comparison, the same scenario was simulated in the HVAC network. This caused a power swing which the distance relay detected. The fault impedance trajectories seen by all of the distance relay comparators were similar. The A-G fault impedance trajectory is shown in fig.8-26 (a) and (b). Fig.8-26 (a) shows the overview of the fault impedance trajectory and fig.8-26 (b) shows the fault impedance that settled on the fault impedance and inside the protection zone3 characteristic. The fault impedance settled at the fault impedance at 300km while the fault was on the network. When it was removed, the power swing occurred, and the fault impedance circled the protection characteristics in a clockwise direction. The impedance trajectory entered the protection zone3 characteristic during power swing after 3.15s and left it after 4.0s. The period that the fault impedance stayed inside protection zone3 characteristic was 850ms, which was greater than zone3 time delay and therefore would cause the relay to trip. Fig.8-27 (a) and (b) show the distance

relay A-G protection block-average comparator output and trip signal. The comparator output began to climb when fault impedance entered the protection zone3 characteristic during fault. After 3.2s, the output crossed the trip level. Following the 500ms time delay of zone3 protection, the distance relay tripped after 3.7s. The fault did not cause distance relay to trip because the fault was outside of the distance relay protection zone. The following power swing did caused the distance relay to trip.

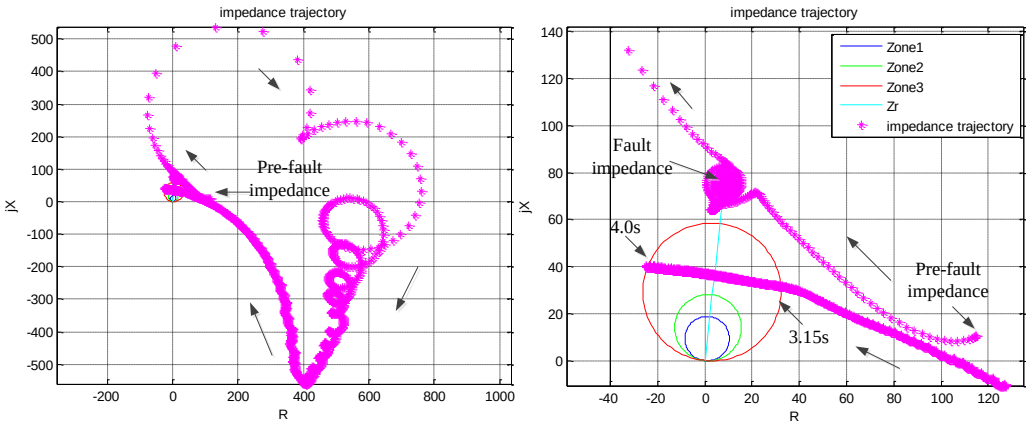

(a) Overview of the A-G impedance trajectory

(b) The A-G impedance trajectory started from the pre-fault point to fault impedance and inside protection zone3 characteristic

Figure 8-26 The impedance trajectory of A-G comparator seen by distance relay for an A-B-C-G fault on 300km from the relay point on the HVAC system

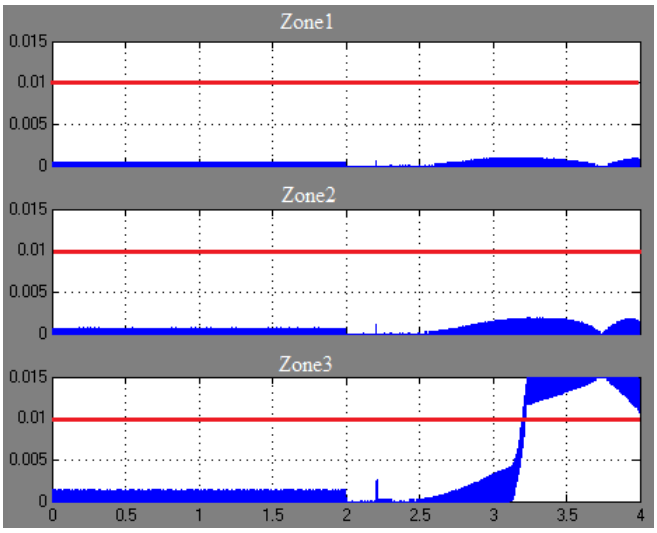

(a) A-G block-average comparator output

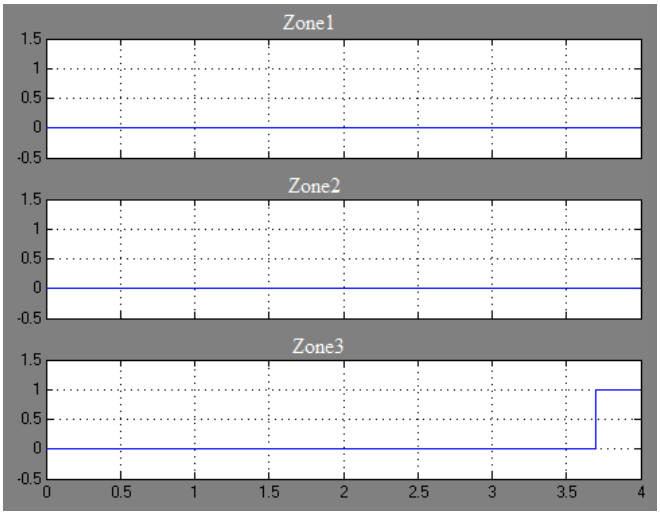

(b) A-G relay trip signals

Figure 8-27 The A-G block-average comparator output and relay trip signals for an A-B-C-G fault at 300km from the relay point on the HVAC system

8.4 Chapter Summary

This chapter investigated the impact of disturbance on a HVAC/HVDC system and subsequent on distance relay. The investigation was carried out based the Kundur's two area system [68]. For comparison, a similar HVAC interconnection system was simulated to demonstrate its response to similar events.

In the HVAC/HVDC system, where there was a disturbance to the system, the HVDC control system modified the power system's voltages and currents. The distance relay apparent impedance trajectories did not enter the protection zones and therefore there was no tripping. Cascading failures or blackouts were therefore prevented.

In the HVAC system, when a sudden change happened in the system became unstable and entered transient conditions. The changing voltage and current caused the distance relay impedance trajectories to enter the protection zones. The distance relay tripped when the apparent impedance duration stayed inside the protection zones for longer than the pre-set time delays. Although the relay did not trip due to the fault, it did trip for the following system disturbance. This could lead to a blackout.

Chapter 9

Conclusions and Future Works

9.1 Conclusions

Worldwide, there is a growing need to transport electrical energy over large distances and within geographically large areas. Historically, North America has offered the greatest opportunities for these wide area systems, however increasingly opportunities are arising in China, Western Europe, Eastern Europe, the Middle-East and Africa.

Unfortunately, the North America experiences with such systems have not been trouble free. Wide area blackouts occasionally occur with loss of power to large geographical areas and affecting large number of consumers.

The trigger for several of these blackouts has been attributed to operation of the protection systems followed by system instability and further protection tripping. Recent major blackouts show that the operation of the distance relay caused by power swing accelerated system collapse. With HVAC networks, system instability led to cascade tripping and the blackout spread to large area affecting many consumers.

The 2003 North America Blackout demonstrated that the inclusion of a HVDC interconnection in the HVAC/HVDC network acted as a 'firewall' against the power outage and prevented the system collapse propagating through the power networks. In this thesis, investigations were undertaken to study the behaviour of distance relays and the HVDC interconnection reactions during faults and transient conditions during a blackout.

This thesis firstly combined the distance relay and the HVDC interconnection together to investigate the behaviour of the distance relay. By investigating the Block-average comparator operations and the fault impedance trajectories, the behaviour of the distance relay was demonstrated in the thesis when protected feeders containing HVDC link during fault conditions and power swing conditions. An HVAC system was also simulated under the similar conditions to give comparable results. These were modelled using HVAC/HVDC power systems based on Kundur's two-area system using MATLAB/SIMULINK.

The thesis focused on the four main areas:

- The distance relay study and modelling;
- The HVDC study and modelling;
- The distance relay operations when the protected network contained both HVDC and HVAC interconnections during fault without power swing conditions;
- The distance relay operations when the protected network contained both HVDC and HVAC interconnections during fault with power swing conditions

9.1.1 The Distance Relay Studies

The distance relay uses the measured voltage and current to determine the apparent impedance. By comparing the apparent impedance and the relay's trip characteristics, the distance relay determines whether there is a fault and generates trip signal.

In a power system, the main purpose of the distance relay is to detect and enable clearing of a fault as reliably and quickly as possible. This minimizes the damage to the power network and maintains the system stability for delivering the electrical energy supplies.

During normal operation, the apparent impedance as seen by the relay is large and located outside the distance relay protection zones. During fault, the decrease voltage and the increase current results in the apparent impedance entering the distance relay protection zones therefore the distance relay trips.

The simulated distance relay in this thesis used a block-average comparator and a Mho characteristic. It used the V and IZ-V signals to generate the Mho circle. The Mho characteristic distance relay tripped when the angle argument between the V and IZ-V phasors was between -90° and 90°.

The block-average comparator used in the simulation is widely recognised as the standard for distance protection. It measured the duration of polarity coincidence of the input signals. When the polarity coincidence differences were between -90° and 90°, the block-average comparator with its trip integrator generated a trip signal.

The fault impedance trajectory plotting circuits used the measuring fault voltage, V, and current, I, to compute the fault impedance. The measured voltage and current signals must be filtered before inputs into the plotting circuits. The low-pass filters and DFTs were used to remove the unwanted high frequency components and extract the fundamental phasor information.

The distance relay's zone3 protection provides the remote back-up protection and covers a wide area along the transmission lines. During power system transient conditions, the voltage and current changes may cause the apparent impedances as seen by distance relay enter the zone3 protection area and lead to a trip. The inappropriate tripping of distance relay zone3 protection due to system instability contributes to the power outage spreading through the whole of the power network.

9.1.2 The HVAC/HVDC Studies

The HVAC/HVDC transmission system offers benefits in long distance power deliveries, in terms of HVAC facilities connections of asynchronous AC system interconnections, AC networks enhancement, economics and environments.

The HVDC link consists of two converter stations operating as rectifier and inverter. These converter stations perform the ac/dc/ac conversion and control the power flow through the HVDC link.

The rectifier is provided with a constant current control and was a constant ignition angle control which includes a minimum α-limit. The minimum firing angle ensures that there is enough voltage across the valves. The constant current control mode controls the dc current at the desired value by varying the α. When the direct current is smaller than a reference value, the α decreases.

The inverter is provided with a constant extinction angle control mode and a constant current control mode. The constant extinction angle control mode maintains the direct voltage.

Under normal operation, the rectifier is under constant current control mode (CC) and the inverter is under constant extinction angle (CEA) control mode. In the situation that the ac voltage decreases, the ignition angle α in rectifier decrease in

order to maintain the dc voltage. When the ignition angle hits its limit value, the rectifier switches to the constant ignition angle control (CIA) and inverter changes to the constant current control mode (CC).

The HVDC control system is also provided with maximum/minimum current control and voltage dependent current order limit (VDCOL) control. The maximum current control limits the maximum direct current value in order to avoid the damaging of the converter valves. The minimum current control limits the minimum direct current value in order to keep the direct current being continuous. The VDCOL control limits the maximum allowable direct current when the voltage drops below a specified value.

9.1.3 The Distance Relay and HVAC/HVDC System Reactions During Fault Conditions

From the simulation studies, it was shown that when a fault occurred in zone1 area, the distance relays trip to the fault both in HVAC/HVDC and HVAC systems. The fault impedances seen by distance relay were similar. Different types of faults led to the distance relay protections tripping as required.

When the fault occurred in zone2 area, the results were different. When fault occurred on HVDC line, the distance relay did not trip. The fault impedances seen by different distance relay comparators were similar. The HVDC line fault led to the voltages and currents in the HVAC feeder responding to the fault but did not result in a trip. When a similar fault occurred at the same location in the HVAC system, the distance relay tripped as expected.

When faults occurred in zone3 area on the HVAC/HVDC network, both on the HVDC line and on the HVAC line beyond the HVDC line, the distance relay did not trip. Different types of faults resulted in similar fault impedances as seen by all of the relay comparators. The HVDC line effectively isolated the fault. When the same faults occurred on the comparable HVAC system, the distance relay tripped as expected.

When a fault occurred outside the protection zones, both distance relays in the HVAC/HVDC system and the HVAC system did not trip. Conversely, the fault impedances seen by the different comparators in the distance relay in HVAC/HVDC system were similar to the fault impedances when the faults occurred inside protection zones.

The results also presented evidence that when faults occurred on the HVAC/HVDC network, and the fault location was on the HVDC line, distance relay did not trip.

For HVAC/HVDC network, when faults occurred both on HVDC line and beyond HVDC link on HVAC line and inside the distance relay protection zones, the distance relay did not trip. The HVDC link isolated the fault. The fault impedances seen by the different comparators of the distance relay were similar irrespective of the fault types. All of the distance relay protection detected similar fault impedances.

There were no further trips of the HVAC lines in HVAC/HVDC system. Distance protection tripping was constrained to the HVAC line before the HVDC interconnection and cascade tripping was prevented.

9.1.4 The Distance Relay and HVAC/HVDC Reactions During Power Swing Conditions

From the simulation studies, it was shown that, when a power swing occurred in the HVAC system caused by line faults, load change and load short circuits did not occur in the HVAC/HVDC system. The HVDC control schemes regulated the network voltages and currents and maintained the power system in a stable state.

In the HVAC network, the power swing was shown to cause the distance relay to trip. During the power swing, the changes in system voltages and currents resulted in the apparent impedance detected by distance relay entering the protection relay's zone3 protection characteristic causing the distance relay to trip. The distance relay tripped in response to power a swing conditions rather than true fault. When power swing occurred, the apparent impedances as seen by the different comparators in the distance relay were similar.

The HVDC link regulated the power swing voltage and current and helped to maintain the power system stable state. The distance relay in the HVAC/HVDC system can detect the power swing voltage and current. However, due to HVDC voltage and current regulation, the variations in the voltages and currents did not result in the distance relay tripping. The power system remained in a stable state. The HVDC acted as a 'firewall' against the power outages and prevented the potential large blackout.

Use of a HVDC interconnection has been shown to provide a significant improvement in the performance of a high voltage power system. The fault on and beyond the HVDC terminal within distance relay protection zones does not trigger the distance relay to trip. The response to unbalance between load and generation does not cause the apparent impedance seen by distance relay to enter the protection zones with HVDC interconnections. The potential for a blackout does not happen in HVAC/HVDC system. Such hybrid AC/DC power system offers significant advantage in terms of power system stability and reliability.

9.2 Future work

HVDC Converter Internal Faults

In this thesis, the response to internal fault inside the HVDC converter has not been considered. The converter internal faults including valve misfire, backfire, commutation failure and short circuits within the converter station. The commutation failure is the most common disturbance during inverter operation. These internal faults affect the network's voltage and current and will cause a disturbance to the nearby HVAC system. The ac voltage and current disturbance will cause the distance relay to respond and probably trip. A subsequent issue stemming from this is scenario in the co-ordination of the converter protection and the network's protection. The zero-sequence current that caused by single phase to ground fault was not considered. These zero-sequence current may cause commutation failure in the converter stations especially on the inverter side AC system fault.

VSC HVDC System

The modelled and tested HVDC scheme in the thesis was CSC HVDC based on thyristor valves. It was a monopolar HVDC scheme which consisted of two converters connected with a single conductor. The return path used ground.

Increasingly VSC HVDC control schemes which utilize self-commutating switches, such as gate turn off thyristors (GTOs) or insulated-gate bipolar transistors (IGBTs) are becoming more popular. The VSC HVDC scheme consists of two conductors, one of which is operated in positive voltage and the other in negative voltage. Since the VSC HVDC has two conductors, the fault types may vary depending on the faulted conductors. The fault types may include single line to ground fault, line to line fault, line to line to ground fault and line to line to ground fault at different locations. Future research should focus on the distance relay's operations during these faults.

The VSC HVDC can control both active and reactive power independently, and is independent of dc voltage level. The VSC HVDC can control reactive power to regulate the ac system voltage. The future studies should also focus on the distance

relay operations during power system dynamic conditions when interconnected by VSC controlled HVDC links.

HVDC and HVAC Parallel

The modelled power system used an HVDC interconnection and HVAC lines connected in series. The fault current was transmitted along the AC and DC lines. The simulation results show that when the fault was on the HVDC interconnection and beyond the HVDC link, it did not cause the distance relay to trip. The absence of power swing following a system unbalance did not result in the distance relay tripping with HVDC interconnection either.

However, the situation where the HVDC interconnection operated in parallel with the HVAC interconnection was not considered in the thesis. The fault current blocked by the HVDC interconnection would be transmitted through the HVAC interconnection and the distance relay may trip. The further investigation should focus on the system where with HVDC interconnection operated parallel with the HVAC interconnection.

Both the CSC and VSC controlled schemes for the HVDC interconnection should be considered.

With CSC HVDC interconnection operated in parallel with HVAC interconnection, following conditions should take in consideration, faults on HVDC interconnection, different types of faults on HVAC interconnection and faults beyond the interconnections. The distance relay response to these faults will be investigated in the future research.

With VSC HVDC interconnection operated in parallel with HVAC interconnection, the following conditions should also be considered with, different types of faults on VSC HVDC terminals, different types of faults on HVAC interconnection, and faults beyond these interconnections. The distance relay's operations will be investigated in the future research.

The voltage collapse can spread through an HVAC system but was constrained by a HVDC link. Under the situation that the power swing occurs, the swing voltage and

current would be blocked by HVDC interconnection, but would pass through the HVAC interconnection. The future research should also focus on the distance relay operations during power swings when the system is interconnected by HVDC interconnection operated parallel with the HVAC interconnection.

Appendix.A

The Kundur's two area system.

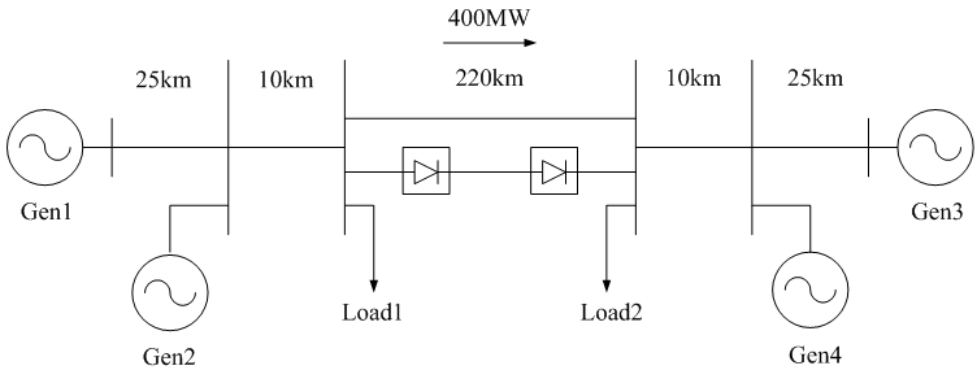

Fig.A-1 The Kundur's two area system

The generator's parameters:

R_s	0.0025pu
X_d	1.8pu
X_q	1.7pu
X_l	0.2pu
X_d'	0.3 pu
X_q'	0.55 pu
X_d''	0.25 pu
X_q''	0.25 pu
T_{d0}'	8.0s
T_{q0}'	0.4s
T_{d0}''	0.03s
T_{q0}''	0.05s
H	6.5s
Rating Power	900MVA
V_{rms}	20kV
f_n	60Hz

The AC line parameters:

Positive-sequence		Zero-sequence	
r_1	x_1	r_0	x_0
0.053Ω/km	0.531 Ω/km	1.638 Ω/km	2.312 Ω/km

The HVDC link parameters:

Rated Power	200MW
Rated Voltage	56 kV
Rated Current	3.6 kA
AC side voltage	230 kV
Commutating Reactance	0.57 Ω
Reactive Power Support	125 MVAr

The DC line parameters:

DC line resistance	1.5 Ω
DC line inductance	100 mH
Smoothing Reactor	50 mH

Appendix.B

Testing distance relay in a simple AC system

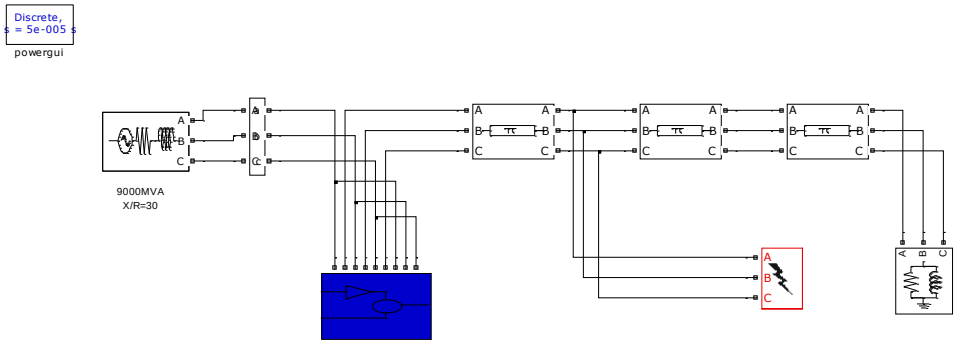

The AC line parameters:

Positive-sequence		Zero-sequence	
r_1	x_1	r_0	x_0
0.053Ω/km	0.531 Ω/km	1.638 Ω/km	2.312 Ω/km

The distance relay settings:

Zone1	1.87 Ω + j18.73 Ω
Zone2	2.8 Ω + j28.1 Ω
Zone3	5.84 Ω + j58.54 Ω

Appendix.C

C.1 B-G Fault at 50 km

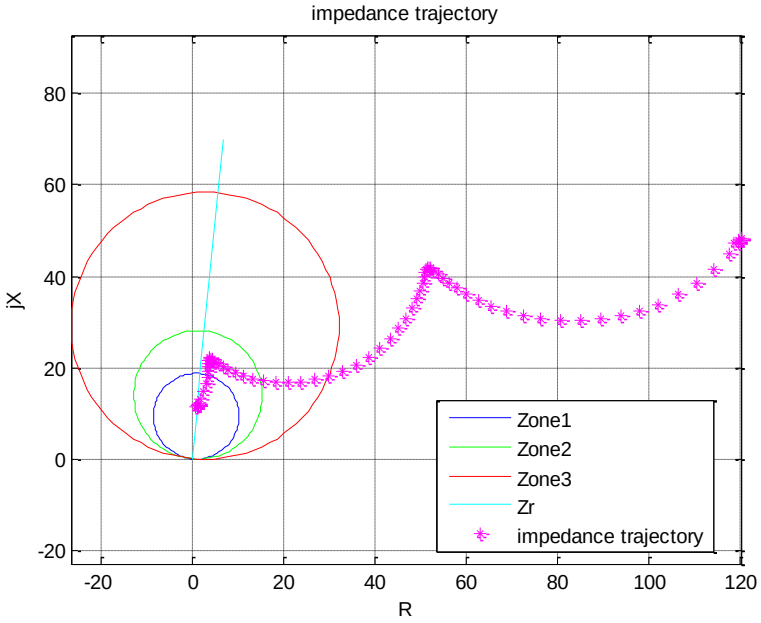

Figure. C-1 The B-G fault impedance trajectory

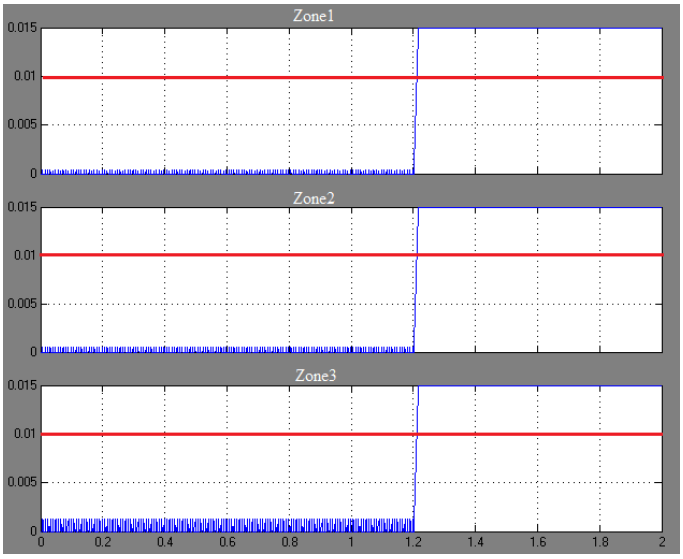

Figure. C-2 B-Gblock-average comparator output

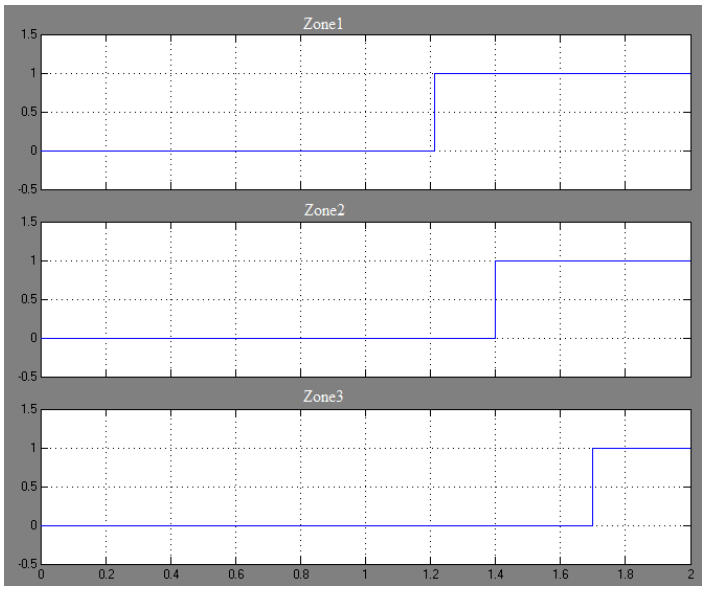

Figure. C-3 Distance relay trip signal

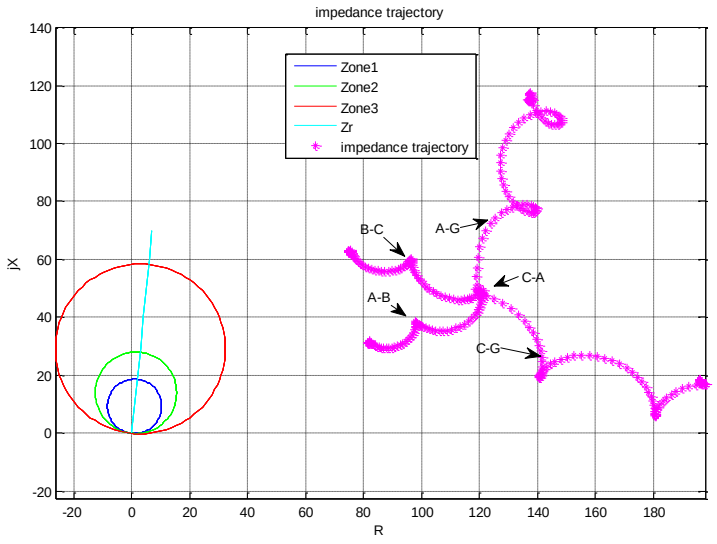

Figure. C-4 A-G, C-G, A-B, B-A, C-A fault impedance trajectories

C.2 C-G Fault at 50km

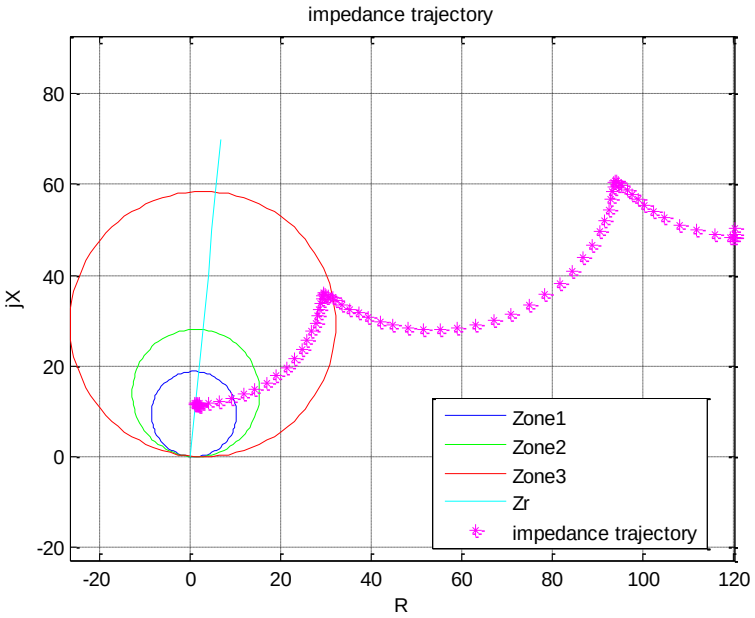

Figure. C-5 C-G fault impedance trajectory

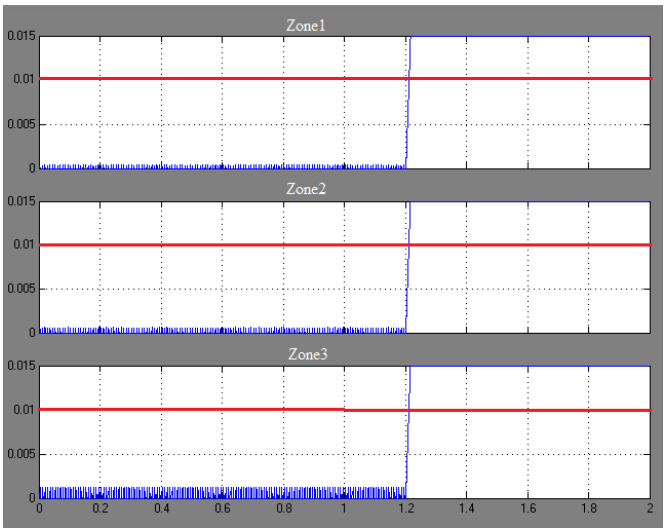

Figure. C-6 C-G block-average comparator output

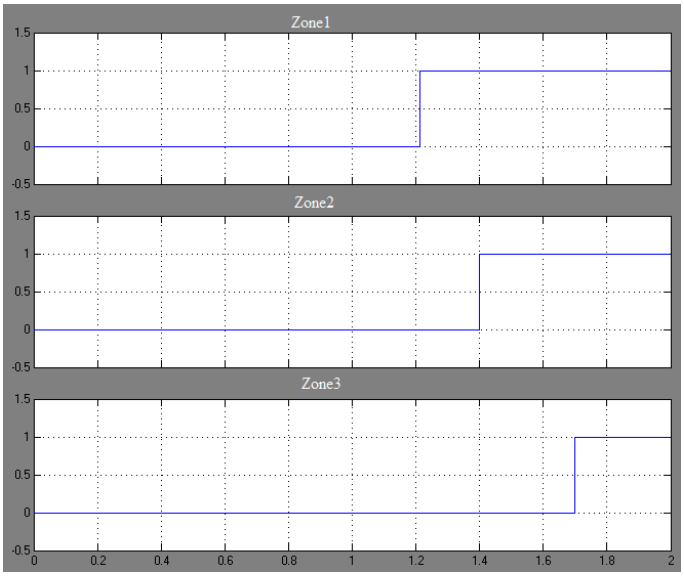

Figure. C-7 Distance relay trip signal

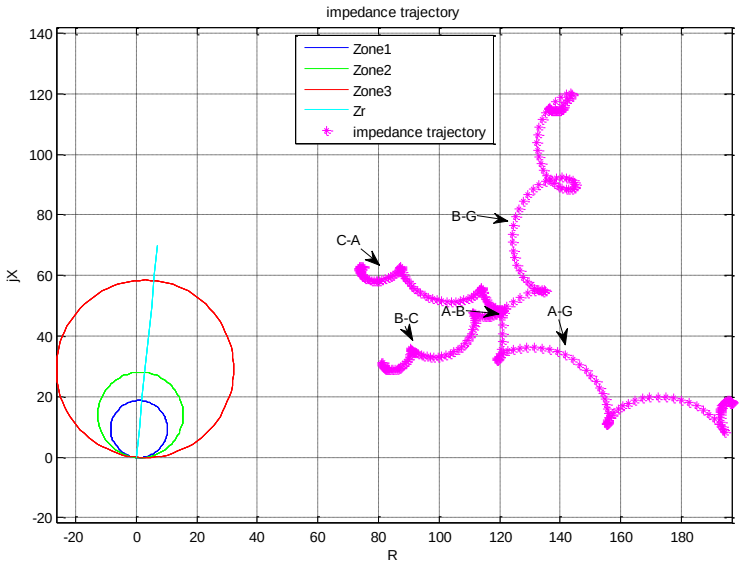

Figure. C-8 A-G, B-G, A-B, B-C, C-A impedance trajectories

C.3 B-C Fault at 50km

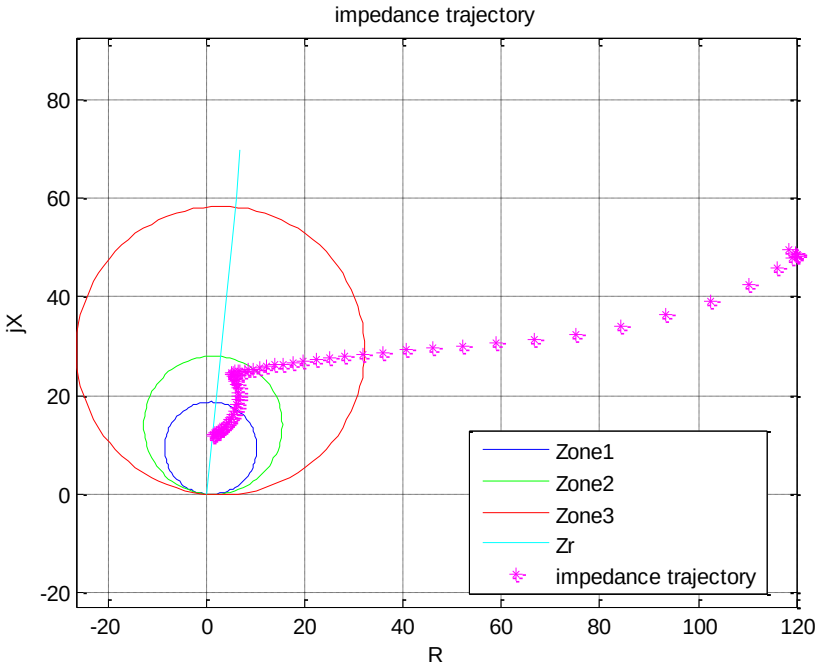

Figure. C-9 B-C fault impedance trajectory

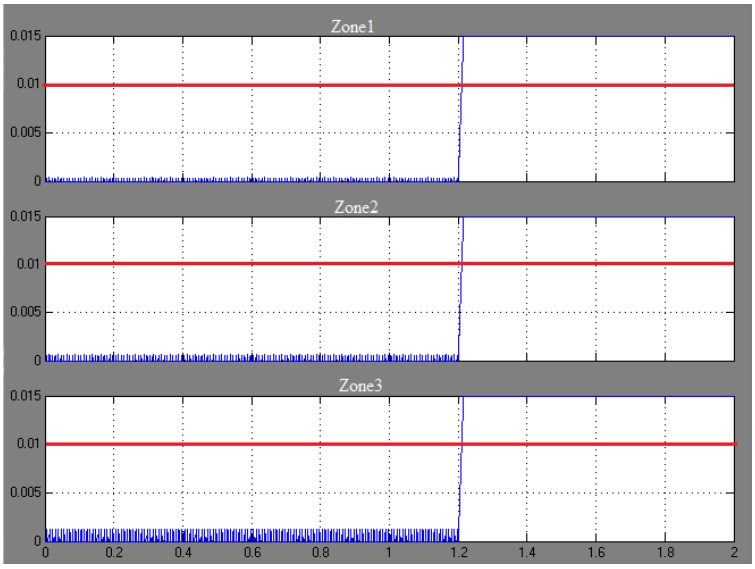

Figure. C-10 B-C block-average comparator output

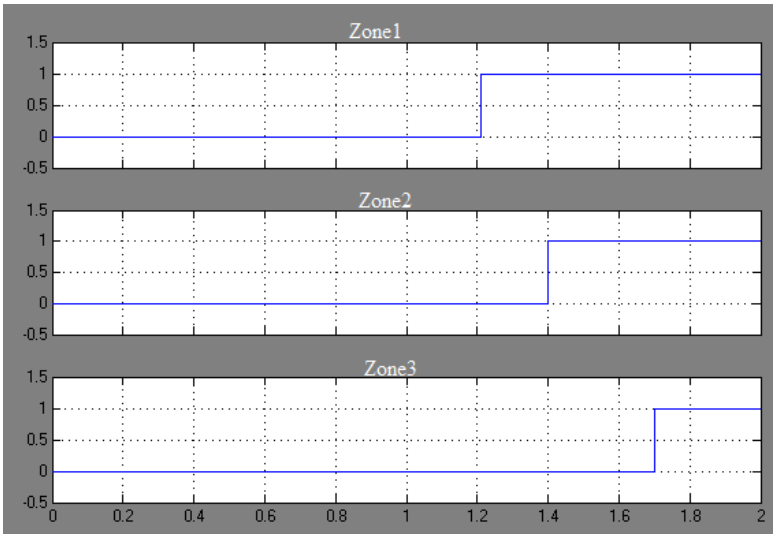

Figure. C-11 Distance relay trip signal

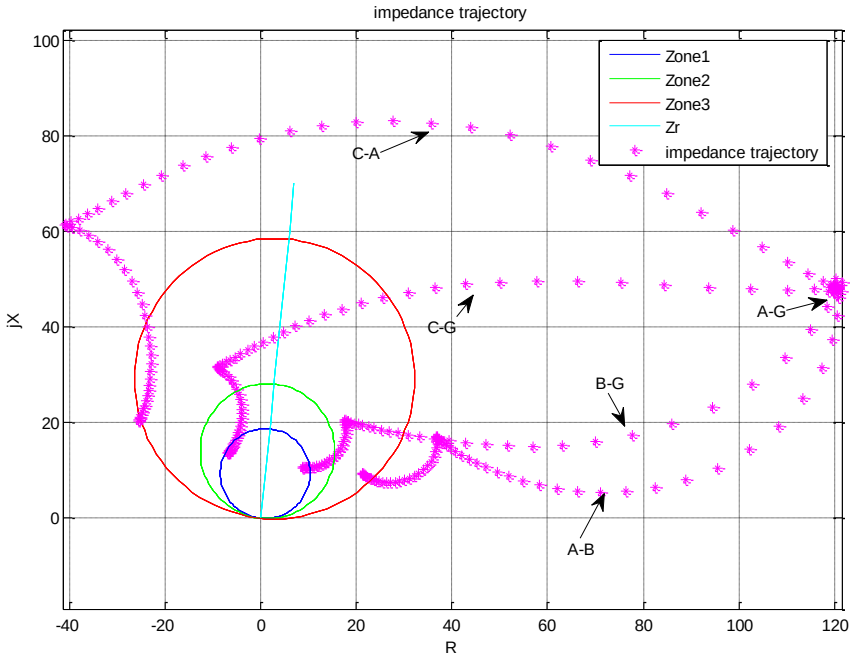

Figure. C-12 A-G, B-G, C-G, A-B, C-A impedance trajectories

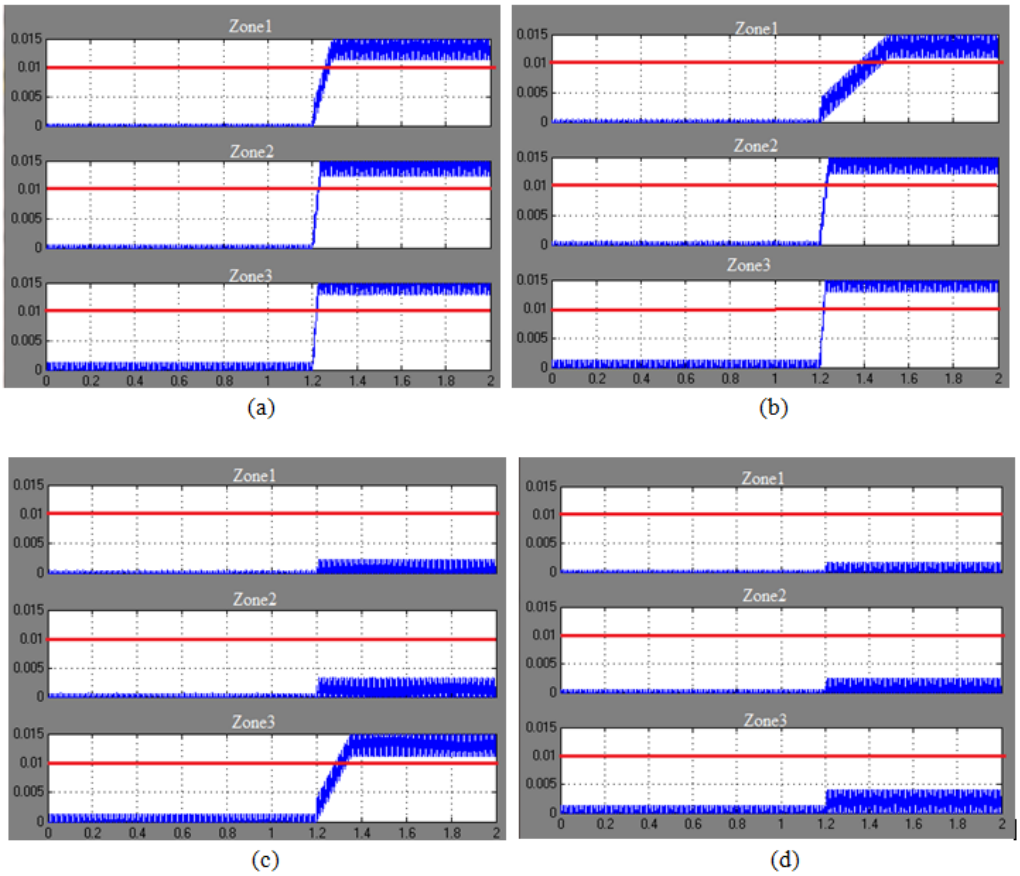

Figure. C-13 Block-average comparator outputs

(a) B-G block-average comparator output

(b) C-G block-average comparator output

(c) A-B block-average comparator output

(d) C-Ablock-average comparator output

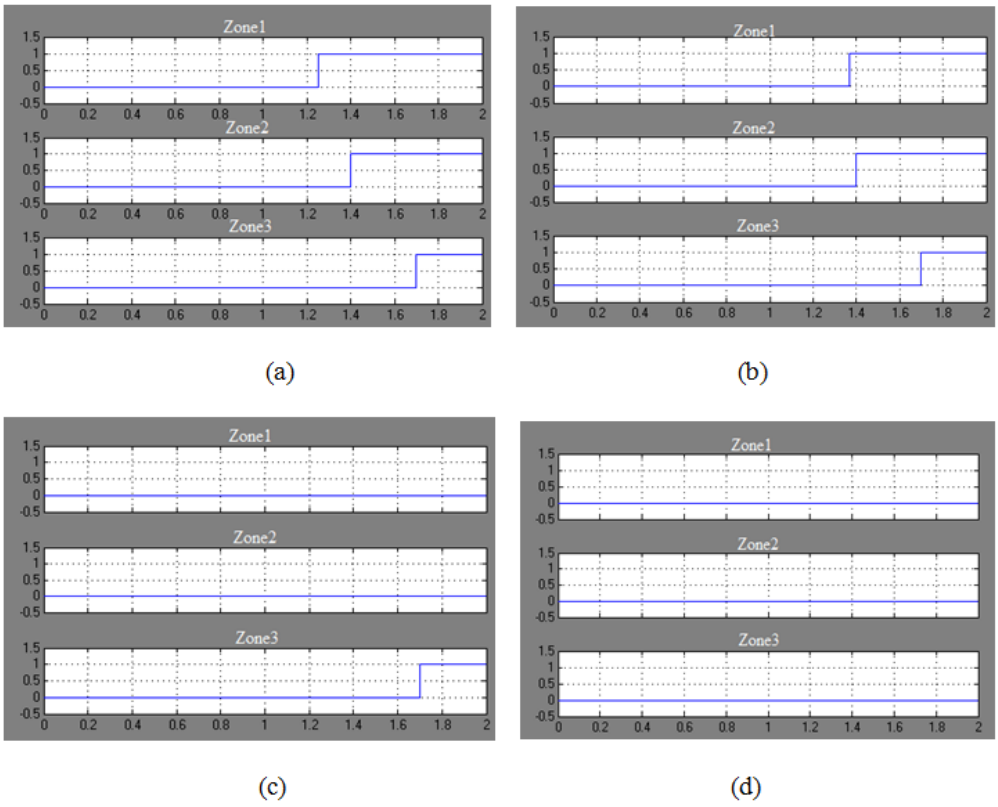

Figure. C-14 Distance relay trip signals

(a) B-G relay trip signals

(b) C-Grelay trip signals

(c) A-Brelay trip signals

(d) C-Arelay trip signals

C.4 C-A Fault at 50km

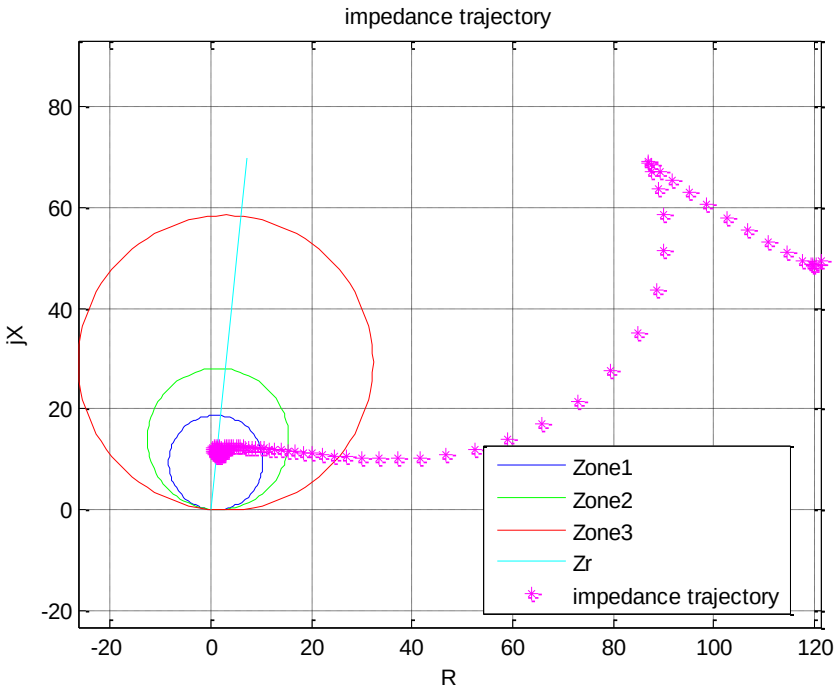

Figure. C-15 C-A fault impedance trajectory

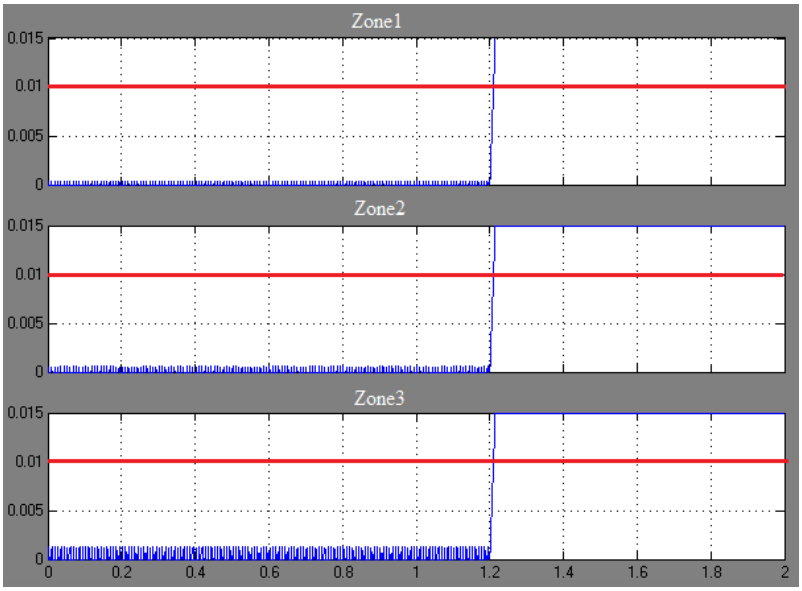

Figure. C-16 C-Ablock-average comparator output

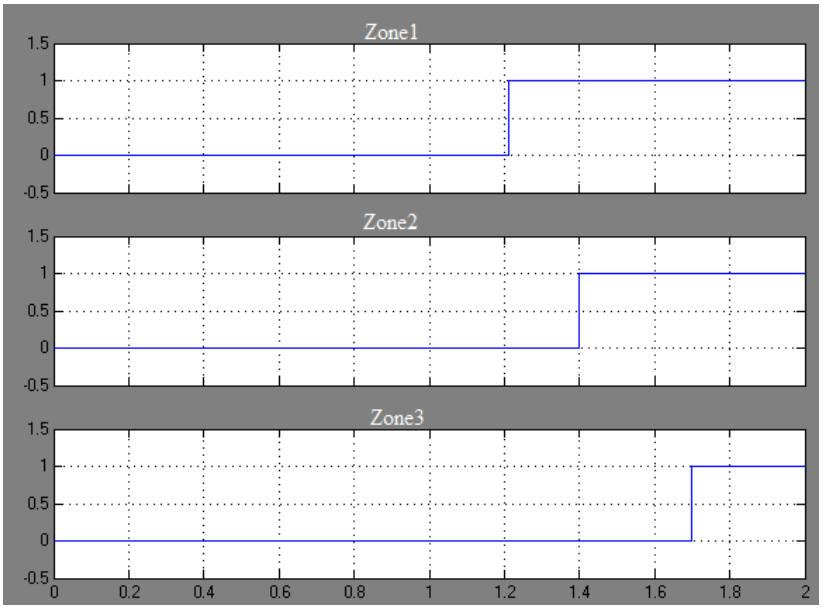

Figure. C-17 Distance relay trip signal

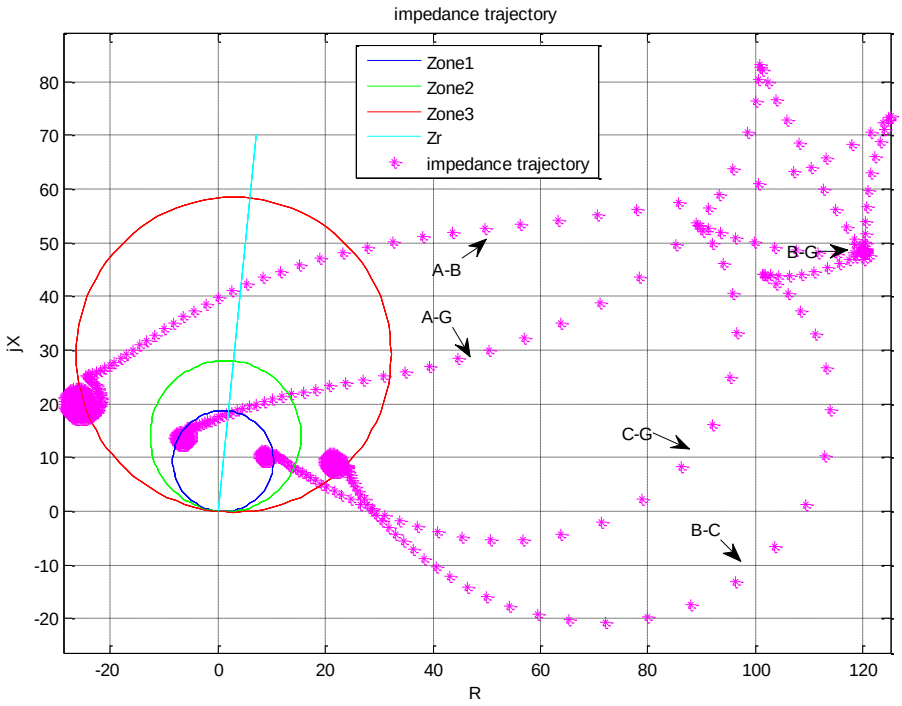

Figure. C-18 A-G, B-G, C-G, A-B, B-C impedance trajectories

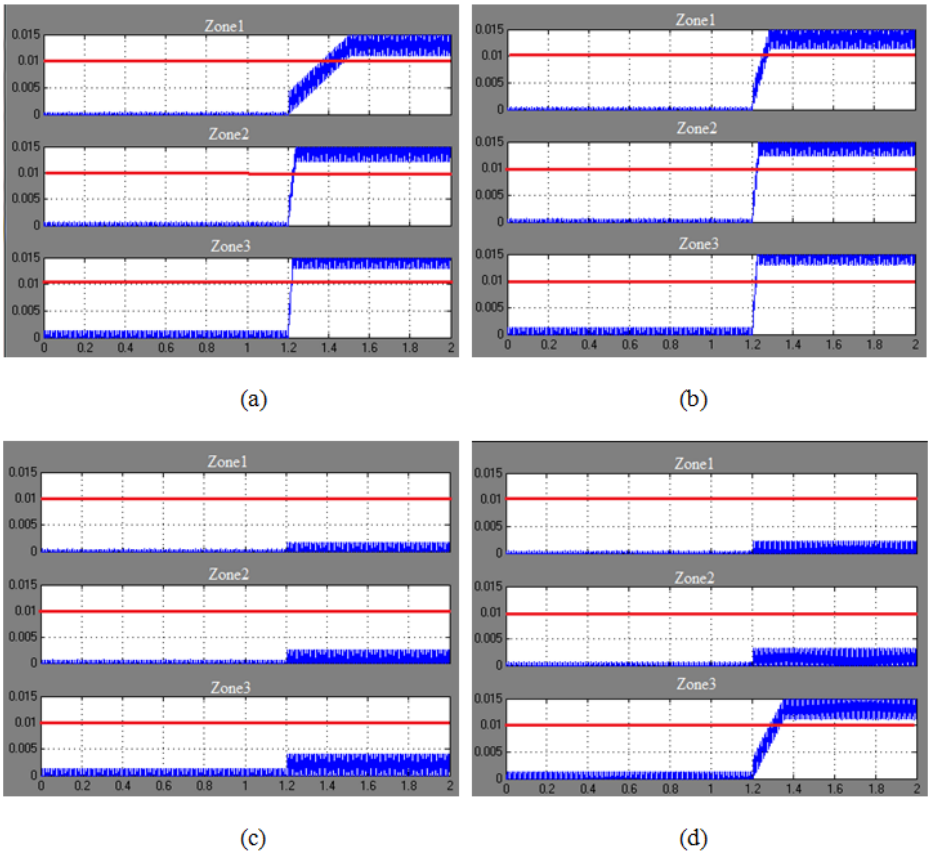

Figure. C-19 Block-average comparator outputs

(a) A-G block-average comparator output

(b) C-Gblock-average comparator output

(c) A-B block-average comparator output

(d) B-Cblock-average comparator output

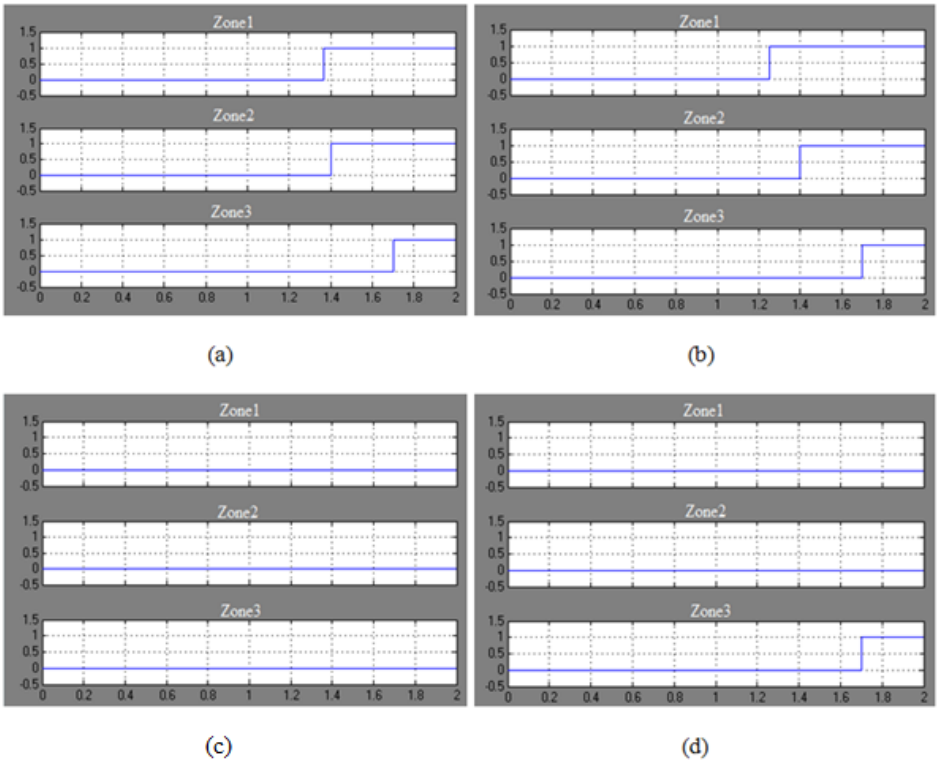

Figure. C-20 Distance relay trip signals

(a) A-G relay trip signals

(b) C-G relay trip signals

(c) A-B relay trip signals

(d) B-Crelay trip signals

C.5 C-A-G Fault at 50km

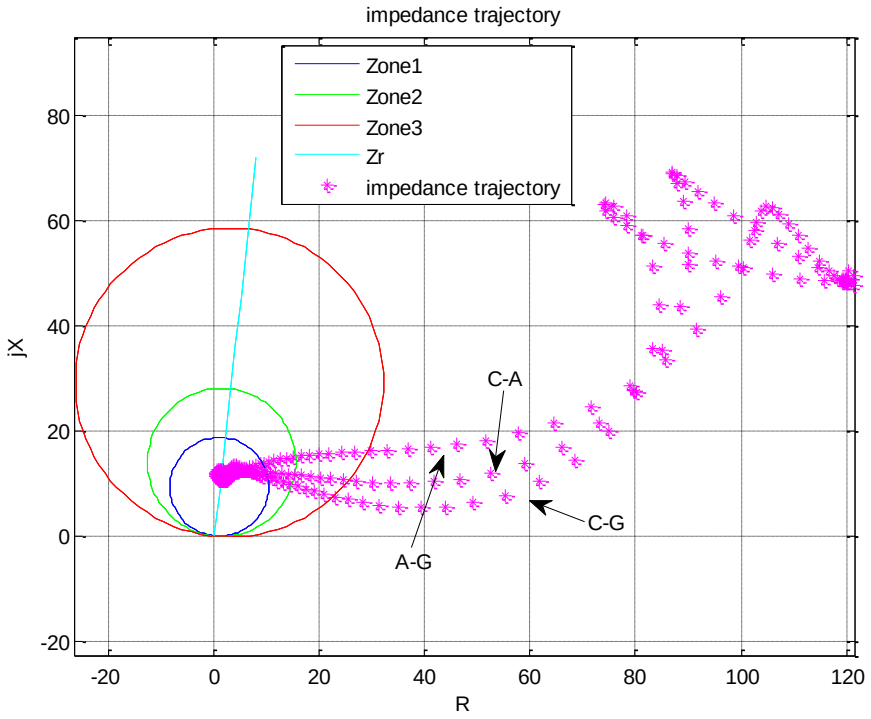

Figure. C-21 A-G, C-G, C-A fault impedance trajectories

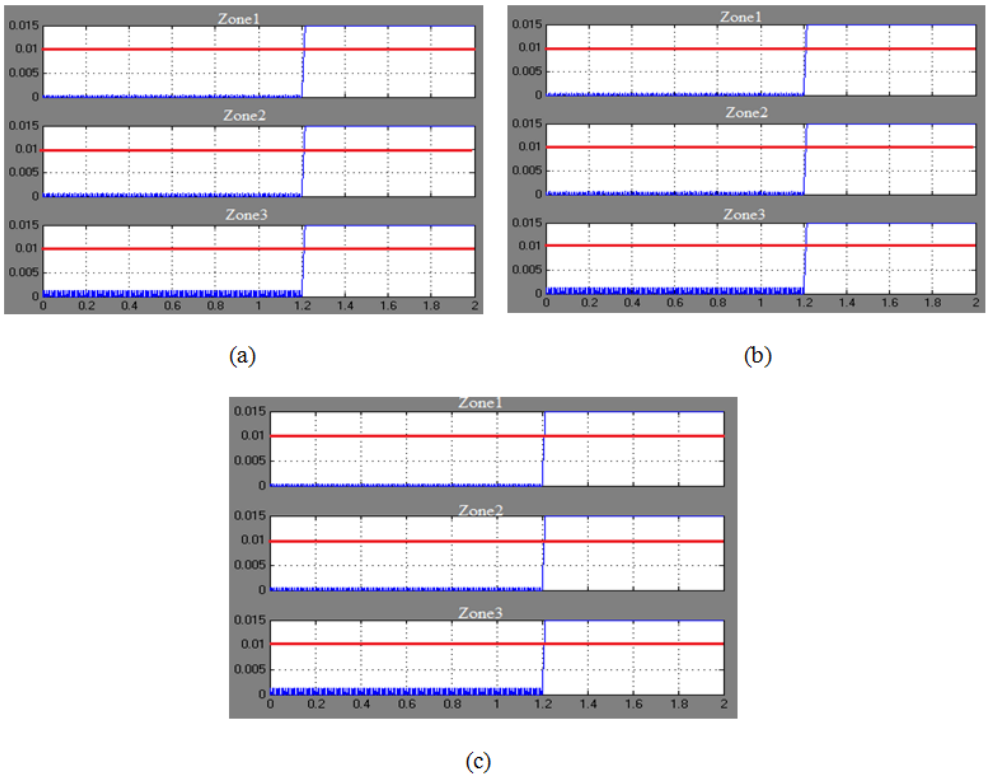

Figure. C-22Block-average comparator outputs

(a) A-G block-average comparator output

(b) C-G block-average comparator output

(c) C-Ablock-average comparator output

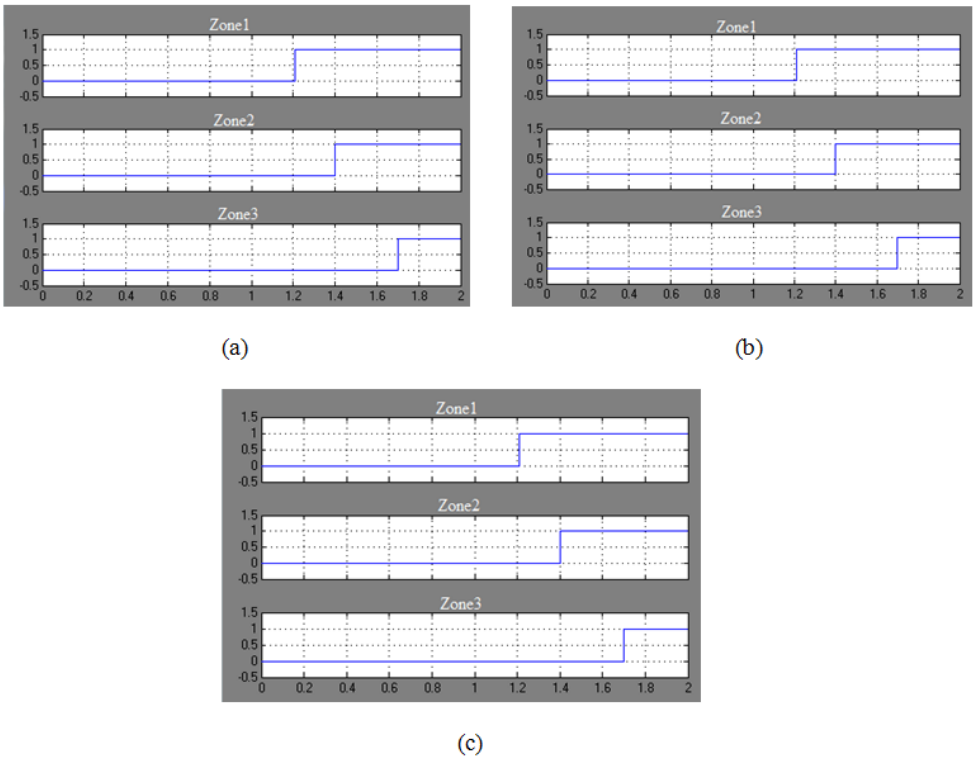

Figure. C-23Distance relay trip signals

(a) A-G relay trip signals

(b) C-G relay trip signals

(c) C-Arelay trip signals

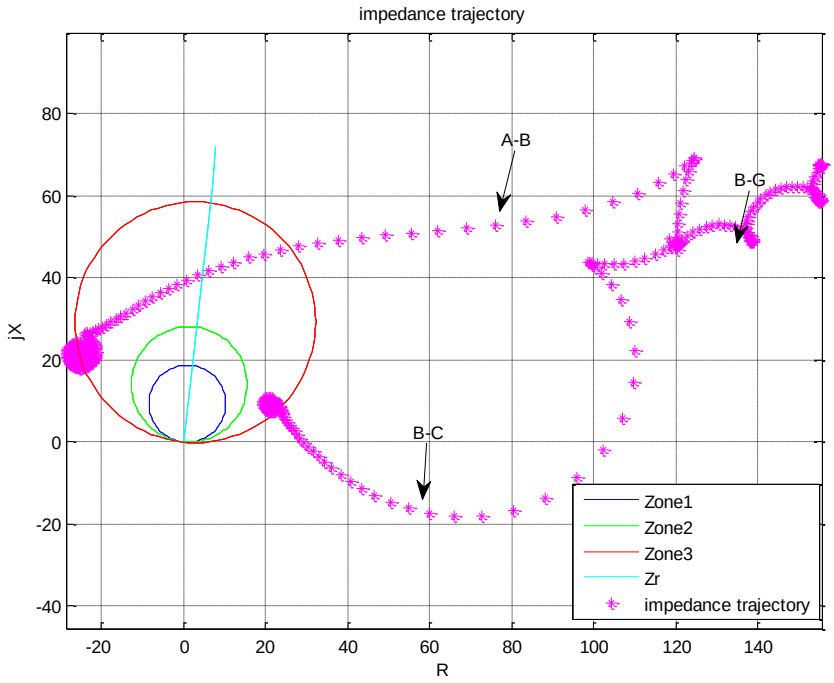

Figure. C-24 B-G, A-B, B-C fault impedance trajectories

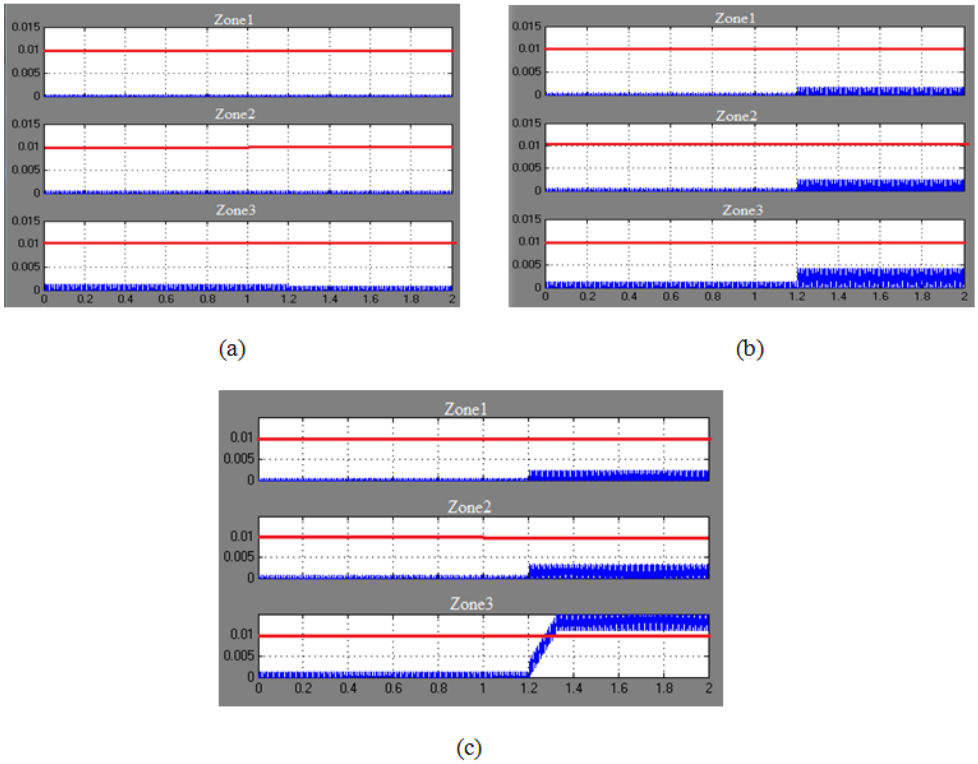

Figure. C-25 Block-average comparator outputs

(a) B-G block-average comparator output

(b) A-B block-average comparator output

(c) B-Cblock-average comparator output

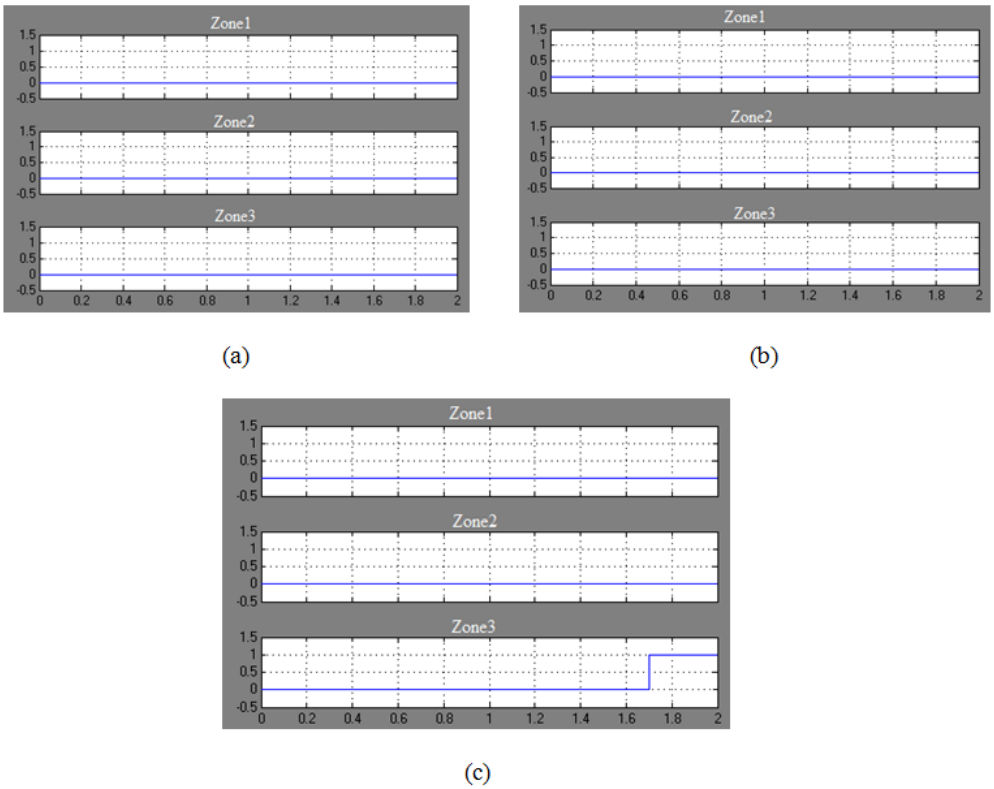

Figure. C-26 Distance relay trip signals

(a) B-G relay trip signals

(b) A-B relay trip signals

(c) B-Crelay trip signals

C.6 A-B-G Fault at 50km

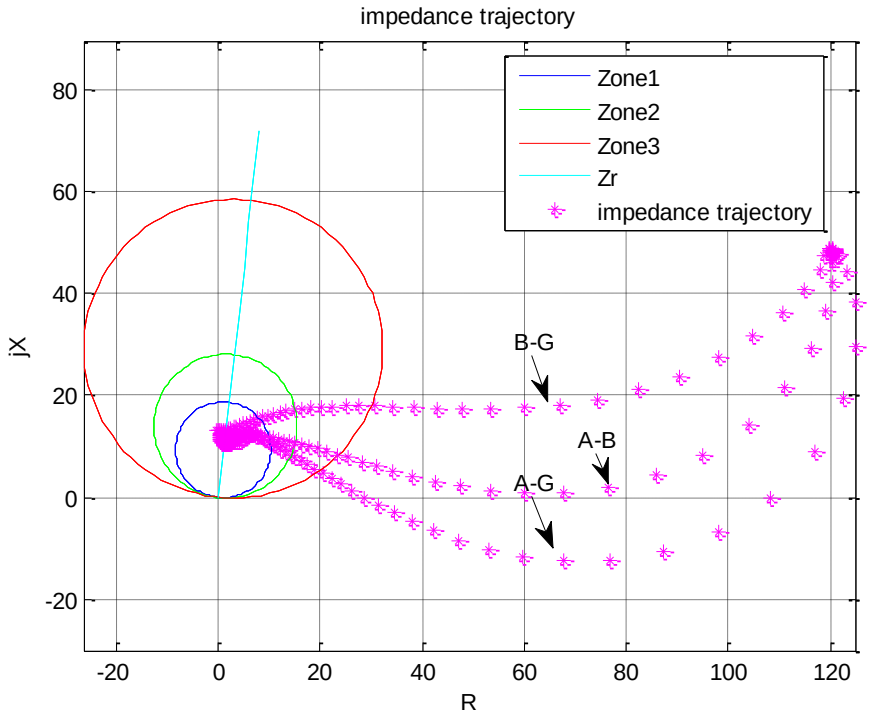

Figure. C-27 A-G, B-G, A-B fault impedance trajectories

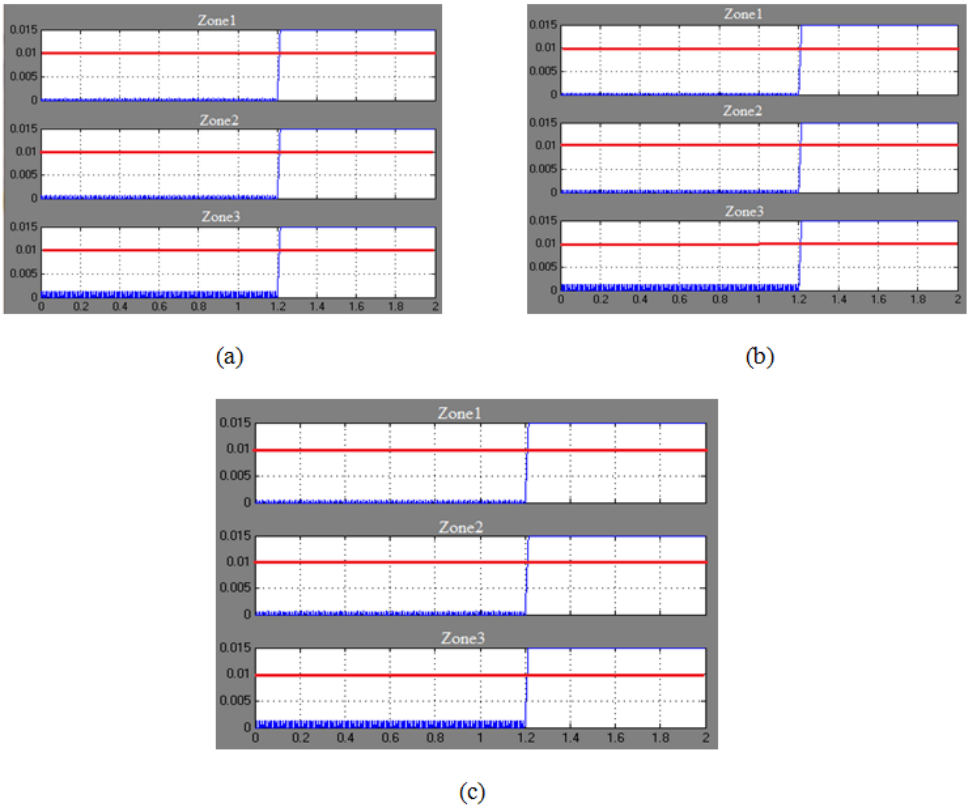

Figure. C-28 Block-average comparator outputs

(a) A-G block-average comparator output

(b) B-G block-average comparator output

(c) A-Bblock-average comparator output

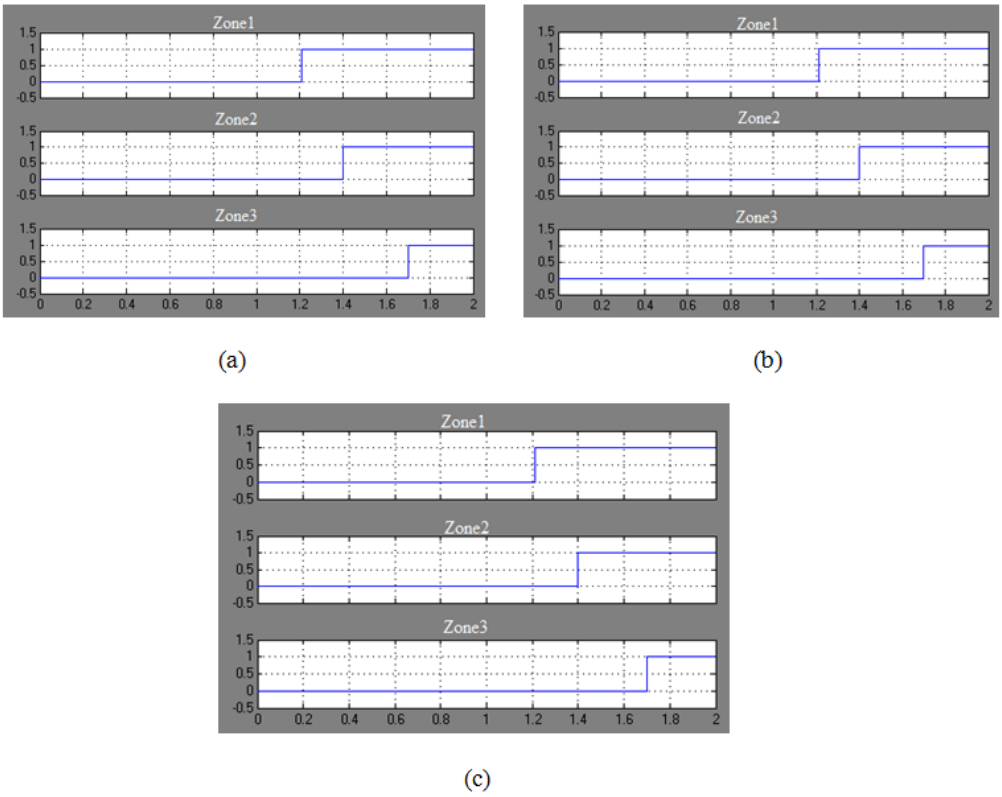

Figure. C-29 Distance relay trip signals

(a) A-G relay trip signals

(b) B-G relay trip signals

(c) A-Brelay trip signals

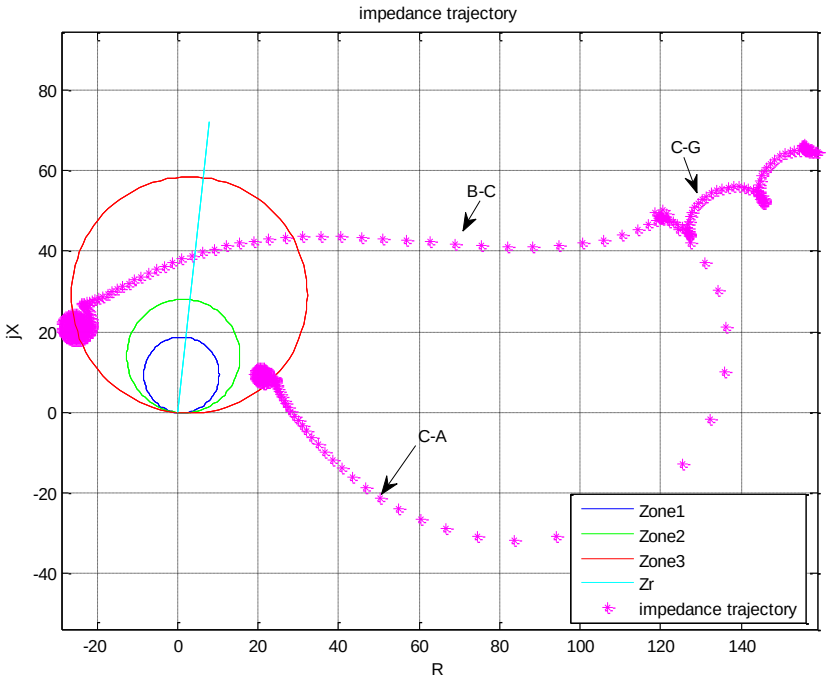

Figure. C-30 C-G, B-C, C-A fault impedance trajectories

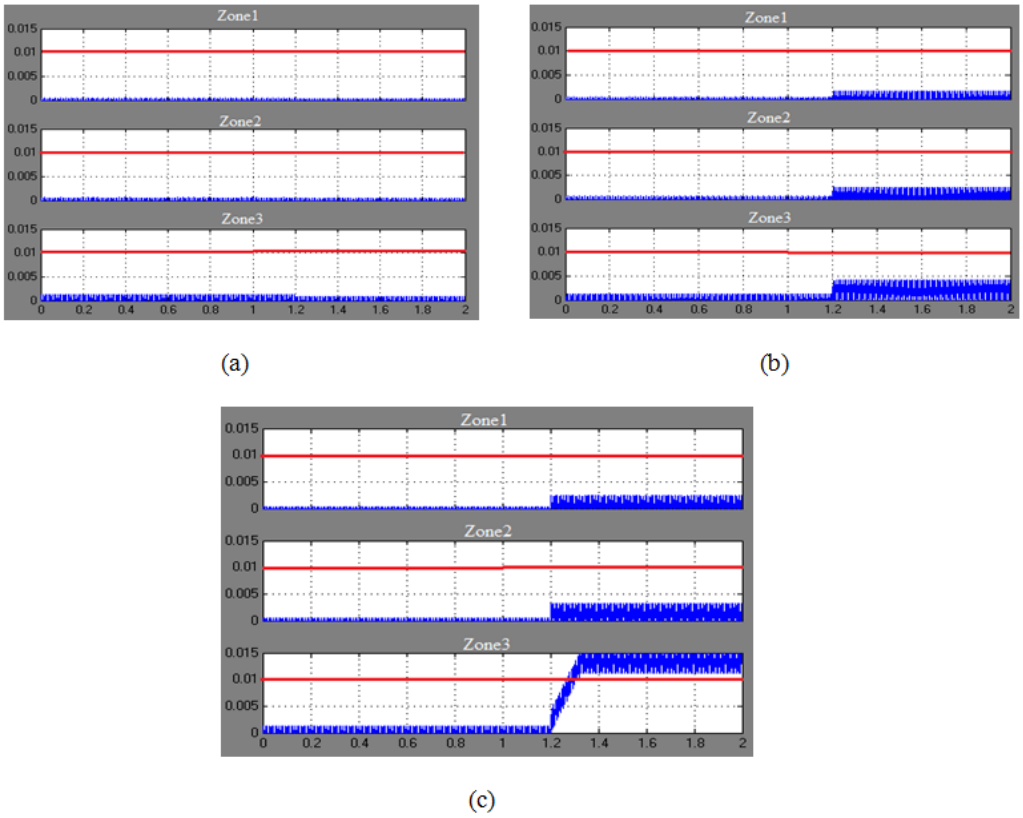

Figure. C-31 Block-average comparator outputs

(a) C-G block-average comparator output

(b) B-C block-average comparator output

(c) C-Ablock-average comparator output

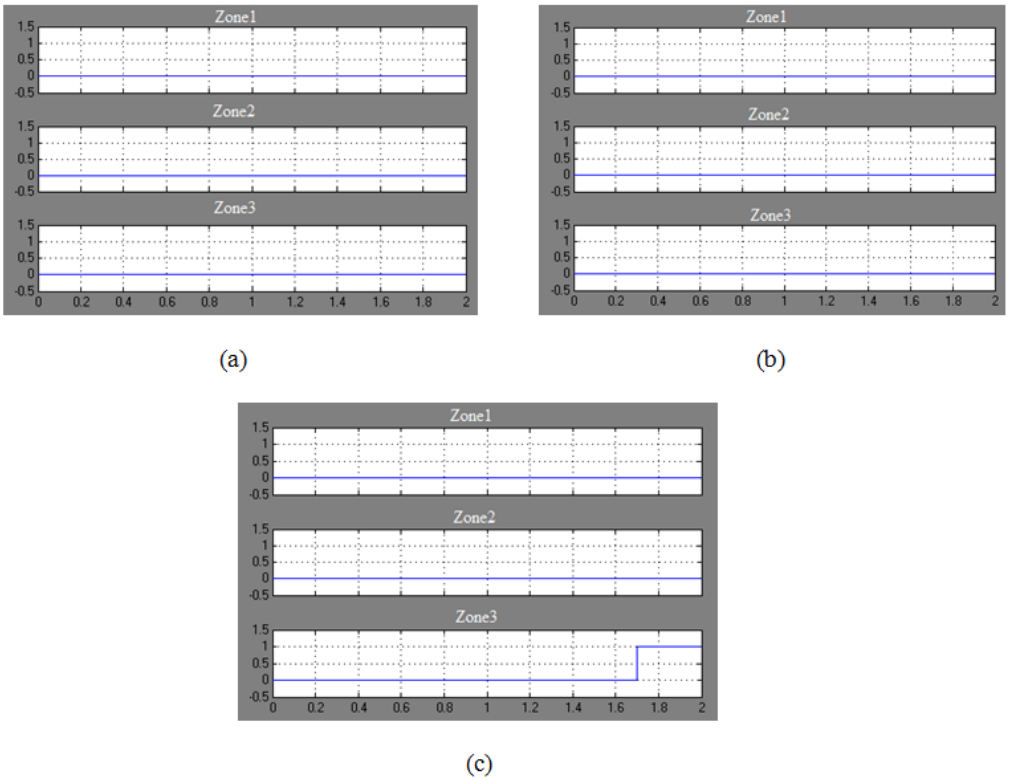

Figure. C-32 Distance relay trip signals

(a) C-G relay trip signals

(b) B-C relay trip signals

(c) C-Arelay trip signals

Appendix.D

D.1 B-G Fault at 100km

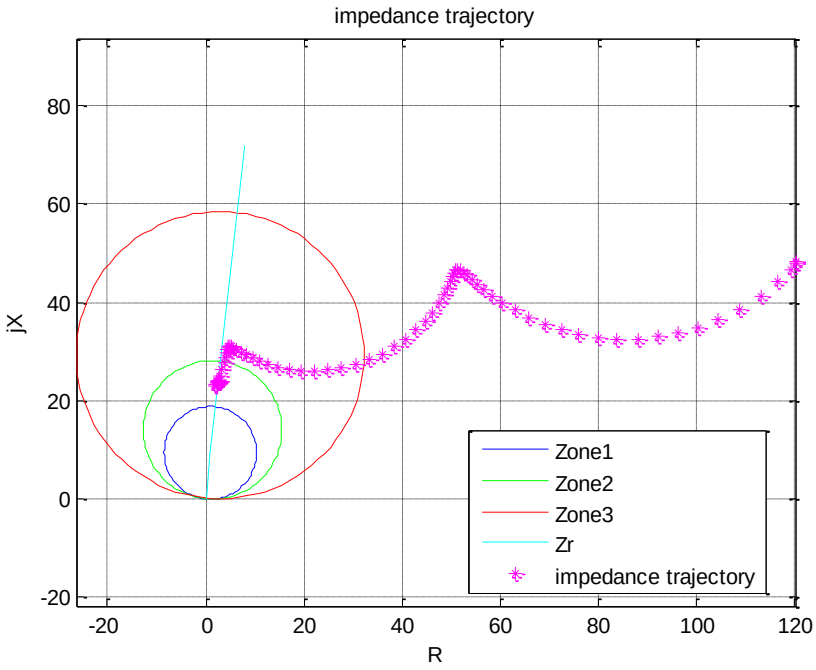

Figure. D-1 B-G fault impedance trajectory

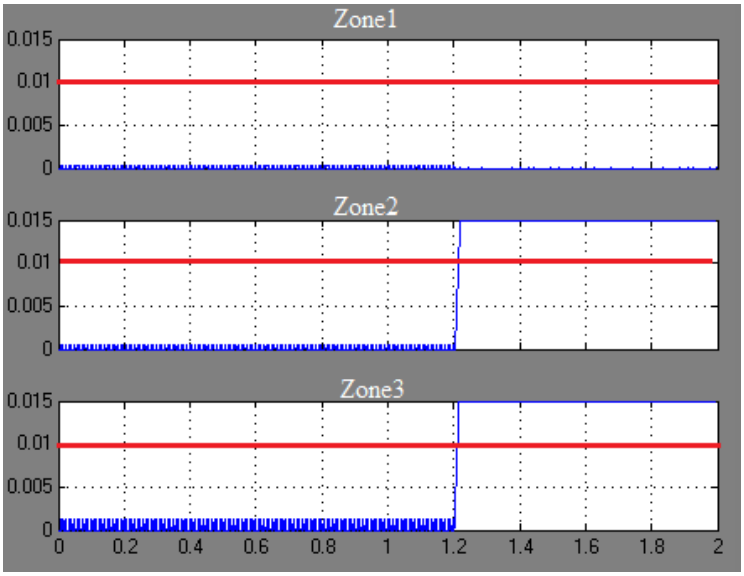

Figure. D-2 B-GBlock-average comparator output

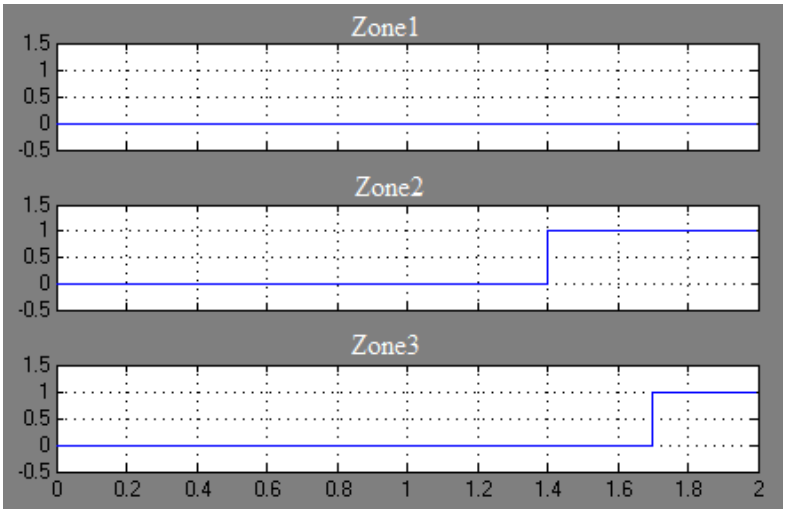

Figure. D-3Distance relay trip signals

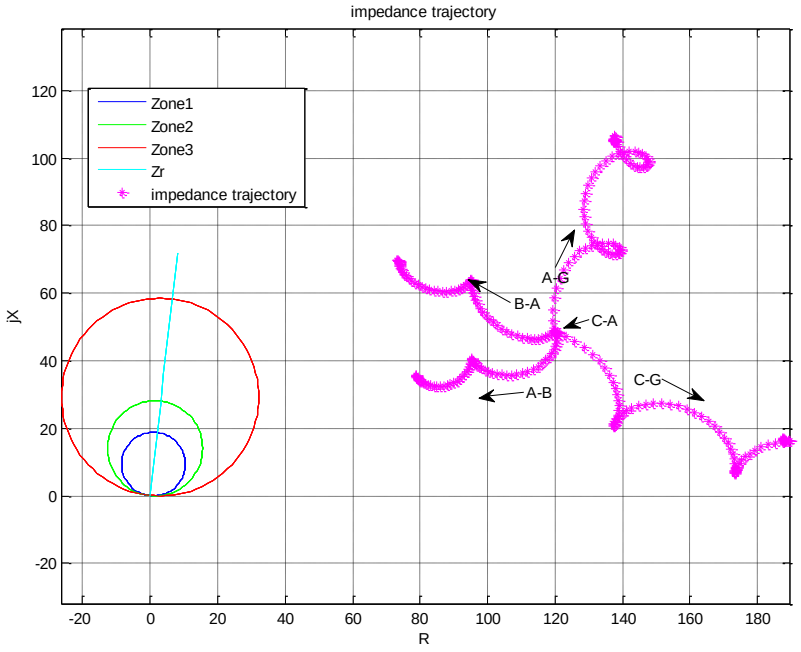

Figure. D-4 A-G, C-G, A-B, B-C, C-A impedance trajectories

D.2 C-G Fault at 100km

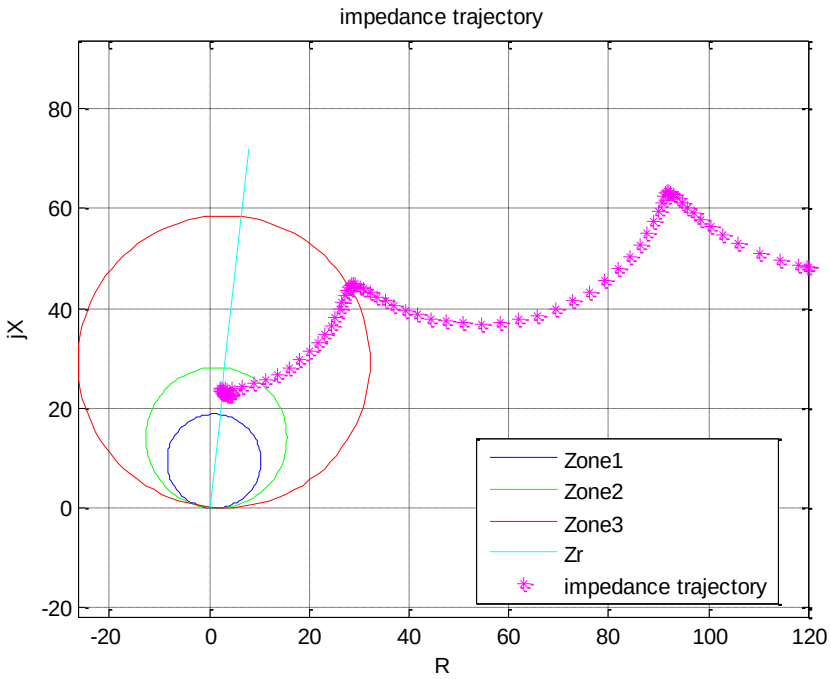

Figure. D-5 C-G fault impedance trajectory

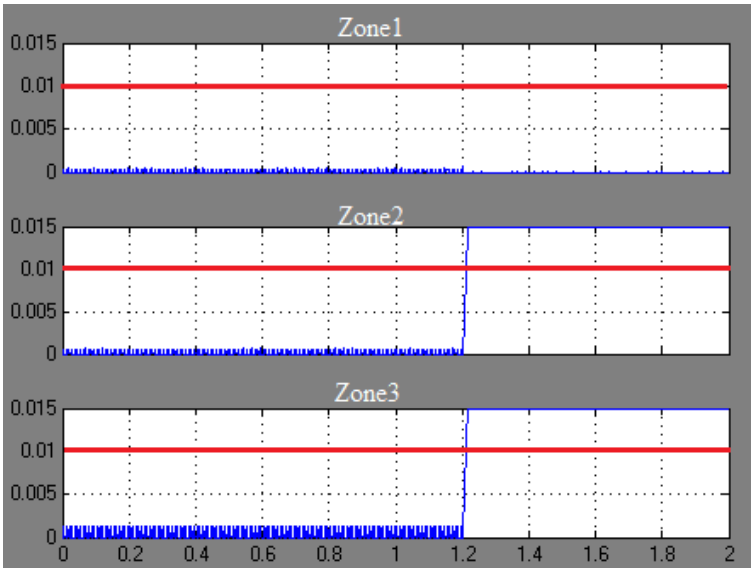

Figure. D-6 C-G Block-average comparator output

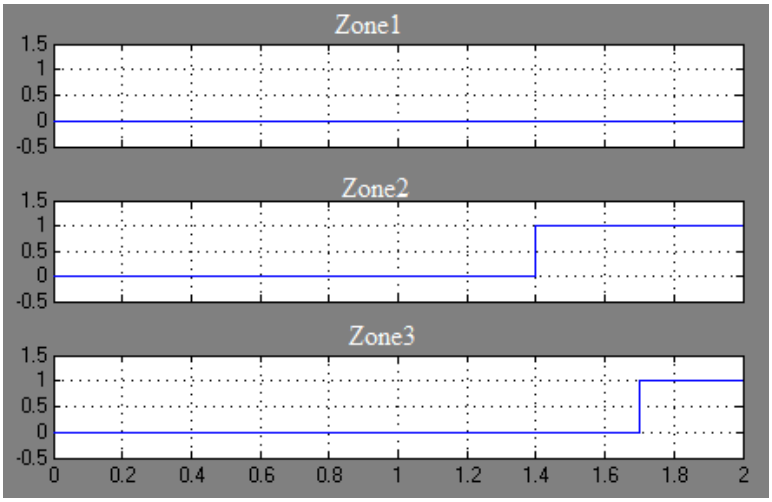

Figure. D-7 Distance relay trip Signals

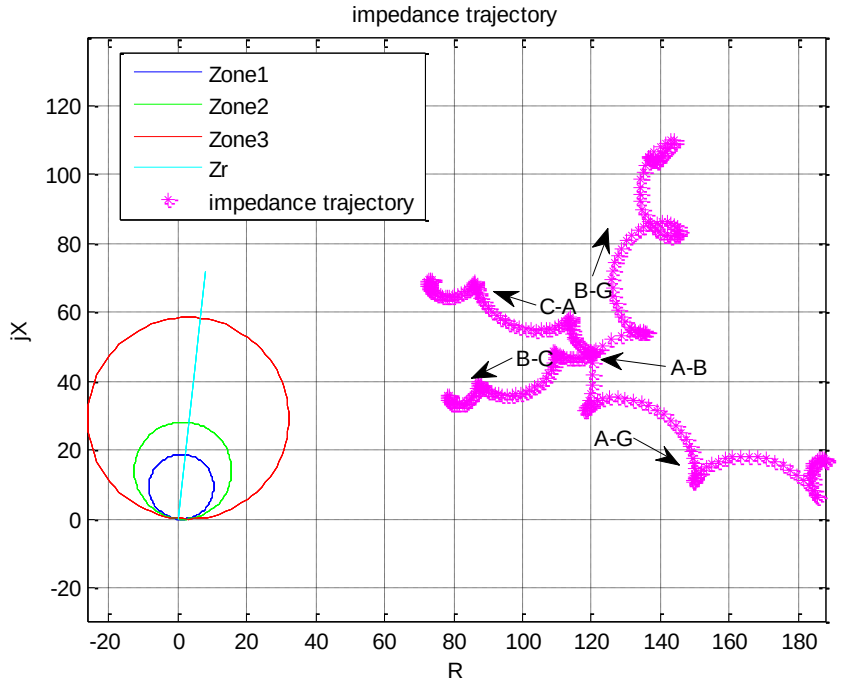

Figure. D-8 A-G, B-G, A-B, B-C, C-A impedance trajectories

D.3 B-C Fault at 100km

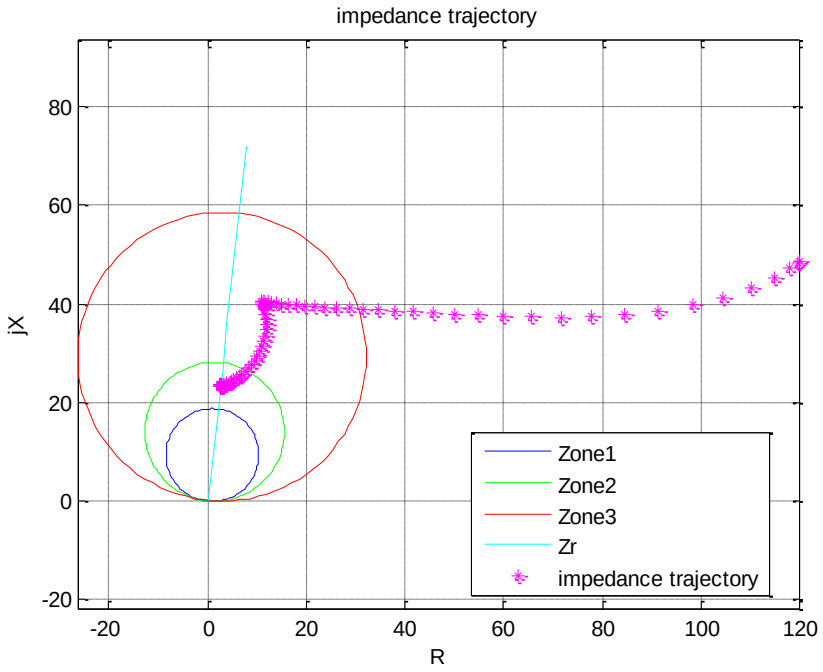

Figure. D-9 B-Cfault impedance trajectory

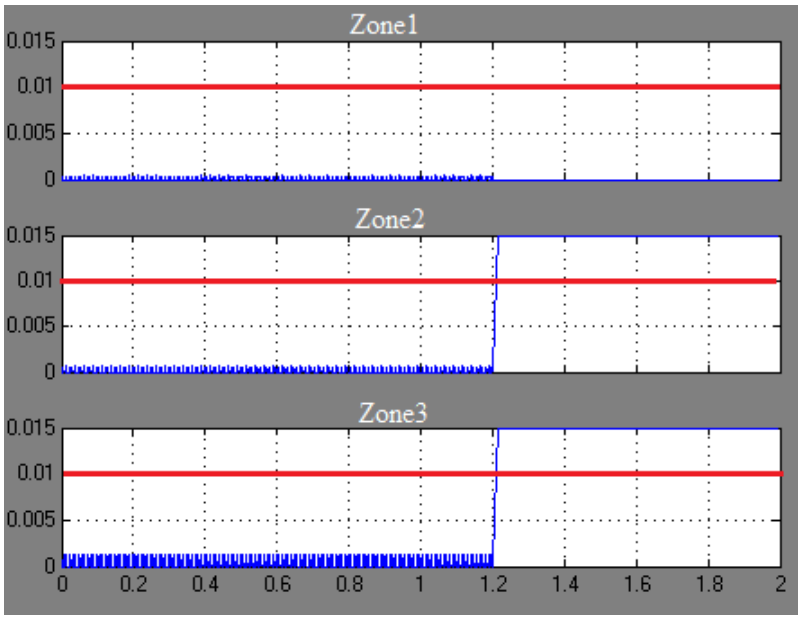

Figure. D-10 B-C block-average comparator output

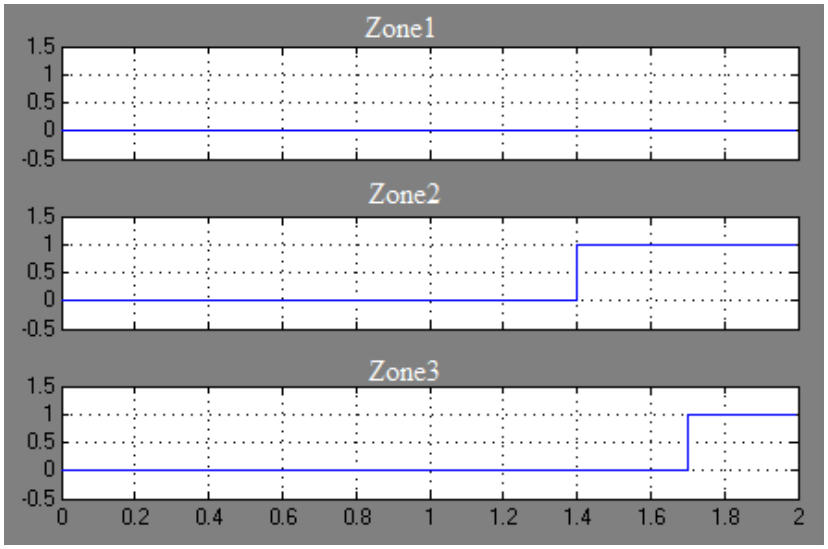

Figure. D-11 Distance relay trip signals

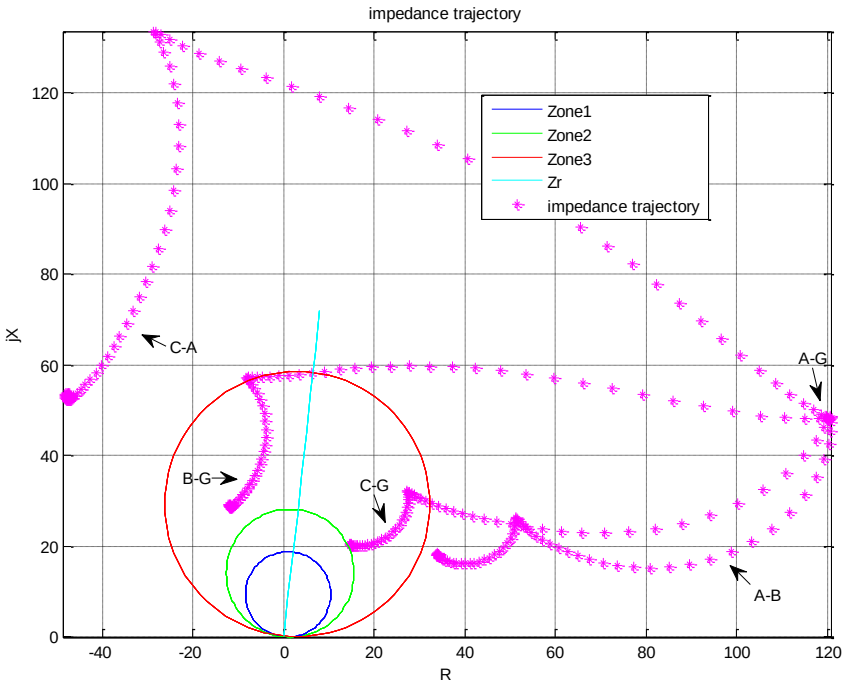

Figure. D-12 A-G, B-G, C-G, A-B, C-A fault impedance trajectories

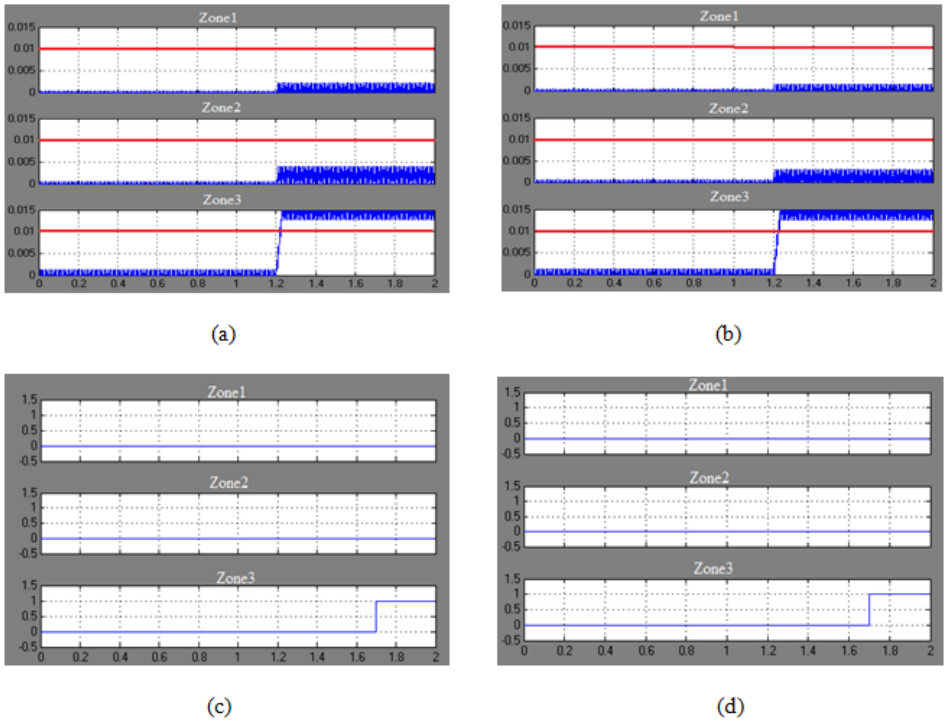

Figure. D-13 Block-average comparator outputs and distance relay trip signals

(a) B-G Block-average comparator outputs

(b) C-GBlock-average comparator outputs

(c) B-G Distance relay trip signals

(d) C-G Distance relay trip signals

D.4 C-A Fault at 100km

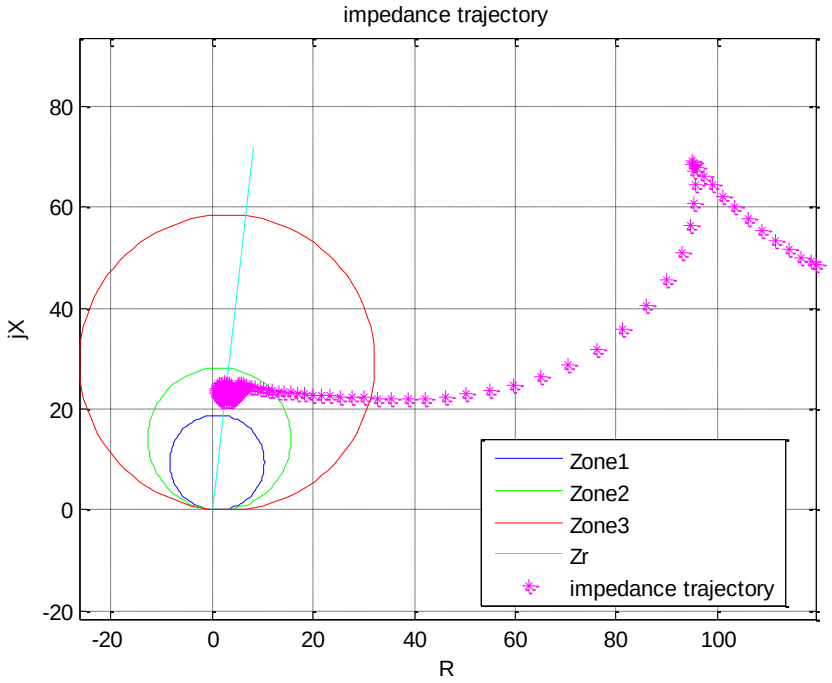

Figure. D-14 C-Afault impedance trajectory

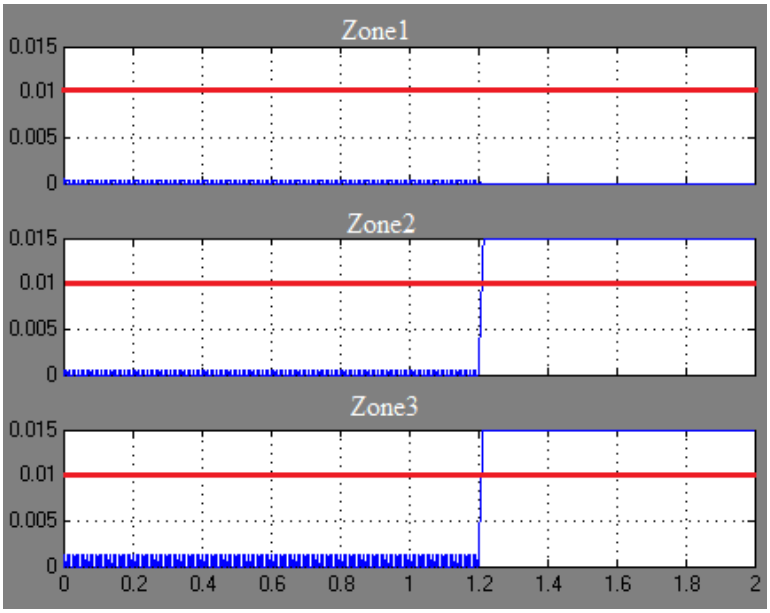

Figure. D-15 C-ABlock-average comparator output

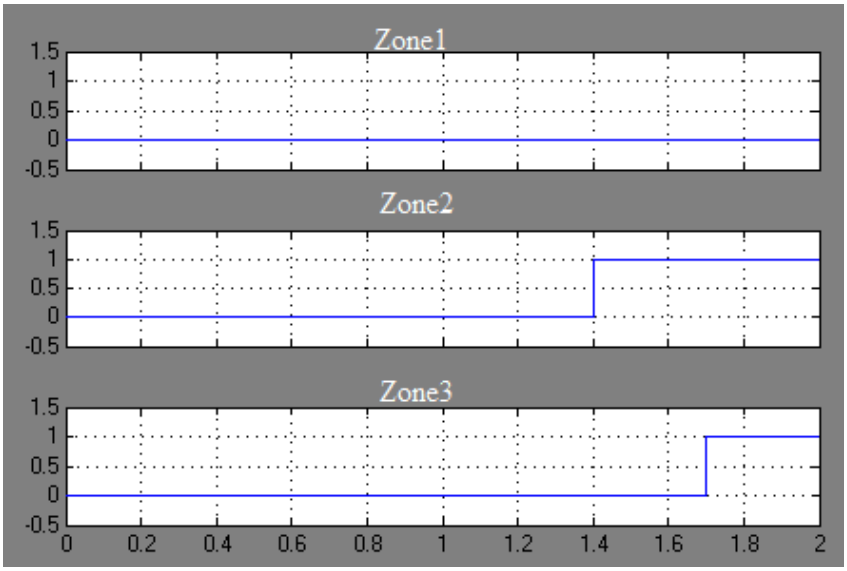

Figure. D-16 C-ADistance relay trip signals

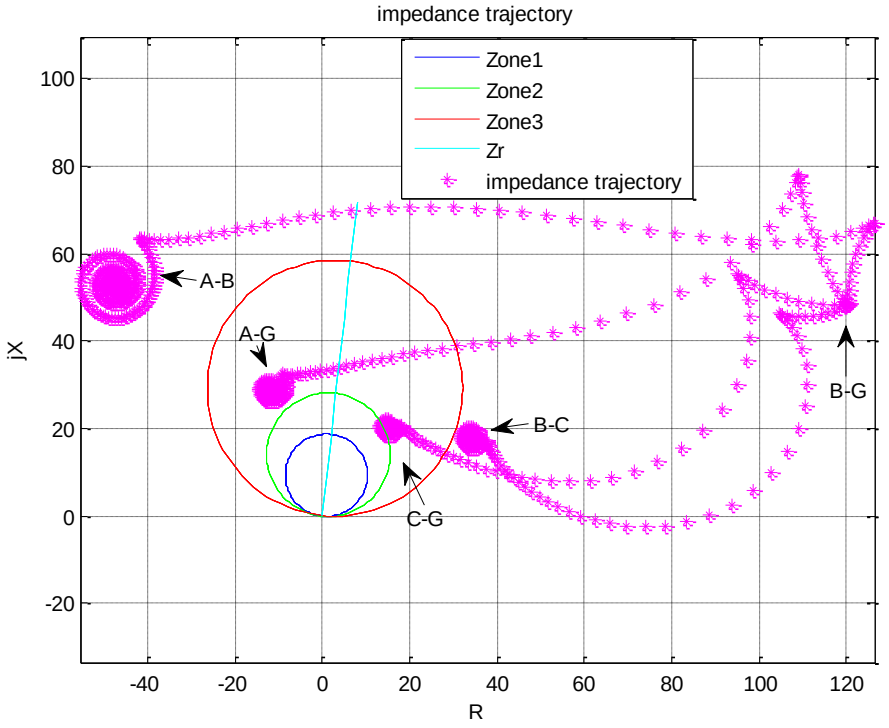

Figure. D-17 A-G, B-G, C-G, A-B, B-C fault impedance trajectories

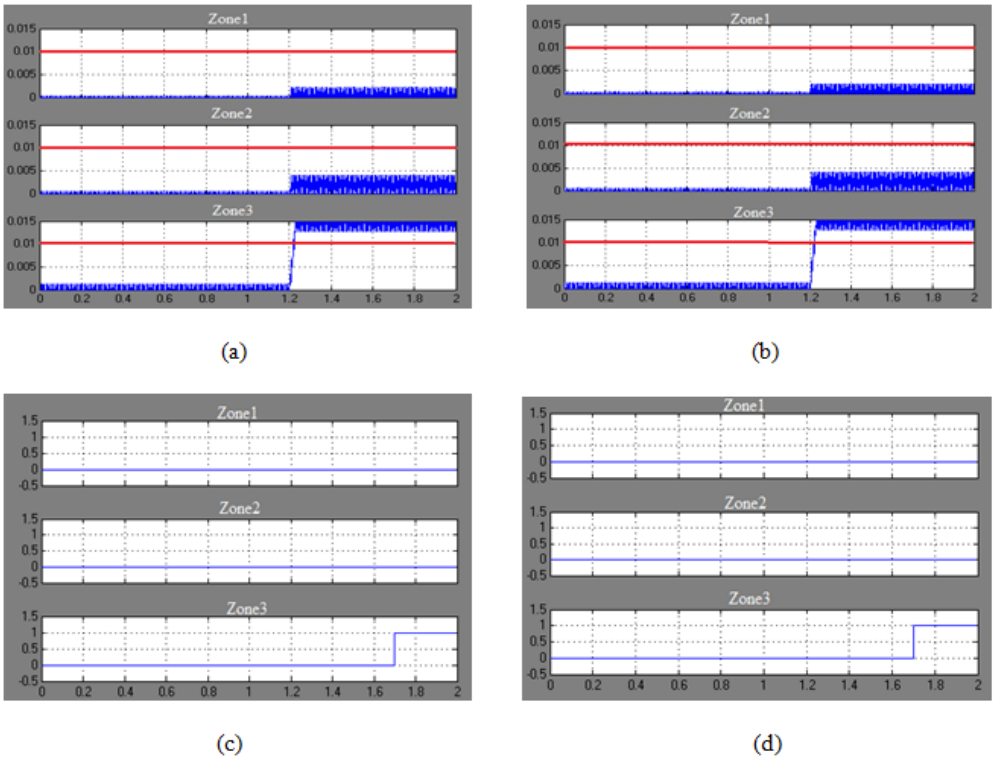

Figure. D-18 Block-average comparator outputs and distance relay trip signals

(a) A-G Block-average comparator outputs

(b) C-GBlock-average comparator outputs

(c) A-G Distance relay trip signals

(d) C-G Distance relay trip signals

D.5 A-B-G Fault at 100km

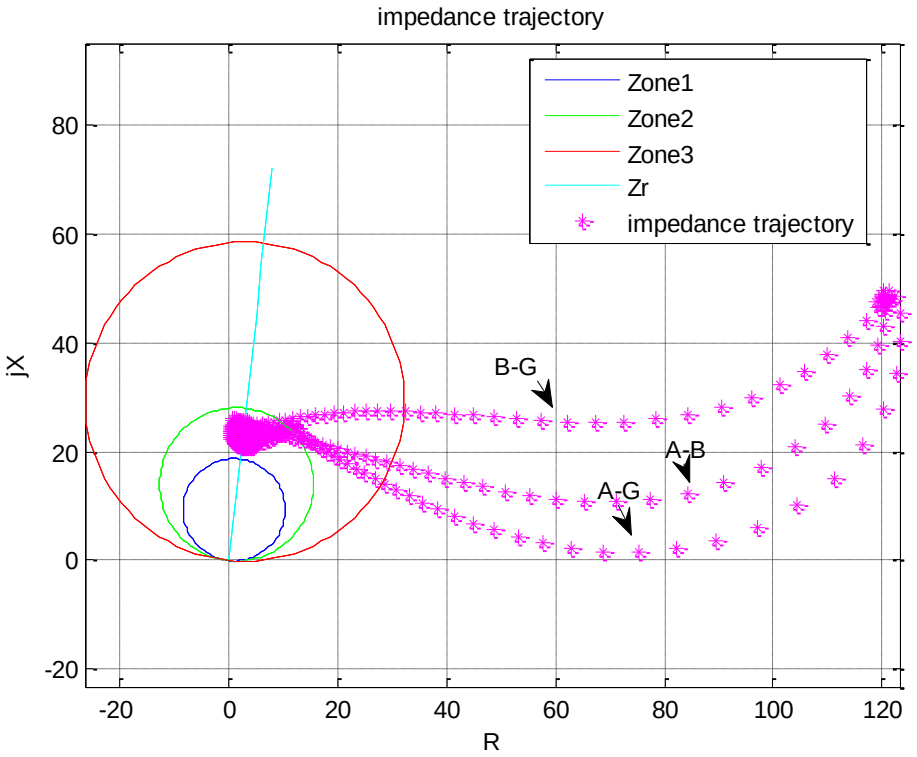

Figure. D-19 A-G, B-G, A-G fault impedance trajectories

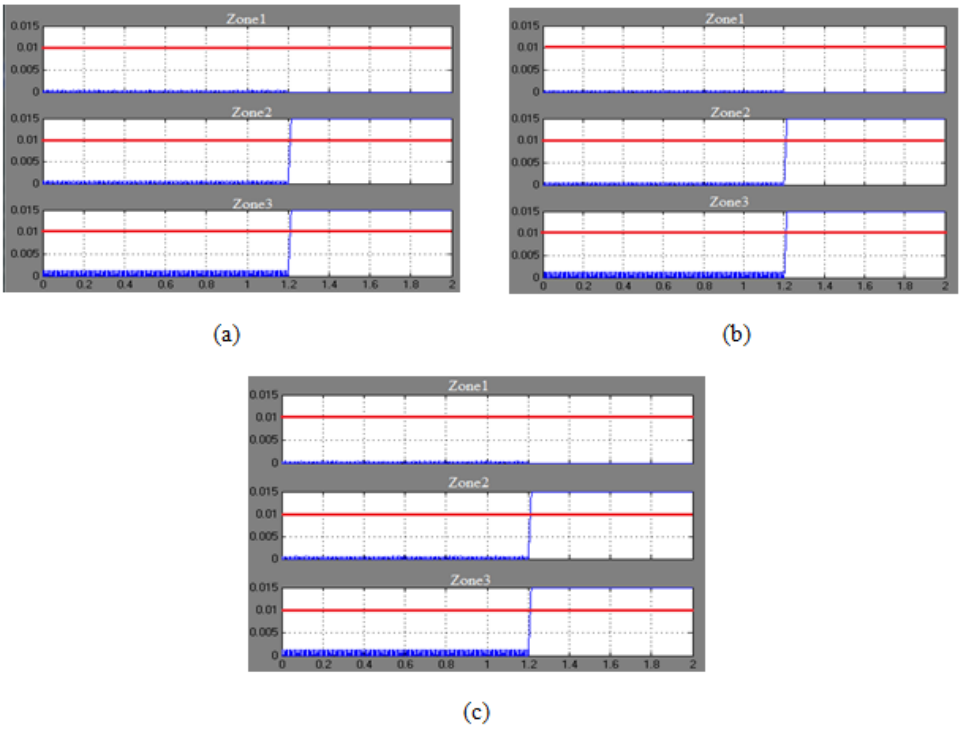

Figure. D-20 Block-average comparator outputs

(a) A-G block-average comparator output

(b) B-G block-average comparator output

(c) A-Bblock-average comparator output

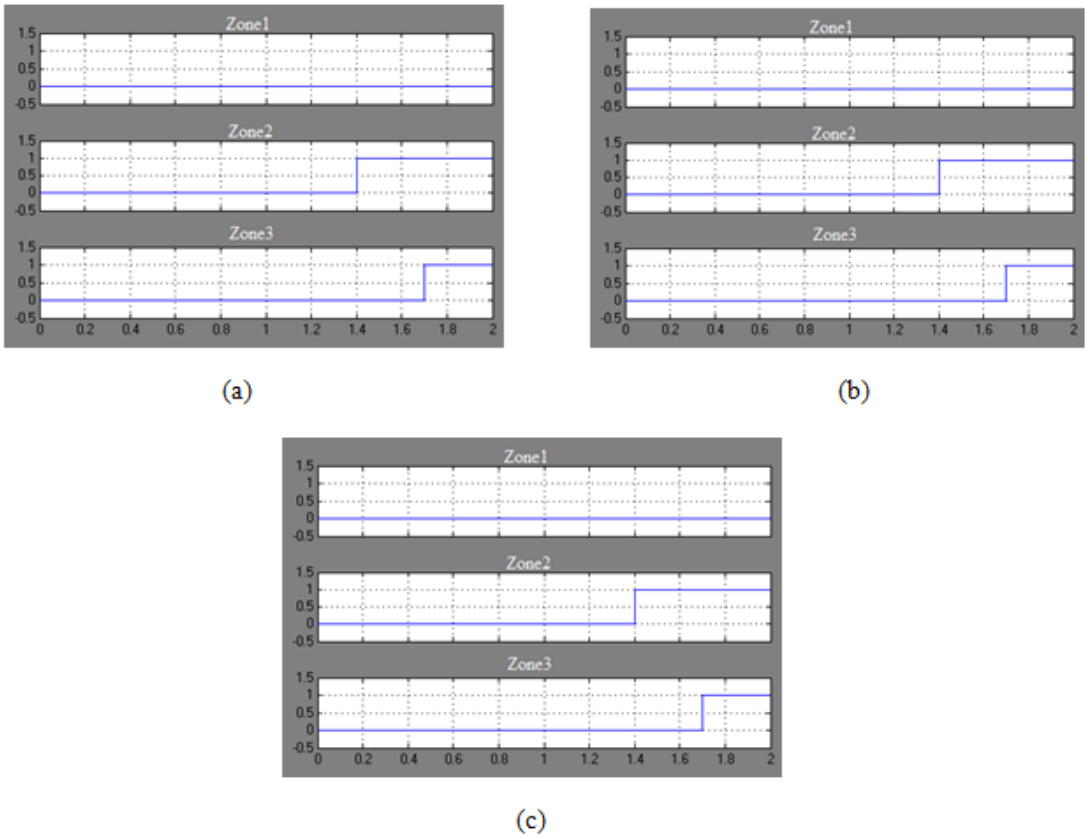

Figure. D-21 Distance relay trip signals

(a) A-G relay trip signals

(b) B-G relay trip signals

(c) A-Brelay trip signals

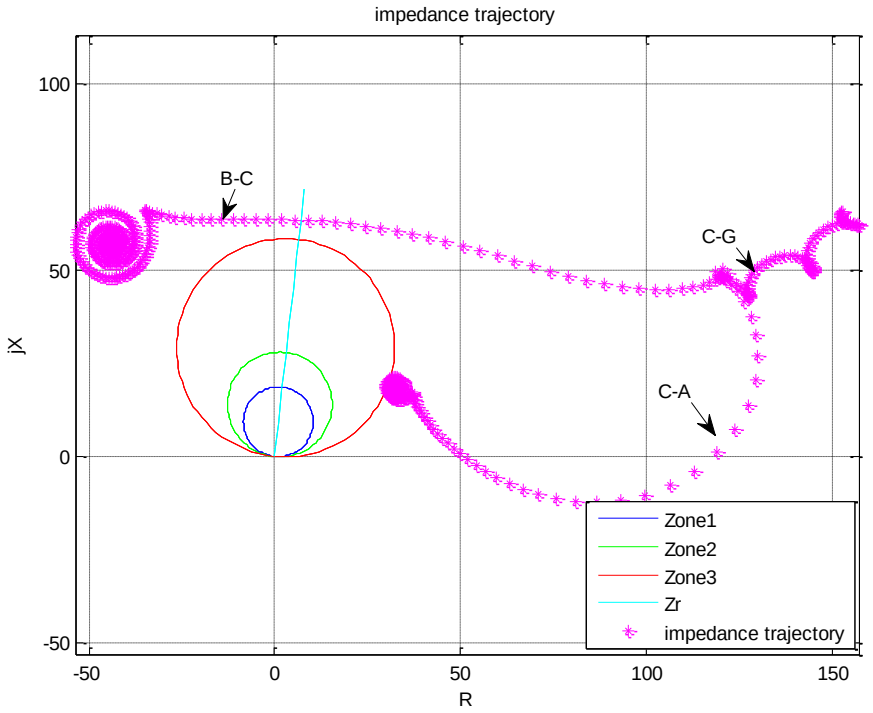

Figure. D-22 C-G, B-C, C-A fault impedance trajectories

D.6 C-A-G Fault at 100km

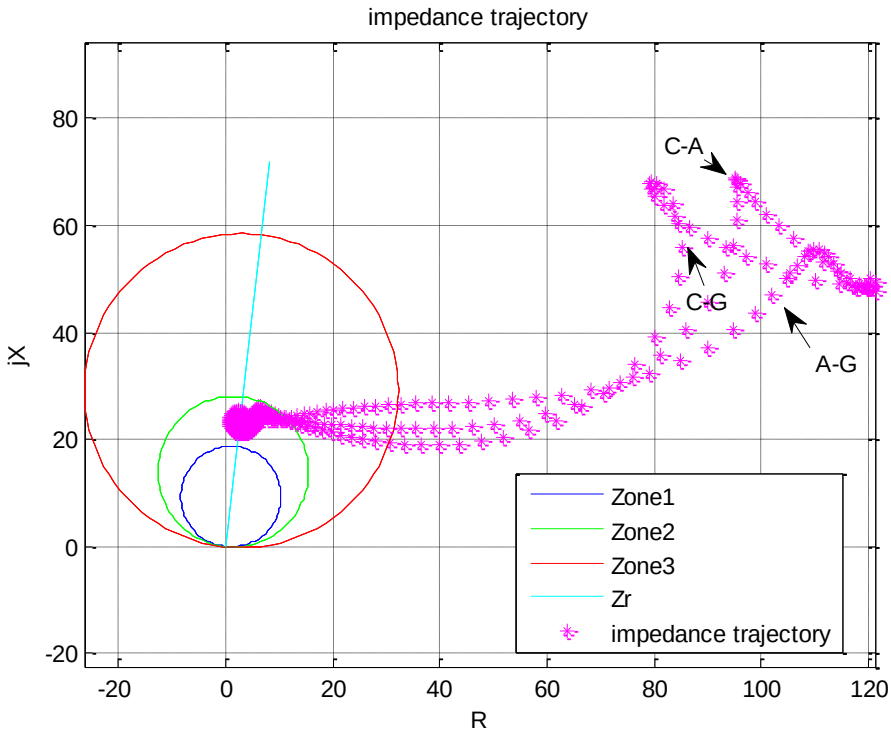

Figure. D-23 A-G, C-G, C-A fault impedance trajectories

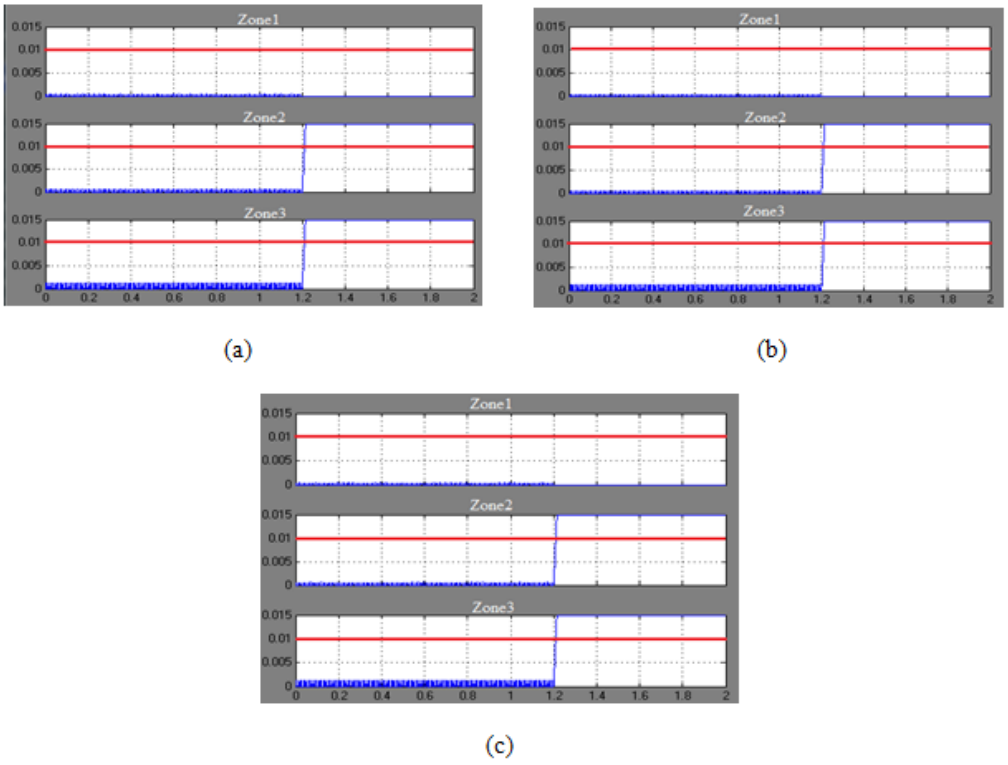

Figure. D-24 Block-average comparator outputs

(a) A-G block-average comparator output

(b) C-G block-average comparator output

(c) C-Ablock-average comparator output

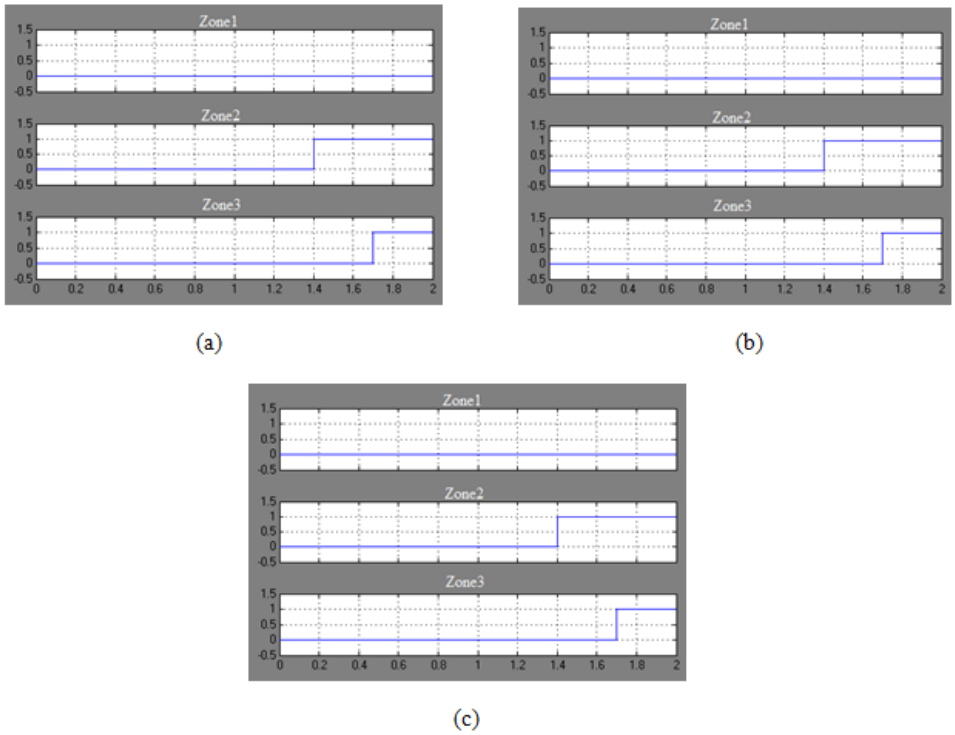

Figure. D-25 Distance relay trip signals

(a) A-G relay trip signals

(b) C-G relay trip signals

(c) C-Arelay trip signals

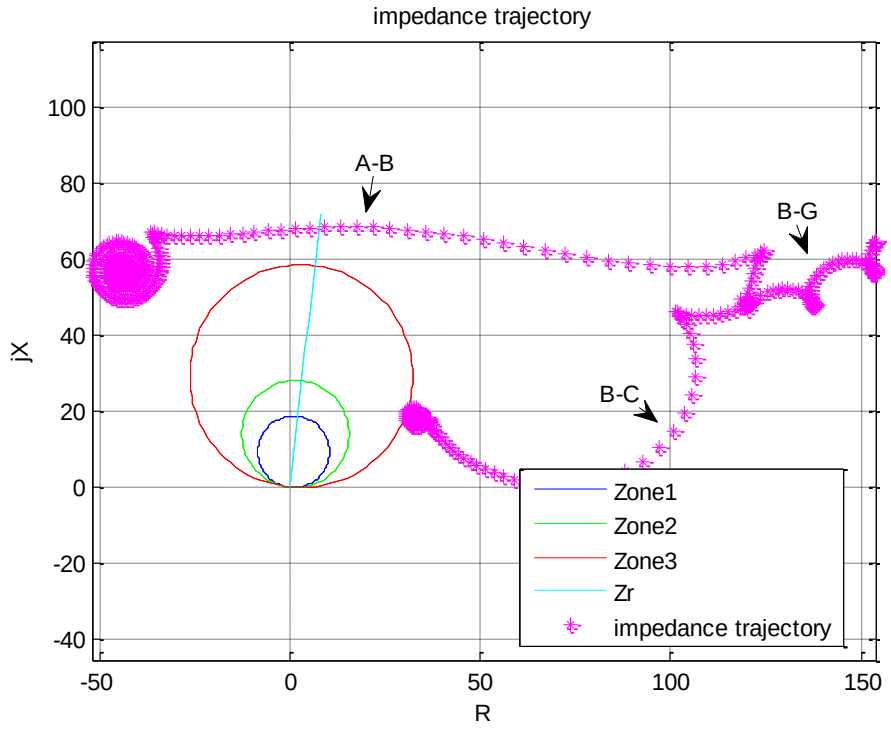

Figure. D-26 B-G, A-G, B-C fault impedance trajectories

Appendix.E

E.1 B-G Fault at 200km

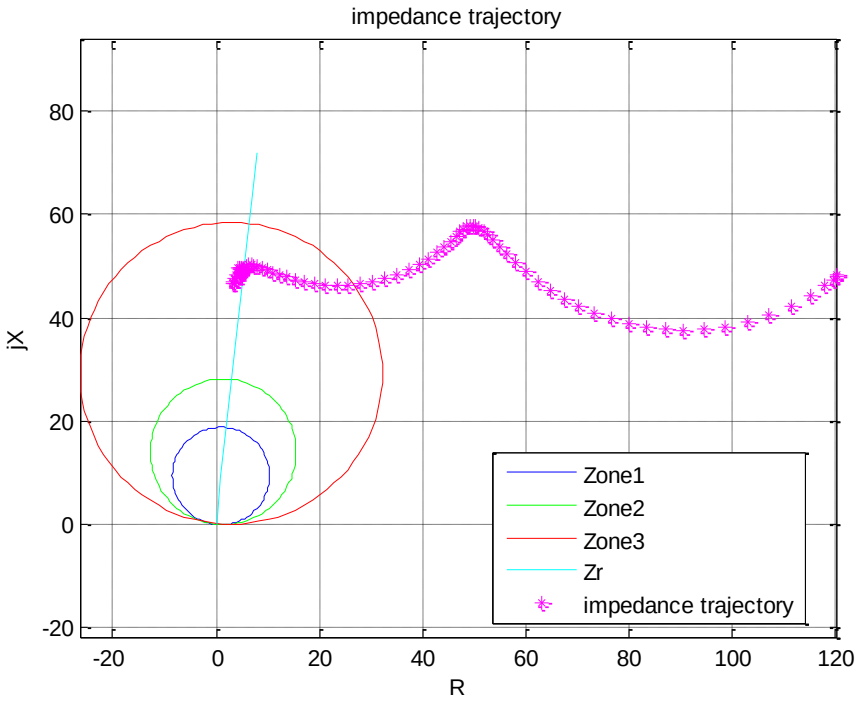

Figure. E-1 B-G fault impedance trajectory

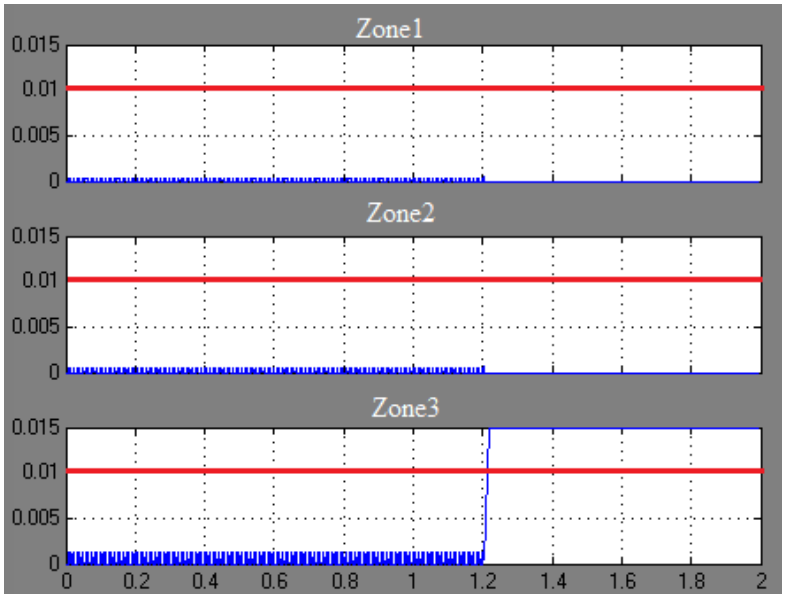

Figure. E-2 B-G Block-average comparator output

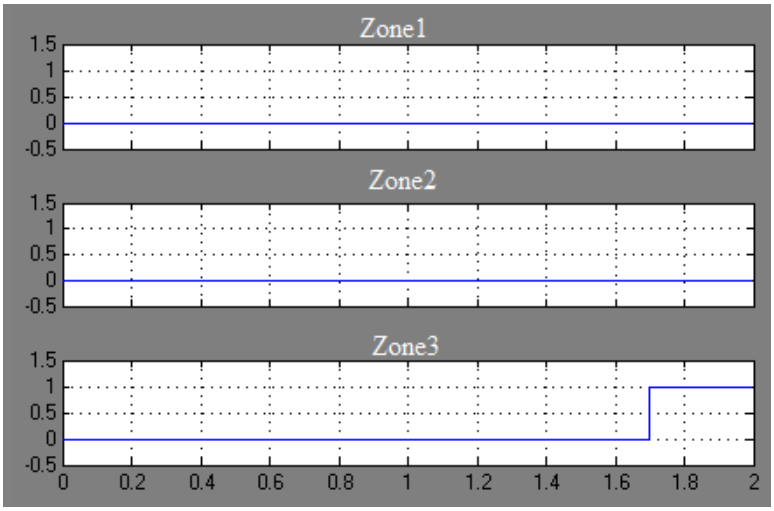

Figure. E-3 B-GDistance relay trip signals

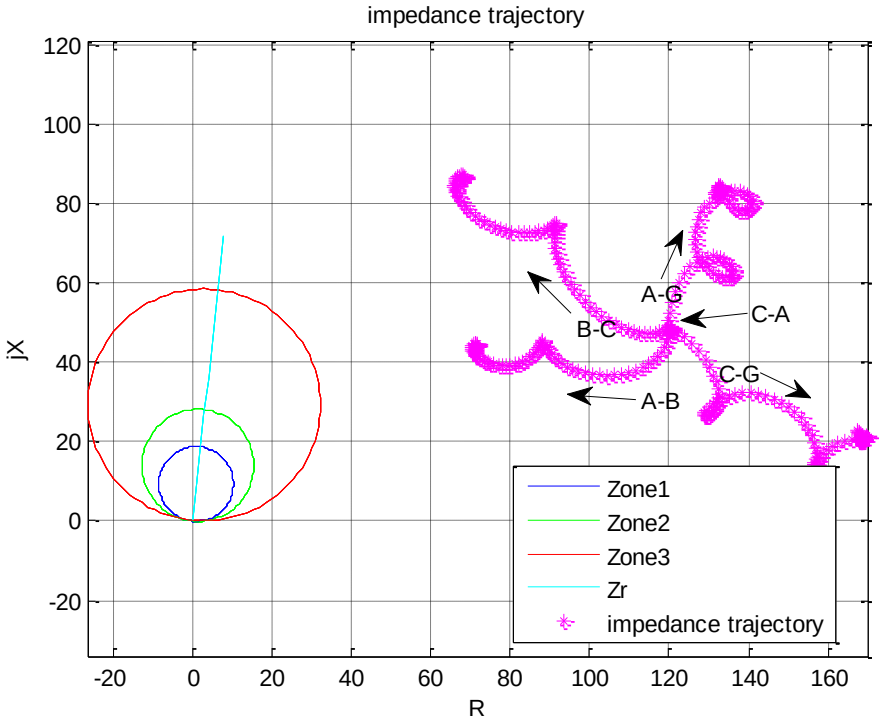

Figure. E-4 A-G, C-G, A-B, B-C, C-A fault impedance trajectories

E.2 C-G Fault at 200km

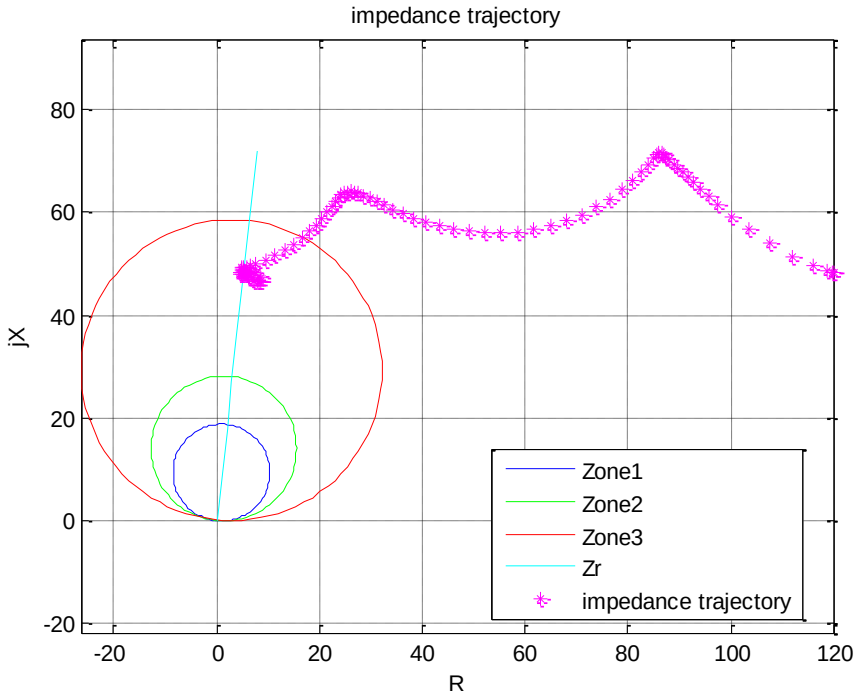

Figure. E-5 C-GFault impedance trajectory

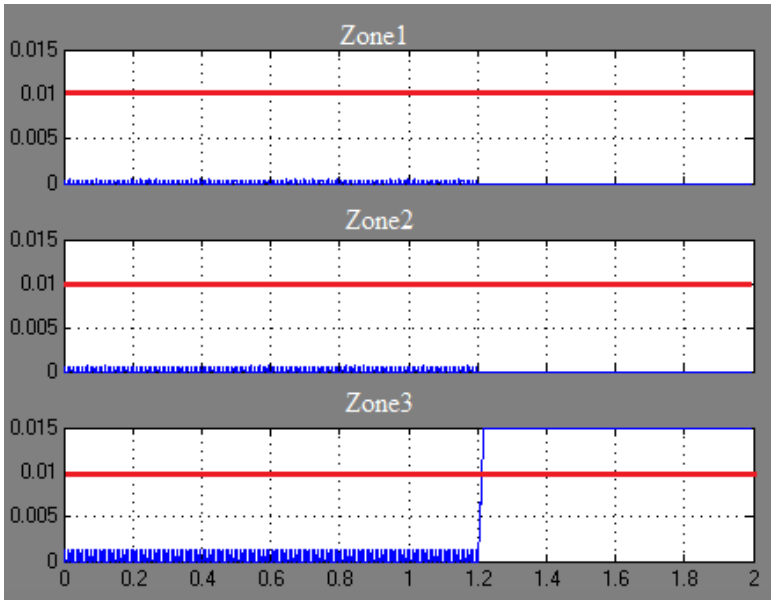

Figure. E-6 C-G Block-average comparator output

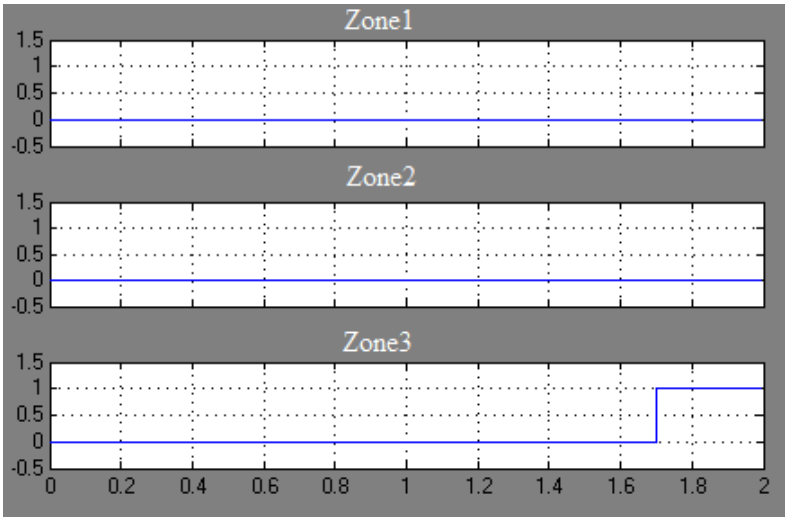

Figure. E-7 C-G Distance relay trip signals

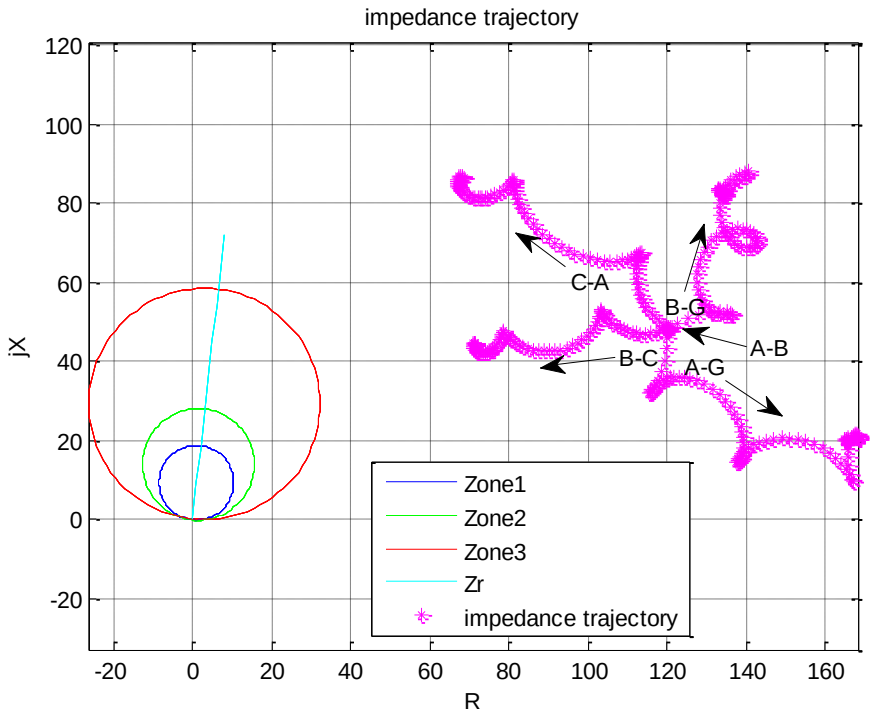

Figure. E-8 A-G, B-G, A-B, B-C, C-Afault impedance trajectories

E.3 B-C Fault at 200km

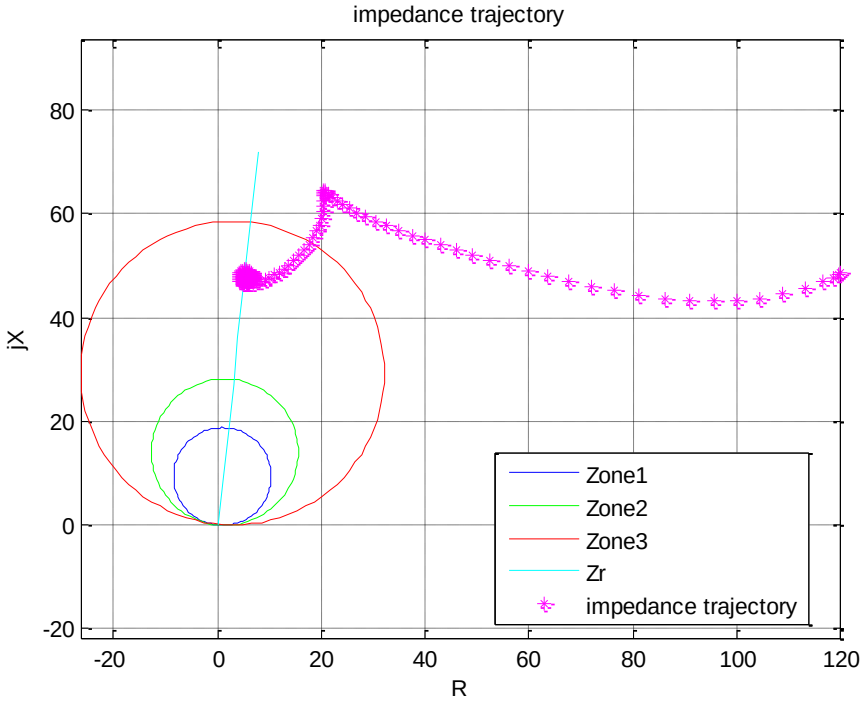

Figure. E-9 B-C Fault impedance trajectory

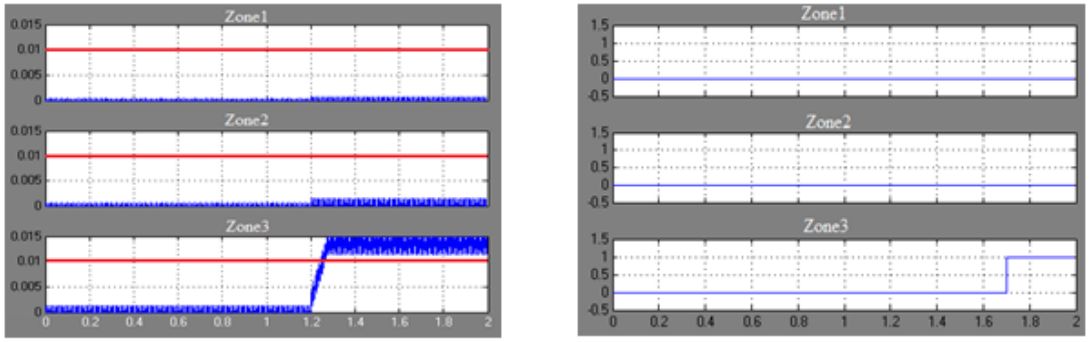

Figure. E-10 B-C block-average comparator output and B-Cdistance relay trip signals

(a) B-C block-average comparator output

(b) B-C relay trip signals

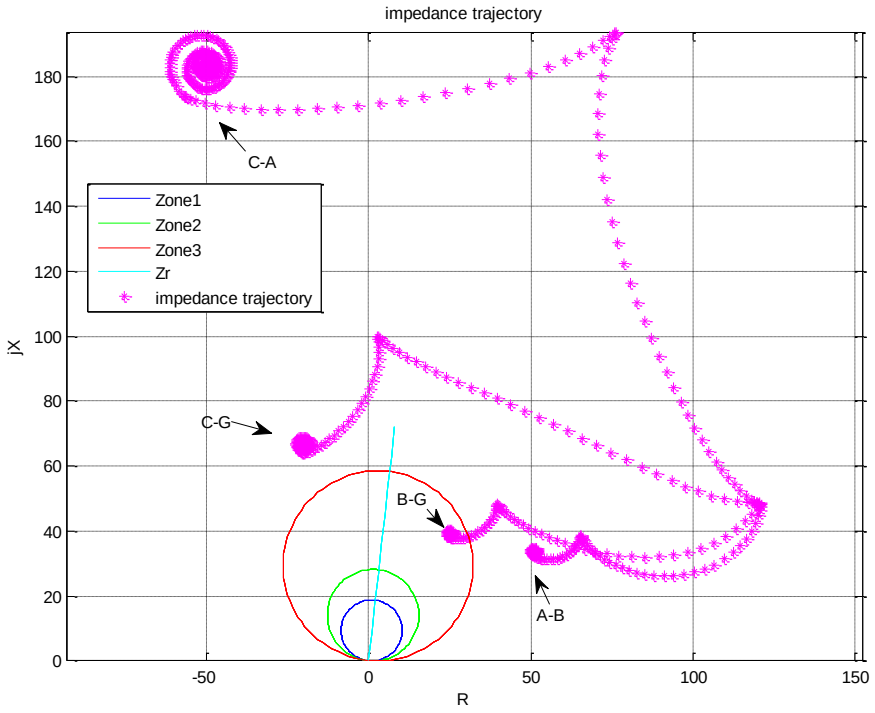

Figure. E-11 A-G, B-G, C-G, A-B, C-A Fault impedance trajectories

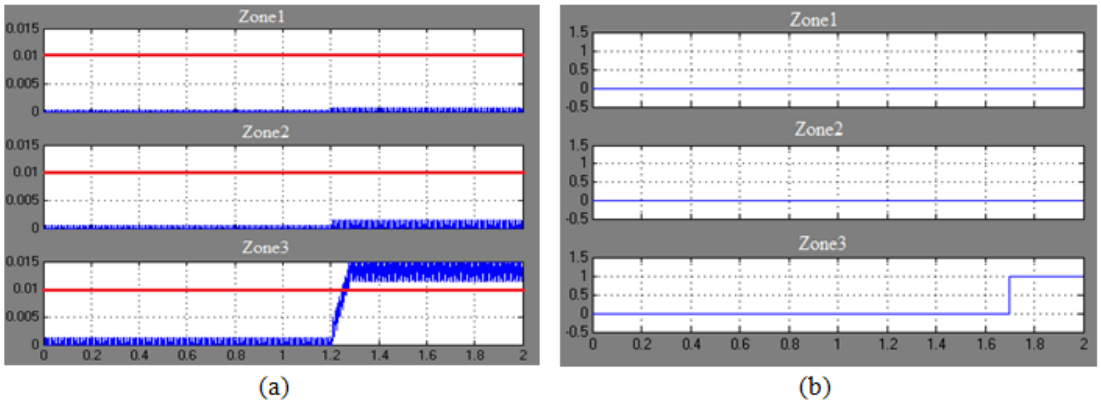

Figure. E-12 B-G Block-average comparator output and B-G distance relay trip signals

(a) B-G block-average comparator output

(b) B-G relay trip signals

E.4 C-A Fault at 200km

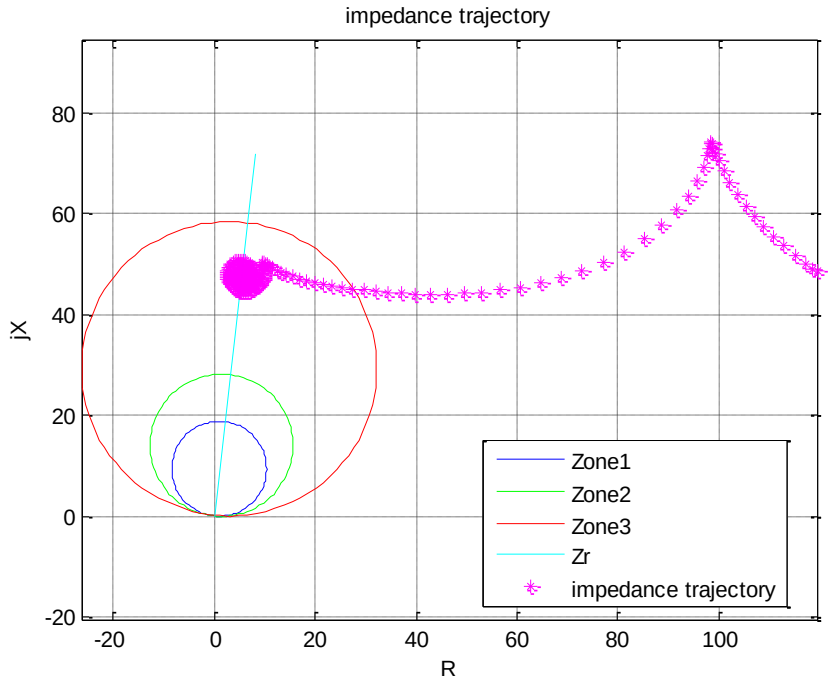

Figure. E-13 C-A Fault impedance trajectory

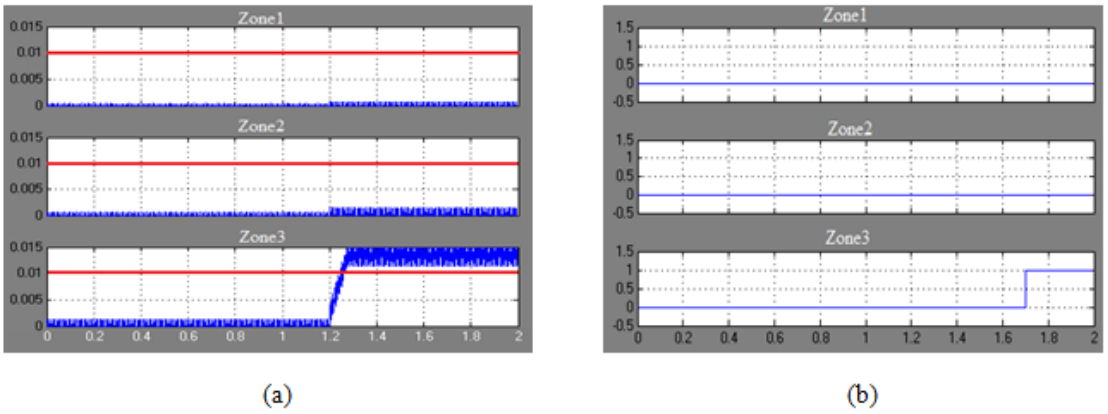

Figure. E-14 C-A Block-average comparator output and C-Adistance relay trip signals

(a) C-A block-average comparator output

(b) C-A relay trip signals

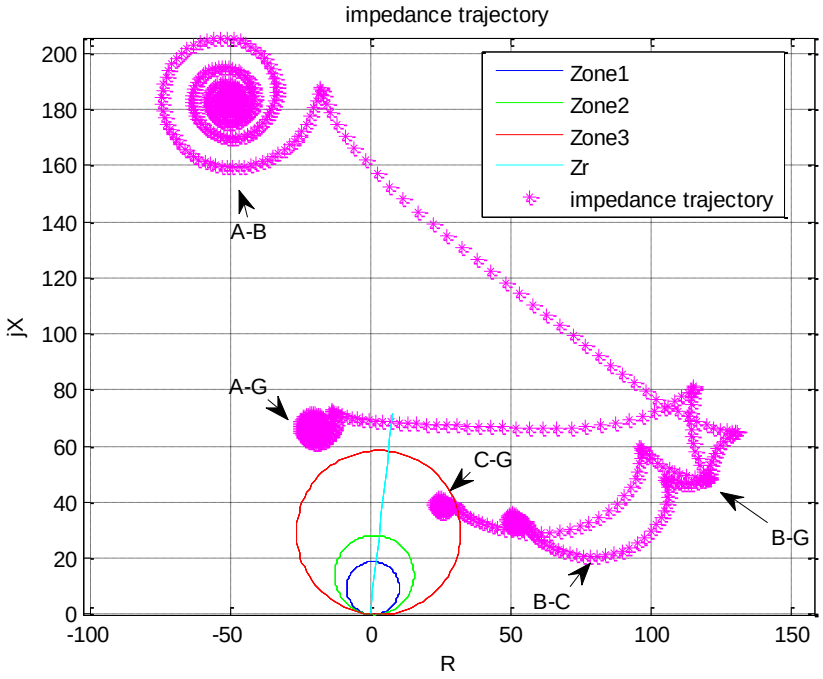

Figure. E-15 A-G, B-G, C-G, A-B, B-Cfault impedance trajectories

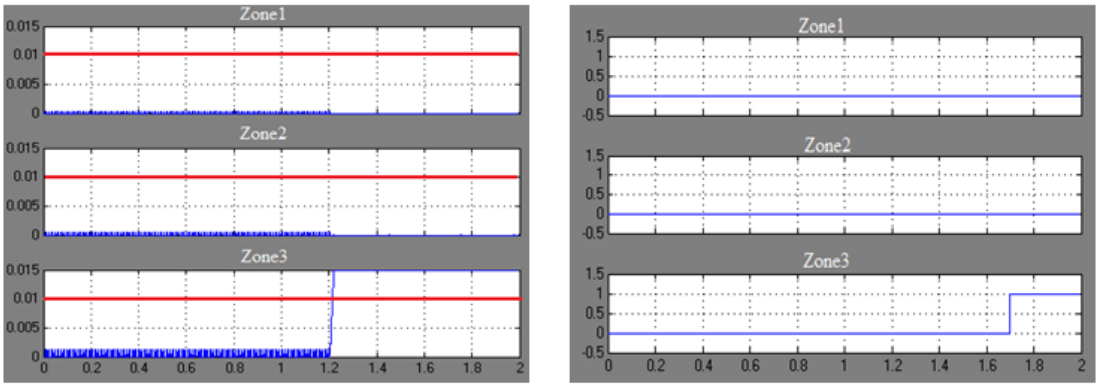

Figure. E-16 C-G block-average comparator output and C-G distance relay trip signals

(a) C-G block-average comparator output

(b) C-G relay trip signals

E.5 A-B-G Fault at 200km

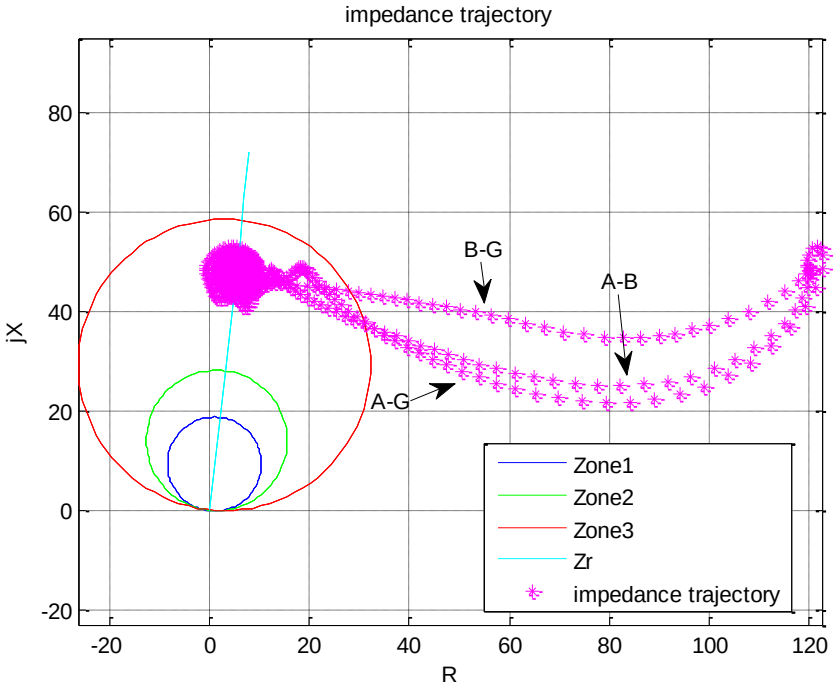

Figure. E-17 A-G, B-G, A-B fault impedance trajectories

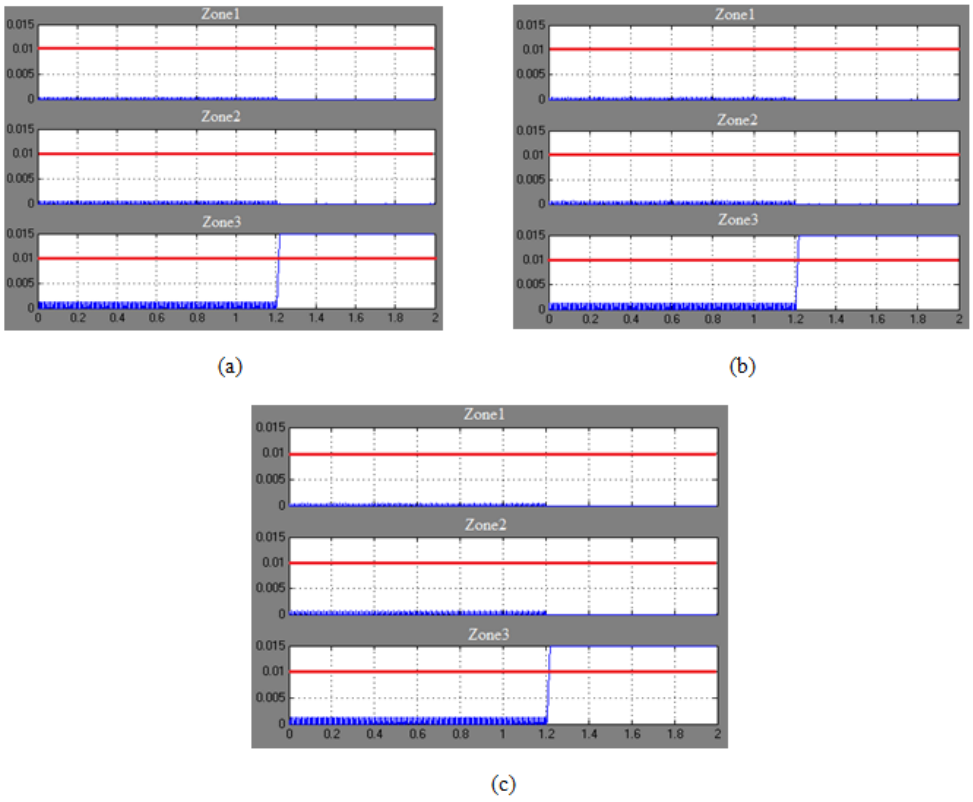

Figure. E-18 Block-average comparator outputs

(a) A-G block-average comparator output

(b) B-G block-average comparator output

(c) A-Bblock-average comparator output

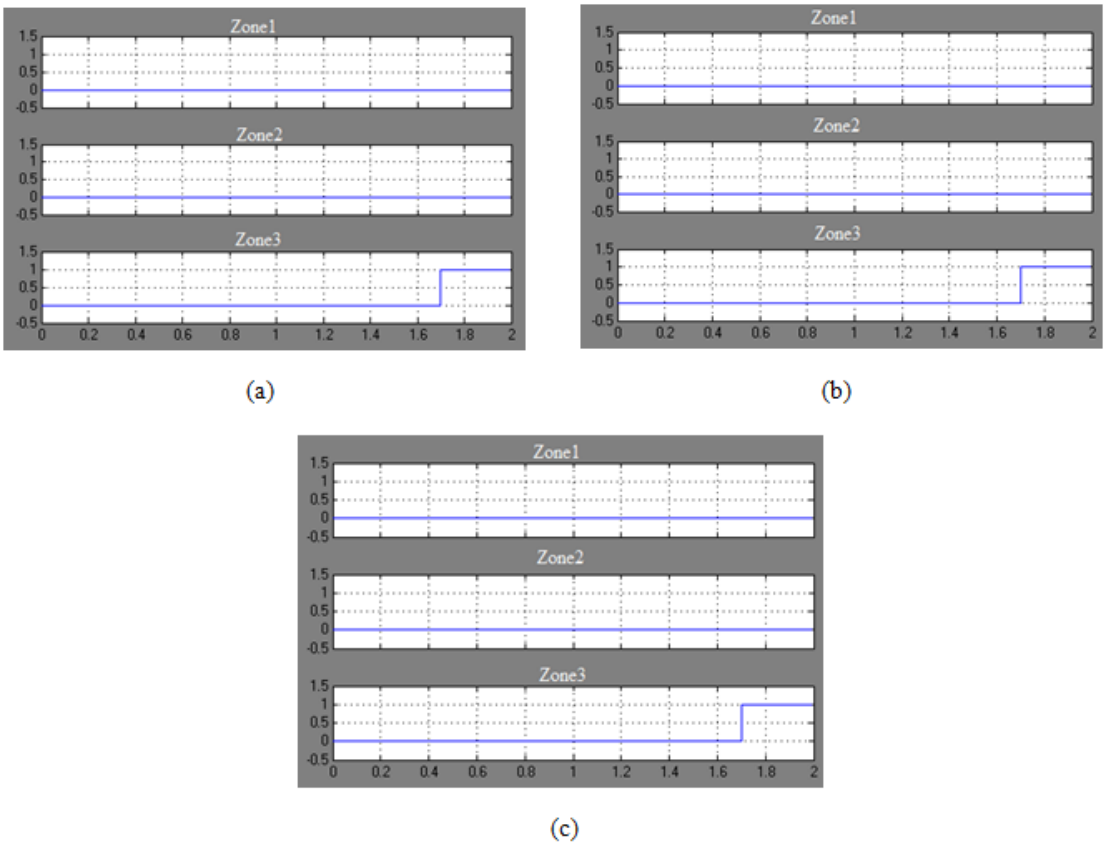

Figure. E-19 Distance relay trip signals

(a) A-G relay trip signals

(b) B-G relay trip signals

(c) A-Brelay trip signals

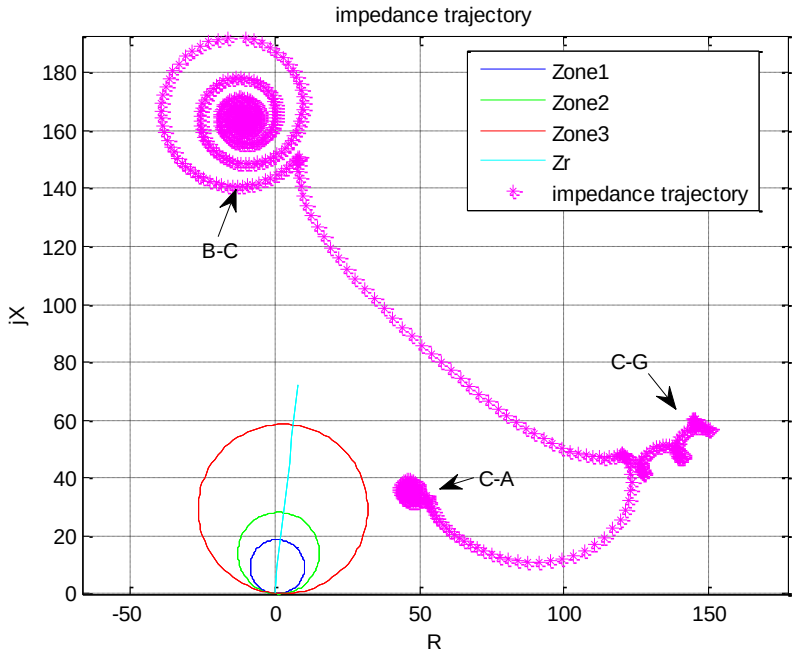

Figure. E-20 C-G, B-C, C-A fault impedance trajectories

E.6 C-A-G Fault at 200km

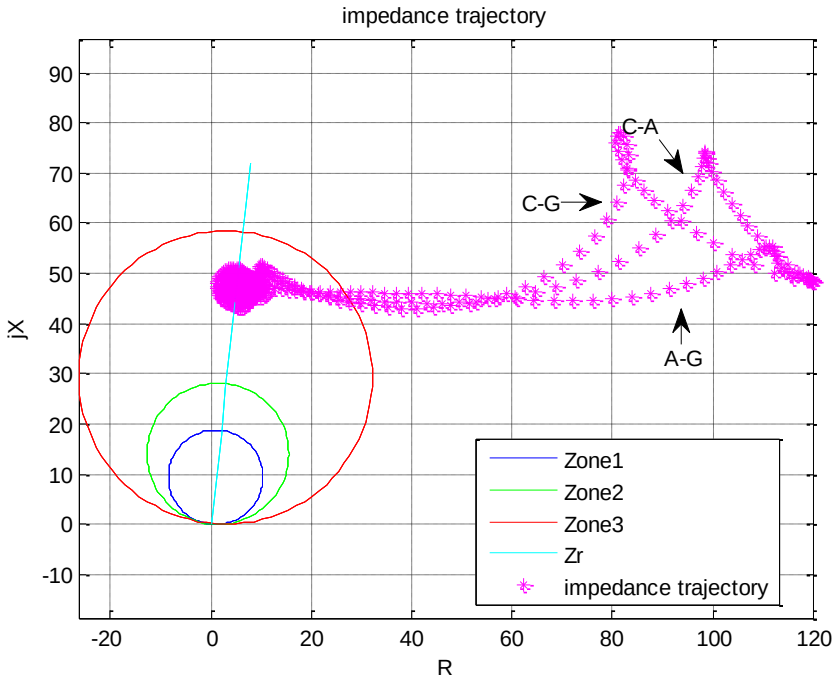

Figure. E-21 A-G, C-G, C-A fault impedance trajectories

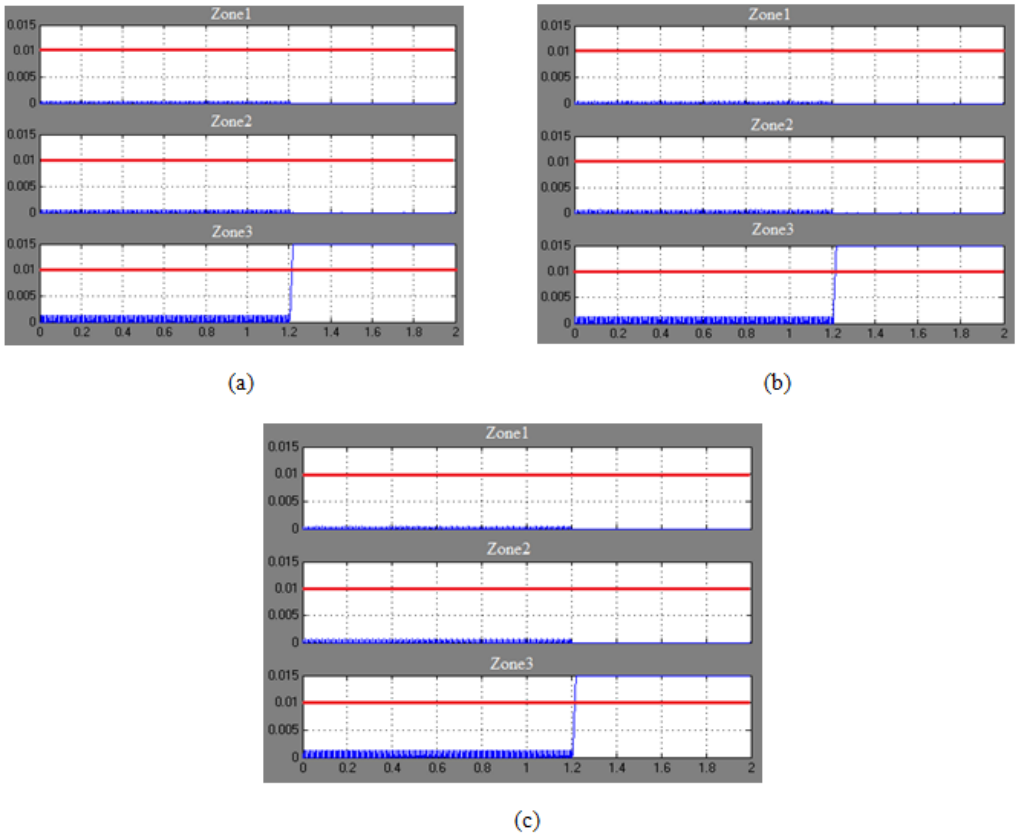

Figure. E-22 Block-average comparator outputs

(a) A-G block-average comparator output

(b) C-G block-average comparator output

(c) C-Ablock-average comparator output

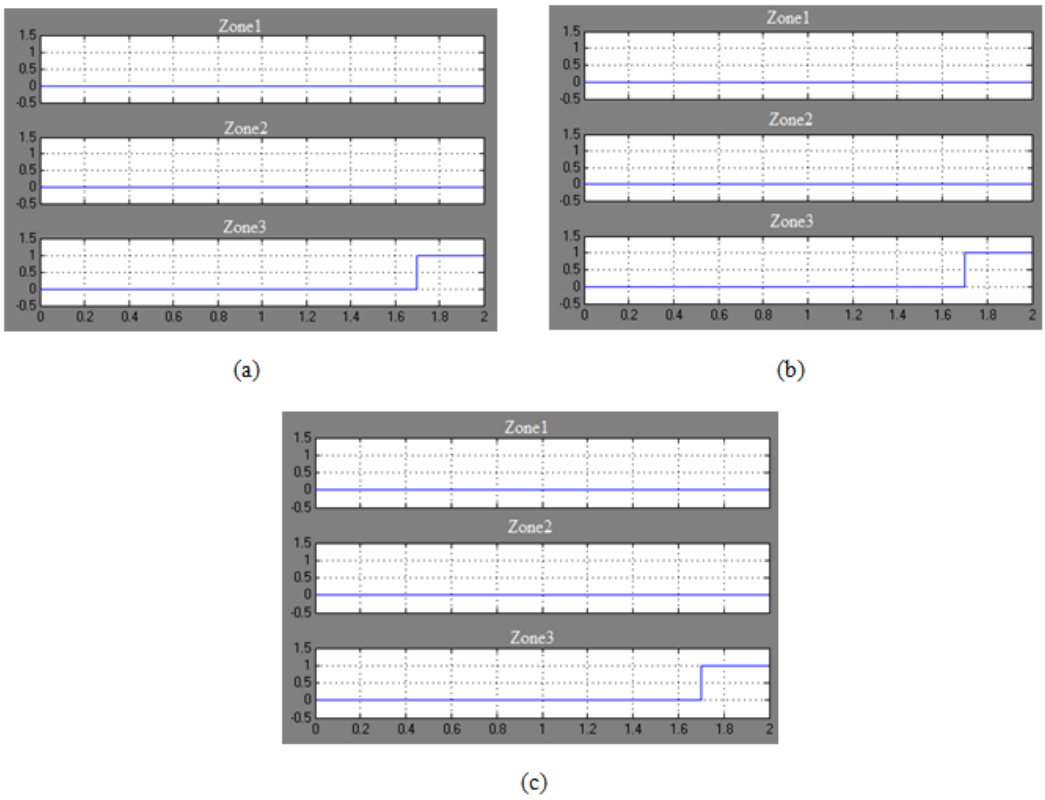

Figure. E-23 Distance relay trip signals

(a) A-G relay trip signals

(b) C-G relay trip signals

(c) C-Arelay trip signals

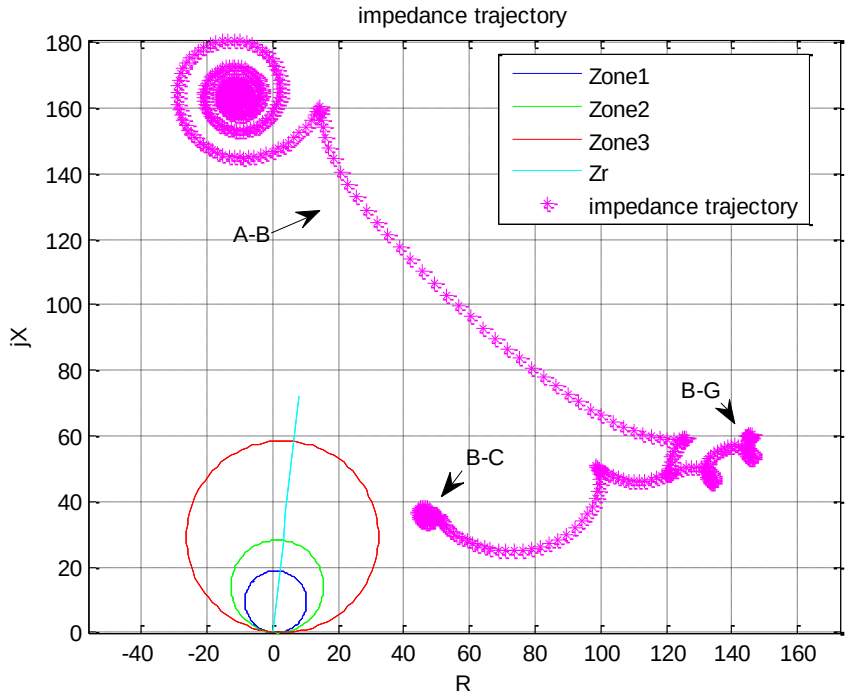

Figure. E-24 B-G, A-B, B-Cfault impedance trajectories

Appendix.F

The HVDC interconnection connects AC network to an infinite bus:

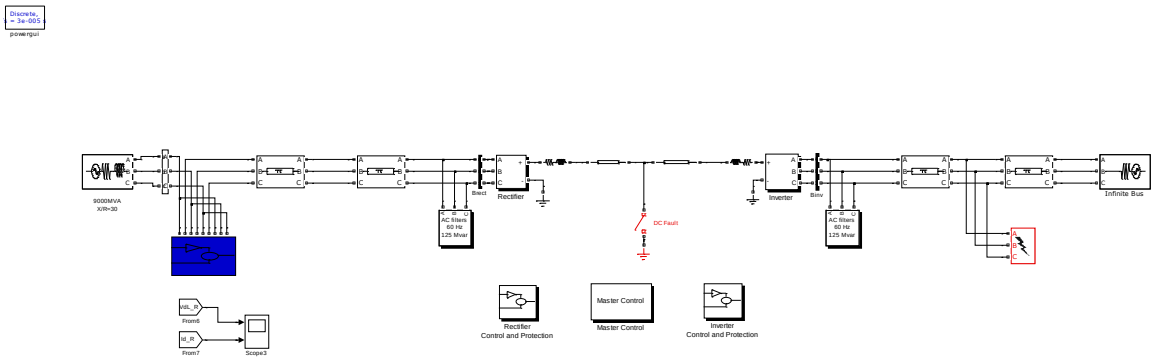

The HVAC interconnection connects AC network to an infinite bus:

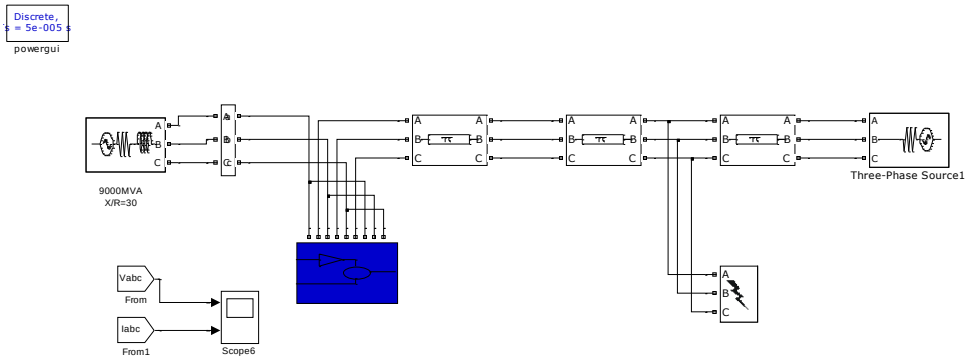

The HVDC interconnection connects AC network to Load 1:

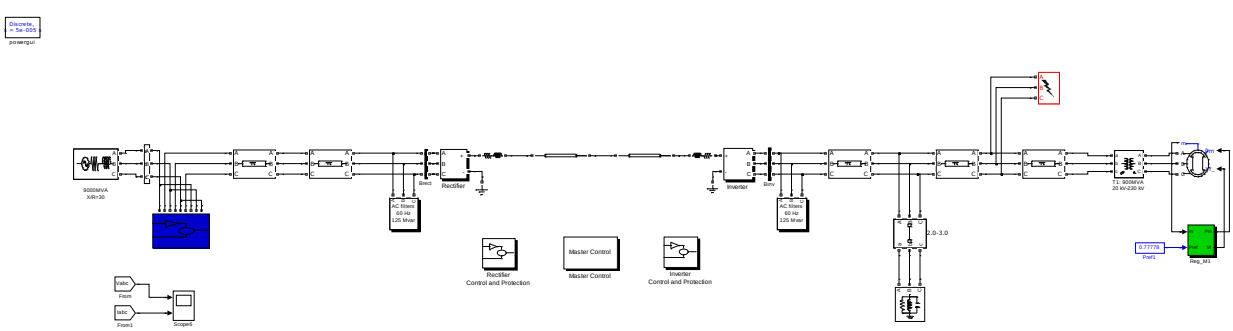

The HVAC interconnection connects AC network to Load 1:

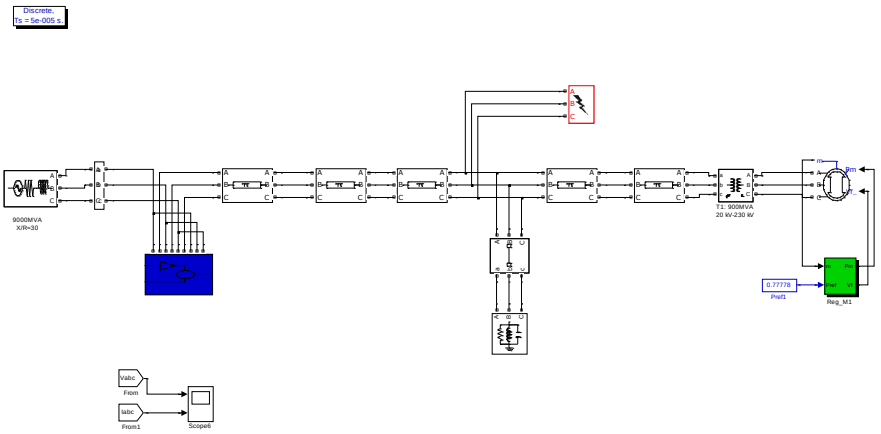

The two area system with HVDC interconnection:

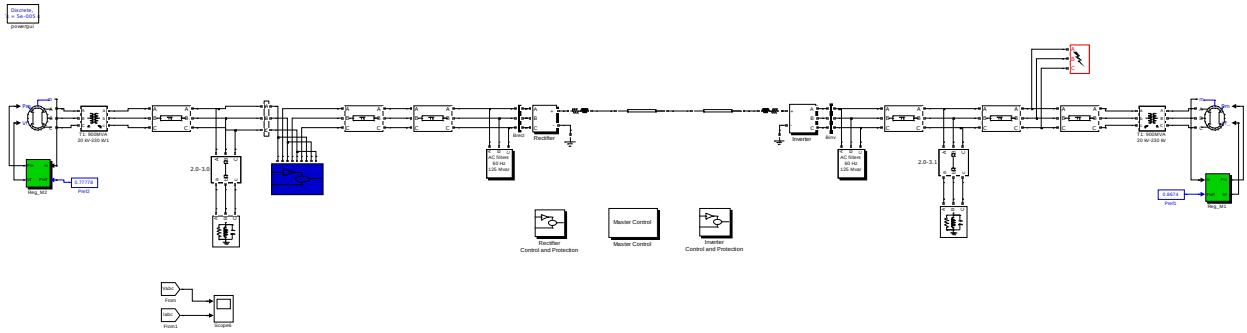

The two area system with HVAC interconnection:

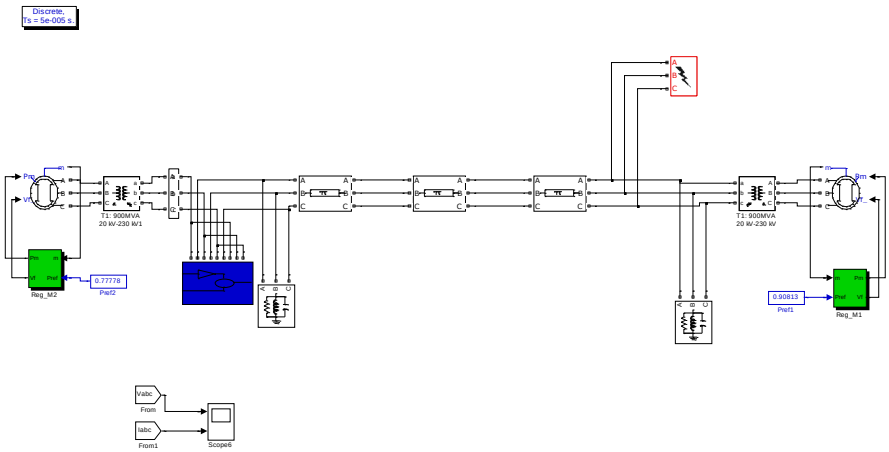

The line parameters and distance relay settings are the same as shown in Appendix. A and B.

Appendix.G

List of Relevant Publications

1. H.L.Wang, M.A.Redfern, "The advantages and disadvantages of using HVDC to interconnect AC networks," *Universities Power Engineering Conference (UPEC), 2010 45th International*, vol., no., pp.1,5, Aug. 31 2010-Sept. 3 2010

2. H.L.Wang, M.A.Redfern, "Enhancing AC networks with HVDC interconnections," *Electricity Distribution (CICED), 2010 China International Conference on*, vol., no., pp.1,7, 13-16 Sept. 2010

3. H.L.Wang, M.A.Redfern, "HVDC to Constrain System Collapse Propagating Through the Power Transmission Networks," *Universities' Power Engineering Conference (UPEC), Proceedings of 2011 46th International*, vol., no., pp.1,6, 5-8 Sept. 2011

References

[1] Beck,G.; Povh, D.; Retzmann, D.; Teltsch, E., “Global Blackouts-Lessons Learned,” in POWER-GEN Europe 2005, Milan, Italy, 2005.

[2] Rahman,M. A.; Ashraf, I.; Alsharari, H.D., “HVDC system for National and Cross Border Grid Interconnections in Saudi Arabia,” *IOSR Journal of Engineering* vol. 2, pp. 529-537, April, 2012.

[3] Carlsson,L. "HVDC A 'firewall' against disturbance in high-voltage grids," 2005.

[4] Andersson,G.;Donalek, P.; Farmer, R.; Hatziargyriou, N.; Kamwa, I.; Kundur, P.; Martins, N.; Paserba, J.; Pourbeik, P.; Sanchez-Gasca, J.; Schulz, R.; Stankovic, A.; Taylor, C.; Vittal, V., “Causes of the 2003 major grid blackouts in North America and Europe, and recommended means to improve system dynamic performance,” *Power Systems, IEEE Transactions on ,,* vol. vol.20,, pp. 1922- 1928,. Nov. 2005.

[5] N. A. E. R. Council, *Technical Analysis of the August 14, 2003, Blackout: What Happened, Why, and What Did We Learn?* , New York, 2004.

[6] Farmer,R. G.; Allen, E.H., “ Power System Dynamic Performance Advancement From History of North American Blackouts,” in Power Systems Conference and Exposition, 2006. PSCE '06. 2006 IEEE PES,, 2006, pp. 293-300, .

[7] U. S.-C. P. S. O. T. Force, *Final Report on the August 14, 2003 Blackout in the United States and Canada: Causes and Recommendations*, 2004.

[8] Pereira,L. “Cascade to Black Similarities Between the 14 August 2003 Blackout and the Western System Collapses of 1996 ” *IEEE power & energy magazine*, pp. 54-57, 2004.

[9] Makarov, Y. V.; Reshetov, V.I.; Stroev, A.; Voropai, N.I., “Blackouts in North America and Europe: Analysis and generalization,” in Power Tech, 2005 IEEE Russia Russia 2005, pp. 1-7,.

[10] Portante,E. C.; Kavicky, J.A.; Folga, S.F.; Craig, B.A.; Talaber, L.E.; Wulfkuhle, G.R., “Simulating the seismic performance of a large-scale electric network in the U.S. Midwest,” in Simulation Conference (WSC), Proceedings of the 2010 Winter,, 2010, pp. 3482-3493.

[11] Apostolov,A. P. “Distance relays operation during the August 2003 North American Blackout and methods for improvement,,” *Power Tech, 2005 IEEE Russia* pp. 1-6, 27-30 June 2005, 2005.

[12] U. S. C. P. O. T. Force, *August 14, 2003 Outage Sequence of Events*, 2003.

[13] Beruer,W.; Hartmann, V.; Povh,D.; Retzmann,D.; Teltsch,E., “APPLICATION OF HVDC FOR LARGE POWER SYSTEM INTERCONNECTIONS,” in CIGRE, Paris, 2004.

[14] Beruer,W.; Lemes, M.; Retzmann, D., “Perspectives of HVDC and FACTS for System Interconnection and Grid Enhacncement,” in Brazil-Chian-Indian Summit Meeting on HVDC & Hybrid Systems: Planning and Engineering Issues, Brazil, 2006.

[15] Cutright,E. “A Tree Falls, and the Lights Go Out,” 2013.

[16] Jiang,H. Y.;Machen.M., “Stability Enhancement and Blackout Prevention by VSC Based HVDC,” in The electric power system of the future-Integrating supergrids and microgrids International Symposium in Bologna, Italy, 2011.

[17] Pan,J. P.; Nuqui,R., Berggren,B., Thorburn,S., Jacobson,B., “The balance of power-Advanced transmission grids are embedding HVDC Light,” *Transmission and distribution*, 2009.

[18] Kreusel,J.; Retzmann, D., “Integrated AC/DC Transmission Systems –Benefits of Power Electronics for Security and Sustainability of Power Supply,” in PSCC 2008, 2008.

[19] Li, C. Y.; Sun,Y.Z.; Chen, X.Y., “Recommendations to improve power system security: Lessons learned from the europe blackout on November 4,” in in Universities Power Engineering Conference, 2007. UPEC 2007. 42nd International 2007, pp. 529-533.

[20] Tu, J.Z.; Gan, D.Q.; Xin, H.H.; Wang, Z., “Cascading Failure and Blackout Risk Analysis of AC/DC Power System - The Impact of AC/DC Interconnection Mode and Capacity Distribution,,” in Power and Energy Engineering Conference (APPEEC), 2012 Asia-Pacific 2012, pp. 1-5.

[21] Perez,S. G. A. “Modeling Relays for Power System Protection Studies,” Department of Electrical Engineering, University of Saskatchewan, Canada, 2006.

[22] Jonsson,M. “Line Protection and Power System Collapse,” Department of Electric Power Engineering, Chalmers University of Technology, Sweden, 2001.

[23] Hemmingsson,M. “Power System Ocsillations Detection Estimation & Control ”, Department of Industrial Electrical Engineering and Automation, LUND University, Sweden, 2003.

[24] Jonsson,M. “Protection Strategies to Mitigate Major Power System Breakdowns,” Department of Electric Power Engineering, Chalmers University of Technology, Sweden, 2003.

[25] PDHengineer, *System Failure Anatomy of a Blackout Part 2 Cascading Failure of the Power System*.

[26] Bialek,J. W. *Recent blackouts in US and continental Europe: is liberalisation to blame?*, 2004.

[27] Horowitz,S. H.; Phadke, A.G., , “Third zone revisited,” *Power Delivery, IEEE Transactions on,* vol. 21, , pp. 23-29, Jan. 2006, 2006.

[28] Suwannakarn,K.; Hoonchreon, N., “Performance analysis of the enhanced zone 3 distance relay on WSCC test system,,” in Electrical Engineering/Electronics, Computer, Telecommunications and Information Technology, 2008. ECTI-CON 2008. 5th International Conference on , , 2008, pp. 941-944.

[29] Richards,S.; Tholomier,D., "Improving the Performance of Distance Protection during Wide Area Disturbances [Online]."

[30] Hodaei,S. A. A.; Ranjbar, A.M.; Amraee,T., “Improvement of Distance Relay Performance During Voltage Instability Conditions,” in The International Conference on Electrical Engineering 2009, 2009.

[31] "Application of Overreaching Distance Relays [Online]."

[32] Zare,M.; Aghamohammadi, M.; Saeedi, M., “Mitigation of power system blackout by blocking zone3 of minimum distance relays,” in Universities Power Engineering Conference, 2008. UPEC 2008. 43rd International , , 2008, pp. 1-5.

[33] Apostolov,A.; Vandiver, B., “Ensuring the Correct Operation of Distance Relays Under Dynamic System Conditions,,” in Protective Relay Engineers, 2008 61st Annual Conference for ,, 2008, pp. 72-77.

[34] Farmer,R. G.; Allen,E.H., “Power System Dynamic Performance Advancement From History of North American Blackouts,,” in Power Systems Conference and Exposition, 2006. PSCE '06. 2006 IEEE PES 2006, pp. 293-300.

[35] Jonsson,M.; Daalder, J., “Distance protection and voltage stability,” in Power System Technology, 2000. Proceedings. PowerCon 2000. International Conference on, 2000, pp. 971-976.

[36] Taylor,C. W. “Improving grid behaviour,” *Spectrum, IEEE* vol. 36, pp. 40-45, Jun 1999, 1999.

[37] Venkatasubramanian.V.; Li, Y., "Analysis of 1996 Western American Electric Blackouts," Italy, 2004.
[38] Taylor,C. W.; Erickson, D. C., "Recording and analyzing the July 2 cascading outage [Western USA power system]," *Computer Applications in Power, IEEE* vol. 10, pp. 26-30, Jan 1997, 1997.
[39] Makarov,Y. V.; Reshetov. V.I.; Stroev, A.; Voropai, N.I., "Blackouts in North America and Europe: Analysis and generalization," in Power Tech, 2005 IEEE Russia, Russia, 2005, pp. 1-7.
[40] Shehu, A. A. "Voltage Stability and Distance Protection Zone3," Division of Electric Power Engineering, Department of Environment and Energy, , CHALMERS UNIVERSITY OF TECHNOLOGY, 2009.
[41] Larsson,S.; Ek, E., "The black-out in southern Sweden and eastern Denmark, September 23, 2003," in Power Engineering Society General Meeting, 2004. IEEE, 2004, pp. 1668-1672.
[42] Berizzi,A. "The Italian 2003 blackout," in Power Engineering Society General Meeting, 2004, pp. 1673-1679.
[43] Corsi,S.; Sabelli. C., "General blackout in Italy Sunday September 28, 2003, h. 03:28:00," in Power Engineering Society General Meeting, 2004. IEEE 2004, pp. 1691-1702.
[44] Sforna,M.; Delfanti. M., "Overview of the events and causes of the 2003 Italian blackout," in Power Systems Conference and Exposition, 2006. PSCE '06. 2006 IEEE PES ,, 2006, pp. 301-308.
[45] Swiss Federal Office of Energy, *Report on the blackout in Italy on 28 September 2003*, 2003.
[46] UCTE, *FINAL REPORT of the Investigation Committee on the 28 September 2003 Blackout in Italy*, 2004.
[47] Chen,X. Y.; Deng, C.H.; Chen, Y.P.; Li, D.Y., "Blackout prevention: Anatomy of the blackout in Europe," in in Power Engineering Conference, 2007. IPEC 2007. International , 2007, 2007, pp. 928-932.
[48] Apostolov,A.; Vandiver. B., "Ensuring the Correct Operation of Distance Relays Under Dynamic System Conditions," in in Protective Relay Engineers, 2008 61st Annual Conference for 2008, pp. 72-77.
[49] Li,C. Y.; Sun. Y.Z.; Chen, X.Y., "Analysis of the blackout in Europe on November 4, 2006," in in Power Engineering Conference, 2007. IPEC 2007. International ,2007, 2007, pp. 939-944.
[50] Richards, S.; Damien, T., "Improving the Performance of Distance Protection during Wide Area Disturbance."
[51] UCTE, *Final Report System Disturbance on 4 November 2006*, 2006.
[52] Magg,T.; Chen, M. M.; Krige, E.; Wasborg, J.; Sundin, J., "Connecting networks with VSC HVDC in Africa: Caprivi Link Interconnector," in IEEE PES PowerAfrica 2012 Conference and Exposition, Johannesburg, South Africa, 2010.
[53] Rudervall,R.; Charpentier,J.P.; Sharma,R., "High Voltage Direct Current (HVDC) Transmission Systems Technology Review Paper," in Energy Week 2000, Washington, D.C, USA, 2000.
[54] Asplund,G.; Carlsson, L.; Tollerz, O., *50 years HVDC Part 1* 2003.
[55] Long,W.; Nilsson. S., "HVDC transmission: yesterday and today," *Power and Energy Magazine, IEEE,* vol. 5, pp. 22-31, March-April 2007, 2007.
[56] Drobik,T. "High-voltage direct current transmission lines."
[57] "High Voltage Direct Current Transmission."
[58] Gunnarsson, C. "The histroy of HVDC transmission-Power transmission in general."

[59] Peake,O. “The History of High Voltage Direct Current Transmission ” in 3rd Australasian Engineering Heritage Conference 2009, 2009.
[60] Asplund,G. Carlsson. L.; Tollerz, O., *50 years HVDC Part 2*, 2003.
[61] Carlsson,G. “'Classical' HVDC: still continuing to evolve,” *Transmission & Distribution*.
[62] J. Z. C. Cao, J.Y.,, “HVDC in China,” in EPRI 2013 HVDC&FACTS Conference, Palo Alto, CA, USA, 2003.
[63] Kreusel,J.; Retzmann, D., “Integrated AC/DC Transmission Systems –Benefits of Power Electronics for Security and Sustainability of Power Supply,” 2008.
[64] ABB, "The evolution of HVDC: Transmitting bulk power over long distancesd."
[65] Siemens Energy, "HVDC Classic."
[66] Andersen,B.; Barker, C., “A new era in HVDC?,” in IEE Review, 2000, pp. 33-39.
[67] Du,C. Q. “The contol of VSC-HVDC and its use for large industrial power systems,” Department of Electri Power Engineering, Chalmers University of Technology, 2003.
[68] Kundur,P. *Power System Stability and Control*.
[69] Larruskain,D. M.; Zamora, I.; Mazon, A.J.; Abarrategui, O.; Monasterio, J., “Transmission and Distribution Networks: AC versus DC.”
[70] Paulinder,J. “Operation and Control HVDC links embedded in AC systems,” Department of Electric Power Engineering, Chalmers University of Technology, Sweden, 2003.
[71] Siemens, "High Voltage Direct Current Transmission-Proven Technology for Power Exchange."
[72] Callavik,M. "ABB achieves antoher milestone in electrical engineering," 2012.
[73] Arrillaga,J. *High Voltage Direct Current Transmission 2nd Edition*, London, uk: The Institution of Engineering and Technology, 2008.
[74] Bahrman,M. P. “HVDC transmission overview,” in Transmission and Distribution Conference and Exposition, 2008. T&D. IEEE/PES 2008, pp. 1-7.
[75] Zhang,L. D. “Modeling and Control of VSC-HVDC Links Connected to Weak AC Systems,” School of Electrical Engineering, Royal Institute of Technology, Stockholm, 2010.
[76] Bahrman,M. P.; Johnson, B.K., “The ABCs of HVDC Transmission Technologies,” *IEEE Power & Energy Magazine*, 2007.
[77] Okba,M. H.; Saied, M.H.; Mostafa, M. Z.; Abdel-Moneim, T.M., “High voltage direct current transmission - A Review, Part II - Converter technologies,” in Energytech, 2012 IEEE, 2012, pp. 1-7.
[78] Andersen,B. R. “HVDC transmission-opportunities and challenges,” in AC and DC Power Transmission, 2006. ACDC 2006. The 8th IEE International Conference on 2006, pp. 24-29.
[79] Meier, S. “System Aspects and Modulation Strategies of an HVDC-based Converter System for Wind Farms,” School of Electrical Engineering, Royal Institute of Technology, Stockholm, 2009.
[80] Andres, J.M. P.; Muhlenkamp, M.;Retzmann, D.; Walz,R., “Prospects for HVDC-Getting more Power out of the Grid,” in Cigre, Madrid, 2006.
[81] Alejandro,B. S. “Operation, Control and Optimization of a Meshed-HVDC System,” Electircal Engineering, 2013.
[82] Arro,T.; Silavwe, O., “Coupling of Transients in HVDC Lines to Adjacent HVAC lines and Its Impact on the AC Line Protection,” Department of Energy & Environment, Chalmers University of Technology, Sweden, 2007.
[83] Siemens, "Enhanced Power Transmission for HVDC," Siemens, 2013.
[84] ABB, "Why HVDC?," 2009.

[85] Retzmann,D.; Uecker, K., “Benefits of HVDC&FACTS for Sustainability and Security of Power Supply,” in Powerafrica 2007 conference and exposition, Johannesburg, South Africa, 2007.

[86] Dandachi,N.; Siddiqui, H.; Masood, A., Uddin,E., “Interconnection Control and Operational Challenges with HVDC Link.”

[87] Kuehn, W. “Real-time method to prevent voltage collapse and power instability of HVDC systems,” in Innovative Smart Grid Technologies Conference Europe (ISGT Europe), 2010 IEEE PES, 2010, pp. 1-8.

[88] Hafner, J. Y.; Manchen, M., “Stability Enhancement and Blackout Prevention by VSC Based HVDC,” in The electic power system of future integrating supergrids and microgrids, Bologna, Italy, 2011, pp. 232-241.

[89] Basu,K. P. “Stability enhancement of power system by controlling HVDC power flow through the same AC transmission line,” in Industrial Electronics & Applications, 2009. ISIEA 2009. IEEE Symposium on, 2009, pp. 663-668.

[90] Ozerdem,O. C.; Habboob, O., “A CASE STUDY OF HVDC SUBMARINE INTERCONNECTION BETWEEN TURKEY AND TRNC.”

[91] Lee,R. L.; Melvold, D. J.; Szumlas, D. J.; Le, L. M.; Finley, A T.; Martin, D.E.; Wong, W. K.; Dickmander, D.L., “Potential DC system support to enhance AC system performance in the Western United States,” *Power Systems, IEEE Transactions on,* vol. 8, pp. 264-274, Feb 1993, 1993.

[92] Corsi,S.; Danelli, A; Pozzi, M., “Emergency-stability controls through HVDC links,” in Power Engineering Society Summer Meeting, 2002 IEEE 2002, pp. 774-779.

[93] Povh,D.; Retzmann, D.; Teltsch,E.; Kerin,U.; Mihalic,R., “Advantages of Large AC/DC System Interconnections,” in CIGRE, 2006.

[94] W. P. Breuer, D.; Retzmann,D.; Urbanke,C.; Weinhold,M., “Prospects of Smart Grid Technologies for a Sustainable and Secure Power Supply,” in The 20th World Energy Contress&Exhibition, Rome, Italy, 2007.

[95] Ramaswami,V.; Retzmann, D.; Uecker,K., “Prospects of Bulk Power EHV and UHV Transmission,” in GRIDTECH 2007, 2007.

[96] Zhang,X. P.; Yao, L.; Chong, B.; Sasse, C.; Godfrey, K.R., “FACTS and HVDC technologies for the development of future power systems,” in Future Power Systems, 2005 International Conference on 2005.

[97] Breuer,W.; Retzmann, D.; Uecker,K.; , “Highly Efficient Solutions for Smart and Bulk Power Transmission of 'Green Energy',” in 21th World Energy Congress, Montreal, Canada, 2010.

[98] Setreus,J.; Bertling, L., “Introduction to HVDC Technology for Reliable Electrical Power Systems,” in Probabilistic Methods Applied to Power Systems, 2008. PMAPS '08. Proceedings of the 10th International Conference on 2008, pp. 1-8.

[99] Fleeman,J. A.; Gutman, R.; Heyeck,M.; Bahrman,M.; Normark,B., “EHV AC and HVDC Transmission Working Together to Integrate Renewable Power,” 2009.

[100] Ragheb, M. “HIGH VOLTAGE DIRECT CURRENT POWER TRANSMISSION,” 2012.

[101] Okba,M. H.; Saied, M.H.; Mostafa, M. Z.; Abdel- Moneim, T. M., “High voltage direct current transmission - A review, part I,” in Energytech, 2012 IEEE, 2012, pp. 1-7.

[102] The Electricity Training. Association, *Power System Protection*: Institution of Engineering and Technology, 1995.

[103] Zhang, B. H.; Yi. X.G., *Power System Protective Relaying (Chinese Version)*, Beijing: China Electric Power Press, 2005.

[104] IEEE, *IEEE Standard Dictionary of Electrical and Electronics Terms*: Wiley Interscience, 1972.

[105] Leoaneka,C. M. “Dynamic Performance of Numerical Distance Protection Relays in Heavily Series Compensated Networks,” School of Electrical, Electronic and Computer Engineering University of KwaZuluNatal South Africa, 2009.
[106] AREVA, *Network Protection & Automation Guide*, Spain: AREVA T&D, 2005.
[107] Phadke,A. G.; Throp, J.S., *Computer Relaying for Power systems*, England: John Wiley & Sons Ltd,, 2009.
[108] Domin,T. J. *Protective Relaying: Principles and Applications*, United States of America: Taylor & Francis Group, 2006.
[109] Blond,S. L. “Intelligent Autoreclosing for Systems with High Penetration of Wind Generation with Real Time Modelling, Development and Deployment,” Department of Electronic and Electrical Engineering, University of Bath, UK, 2011.
[110] Sherwali,H.; Abdlrahem, A., "Simulation of numberical distance relays," *Matlab-Modelling, Programming and Simulations*, India: Sdyo, 2010.
[111] Redfern,M. A. *Power System Protection*, 2008.
[112] Redfern,M. A. “Signal Processing Techniques in Distacen Protection Applications,” University of Cambridge, Cambridge, 1976.
[113] Lundqvist,B. “100 years of relay protecion, the Swedish ABB relay history.”
[114] Saengsuwan,T. “Modelling of Distance Relays in EMTP,” in IPST'99- International Conference on Power Systems Transients, Budapest, 1999.
[115] Kennedy,J. M.; Alexander. G.E.; Thorp, J.S., “Variable Digital Filter Response Time in a Digital Distance Relay.”
[116] Kasztenny,B.; Finney, D., “Fundamentals of Distance Protection,” in Protective Relay Engineers, 2008 61st Annual Conference for, 2008, pp. 1-34.
[117] Andrichak,J. G. Alexander, G.E., “Distance Relay Fundamentals.”
[118] El-Arroudi,K.; Joos, G.; McGillis, D.T., “Operation of impedance protection relays with the STATCOM,” *Power Delivery, IEEE Transactions on,* vol. 17, pp. 381-387, Apr 2002, 2002.
[119] Zou,J. X. “Demonstration of Healthy-Phase Polarisation for Distance Protection,” Department of Electronic & Electrical Engineering, University of Bath, Bath, 2012.
[120] Jackson,L.; Patrickson. J.B.; Wedepohl, L.M., “Distance protection: optimum dynamic design of static relay comparators,” *Electrical Engineers, Proceedings of the Institution of,* vol. 115, pp. 280-287, February 1968, 1968.
[121] McLaren,P. G.; Redfern,M. A., “Fourier-series techniques applied to distance protection,” *Electrical Engineers, Proceedings of the Institution of* vol. 122, pp. 1301-1305, November 1975, 1975.
[122] Abdlrahem,A. A.; Sherwali. H.H., “Modelling of numerical distance relays using MATLAB,” in Industrial Electronics & Applications, 2009. ISIEA 2009. IEEE Symposium on, 2009, pp. 389-393.
[123] Bentarzi, H.; Duadi, A.; Zitouni, A., “Distance Protective System Performance Enhancement Using Optimized Digital Filter.”
[124] Ouadi,A.; Bentarzi, H.; Maun,J.C., “Digital Distance Relay Reliability Enhancement Using Real-Time Filter.”
[125] Wu,L. C.; Lie, C.W.; Chen, C.S., “Modeling and testing of a digital distance relay MATLAB/SIMULINK,” in Power Symposium, 2005. Proceedings of the 37th Annual North American 2005, pp. 253-259.
[126] Vaidya,A. P.; Venikar, P.A., “ANN based distance protection of long transmission lines by considering the effect of fault resistance,” in Advances in Engineering, Science and Management (ICAESM), 2012 International Conference on 2012, pp. 590-594.

[127] Tziouvaras, D. A.; Hou, D.Q., "Out-of-step protection fundamentals and advancements," in Protective Relay Engineers, 2004 57th Annual Conference for 2004, pp. 282-307.
[128] IEEE Power Engineering Society, *Power Swing and Out-of-step Considerations on Transmission Lines*, 2005.
[129] Khan,U. N.; Yan, L., "Power Swing Phenomena and its Detection and Prevention."
[130] Abidin,A. F. B.; Mohamed, A.; Shareef, H., "A New Power Swing Detection Scheme for Distance Relay Operations," *International Journal of Energy,* vol. 3, pp. 9-17, 2009.
[131] Sena,C.; Franco, R.; Giusto, A., "Assessment of power swing blocking functions of line protective relays for a near scenario of the Uruguayan system," in Transmission and Distribution Conference and Exposition 2008 IEEE/PES, Latin America, 2008, pp. 1-7.
[132] Taheri,S. S.; Abyaneh, H.A., "Detecting of a Power Swing Phenomenon during Two Worst Simultaneous Faults Using System Characteristics," in International Conference on Advancements in Electronics and Power Engineering (ICAEPE'2011), Bangkok, 2011, pp. 86-91.
[133] Sood,V. K. *HVDC AND FACTS CONTROLLERS*, Boston: Kluwer Academic Publishers, 2004.
[134] Rahman,H.; Khan, B. H., "Enhanced power transfer by simultaneous transmission of AC-DC: A new facts concept," in Power Electronics, Machines and Drives, 2004. (PEMD 2004). Second International Conference on (Conf. Publ. No. 498), 2004, pp. 186-191.
[135] Ebasco Services Incorporated, *Methodology for Integraeion of HVDC Link in Large AC Systems - Phase 1: Reference Manual*, 1983.
[136] Avilar,H. A. "Study of Supplementary Controls for Embedded HVDC Links in AC Power Systems," Department of Energy and Environment, Chalmers University of Technology, Goteborg, Sweden, 2008.
[137] Li,X. Y. *High Voltage Direct Current Transmission System (Chinese)*, 2010.
[138] IEEE Standards Board, *IEEE Guide for Planning DC Links Terminating at AC Locations Having Low Short-Circuit Capacities*, p.^pp. 1-214, New York, USA: The Institute of Electrical and Electronics Enginerrs Inc, 1997.
[139] Meah,K.; Sadrull, U. A.M., "Simulation study of the Frontier Line as a multi-terminal HVDC system," in Power and Energy Society General Meeting - Conversion and Delivery of Electrical Energy in the 21st Century, 2008 IEEE, 2008, pp. 1-7.
[140] Abdulla,A. M.; EIdin, A. A. H.; Abbas, A, "Investigation of HVDC link under constant power control," in Power Systems Conference, 2006. MEPCON 2006. Eleventh International Middle East 2006, pp. 447-451.
[141] Kim,C. K.;Sood, V. K.; Jang,G.S.; Lim,S.J.; Lee,S.J., *HVDC Transmission*: John Wiley & Sons (Asia) Pte Ltd, 2009.
[142] Bayliss,C.; Hardy,B., *Transmission and Distribution Electrical Engineering*: Elsevier Ltd, 2012.
[143] Wang,H.; Heng; W.H., "The application research of Matlab in the simulation of Power System," *Journal of Anyang Institute of Technology,* vol. 1, pp. 61-65, 2007.
[144] Li,Z.; Yu, G.B.; Wang, Y.F., "Simulation of power transmission line based on SPS module of Matlab/Simulink," *Colliery Mechanical & Electrical Technology* vol. 6, no. 65-67, 2007.
[145] Liu,X. G.; Jia, M.H.; Qin, C., "Application of the Matlab-based SPS module into power systems," *Electrical Machinery Technology,* vol. 4, pp. 39-40, 2006.
[146] Klein,M.; Rogers, G.J.; Kundur, P., "A fundamental study of inter-area oscillations in power systems," *Power Systems, IEEE Transactions on,* vol. 6, pp. 914-921, Aug 1991, 1991.
[147] MathWorks, *SimPowerSystems User's Guide R2012b*: The MathWorks Inc, 2012.

[148] Mathworks, "SimPowerSystem User's Guide," H.-Q. R. Institute, ed., 2012.
[149] Zhang,Z. Y.; Voloh, I.; Cardenas, J.; Antiza, I.; Iliceto, F., “Inter-area Oscillation Detection by Modern Digital Relays,” in The International Conference on Advanced Power System Automation and Protection, 2011.
[150] Sanchez,J. J.; Miller, N.W.; Price, W.W., “A Modal Analysis of a Two-Area System with Significant Wind Power Penetration,” 2004.